

Controlling topology, dynamics and function of polymer brushes via post-polymerization modification

Thèse N° 9433

Présentée le 14 juin 2019

à la Faculté des sciences et techniques de l'ingénieur
Laboratoire des polymères
Programme doctoral en science et génie des matériaux

pour l'obtention du grade de Docteur ès Sciences

par

Piotr MOCNY

Acceptée sur proposition du jury

Prof. P. Muralt, président du jury
Prof. H.-A. Klok, directeur de thèse
Prof. A. Anastasaki, rapporteuse
Prof. A. Kilbinger, rapporteur
Prof. F. Stellacci, rapporteur

2019

The work described in this Thesis has been performed at the École Polytechnique Fédérale de Lausanne from August 2013 until April 2019 under the supervision of Prof. Harm-Anton Klok.

This work was financially supported by the Swiss National Science Foundation (SNSF).

Acknowledgments

First, I would like to thank Prof. Harm-Anton Klok for hosting me in his lab and giving me a chance to work on challenging and interesting projects. Many thanks for trusting me and giving independence to realize these projects. His guidance, advice and support has been integral, especially during quite complicated times at the end. Thanks HAK for your understanding!

I would like to express my gratitude to the jury members of my doctoral thesis committee: Prof. Paul Muralt, Prof. Athina Anastasaki, Prof. Francesco Stellacci and Prof. Andreas Kilbinger for evaluating this work, inspiring discussion and valuable remarks.

I also would like to thank Dr. Stefano Mischler, who participated in my candidacy exam and shared his tribology experience.

Special acknowledgements go to Prof. Xile Hu and Lucas-Alexandre Stern from LSCI, with whom I had a pleasure to work with during the hydrogen evolution project, which is described in Chapter 4 of this Thesis.

Many thanks to Pierre Mettraux for all help and expertise regarding XPS analysis. I thank Péter Péchy for his introduction to NMR equipment and interesting political talks. ☺

I wish to thank all of my former and present colleagues within LP. I am grateful for the great atmosphere during my stay and our time together: all the jokes, drinks, etc. – though limited due to my family commitment. I am grateful to Jian Wang for being such a nice colleague. I enjoyed all our talks on language, culture, as well as Dragon Ball. *Haha!* I am happy we share a similar situation and see how it is to start a family during doctoral studies. All the best to your kids! I also appreciate much our exciting discussions on science. Big thanks for my office mates: Tuğba (so sad you left just after my arrival... you were very supportive during these days), Julian (who saved me after ca. 5 months from loneliness of the empty and silent office) and Maria (who added a Polish atmosphere to the LP during my last year). Special thanks goes to post-docs: Corey, Michael, Mark, Justin and Ioana for all of your advice on conducting science, writing papers, proposals, and also, revising these work pieces. I am truly indebted to you. I thank Markus (regards to your wife Tianyu!), Tanja, Frieda, Lisa, Cristiana, Sabrina, Alice, Zhao and a newcomer Ghazae. Cheers to our lab technicians Jacques, Philippe and Cindy Känel. Jacques: thanks for your sense of humor and fixing stuff. May your picture stay long on the seminar room's ceiling! ☺ Special thanks to the current (Susanne) and former secretaries (Cindy Ravey) for all help with administration. I would also like to thank and acknowledge former lab members: Ana, Arda, Maxime, Raoul, Nariye, Jirawan, Thawinda, Sorin, Caroline, Vitaliy and Solenne,

and visitors: Alexandre, Chie, Yasushi, Thomas. I would also like to thank Reuben from LMOM for our frequent talks on the way to the oxygen plasma generator!

I am grateful for work of my students: Joan Jornod, Maxence Ménetrey, and Marcelo Alejandro González Alanís. I wish you all the best for your future careers!

I must also mention the members of the Polish community in Lausanne Kasia and I have met: Kuba, Maja, Jakub, Kasia, Konrad, Agata, Paulina and Dawid. You have helped us and brought joy to this place. Thanks for that and all your support.

Raising a family is an uneasy task, when abroad and far from family. We have experienced these challenges. One particularly difficult and stressful event was the second childbirth, when we had to provide care to Emilia, and my thesis defense was approaching. Special thanks to Maria Carmona, who was so kind to offer herself. You helped us a lot on that day!

I also must mention our best friends in Poland. I very much appreciate our tight bonds and continuous gatherings whenever we are in Poland. Thank you Tomek, Dorota, Dawid, Ola, Kamil and Ewelina! *Mam nadzieję, że będziemy kontynuować naszą tradycję!*

I am grateful to people who guided me before I came to EPFL: Prof. Jan F. Biernat, Dr Lidia Jasińska-Walc and Dr Robbert Duchateau. They inspired me and stimulated to undertake scientific career, which I hope to continue.

And last but not least, thanks to my family: parents for raising me and telling me to follow my dreams, my brothers Jakub and Wawrzyniec for your support now and before, and finally and most importantly to my wife Kasia. You may never believe me on your impact, but without your help, support and belief none of these would be possible. You helped me in more ways you can imagine. Also now, when we are a happy family with our lovely kids: Emilia and Alicja, I am happier than ever! *Dziękuję Ci bardzo za to wszystko! Wiedz, że żadne słowa nie oddadzą mojej wdzięczności!* A last acknowledgement is to Emilia for her smiles and Alicja, who was particularly kind to not cry during the nights leading up to my thesis examination. ☺

Table of contents

Summary.....	1
Résumé.....	4
1. Complex Polymer Topologies and Polymer – Nanoparticles Hybrid Films Prepared via Surface-Initiated Polymerization.....	7
1.1. Introduction.....	7
1.2. Architectures of polymer brushes	10
1.2.1. Homopolymer, block and statistical copolymer brushes.....	11
1.2.2. Cyclic, loop-type, Y-shaped and branched polymer brushes	12
1.2.3. Crosslinked polymer brushes	13
1.2.4. Binary mixed, two-layer, bimodal and gradient polymer brushes	14
1.2.5. Free-standing polymer carpets	16
1.3. Incorporation of nanoparticles into polymer brushes.....	17
1.3.1. Infiltration of polymer brushes with preformed nanoparticles	18
1.3.2. Synthesis of nanoparticles in polymer brush templates	19
1.4. Outlook and recommendations	28
1.5. References.....	29
2. Synthesis of Loop Polymer Brushes via Chain-End Post-Polymerization Modification.....	40
2.1. Introduction.....	40
2.2. Experimental Section	41
2.2.1. Materials	41
2.2.2. Analytical methods	42
2.2.3. Procedures.....	42
2.3. Results and Discussion	49
2.3.1. PMMA brush synthesis.....	49
2.3.2. Brush cleavage.....	50
2.3.3. Chain-end modification.....	51
2.3.4. Synthesis of PMMA loop brushes.....	55
2.4. Conclusions.....	59
2.5. References.....	59
2.6. Supporting Information.....	62
3. Reversibly Crosslinked Polymer Brushes	83
3.1. Introduction.....	83
3.2. Experimental Section.....	84
3.2.1. Materials	84
3.2.2. Analytical methods	85
3.2.3. Procedures.....	87

3.3.	Results and Discussion.....	90
3.3.1.	Synthesis and characterization of P(DMAEMA-co-AzHPMA) copolymer brushes.....	90
3.3.2.	Post-polymerization modification of P(DMAEMA-co-AzHPMA) copolymer brushes.....	94
3.3.3.	Dynamic behavior of reversibly crosslinked polymer brushes.....	98
3.4.	Conclusions.....	101
3.5.	References.....	102
3.6.	Supporting Information.....	104
4.	A Polymer-Brush Templated Three-Dimensional Molybdenum Sulfide Catalyst for Hydrogen Evolution	119
4.1.	Introduction.....	119
4.2.	Experimental Section.....	120
4.2.1.	Materials.....	120
4.2.2.	Analytical methods.....	121
4.2.3.	Procedures.....	122
4.3.	Results and Discussion.....	124
4.3.1.	Synthesis and characterization of polymer-brush templated 3D MoS _x catalysts.....	124
4.3.2.	Hydrogen evolution using polymer-brush templated 3D MoS _x catalysts.....	129
4.4.	Conclusions.....	134
4.5.	References.....	135
4.6.	Supporting Information.....	137
5.	Conclusions and Perspectives	159
	Curriculum vitae.....	a

List of Symbols and Abbreviations

2D	two-dimensional
3D	three-dimensional
4-NDT	(4-Nitrophenyl)diazonium tetrafluoroborate
¹³ C NMR	carbon-13 nuclear magnetic resonance
¹ H NMR	proton nuclear magnetic resonance
ACN	acetonitrile
AFM	atomic force microscopy
AIBN	2,2'-azobis(isobutyronitrile)
A(R)GET	activators (re)generated by electron transfer
ATR	attenuated total reflectance
ATRP	atom transfer radical polymerization
AzHPMA	3-azido-2-hydroxypropyl methacrylate
BDT	benzenediazonium tetrafluoroborate
bisAAm	bis-acrylamide
bpy	2,2'-bipyridine or 2,2'-bipyridyl
Cd(Ac) ₂	cadmium acetate
CS	core-shell
CTA	chain transfer agent
CuAAC	copper(I)-catalyzed alkyne-azide cycloaddition
Cu-CRP	copper(0)-mediated controlled radical polymerization
Cu ⁰ -SI-ATRP	copper(0)-mediated surface-initiated atom transfer radical polymerization
d	diameter
d*	swollen polymer brush thickness calculated as twice the second moment of the brush profile
DCM	dichloromethane
DEGDMA	diethylene glycol dimethacrylate
DG	double gyroid
DLS	dynamic light scattering
DMF	dimethylformamide
DMSO	dimethyl sulfoxide
DP	degree of polymerization
DMAEMA	2-(dimethylamino)ethyl methacrylate
dNbp	4,4'-dinonyl-2,2'-dipyridyl
Đ	dispersity (M_w/M_n)
EBiB	ethyl 2-bromoisobutyrate
EDA	ethylene glycol diacrylate
EDTA	ethylenediaminetetraacetic acid
EDX	energy dispersive X-ray
EDXS	energy dispersive X-ray spectroscopy
EGDMA	ethylene glycol dimethacrylate
ESCA	electrochemical active surface area
Et ₃ N	triethylamine
EtOAc	ethyl acetate
EtOH	ethanol
FIB	focused-ion beam
FRP	free-radical polymerization
FTIR	Fourier-transform infrared
GD	grafting density

List of Abbreviations

GPC	gel permeation chromatography
h	brush thickness
HDA	hexanediol diacrylate
HDI	hexamethylene diisocyanate
HER	hydrogen evolution reaction
Hex	n-hexane
HMTETA	1,1,4,7,10,10-hexamethyltriethylenetetramine
HOPG	highly-ordered / highly-oriented pyrolytic graphite
HRSEM	high resolution scanning electron microscopy
ICAR	initiators for continuous activator regeneration
IR	infrared
j	current density
j_m	mass activity
j_s	specific activity
K_{ATRP}	atom transfer radical polymerization equilibrium constant
k_p	propagation rate constant
k_t	termination rate constant
LbL	layer-by-layer
LSPR	localized surface plasmon resonance
LSV	linear sweep voltammetry
m	mass
M	monomer or molecular weight
MALDI-TOF MS	matrix assisted laser desorption ionization – time-of-flight mass spectrometry
M_{av}	average molecular weight
MBA	<i>N,N</i> -methylene-bisacrylamide
MEMs	microelectromechanical devices
METAI	2-(methacryloyloxy)ethyl ammonium iodide
MeOH	methanol
MMA	methyl methacrylate
M_n	number average molecular weight
M_w	weight average molecular weight
n	molar amount
<i>n</i>	refractive index
NaSAc	sodium thiomethoxide
N_{AV}	Avogadro's number
NMP	nitroxide-mediated polymerization
NMR	nuclear magnetic resonance
OER	oxygen evolution reaction
PAA	poly(acrylic acid)
PAAm-ETA-CIPPh ₂	poly(acrylamide) reacted with ethanolamine and chlorodiphenylphosphine
PAA(Na)	poly(sodium acrylate)
PAA(Ag)	poly(silver acrylate)
PAEMA-HCl	poly((2-aminoethyl)methacrylate hydrochloride)
PAzHPMA	poly(3-azido-2-hydroxypropyl methacrylate)
PBpyClCl	poly(<i>N</i> -benzyl- <i>N'</i> -(4-vinylbenzyl)-4,4'-bipyridium dichloride)
PDI	polydispersity index
PDMAEMA	poly(2-(dimethylamino)ethyl methacrylate)
PDMAEMA-EtBr	poly(2-(dimethylamino)ethyl methacrylate) quaternized with bromoethane

PDMAEMA-HexBr	poly(2-(dimethylamino)ethyl methacrylate) quaternized with 1-bromohexane
PDMS	polydimethylsiloxane
PEEK	poly(ether ether ketone)
PEGDMA	poly(ethylene glycol) dimethacrylate
PEOXA	poly(2-ethyl-2-oxazoline)
Pg-SAc	S-propargyl thioacetate
PHEMA	poly(2-hydroxyethyl methacrylate)
PHEMA-SA	poly(2-hydroxyethyl methacrylate) reacted with succinic anhydride
PMAA	poly(methacrylic acid)
PMDETA	<i>N,N,N',N'',N'''</i> -pentamethyldiethylenetriamine
PMETAC	poly(2-(methacryloyloxy)ethyl ammonium chloride)
PMETAI	poly(2-(methacryloyloxy)ethyl ammonium iodide)
PMMA	poly(methyl methacrylate)
PNIPAAm	poly(<i>N</i> -isopropylacrylamide)
POEGEEMA	poly(oligo(ethylene glycol) ethyl ether methacrylate)
PPEGMA	poly(poly(ethylene glycol) methacrylate)
PPEGMEMA	poly(poly(ethylene glycol) methyl ether methacrylate)
PPM	post-polymerization modification
PSPMA(Na)	poly(3-sulfopropyl methacrylate, sodium salt)
PSSA	poly(styrene sulfonic acid)
PTEPM	poly(3-(triethoxysilyl)propyl methacrylate)
PTHFMA	poly(tetrahydrofurfuryl methacrylate)
PVOH	poly(vinyl alcohol)
P4VP	poly(4-vinylpyridine)
P2VP	poly(2-vinylpyridine)
P(MAA) ₂ Cd	poly(cadmium dimethacrylate)
P(MAA) ₂ Pb	poly(lead dimethacrylate)
Q	charge
QCM	quartz crystal microbalance
QCM-D	quartz crystal microbalance with dissipation monitoring
RAFT	reversible addition-fragmentation chain-transfer
RGO	reduced graphene oxide
RHE	reversible hydrogen electrode
ROP	ring-opening polymerization
r_i	reactivity ratio
R_f	retention factor
SA	specific surface area
SAMs	self-assembled monolayers
SERS	surface enhanced Raman scattering
S-RAFT	surface reversible addition-fragmentation chain-transfer
SARA ATRP	supplemental activator and reducing agent atom transfer radical polymerization
SET-LRP	single-electron transfer living radical polymerization
SI-A(R)GET-ATRP	surface-initiated activators (re)generated by electron transfer atom transfer radical polymerization
SI-ATRP	surface-initiated atom transfer radical polymerization
SI-CRP	surface-initiated controlled radical polymerization
SI-FRP	surface-initiated free-radical polymerization
SI-FRPP	surface-initiated free-radical photopolymerization

List of Abbreviations

SI-NMP	surface-initiated nitroxide-mediated polymerization
SIP	surface-initiated polymerization
SIPGP	self-initiated photografting and photopolymerization
SI-PIMP	surface-initiated photoiniferter-mediated polymerization
TBAF	tetra- <i>n</i> -butylammonium fluoride
TCEP	tris(2-carboxyethyl)phosphine hydrochloride
TEGDMA	tetra(ethylene glycol) dimethacrylate
TEM	transmission electron microscopy
TEMPO	2,2,6,6-tetramethylpiperidinyloxy
TGA	thermogravimetric analysis
THF	tetrahydrofuran
TOF	turnover frequency
UV	ultraviolet
V	volume
XPS	X-ray photoelectron spectroscopy
z_i	thickness of <i>i</i> th layer
Δ	phase difference
Δf_n	change of <i>n</i> th harmonic frequency
ΔD_n	change of dissipation factor of <i>n</i> th overtone
η	reaction yield
η	overpotential
λ	wavelength
ρ	density
φ	weight fraction
φ_i	volume fraction of <i>i</i> th layer
Ψ	amplitude ratio

Summary

Polymer brushes are a class of thin coatings, where each of chains is tethered to the underlying substrate via one chain end. Densely grafted polymer brushes feature a stretched chain conformation, which in a unique way enhances their lubrication and non-biofouling properties. Polymer brushes also present a high density of functional groups, whose exposure in solvated brushes is useful for catalysis or in medical applications, including diagnostics. Advances in surface-initiated controlled radical polymerizations (SI-CRP) have facilitated the synthesis of high grafting density polymer brushes with a great control over film thickness / polymer molecular weight and composition. These techniques enable access to plethora of polymer architectures. Due to the fact that SI-CRP strategies allow the use of a wide range of monomers, multiple routes for the post-polymerization modification of polymer brushes are possible. Combination of SI-CRP with post-polymerization modification provides possibilities to systematically study architecture- and composition-property relationships of polymer brushes. This Thesis aims to manipulate the topology and crosslinking dynamics of polymer brushes, whose effect on properties of the coatings will help to understand these relationships. Additionally, functions of polymer brushes can be extended by their modification. As an example, incorporation of nanoparticles is a way to provide catalytic functions. Swelling of the nanoparticle – polymer brush assemblies can expose the catalytically active sites and potentially maximize its activities. These topics are explored within four chapter of this Thesis and are briefly summarized below.

Chapter 1 provides an overview of manipulation strategies over the composition and topologies of polymer brushes including, among others, block, statistical and gradient copolymer brushes, cyclic and loop polymer brushes, bimodal, Y-shaped and branched polymer brushes. Routes toward crosslinking of polymer brushes with a range of chemistries is also presented. This Chapter concludes with methods for assembly of nanoparticles within polymer brushes.

Chapter 2 demonstrates a two-step post-polymerization synthetic approach to generate loop polymer brushes that have been demonstrated previously to possess improved resistance to biofouling as well as superior lubrication properties as compared to their single chain-end tethered analogues. In the first step, olefin groups are installed at the polymer chain-ends and then metathesis is used to induce loop closure. The loop-formation is followed by gel permeation chromatography (GPC) analysis of cleaved polymer chains.

Chapter 3 presents a synthetic strategy to install different crosslinks onto polymer brush platforms, which will allow for the systematic investigation of their impact on the stability and properties of polymer brushes. The synthesis comprises a two step-process: surface-initiated atom transfer polymerization (SI-ATRP) to generate a copolymer platform bearing azide groups for subsequent copper(I)-catalyzed alkyne-azide cycloaddition (CuAAC) using propargyl-modified thiol precursors. The reactions steps are followed by Fourier-transform infrared (FTIR) spectroscopy and X-ray photoelectron spectroscopy (XPS). Multiple crosslinking and decrosslinking cycles are studied under oxidative and reductive conditions. This reversibility was followed by swelling changes (ellipsometry), chain hydration and mobility (quartz crystal microbalance with dissipation monitoring, QCM-D).

Chapter 4 explores the catalytic properties of 3-dimensional (3D) assemblies of amorphous molybdenum sulfide in polymer brushes as a template. Poly(dimethylaminoethyl methacrylate) (PDMAEMA) brushes are grown from highly-oriented pyrolytic graphite (HOPG) and used to bind anionic MoS_4^{2-} through an anion exchange reaction. In a final oxidation step, the polymer-bound MoS_4^{2-} is converted into the amorphous MoS_x catalyst. The incorporation of MoS_x within PDMAEMA brushes is studied by FTIR spectroscopy and XPS, and its distribution within the layer is analyzed by transmission electron microscopy (TEM) and energy dispersive X-ray spectroscopy (EDXS). The performance of polymer brush-catalyst system during hydrogen evolution reaction (HER) is studied. Turnover frequencies are compared with other reported molybdenum sulfide catalysts.

Keywords: Surface-initiated controlled radical polymerization (SI-CRP), surface-initiated atom transfer radical polymerization (SI-ATRP), polymer brushes, post-polymerization modification, loop polymer brushes, reversible crosslinks, nanoparticles, hybrids, nanocomposites, hydrogen evolution reaction (HER)

Résumé

Les polymères appelés brosses sont une classe de revêtement de surface fins pour lesquels chaque chaîne de polymère est attachée au substrat sous-jacent par une de ses extrémités. Des brosses greffées de manière dense se présentent de manière étirée, ce qui de manière unique modifie certaines propriétés comme l'amélioration l'effet lubrifiant ou la réduction l'encrassement biologique. Les polymères en brosse présentent aussi une forte densité de groupes fonctionnels, ce qui, lorsque ces brosses sont dans un état de solvation, est un avantage en catalyse ou pour des applications médicales, tel que le développement de méthodes de diagnostic. Les avancées dans le domaine de la polymérisation radicalaire contrôlée initiée en surface (SI-CRP) ont facilité la synthèse de polymères en brosse greffés de manière dense avec un excellent contrôle de l'épaisseur du film / du poids moléculaire et de la composition du film. Ces techniques permettent une pléthore d'architectures de polymère. Comme la polymérisation radicalaire contrôlée initiée en surface permet l'utilisation d'un large éventail de monomères, de nombreuses routes pour la modification post-polymérisation sont possibles. La combinaison entre la méthode de polymérisation SI-CRP et les possibles modifications post-polymérisation permet l'étude systématique des propriétés des brosses de polymère selon leur architecture ou leur composition. Cette thèse a pour but d'étudier l'effet des modifications de topologies et la dynamique des réticulations des brosses de polymères. Les changements de propriété de ces polymères aideront à la compréhension de la relation entre l'architecture et la composition. De plus, la fonction de ces polymères peut être élargie par leur modification. Par exemple, l'incorporation de nanoparticules est un moyen d'introduire des fonctions catalytiques. La solvation de ces assemblages de brosses de polymères et de nanoparticules permet d'exposer les sites catalytiques actifs et peut potentiellement maximiser leur activité. Ces sujets sont développés dans quatre chapitres et sont résumés ci-dessous.

Le Chapitre 1 est une vue d'ensemble des stratégies de manipulations de la composition et de la topologie des brosses de polymères, incluant entre autre des brosses de copolymères en blocs, statistiques et en gradient, des brosses cycliques, en boucle, bimodal, en forme de Y ou ramifiée. La réticulation des brosses de polymère utilisant différents types de réactions chimiques est aussi présentée. Ce chapitre se conclut avec des méthodes d'assemblage de nanoparticules dans des brosses de polymère.

Le Chapitre 2 décrit une approche synthétique post-polymérisation en deux étapes pour la création de boucles sur des brosses de polymère. Il a été démontré que ces boucles

améliorent la résistance contre l'encrassement biologique et montrent de meilleures propriétés lubrifiantes en comparaison avec des brosses de polymère sans boucle. Dans une première étape, les bouts de chaînes sont modifiés pour présenter des oléfines qui par métathèse peuvent être couplées ensemble pour créer des boucles. La formation de ces boucles est suivie par l'analyse de ces chaînes de polymère clivées de la surface par chromatographie d'exclusion stérique (GPC).

Le Chapitre 3 présente différentes stratégies synthétiques pour l'insertion d'agents de réticulation dans des brosses de polymère. Ces agents vont permettre l'analyse systématique de l'influence de la réticulation sur la stabilité et les propriétés des brosses. Ces brosses sont préparées par un processus en deux étapes comprenant la préparation des brosses par polymérisation radicalaire par transfert d'atomes initiée en surface (SI-ATRP) et qui contiennent des fonctions azide. La seconde étape est la réaction des résidus azide avec du 2-propyne-1-thiol utilisant une alcyne-azide cyclo-addition catalysée par du cuivre (I). Chaque étape est étudiée par spectroscopie infrarouge à transformée de Fourier (FTIR) et par spectrométrie photo électronique X (XPS). La réticulation multiple et la réaction inverse par l'utilisation de conditions oxydatives ou réductives sont étudiées. Cette réversibilité a été analysée par les changements de solvatation (ellipsométrie), l'hydratation et la mobilité des chaînes (microbalance à cristal de quartz avec contrôle de la dissipation).

Le Chapitre 4 explore les propriétés catalytiques d'assemblage tridimensionnel (3D) de sulfure de molybdène amorphe dans des brosses de polymère comme modèle. Des brosses composées de poly(diméthylaminoéthyle méthacrylate) (PDMAEMA) ont été préparées sur du graphite pyrolytique hautement orienté (HOPG) et utilisées pour attacher du MoS_4^{2-} anionique par une réaction d'échange anionique. Dans une dernière étape d'oxydation, le MoS_4^{2-} attaché sur le polymère est converti en MoS_x catalytique amorphe. L'incorporation de MoS_x dans des brosses de PDMAEMA est étudiée par spectroscopie FTIR et XPS et sa distribution dans la couche de polymère analysée par microscopie à transmission d'électrons (TEM) et par spectroscopie à analyse dispersive de rayon X (EDXS). La performance de ce système catalyseur/brosses durant la réaction d'évolution d'hydrogène (HER) est également étudiée. La fréquence de turnover est comparée avec d'autres catalyseurs au sulfure de molybdène répertoriés.

Mots clés : Polymérisation radicalaire contrôlée initiée en surface (SI-CRP), polymérisation radicalaire par transfert d'atomes initiée en surface (SI-ATPR), brosses de polymère, modification post-polymérisation, brosses de polymères en boucle, nanoparticules, hybrides, nano composites, réaction d'évolution d'hydrogène (HER)

1. Complex Polymer Topologies and Polymer – Nanoparticles Hybrid Films Prepared via Surface-Initiated Polymerization

1.1. Introduction

Polymer brushes are thin coatings in which each of polymer chains is tethered to an underlying substrate. They are typically synthesized by surface-initiated polymerization (SIP).^{1,2} This polymerization represents a grafting-from strategy (**Figure 1.1**) that allows for high grafting densities and a great control over films thickness / polymer molecular weights and composition.² Controlled radical polymerization (CRP) methods are most frequently used to generate polymer brushes. These include, among others, atom transfer radical polymerization (ATRP) and reversible addition-fragmentation chain-transfer (RAFT) polymerization.¹ These polymerizations require simple experimental setups and permit mild reaction conditions. They are tolerant against a wide range of functional groups and are compatible with both aqueous and organic media.¹

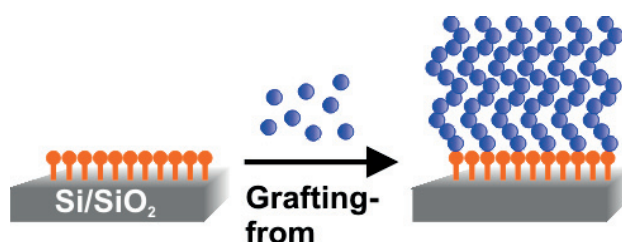
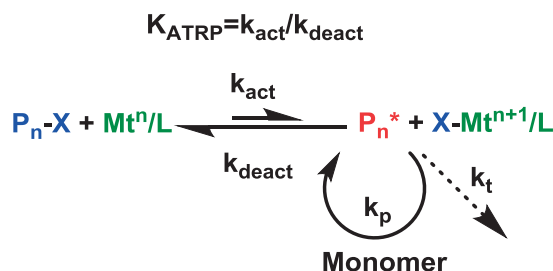


Figure 1.1. Schematic illustration of the grafting-from strategy for the preparation of polymer brushes. Orange and blue spheres correspond to initiator and monomer molecules, respectively.

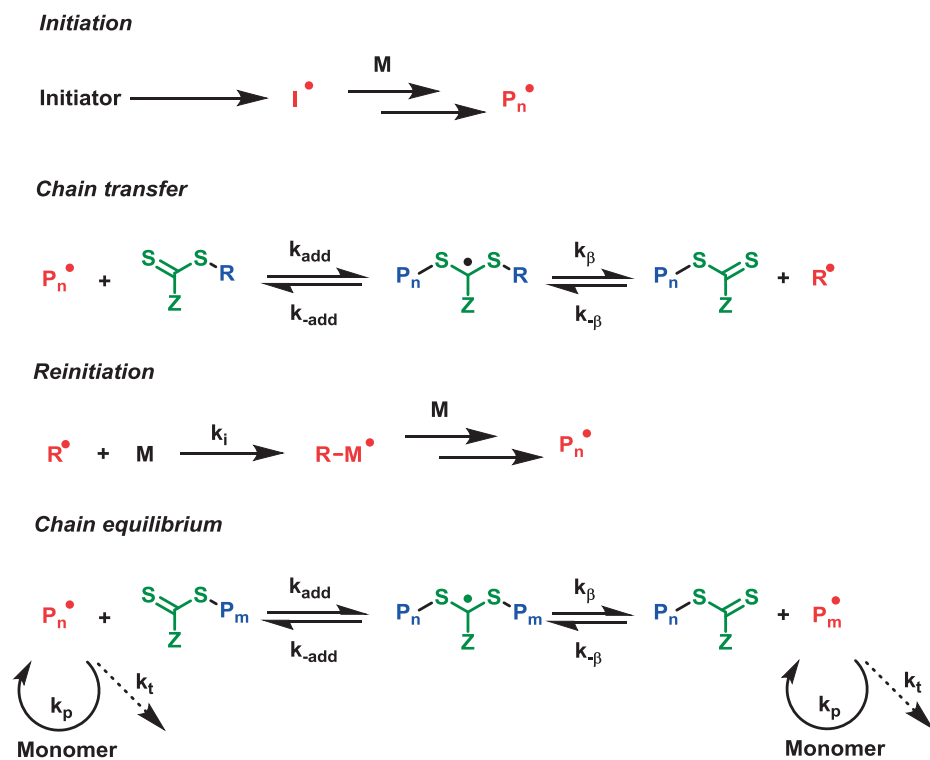
ATRP relies on a reversible activation-deactivation equilibrium between a transition metal complex (activator Mt^v/L and deactivator Mt^{v+1}/L) and dormant halide-terminated polymer chains (P_n-X) as depicted in **Scheme 1.1**.³ Its equilibrium constant K_{ATRP} is governed by structure of the alkyl halide, the catalyst, and the solvents. Intermittently formed radicals P_n^* react with a monomer (propagation rate constant k_p) or terminate

(propagation rate constant k_p). Several variations of ATRP have been developed, such as activators (re)generated by electron transfer (A(R)GET) ATRP, initiators for continuous activator regeneration (ICAR) ATRP, metal-free ATRP or ATRP in the presence of Cu(0).⁴ The latter is termed supplemental activator and reducing agent (SARA) ATRP or single-electron transfer living radical polymerization (SET-LRP) depending on the exact mechanism of the polymerization in solution. For SIP it is often termed Cu(0) mediated controlled radical polymerization (Cu-CRP)^{5,6} or Cu⁰-SI-ATRP.⁷ The purpose of the aforementioned methods is mainly to decrease amount of the metal catalyst in the polymerization medium and allow for milder polymerization conditions (less stringent deoxygenation, lower temperature, faster polymerization rates), which is beneficial for biological or electronic applications and easier implementation in industrial processes.

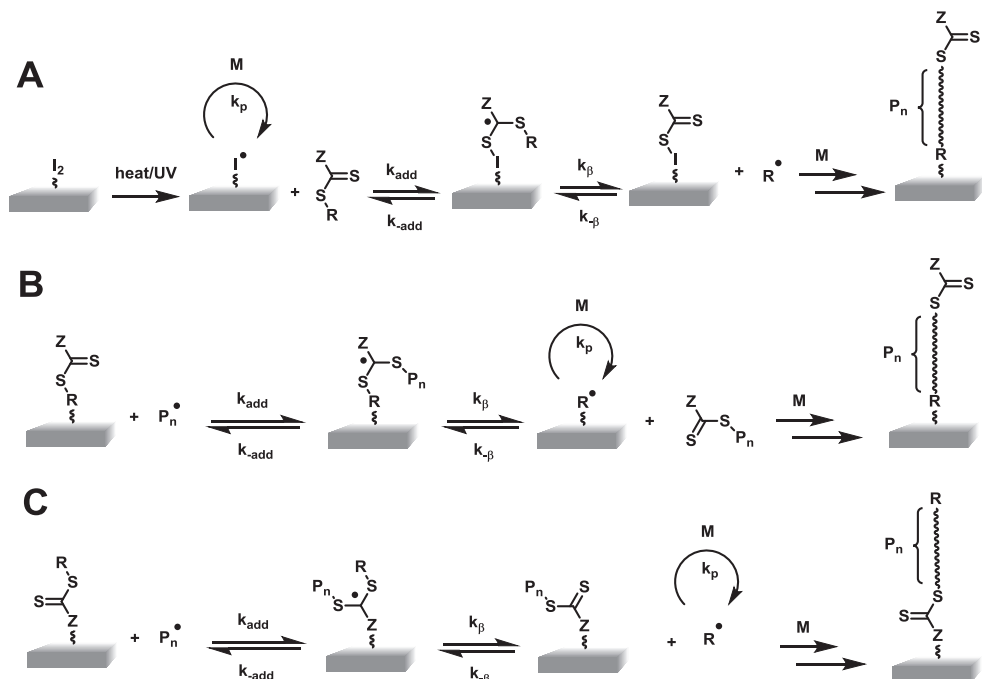


Scheme 1.1. Mechanism of ATRP.³

RAFT is based on a reversible chain-transfer between a chain transfer agent (CTA) and an active, polymer radical (**Scheme 1.2**).⁸ CTAs are thiocarbonylthio compounds of general structure $Z-C(=S)-R$, which react reversibly with a propagating radical (addition) and form the intermediate radical, which can fragment into the new CTA and radical species. Thus, the radicals are activated and deactivated in similar manner as in ATRP, which prevents termination reactions and facilitate synthesis of polymers with low dispersities. It is worth noting, that in contrast to ATRP, where dormant species are also source of radicals, RAFT polymerization requires an external source of free radicals for initiation of the polymerization (**Scheme 1.2, Initiation**). Its CTAs alone neither form nor destroy the radicals. The free radical initiators are typical to conventional free radical polymerization, which cleave homolytically under heating or UV light irradiation. For the generation of polymer brushes, these initiators must be attached to a substrate or be present in the polymerization medium.⁹ For the latter strategy, CTAs must be grafted via their R-¹⁰ or Z-group.¹¹ Depending on the method, the final polymer brushes have CTA either at the chain-ends (substrates grafted with radical initiator or CTA via R-group^{9,10}) or at the bottom of the brush (substrates grafted with CTA via Z-group¹¹) (**Scheme 1.3**).



Scheme 1.2. Mechanism of RAFT.⁸



Scheme 1.3. Mechanism of S-RAFT for (A) radical initiator grafted, (B) R-group attached CTA and (C) Z-group attached CTA to substrates.^{12,13}

Two other used SI-CRP methods are surface-initiated nitroxide-mediated polymerization (SI-NMP) and photoiniferter-mediated polymerization (SI-PIMP).¹ In SI-NMP nitroxides (usually alkoxyamines) are used as mediators. During the polymerization, mediators like 2,2,6,6-tetramethylpiperidinyloxy (TEMPO) trap carbon-centered propagating radicals.¹⁴ At low temperatures (e.g. 60°C) the adducts are stable and the polymerization does not occur. However, at higher temperatures (e.g. 130 °C) the C-ON bond is weak enough to promote reversible deactivation of propagating radicals, which enables controlled polymerization with characteristics of a living system.

In SI-PIMP photo-labile iniferters are used that act simultaneously as *initiators*, chain *transfer* agents and *terminators*.¹⁵ Intensity of UV light controls deactivation of propagating radicals and thus rate of the polymerization. It also provides spatial and temporal control over generation of polymer brush films.

Grafting-onto method (**Figure 1.2**) involves adsorption (physi- or chemisorption) of pre-synthesized polymers that contain appropriate chain-end functional groups, which either have a high affinity to or can react with a complementary reactive group on the substrate of interest.¹⁶ As opposed to grafting-from, this method, although straightforward, is limited to low grafting densities, as the chains approaching the surfaces exert higher steric hindrance than monomers used in grafting-from methods.

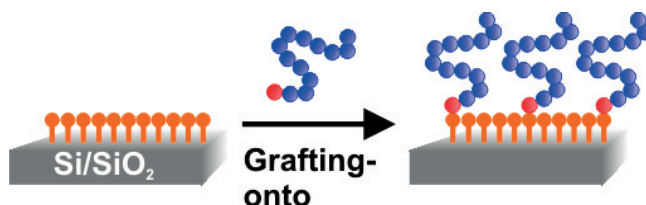


Figure 1.2. Schematic illustration of the grafting-onto strategy for the preparation of polymer brushes. Orange, red, and blue spheres correspond to reactive surface groups, reactive / sticky polymer segments and monomer molecules, respectively.

1.2. Architectures of polymer brushes

The use of controlled radical polymerization techniques allow researchers to generate a wide range of polymer brush architectures. They will be discussed together with their synthetic strategies in the following sections.

1.2.1. Homopolymer, block and statistical copolymer brushes

The chemical composition of surface-grafted polymers can be tuned, so that, apart from homopolymer brushes,^{17,18} also block^{19,20} or statistical^{20,21} copolymer brushes can be generated (**Figure 1.3**).

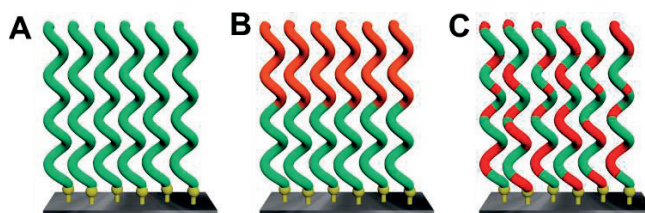


Figure 1.3. (A) Homopolymer, (B) Block copolymer and (C) Statistical copolymer brushes.

Block copolymer brushes are obtained by sequential polymerizations of the respective monomers. This is possible, because of limited termination reactions and high retention of chain-end functionality in CRP. However, it is important to adjust the reactivity of the end group of one block with that of the second block.²² If the cross-propagation is slow compared to polymerization of the subsequent monomer, initiation efficiency will be low²³ and bimodal brushes will be formed.²⁴ An example of this problem is polymerization of methacrylates from polystyrene²⁵ or polyacrylate²⁴ macroinitiators. Here, however, one can utilize halogen exchange technique in ATRP, where a mixed halide system is used,²⁶ i.e. bromo-containing initiator (polystyrene) is used with CuCl catalyst for the polymerization of the second block-monomer. In this way, the polymerization will be retarded, which will compensate for initiation and polymerization rate differences. Another important aspect in building block copolymer brushes is to maintain good swelling of the blocks in polymerization media.¹⁸ Therefore, synthesis of copolymer brushes composed of monomers of very different polarities can be challenging and accessible only by post-polymerization modification. This was demonstrated by Paripovic and Klok, who could not directly copolymerize hydrophilic sodium methacrylate on top of poly(methyl methacrylate) or poly(2-ethylhexyl methacrylate), as the bottom blocks did not swell in water required for the second polymerization.¹⁸ Instead, they extended them with poly(*tert*-butyl methacrylate), which then deprotected with trifluoroacetic acid to afford poly(metacrylic acid) block.

Statistical copolymer brushes are typically obtained by a one batch copolymerization of two monomers, whose arrangement in the chains is governed by the monomer

reactivities and their relative concentrations in the polymerization medium.²⁷ If additionally monomer conversion is significant (as for SI-ATRP from nanoparticles with substantial amount of grafted initiator compared to monomer volume), a compositional drift can be observed,^{28,29} which leads to gradient polymers.³⁰ Reactivity ratios r_1 , r_2 , which can be used to predict the behavior of monomers, are usually different.²⁷ High r values indicate preferential homopolymerization of the corresponding monomer, thus the brush will grow with higher content of this monomer. If $r_1 = r_2$, each of the monomers will propagate with the same probability. Moreover, if the product $r_1 \cdot r_2 = 1$, the monomers will have no preference whether to cross-propagate or homopolymerize and will generate true random copolymer brushes.

1.2.2. Cyclic, loop-type, Y-shaped and branched polymer brushes

Aside from linear polymer chains also cyclic,^{31,32} loop-type,^{33,34} Y-shaped³⁵ and branched³⁶⁻³⁸ brushes can be grafted (**Figure 1.4**).

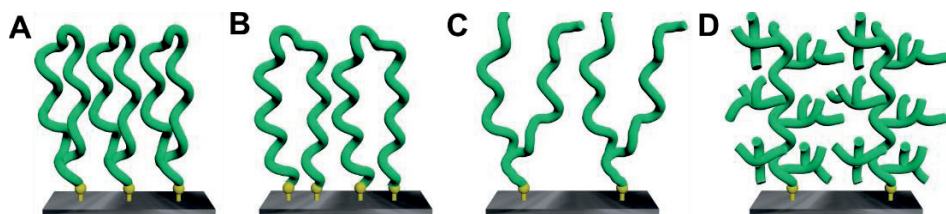


Figure 1.4. (A) Cyclic, (B) Loop-type, (C) Y-shaped and (D) Branched polymer brushes.

Synthesis of cyclic polymer brushes has been exclusively accomplished by grafting-onto of presynthesized cyclic polymers bearing one anchoring unit, a strategy explored by Benetti et al.^{32,39-41} and Wei et al.⁴²

Loop-type brushes can be prepared in a similar manner using presynthesized α,ω -telechelic polymers bearing a pair of reactive groups, such as thiol,^{33,43-45} siloxane,⁴⁶ carboxylic acid^{47,48} or catechol.^{40,49,50} Alternatively, block copolymers with physisorbing hydrophobic or charged domains at both sides can be used.⁵¹⁻⁵⁵ There are also two examples, where grafting-from approach was exploited.^{34,56} More specifically, Rotzoll et al. utilized bipedal azo initiators and trimethoxysilane functionalized RAFT agents via both R and Z group.

Y-shaped polymer brushes are synthesized from Y-shaped initiators. Growth of asymmetric Y-shaped brushes with different polymers at each arm can be realized by using initiator groups designed to be selectively activated at given conditions, e.g. ATRP initiators were combined with nitroxide-mediated polymerization (NMP) initiators,^{35,57-62}

ring-opening polymerization (ROP) with NMP initiators,⁶³ and RAFT polymerization with ATRP initiators.⁶⁴

Branched polymer brushes can be subdivided into several categories depending on number n of generations of graft-chains. The most simple branched polymer brushes are grafted bottlebrush polymers with second generation grafts ($n=2$), obtained by e.g. polymerization of poly(2-hydroxyethyl methacrylate) (PHEMA) (a stem) followed by ROP^{65,66} to form branches. Higher generation-grafts can be prepared by multiple polymerization/initiator-grafting reactions. For example, third generation branched polymer chains were synthesized by sequential polymerizations with chloromethylstyrene as a comonomer that can be subsequently modified with *N,N*-diethyldithiocarbamate. Then, the grafted photoiniferter functions can be used for growing the next generation grafts.^{36,67} A similar approach relied on ATRP with 4-vinylbenzyl chloride as a comonomer, which also acts as an initiator (a so-called inimer), which can lead to further polymerizations and branching.⁶⁸ This strategy represent a concept of self-condensing vinyl copolymerization or self-condensing ATRP and was also explored by others.^{69,70}

1.2.3. Crosslinked polymer brushes

Polymer brush layers can also be crosslinked (**Figure 1.5**).^{71,72} Two approaches can be used, viz. direct copolymerization and post-polymerization modification.

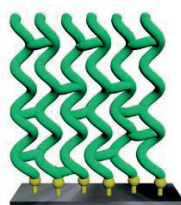


Figure 1.5. Crosslinked polymer brushes.

The direct copolymerization requires multifunctional monomers that connect multiple chains during polymerization, while post-polymerization modification relies on reactive groups of polymer brushes. To date, a number of vinyl comonomers as crosslinkers have been used for the first strategy, i.e. ethylene glycol dimethacrylate (EGDMA),^{71,73,74} diethylene glycol dimethacrylate (DEGDMA),⁷⁵⁻⁷⁸ tetra(ethylene glycol) dimethacrylate (TEGDMA),⁷⁶ polyethylene glycol dimethacrylate (PEGDMA), bis-acrylamide (bisAAm),⁷⁹⁻⁸² ethylene glycol diacrylate (EDA),⁸³ hexanediol diacrylate (HDA),⁸³ *N,N'*-methylenebisacrylamide,⁸⁴ divinylbenzene,⁸⁵⁻⁸⁷ and *N,N*-methylene-bisacrylamide (MBA).^{88,89}

Post-polymerization crosslinking of polymer brushes is used less frequently. Chemical crosslinking with difunctional compounds has been carried out with cystamine, (reacting with maleic anhydride or succinimide groups),^{90,91} hexamethylene diisocyanate (HDI) (reacting with amine groups),⁷² bis(2-iodoethoxy)ethane (quaternization of amine groups),⁹² or Zn^{2+} (complexation of amine groups).⁹² UV-light, frequently used to cure resins, has been surprisingly reported few times. The examples include dimerization of dimethyl maleimide⁹³ and coumarin side groups.⁹⁴ Polystyrene has also been used as a UV-curable block within polymer brushes.⁹⁵

1.2.4. Binary mixed, two-layer, bimodal and gradient polymer brushes

Finally, different compositions of grafts can be created, which include binary mixed,⁹⁶ two-layer, bimodal^{97,98} or gradient polymer brushes⁹⁹⁻¹⁰¹ (Figure 1.6).

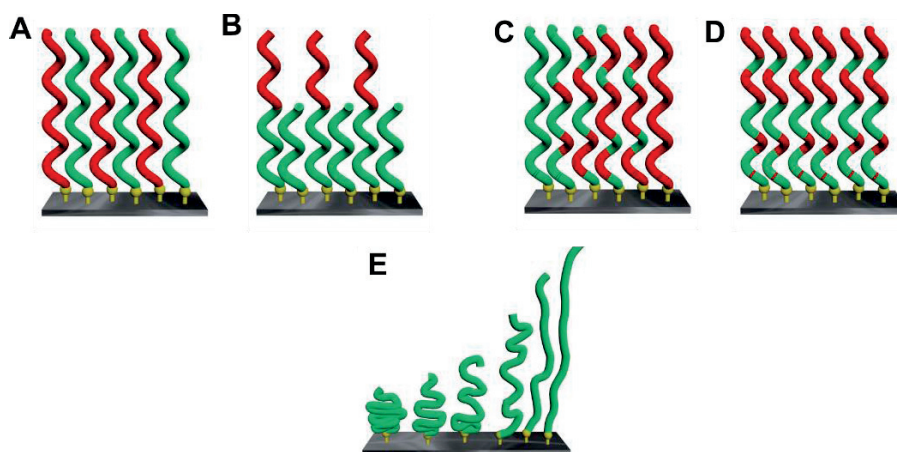


Figure 1.6. (A) Binary mixed, (B) Two-layer, bimodal, (C, D) Compositional gradient (C - horizontal or D - vertical) and (E) Grafting density gradient polymer brushes.

Binary “mixed” homopolymer brushes are thin films, in which two distinct, immiscible polymers are immobilized on surfaces in random or alternating arrangements. A typical synthetic strategy involves grafting of a mixture of different initiators onto a substrate of interest. The initiators are selected to be orthogonally active in subsequent polymerization steps. The reported initiator pairs that were used to obtain binary polymer brushes are ROP/ATRP,¹⁰² ATRP/PIMP,¹⁰³ ATRP/NMP⁵⁷ and ATRP/free-radical polymerization (FRP)^{96,104} initiators. An interesting example is two-step reverse ATRP,¹⁰⁵ where grafted diazo initiators were, first, only partially decomposed at elevated temperature to initiate following polymerization that proceeded at milder conditions. Then, the halide polymer chain-ends were deactivated with tri(*n*-butyl)tin hydride and the process was repeated with

another monomer. Alternatively, a grafting-from can be combined with a grafting-onto method.^{106,107}

Polymer brushes of two-layer or bimodal structure can be obtained by controlled termination or regeneration of polymer brush end-groups^{97,98,108} and post-polymerization patterning methods.¹⁰⁹⁻¹¹³ End-groups of ATRP grown polymer brushes can be deactivated in a controlled manner by tuning exposure time of the brushes to sodium azide solution.^{98,108} This allows the growth of top polymer-brush layer of different grafting density. The initiator functionalities can also be regenerated. For example, Rungta et al.⁹⁷ partially grafted silica nanoparticles with RAFT agent to grow first layer of short and dense polymer brushes. Then, they deactivated the polymer end-groups by cleaving them with 2,2'-azobis(isobutyronitrile) (AIBN) and attached second RAFT agent on remaining amine sites of the nanoparticles. In final polymerization step, they grew long polymer brushes, so that the second layer of low grafting density was formed. Post-polymerization patterning methods confine polymer brush growth to specific regions and have been accomplished with UV-mediated polymerization,^{109,113} photolithography (protection of initiator with photoresist)^{110,112} or soft lithography (with initiator coated polydimethylsiloxane, PDMS, stamps).¹¹¹

Gradient polymer brushes include chemical and grafting density gradients. Composition of monomers can be varied both horizontally (**Figure 1.6C**) and vertically (**Figure 1.6D**). Horizontal composition gradients were obtained by SIP in microchannel chamber,⁹⁹ which was filled with one monomer at the top and second monomer at the bottom, providing a solution gradient in between. The confinement of the microchannel preserved this gradient over long period of time. The vertical gradient can be obtained by feeding a polymerization solution comprising one monomer with portions of a second monomer throughout the polymerization process.¹⁰⁰ Grafting density gradient (**Figure 1.6E**) can be varied by either bottom-up or top-down approach. For example, initiator gradients can be prepared by diffusion-controlled deposition of initiator vapors,^{101,114} solutes¹¹⁵ or functionalization of gradient polymer substrates, e.g. obtained by moving mask plasma copolymerization.¹¹⁶ Then these surfaces can be used to grow polymer brush gradients (bottom-up). Alternatively, polymer brushes grafted from silicon wafers can be exposed to tetra-*n*-butylammonium fluoride (TBAF) etching solutions, which slowly detach single polymer chains and thus can be used to create gradients in a top-down approach.¹¹⁷

1.2.5. Free-standing polymer carpets

Also free-standing “polymer carpets” have been obtained,^{118,119} which are polymer brushes grafted from ultrathin substrates (**Figure 1.7**), such as initiator-modified gold films,¹²⁰ carbon nanosheets¹²¹ and polymers,^{122,123} crosslinked self-assembled monolayers (SAMs)^{119,124} or layer-by-layer (LbL) deposited macroinitiator films.^{96,125} In general, polymer brushes are grown from the ultrathin films (thickness of a few nm) supported by bulk and thus much more rigid substrates to facilitate the process. It is required to carefully lift-off and transfer the prepared polymer carpets, as their structure can be easily damaged. Usually, it is done with a sacrificial polymer used as a top⁹⁶ or bottom layer^{126,127} (**Figure 1.8**). When placed at the top it embeds and stabilizes the brushes, which allows them to be peeled off⁹⁶ (**Figure 1.8A**). Then, the sacrificial layer is removed in a good solvent. For the bottom layer approach, a sacrificial layer is coated before growing polymer brushes. Final immersion in a good solvent triggers release of the films^{126,127} (**Figure 1.8B**). Alternatively, a thin sacrificial inorganic substrate can be used and etched away, such as silicon nitride removed with hydrofluoric acid.¹²⁴ Edmondson and Huck exploited another strategy.¹¹⁸ They used cathodic stripping to lift-off polymer carpets from gold-coated surfaces.

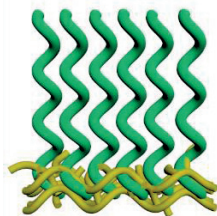


Figure 1.7. Free-standing polymer carpets.

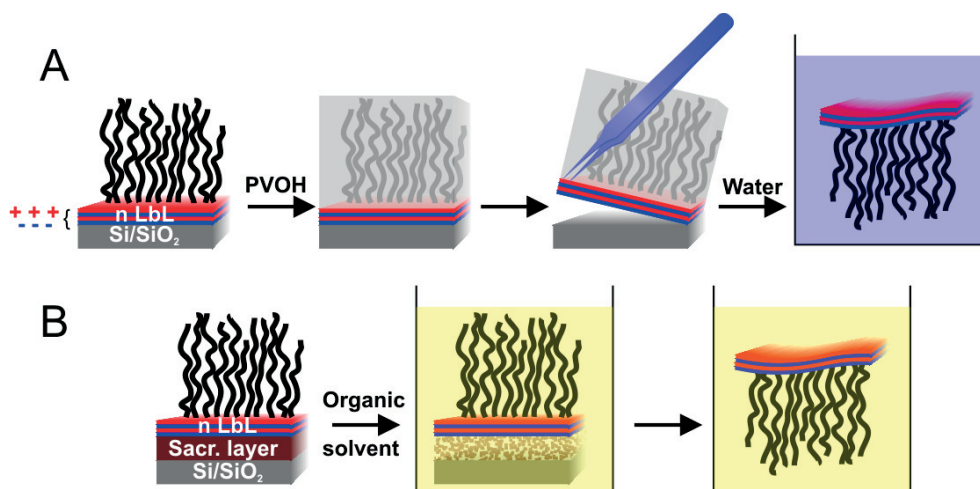


Figure 1.8. Lift-off strategies to afford polymer brush free-standing carpets using sacrificial polymer layer as (A) the top⁹⁶ and (B) the bottom layer.¹²⁶ The polymer brushes were grown from n LbL deposited macroinitiator films onto silicon wafers.

1.3. Incorporation of nanoparticles into polymer brushes

The introduction of nanoparticles into polymer brushes results in new hybrid materials (**Figure 1.9**) with enriched functions, which can be used to develop, among others, novel optical sensors and actuators benefiting from localized surface plasmon resonance (LSPR) and surface enhanced Raman scattering (SERS) phenomena.¹²⁸ Stimuli-responsiveness features of certain polymer brushes have been frequently exploited to provide sensitivity to pH,^{129,130} temperature,¹³¹ ionic strength or medium polarity.¹³²⁻¹³⁴ Polymer brush/nanoparticle hybrids have also been used as catalysts with tunable activity. Other applications include nanostructured solar cells and photonic band-gap materials¹²⁸ or anti-infection biomaterials.¹³⁵

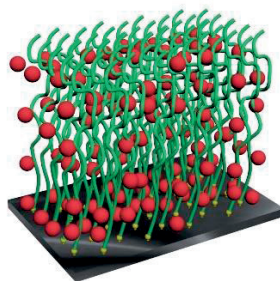


Figure 1.9. Nanoparticle-embedded polymer brushes.

The incorporation of nanoparticles can be achieved in two ways. Polymer brushes can be either incubated in a separately prepared nanoparticle suspension (one step with

nanoparticle synthesis *ex situ*) or exposed to nanoparticle precursor (such as metal salt) solution followed by a final nanoparticle forming reaction, typically wet chemical reduction (two steps with nanoparticle synthesis *in situ*).^{136,137}

1.3.1. Infiltration of polymer brushes with preformed nanoparticles

The *ex situ* synthesis allows to use uniform nanoparticles, which can be fine-tuned to obtain desired properties. Because infiltration of nanoparticles to polymer brushes greatly depends on their size and grafting density, respectively (see theoretical work¹³⁸), both factors can be optimized to afford 2D or 3D distributions within the brushes.^{128,139-141} The true infiltration has been reported to proceed only when the nanoparticle size is close to the inter-grafting distance. The grafting density can be further optimized to maximize uptake of particles.¹³⁹ Importantly, a strategy to achieve 3D assembly also for bigger nanoparticle sizes was reported by Ferhan and Kim¹⁴⁰ (**Figure 1.10**). Their “in-stacking” method comprises multiple immersion and drying steps. During the immersion, nanoparticles are adsorbed on the top region of a brush and after drying and re-immersion, polymer chains at regions free from the adsorbed nanoparticles swell more and are accessible for further nanoparticles. Thus, several layers of nanoparticles can be captured within the brushes. Other parameters that influence the organization of nanoparticles within polymer brushes are strength of nanoparticle/polymer interaction,^{139,142,143} polymer chain length^{141,144} and solvent quality. So far, polymer brushes have been infiltrated with Au,^{129-134,139-141,144-154} Ag,^{135,155-157} SiO₂,^{142,158} Fe₃O₄¹⁵⁹⁻¹⁶² nanoparticles, CdSe¹²⁸ quantum dots or fullerenes.¹⁶³

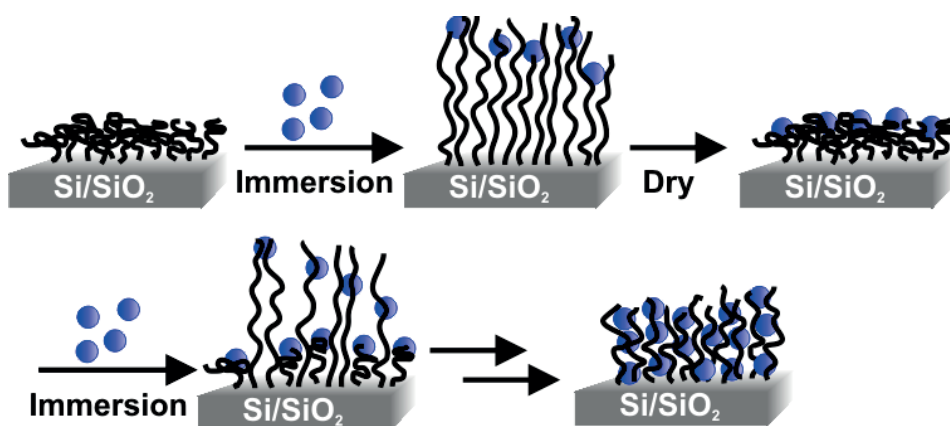


Figure 1.10. In-stacking process for incorporation of nanoparticles in polymer brushes.¹⁴⁰

1.3.2. Synthesis of nanoparticles in polymer brush templates

On the other hand, the *in situ* process, can be well controlled by careful selection of type and thickness of a polymer brush, which serves as a reaction medium.¹⁶⁴ Polymer brushes, as templates, enable formation and immobilization of the nanoparticles and also serve as a capping agent that limits their growth and aggregation.¹³⁶ Crosslinking is another important parameter. Introduction of physical constraints generates a polymer brush network with a tunable mesh size, which serves as a barrier for growth of the nanoparticles.¹³⁷ Higher degrees of crosslinking in general facilitates formation of smaller nanoparticles, but it can also improve their size distribution and reduce anisotropy (**Figure 1.11**). An amount of loaded nanoparticle precursor can be easily varied, which also influences formation of nanoparticles.^{164,165} Another factors that affect the formation are type¹⁶⁶ and concentration¹³⁶ of a reducing agent used to treat precursor-loaded polymer brushes. Loading with nanoparticle precursor has been realized on polymer brushes having carboxylic acid,^{137,167,168} basic,^{165,166,169-171} quaternized^{136,172} or complexing^{164,173,174} functionalities. Also anionic^{175,176} and cationic¹⁷⁵ charges can be used to interact with impregnating salts. Interestingly, charging state of ionic polymer brushes, such as poly(2-(dimethylamino)ethyl methacrylate) (PDMAEMA), can be tuned with pH and used to direct uptake of counterions permitting control over spatial distribution of synthesized nanoparticles.¹⁷⁵ Nanoparticle precursors have been used to obtain quantum dots (PbS,¹⁷⁷ CdS,^{168,176,178} CdS/CdSe¹⁶⁸), metallic (Ag,^{137,164,166,167,171,174,179-186} Au,^{136,165,166,170,175,187-191} Pt,^{169,187,189,192} Pd^{136,167,172,175,193-195} and Cu^{173,196}), bimetallic (Au/Pt¹⁸⁷) and inorganic (Fe_{0.67}-₁O,¹⁷⁶ TiO₂, SiO₂,¹⁹⁰ La₂O₃¹⁹⁷) nanoparticles. An overview of these syntheses is presented in **Table 1.1**.

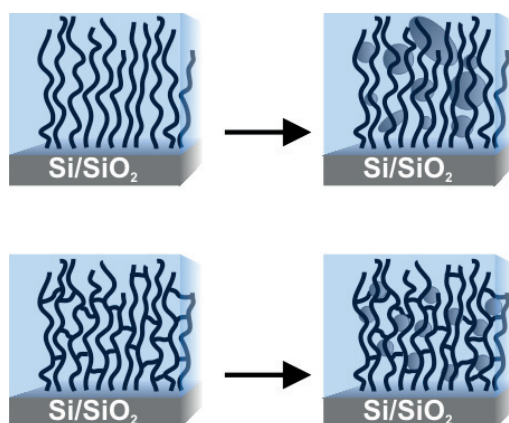


Figure 1.11. Effect of crosslinking on size, size distribution and anisotropy of nanoparticles synthesized *in situ* in polymer brushes.¹³⁷

Table 1.1. Overview of metal, inorganic nanoparticles and quantum dots synthesized *in situ* in polymer brush templates.

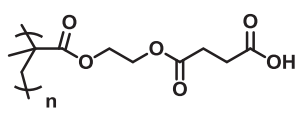
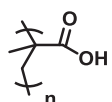
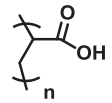
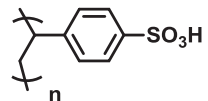
Nano-particle	Polymer brush	Nanoparticle precursor	Particle forming reagent	Nanoparticle diameter	Ref.
<i>Metal nanoparticles</i>					
Ag	Carboxylic acid functionalities				
	PHEMA-SA ^a 	AgNO ₃	NaBH ₄	13, 15, 20 nm	137
				20 nm	167
	PMAA ^a 			7.5 nm	184
	PAA ^a 			N.A.	186
	PSSA ^d 		Tollens reagent, [Ag(NH ₃) ₂] ⁺	3-5 μm super-structures composed of 50 nm particles	179

Table 1.1. (Continued).

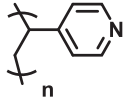
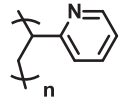
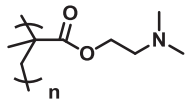
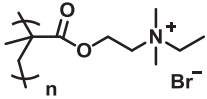
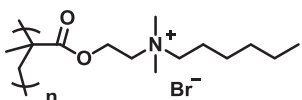
Nano-particle	Polymer brush	Nanoparticle precursor	Particle forming reagent	Nanoparticle diameter	Ref.
<i>Metal nanoparticles</i>					
Ag	Basic functionalities				
	P4VP ^{c, f}	AgNO ₃	NaBH ₄	2.5 nm	166
					
				38 nm	181
	P2VP ^g			N.A.	182
					
	PDMAEMA ^d			N.A.	171
					
	Quaternized functionalities				
	PDMAEMA-EtBr ^a	AgClO ₄	PDMAEMA (internal)	35 nm	180
					
	PDMAEMA-HexBr ^a			35 nm, aggregated	180
					

Table 1.1. (Continued).

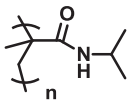
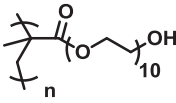
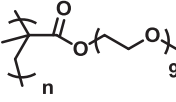
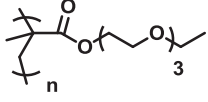
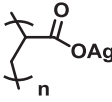
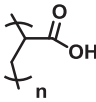
Nano-particle	Polymer brush	Nanoparticle precursor	Particle forming reagent	Nanoparticle diameter	Ref.
<i>Metal nanoparticles</i>					
Ag	Complexing functionalities				
	PNIPAAm ^a	AgNO ₃	NaBH ₄	4-10 nm	164
					
	PPEGMA ^e			7.5 nm	183
					
	PEGMEMA ^a	AgCF ₃ SO ₃		5 nm	174
					
	POEGEEMA ^f	AgNO ₃		20x60 and 7x20 nm (nanorods)	181
					
Nanoparticle precursor functionalities					
	PAA(Ag) ^e	Silver acrylate (internal)	UV	3 nm	185
					
Au	Carboxylic acid functionalities				
	PAA ^f	HAuCl ₄	NaBH ₄	10-20 nm	191
					

Table 1.1. (Continued).

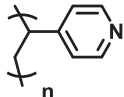
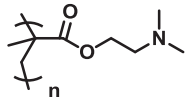
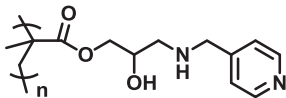
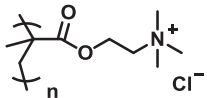
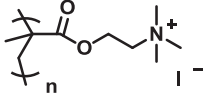
Nano-particle	Polymer brush	Nanoparticle precursor	Particle forming reagent	Nanoparticle diameter	Ref.
<i>Metal nanoparticles</i>					
Au	Basic functionalities				
	P4VP ^c	HAuCl ₄	NaBH ₄	3.0, 15 nm	166
					
	PDMAEMA ^{b,a}		PDMAEMA	5-25 nm	165
			(internal)	60-80 nm	
			NaBH ₄	4.2 nm	170
			PDMAEMA	19.6 nm	170
			(internal)		
	PGMA-pyridinemethanamine ^e		LiAlH ₄	N.A.	190
					
	Quaternized functionalities				
	PMETAC ^a	HAuCl ₄	NaBH ₄	14, 24, 28, 41, 49, 54, 95, 96, 104 nm	136
					
				9 nm	188
	PMETA ^a			15-80 nm	175
					

Table 1.1. (Continued).

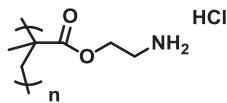
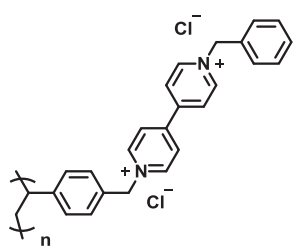
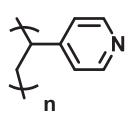
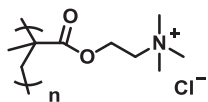
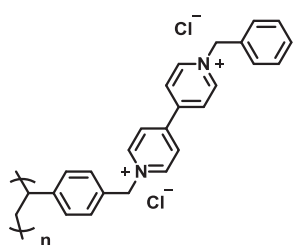
Nano-particle	Polymer brush	Nanoparticle precursor	Particle forming reagent	Nanoparticle diameter	Ref.
<i>Metal nanoparticles</i>					
Au	Quaternized functionalities				
	PAEMA-HCl ^e	HAuCl ₄	NaBH ₄	1.5 nm	189
					
	PBpyClCl ^a	AuCl ₄ ²⁻	1. UV 2. Air	< 5 nm	187
					
Pt	Basic functionalities				
	P4VP ^a	H ₂ PtCl ₆	NaBH ₄	2-3 nm	169
					
	Quaternized functionalities				
	PMETAC ^e	H ₂ PtCl ₆	NaBH ₄	2.3 nm 2 nm	189 192
					
	PBpyClCl ^a	PtCl ₆ ²⁻	1. UV 2. Air	< 5 nm	187
					

Table 1.1. (Continued).

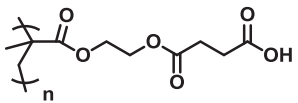
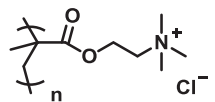
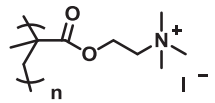
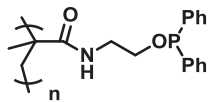
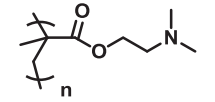
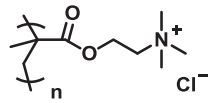
Nano-particle	Polymer brush	Nanoparticle precursor	Particle forming reagent	Nanoparticle diameter	Ref.	
<i>Metal nanoparticles</i>						
Pd	Carboxylic acid functionalities					
		PHEMA-SA ^a	Pd(NO ₃) ₂	NaBH ₄	30 nm	167
						
	Quaternized functionalities					
		PMETAC ^f	Na ₂ PdCl ₄	NaBH ₄	2.4, 3.8 nm	193
						
		PMETAI ^a	(NH ₄) ₂ PdCl ₄	NaBH ₄	2-4 nm	172
						
	Complexing functionalities					
		PAAm-ETA-CIPPh ₂ ^{g,c}	Pd(OAc) ₂	None	10-15 nm	194
				9.7, 10.0, 14.8, 15.6 nm	195	
Sterically trapping structures						
	PDMAEMA ^a	Pd(NH ₃) ₄ Cl ₂	NaBH ₄	2-5 nm	175	
						
Cu	Quaternized functionalities					
		PMETAC ^a	CuSO ₄ , KNaC ₄ H ₄ O ₆ · 4H ₂ O	HCHO	130 nm	196
						

Table 1.1. (Continued).

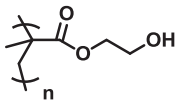
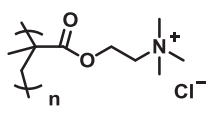
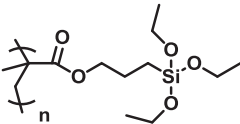
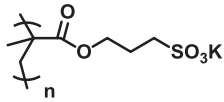
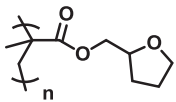
Nano-particle	Polymer brush	Nanoparticle precursor	Particle forming reagent	Nanoparticle diameter	Ref.
<i>Metal nanoparticles</i>					
Cu	Complexing functionalities				
	PHEMA ^a	CuCl ₂	NaBH ₄	200 nm	173
					
<i>Bimetallic nanoparticles</i>					
Au/Pd	Quaternized functionalities				
	PMETAC ^a	Na ₂ PdCl ₄ , HAuCl ₄	NaBH ₄	N.A.	136
					
<i>Inorganic nanoparticles</i>					
SiO ₂	Nanoparticle precursor functionalities				
	PTEPM ^b	PTEPM (internal)	NH ₃ ·H ₂ O (hydrolysis and condensation catalyst)	N.A.	190
					
Fe ²⁺ /Fe ³⁺ ₂ O ₄ (magnetite) / FeO (maghemite)	Sulfonate functionalities				
	PSPMA ^a	FeCl ₂ or Fe(NO ₃) ₂	NaOH (pH 12 or 13), O ₂	2-4 nm	176
					
La ₂ O ₃	Complexing functionalities				
	PTHFMA ^a	La(NO ₃) ₃	NaBH ₄	20-30 nm	197
					

Table 1.1. (Continued).

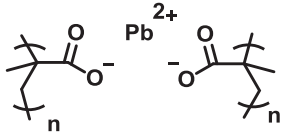
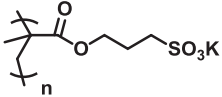
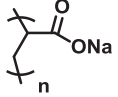
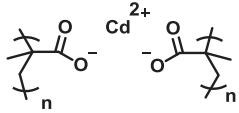
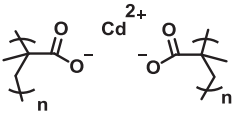
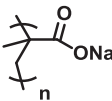
Nano-particle	Polymer brush	Nanoparticle precursor	Particle forming reagent	Nanoparticle diameter	Ref.
Quantum dots					
PbS	Nanoparticle precursor functionalities				
	P(MAA) ₂ Pb ^a	P(MA) ₂ Pb (internal)	H ₂ S (sulfurization agent)	1 nm	177
					
CdS	Sulfonate functionalities				
	PSPMA ^a	Cd(NO ₃) ₂	Na ₂ S (sulfurization agent), pH 12-13	5-8 nm	176
					
	Carboxylate functionalities				
	PAA(Na) ^a	Cd(Ac) ₂	H ₂ S (sulfurization agent)	4-5 nm	178
					
	Nanoparticle precursor functionalities				
	P(MAA) ₂ Cd ^a	PCd(MA) ₂ (internal)	H ₂ S (sulfurization agent)	3-5 nm	168
					

Table 1.1. (Continued).

Nano-particle	Polymer brush	Nanoparticle precursor	Particle forming reagent	Nanoparticle diameter	Ref.
Quantum dots					
CdS/CdSe	Nanoparticle precursor functionalities				
	Carboxylate functionalities				
	1. P(MAA) ₂ Cd ^a	1. P(MA) ₂ Cd (internal)	1. H ₂ S (sulfurization agent)	5-10 nm	168
	2. PMAA(Na) ^a	2. Cd(Ac) ₂	2. Na ₂ SeSO ₃ (selenization agent)		
					
					

a-g: polymer brushes obtained by: a: SI-ATRP, b: SI-AGET-ATRP, c: S-RAFT, d: self-initiated photografting and photopolymerization (SIPGP), e: surface-initiated free-radical photopolymerization (SI-FRPP), f: surface-initiated free-radical polymerization (SI-FRP), g: grafting-onto

1.4. Outlook and recommendations

Surface-initiated controlled radical polymerization with its advances in the most frequently applied ATRP and RAFT polymerization techniques has enabled generation of plethora of architectures of polymer brushes. Manipulation over the compositions and topologies has been explored in depth, which has covered, among others, syntheses of block, statistical and gradient copolymer brushes, cyclic and loop polymer brushes, bimodal, Y-shaped and branched polymer brushes. Also crosslinking has been widely utilized for improvement of their properties. Finally, these polymer coatings have been integrated with a range of nanoparticles to further broaden the scope of their applications. The flexibility of controlled radical polymerization allows almost unlimited ways for manipulation and fine-tuning. Surface-initiated polymerization, as a younger discipline to conventional polymerization in solution, presents many similar, but still challenging topics, when transferred to surface-initiated systems. The syntheses are still demanding and time-consuming, as they often require oxygen-free atmosphere and careful purifications. Both can be very challenging for a non-expert. New techniques are being developed that will

ease the experiments, e.g. recent reports on copper plate SI-ATRP,^{6,149} photoinduced, metal free polymerization techniques¹⁵⁰ or air-tolerant enzyme-assisted ATRP¹⁵¹ or RAFT polymerization¹⁵² or even biocatalytic “oxygen-fueled” ATRP¹⁵³ that actually requires oxygen to proceed, which is in stark contrast to so-far CRP methods. Additionally, full characterization often requires cleaving the polymer chains from the surfaces¹⁵⁴ for their analysis via GPC, MALDI-TOF MS or NMR spectroscopy. The process and purification of collected polymers is usually a lengthy task. It can be additionally impeded in case of flat surfaces, where the amount of tethered polymer chains is dramatically small, often insufficient for the analyses. Thus, also estimation of initiator and polymer brush grafting density is challenging. Much easier synthetic and characterization techniques would be vital to establish accurate composition-property relationships.

1.5. References

- (1) Zoppe, J. O.; Ataman, N. C.; Mocny, P.; Wang, J.; Moraes, J.; Klok, H.-A. *Chemical Reviews* **2017**, *117*, 1105.
- (2) Edmondson, S.; Osborne, V. L.; Huck, W. T. *Chemical Society Reviews* **2004**, *33*, 14.
- (3) Matyjaszewski, K. *Macromolecules* **2012**, *45*, 4015.
- (4) Matyjaszewski, K. *Advanced Materials* **2018**, 1706441.
- (5) Dehghani, E. S.; Du, Y.; Zhang, T.; Ramakrishna, S. N.; Spencer, N. D.; Jordan, R.; Benetti, E. M. *Macromolecules* **2017**, *50*, 2436.
- (6) Che, Y.; Zhang, T.; Du, Y.; Amin, I.; Marschelke, C.; Jordan, R. *Angewandte Chemie International Edition* **2018**.
- (7) Fantin, M.; Ramakrishna, S. N.; Yan, J.; Yan, W.; Divandari, M.; Spencer, N. D.; Matyjaszewski, K.; Benetti, E. M. *Macromolecules* **2018**, *51*, 6825.
- (8) Moad, G.; Rizzardo, E.; Thang, S. H. *Australian Journal of Chemistry* **2005**, *58*, 379.
- (9) Baum, M.; Brittain, W. J. *Macromolecules* **2002**, *35*, 610.
- (10) Li, C.; Benicewicz, B. C. *Macromolecules* **2005**, *38*, 5929.
- (11) Zhao, Y.; Perrier, S. *Macromolecules* **2007**, *40*, 9116.
- (12) Barbey, R.; Lavanant, L.; Paripovic, D.; Schüwer, N.; Sugnaux, C.; Tugulu, S.; Klok, H.-A. *Chemical Reviews* **2009**, *109*, 5437.
- (13) Wu, L.; Glebe, U.; Boeker, A. *Polymer Chemistry* **2015**, *6*, 5143.
- (14) Hawker, C. J.; Bosman, A. W.; Harth, E. *Chemical Reviews* **2001**, *101*, 3661.

- (15) Otsu, T. *Journal of Polymer Science Part A: Polymer Chemistry* **2000**, *38*, 2121.
- (16) Zhao, B.; Brittain, W. J. *Progress in Polymer Science* **2000**, *25*, 677.
- (17) Kizhakkedathu, J. N.; Norris-Jones, R.; Brooks, D. E. *Macromolecules* **2004**, *37*, 734.
- (18) Paripovic, D.; Klok, H. -A. *Macromolecular Chemistry and Physics* **2011**, *212*, 950.
- (19) Xu, F.; Cai, Q.; Kang, E.; Neoh, K. *Langmuir* **2005**, *21*, 3221.
- (20) Liu, T.; Jia, S.; Kowalewski, T.; Matyjaszewski, K.; Casado-Portilla, R.; Belmont, J. *Macromolecules* **2006**, *39*, 548.
- (21) Skaff, H.; Emrick, T. *Angewandte Chemie* **2004**, *116*, 5497.
- (22) Davis, K. A.; Matyjaszewski, K. In *Statistical, gradient, block and graft copolymers by controlled/living radical polymerizations*; Springer, 2002.
- (23) Matyjaszewski, K.; Wang, J.-L.; Grimaud, T.; Shipp, D. A. *Macromolecules* **1998**, *31*, 1527.
- (24) Shipp, D. A.; Wang, J.-L.; Matyjaszewski, K. *Macromolecules* **1998**, *31*, 8005.
- (25) Zou, Y.; Zhuang, R.; Qiu, Z.; Dai, L. *Chinese Journal of Reactive Polymers* **1998**, *7*, 75.
- (26) Matyjaszewski, K.; Shipp, D. A.; Wang, J.-L.; Grimaud, T.; Patten, T. E. *Macromolecules* **1998**, *31*, 6836.
- (27) Matyjaszewski, K.; Ziegler, M. J.; Arehart, S. V.; Greszta, D.; Pakula, T. *Journal of Physical Organic Chemistry* **2000**, *13*, 775.
- (28) Moraes, J.; Simionca, I.-M.; Ketari, H.; Klok, H.-A. *Polymer Chemistry* **2015**, *6*, 3245.
- (29) Patton, D. L.; Page, K. A.; Xu, C.; Genson, K. L.; Fasolka, M. J.; Beers, K. L. *Macromolecules* **2007**, *40*, 6017.
- (30) Ting, J. M.; Navale, T. S.; Bates, F. S.; Reineke, T. M. *ACS Macro Letters* **2013**, *2*, 770.
- (31) Morgese, G.; Trachsel, L.; Romio, M.; Divandari, M.; Ramakrishna, S. N.; Benetti, E. M. *Angewandte Chemie* **2016**, *128*, 15812.
- (32) Yan, W.; Divandari, M.; Rosenboom, J.-G.; Ramakrishna, S. N.; Trachsel, L.; Spencer, N. D.; Morgese, G.; Benetti, E. M. *Polymer Chemistry* **2018**, *9*, 2580.
- (33) Patton, D.; Knoll, W.; Advincula, R. C. *Macromolecular Chemistry and Physics* **2011**, *212*, 485.

- (34) Rotzoll, R.; Vana, P. *Journal of Polymer Science Part A: Polymer Chemistry* **2008**, *46*, 7656.
- (35) Jiang, X.; Zhao, B.; Zhong, G.; Jin, N.; Horton, J. M.; Zhu, L.; Hafner, R. S.; Lodge, T. P. *Macromolecules* **2010**, *43*, 8209.
- (36) Nakayama, Y.; Sudo, M.; Uchida, K.; Matsuda, T. *Langmuir* **2002**, *18*, 2601.
- (37) Yang, W. J.; Neoh, K.-G.; Kang, E.-T.; Teo, S. L.-M.; Rittschof, D. *Polymer Chemistry* **2013**, *4*, 3105.
- (38) Zhang, C.; Lu, J.; Hou, Y.; Xiong, W.; Sheng, K.; Lu, H. *ACS Applied Materials & Interfaces* **2018**.
- (39) Morgese, G.; Trachsel, L.; Romio, M.; Divandari, M.; Ramakrishna, S. N.; Benetti, E. M. *Angewandte Chemie International Edition* **2016**, *55*, 15583.
- (40) Divandari, M.; Morgese, G.; Trachsel, L.; Romio, M.; Dehghani, E. S.; Rosenboom, J.-G.; Paradisi, C.; Zenobi-Wong, M.; Ramakrishna, S. N.; Benetti, E. M. *Macromolecules* **2017**, *50*, 7760.
- (41) Morgese, G.; Cavalli, E.; Rosenboom, J. G.; Zenobi-Wong, M.; Benetti, E. M. *Angewandte Chemie* **2018**, *130*, 1637.
- (42) Wei, T.; Zhou, Y.; Zhan, W.; Zhang, Z.; Zhu, X.; Yu, Q.; Chen, H. *Colloids and Surfaces B: Biointerfaces* **2017**, *159*, 527.
- (43) Lu, H. B.; Campbell, C. T.; Castner, D. G. *Langmuir* **2000**, *16*, 1711.
- (44) Yamada, K.; Katoono, R.; Yui, N. *Polymer Journal* **2011**, *44*, 286.
- (45) Han, Y.; Ma, J.; Hu, Y.; Jin, J.; Jiang, W. *Langmuir* **2018**.
- (46) Sakurai, S.; Watanabe, H.; Takahara, A. *Polymer Journal* **2013**, *46*, 117.
- (47) Huang, Z.; Ji, H.; Mays, J. W.; Dadmun, M. D. *Macromolecules* **2008**, *41*, 1009.
- (48) Haung, Z.; Ji, H.; Mays, J.; Dadmun, M.; Smith, G.; Bedrov, D.; Zhang, Y. *Langmuir* **2010**, *26*, 202.
- (49) Kang, T.; Banquy, X.; Heo, J.; Lim, C.; Lynd, N. A.; Lundberg, P.; Oh, D. X.; Lee, H.-K.; Hong, Y.-K.; Hwang, D. S. *ACS Nano* **2016**, *10*, 930.
- (50) Li, L.; Yan, B.; Zhang, L.; Tian, Y.; Zeng, H. *Chemical Communications* **2015**, *51*, 15780.
- (51) Ren, X.; Weng, L. T.; Fu, Y.; Ng, K. M.; Chan, C. M. *Surface and Interface Analysis* **2015**, *47*, 953.
- (52) Goren, T.; Spencer, N.; Crockett, R. *RSC Advances* **2014**, *4*, 21497.
- (53) Banquy, X.; Burdynska, J.; Lee, D. W.; Matyjaszewski, K.; Israelachvili, J. *Journal of the American Chemical Society* **2014**, *136*, 6199.

- (54) Alonzo, J.; Huang, Z.; Liu, M.; Mays, J. W.; Toomey, R. G.; Dadmun, M. D.; Kilbey, S. M. *Macromolecules* **2006**, *39*, 8434.
- (55) Liu, S.; Jamali, S.; Liu, Q.; Maia, J.; Baek, J.-B.; Jiang, N.; Xu, M.; Dai, L. *Macromolecules* **2016**, *49*, 7434.
- (56) Rotzoll, R.; Vana, P. *Australian Journal of Chemistry* **2009**, *62*, 1473.
- (57) Thiessen, W.; Wolff, T. *Designed Monomers and Polymers* **2011**, *14*, 287.
- (58) Horton, J. M.; Tang, S.; Bao, C.; Tang, P.; Qiu, F.; Zhu, L.; Zhao, B. *ACS Macro Letters* **2012**, *1*, 1061.
- (59) Jiang, X.; Zhong, G.; Horton, J. M.; Jin, N.; Zhu, L.; Zhao, B. *Macromolecules* **2010**, *43*, 5387.
- (60) Tang, S.; Lo, T.-Y.; Horton, J. M.; Bao, C.; Tang, P.; Qiu, F.; Ho, R.-M.; Zhao, B.; Zhu, L. *Macromolecules* **2013**, *46*, 6575.
- (61) Bao, C.; Tang, S.; Horton, J. M.; Jiang, X.; Tang, P.; Qiu, F.; Zhu, L.; Zhao, B. *Macromolecules* **2012**, *45*, 8027.
- (62) Bao, C.; Tang, S.; Wright, R. A.; Tang, P.; Qiu, F.; Zhu, L.; Zhao, B. *Macromolecules* **2014**, *47*, 6824.
- (63) Li, W.; Bao, C.; Wright, R. A.; Zhao, B. *RSC Advances* **2014**, *4*, 18772.
- (64) Huang, X.; Hauptmann, N.; Appelhans, D.; Formanek, P.; Frank, S.; Kaskel, S.; Temme, A.; Voit, B. *Small* **2012**, *8*, 3579.
- (65) Yang, Q.; Wang, L.; Huo, J.; Ding, J.; Xiang, W. *Journal of Applied Polymer Science* **2010**, *117*, 824.
- (66) Zeng, L.; Wang, H.; Fu, G.; Jiang, J.; Zhang, X. *Journal of Colloid and Interface Science* **2010**, *352*, 36.
- (67) Lee, H. J.; Nakayama, Y.; Matsuda, T. *Macromolecules* **1999**, *32*, 6989.
- (68) Xu, F.; Yuan, Z.; Kang, E.; Neoh, K. *Langmuir* **2004**, *20*, 8200.
- (69) Gao, C.; Muthukrishnan, S.; Li, W.; Yuan, J.; Xu, Y.; Müller, A. H. *Macromolecules* **2007**, *40*, 1803.
- (70) Mori, H.; Böker, A.; Krausch, G.; Müller, A. H. *Macromolecules* **2001**, *34*, 6871.
- (71) Wang, J.; Wei, J. *Applied Surface Science* **2016**, *382*, 202.
- (72) Mu, B.; Shen, R.; Liu, P. *Colloids and Surfaces B: Biointerfaces* **2009**, *74*, 511.
- (73) Ramakrishna, S. N.; Cirelli, M.; Kooij, E. S.; Klein Gunnewiek, M.; Benetti, E. M. *Macromolecules* **2015**, *48*, 7106.
- (74) Li, G. L.; Yu, R.; Qi, T.; Möhwald, H.; Shchukin, D. G. *Macromolecules* **2016**, *49*, 1127.

- (75) Dehghani, E. S.; Aghion, S.; Anwand, W.; Consolati, G.; Ferragut, R.; Panzarasa, G. *European Polymer Journal* **2018**, *99*, 415.
- (76) Dehghani, E. S.; Spencer, N. D.; Ramakrishna, S. N.; Benetti, E. M. *Langmuir* **2016**, *32*, 10317.
- (77) Dehghani, E. S.; Ramakrishna, S. N.; Spencer, N. D.; Benetti, E. M. *Macromolecules* **2017**, *50*, 2932.
- (78) Iuster, N.; Tairy, O.; Driver, M. J.; Armes, S. P.; Klein, J. *Macromolecules* **2017**, *50*, 7361.
- (79) Lilge, I.; Schönherr, H. *Angewandte Chemie* **2016**, *128*, 13308.
- (80) Li, A.; Benetti, E. M.; Tranchida, D.; Clasohm, J. N.; Schönherr, H.; Spencer, N. D. *Macromolecules* **2011**, *44*, 5344.
- (81) Zhang, J.; Xiao, S.; Shen, M.; Sun, L.; Chen, F.; Fan, P.; Zhong, M.; Yang, J. *RSC Advances* **2016**, *6*, 21961.
- (82) Lilge, I.; Schönherr, H. *European Polymer Journal* **2013**, *49*, 1943.
- (83) Iqbal, D.; Rechmann, J.; Sarfraz, A.; Altin, A.; Genchev, G.; Erbe, A. *ACS Applied Materials & Interfaces* **2014**, *6*, 18112.
- (84) Glass, J. J.; Li, Y.; De Rose, R.; Johnston, A. P.; Czuba, E. I.; Khor, S. Y.; Quinn, J. F.; Whittaker, M. R.; Davis, T. P.; Kent, S. J. *ACS Applied Materials & Interfaces* **2017**, *9*, 12182.
- (85) Ding, H.; Yan, J.; Wang, Z.; Xie, G.; Mahoney, C.; Ferebee, R.; Zhong, M.; Daniel, W. F.; Pietrasik, J.; Sheiko, S. S. *Polymer* **2016**, *107*, 492.
- (86) Gao, L.; Zhu, W.; Zhang, K.; Chen, Y. *Macromolecular Materials and Engineering* **2012**, *297*, 639.
- (87) Mazurowski, M.; Gallei, M.; Li, J.; Didzoleit, H.; Stühn, B.; Rehahn, M. *Macromolecules* **2012**, *45*, 8970.
- (88) Mu, B.; Liu, P.; Tang, Z.; Du, P.; Dong, Y. *Nanomedicine: Nanotechnology, Biology and Medicine* **2011**, *7*, 789.
- (89) Mu, B.; Liu, P. *Reactive and Functional Polymers* **2012**, *72*, 983.
- (90) Guo, W.; Reese, C. M.; Xiong, L.; Logan, P. K.; Thompson, B. J.; Stafford, C. M.; Ievlev, A. V.; Lokitz, B. S.; Ovchinnikova, O. S.; Patton, D. L. *Macromolecules* **2017**, *50*, 8670.
- (91) Wan, X.; Wang, D.; Liu, S. *Langmuir* **2010**, *26*, 15574.
- (92) Han, G.; Ju, Y.; Zhao, H. *Polymer Chemistry* **2016**, *7*, 1197.

- (93) Arisaka, Y.; Nishijima, Y.; Yusa, S.-i.; Takeda, N. *Journal of Biomaterials Science, Polymer Edition* **2016**, *27*, 1331.
- (94) Dong, Z.; Mao, J.; Wang, D.; Yang, M.; Ji, X. *Langmuir* **2015**, *31*, 8930.
- (95) Mu, B.; Liu, P.; Pu, Q. *Reactive and Functional Polymers* **2010**, *70*, 578.
- (96) Estillore, N. C.; Advincula, R. C. *Langmuir* **2011**, *27*, 5997.
- (97) Rungta, A.; Natarajan, B.; Neely, T.; Dukes, D.; Schadler, L. S.; Benicewicz, B. C. *Macromolecules* **2012**, *45*, 9303.
- (98) Brault, N. D.; Sundaram, H. S.; Huang, C.-J.; Li, Y.; Yu, Q.; Jiang, S. *Biomacromolecules* **2012**, *13*, 4049.
- (99) Xu, C.; Barnes, S. E.; Wu, T.; Fischer, D. A.; DeLongchamp, D. M.; Batteas, J. D.; Beers, K. L. *Advanced Materials* **2006**, *18*, 1427.
- (100) Xu, C.; Wu, T.; Mei, Y.; Drain, C. M.; Batteas, J. D.; Beers, K. L. *Langmuir* **2005**, *21*, 11136.
- (101) Wu, T.; Efimenko, K.; Vlček, P.; Šubr, V.; Genzer, J. *Macromolecules* **2003**, *36*, 2448.
- (102) Priftis, D.; Sakellariou, G.; Baskaran, D.; Mays, J. W.; Hadjichristidis, N. *Soft Matter* **2009**, *5*, 4272.
- (103) Sui, X.; Zapotoczny, S.; Benetti, E. M.; Memesa, M.; Hempenius, M. A.; Vancso, G. J. *Polymer chemistry* **2011**, *2*, 879.
- (104) Qian, X.; Lei, J.; Wickramasinghe, S. R. *RSC Advances* **2013**, *3*, 24280.
- (105) Ye, P.; Dong, H.; Zhong, M.; Matyjaszewski, K. *Macromolecules* **2011**, *44*, 2253.
- (106) Song, J.; Cheng, L.; Liu, A.; Yin, J.; Kuang, M.; Duan, H. *Journal of the American Chemical Society* **2011**, *133*, 10760.
- (107) Yin, J.; Wu, T.; Song, J.; Zhang, Q.; Liu, S.; Xu, R.; Duan, H. *Chemistry of Materials* **2011**, *23*, 4756.
- (108) Huang, C. J.; Brault, N. D.; Li, Y.; Yu, Q.; Jiang, S. *Advanced Materials* **2012**, *24*, 1834.
- (109) Poelma, J. E.; Fors, B. P.; Meyers, G. F.; Kramer, J. W.; Hawker, C. J. *Angewandte Chemie* **2013**, *125*, 6982.
- (110) Takahashi, H.; Nakayama, M.; Itoga, K.; Yamato, M.; Okano, T. *Biomacromolecules* **2011**, *12*, 1414.
- (111) Wei, Q.; Yu, B.; Wang, X.; Zhou, F. *Macromolecular Rapid Communications* **2014**, *35*, 1046.
- (112) Yom, J.; Lane, S. M.; Vaia, R. A. *Soft Matter* **2012**, *8*, 12009.

- (113) Ma, J.; Luan, S.; Song, L.; Jin, J.; Yuan, S.; Yan, S.; Yang, H.; Shi, H.; Yin, J. *ACS Applied Materials & Interfaces* **2014**, *6*, 1971.
- (114) Wu, T.; Efimenko, K.; Genzer, J. *Journal of the American Chemical Society* **2002**, *124*, 9394.
- (115) Mei, Y.; Wu, T.; Xu, C.; Langenbach, K. J.; Elliott, J. T.; Vogt, B. D.; Beers, K. L.; Amis, E. J.; Washburn, N. R. *Langmuir* **2005**, *21*, 12309.
- (116) Coad, B. R.; Bilgic, T.; Klok, H.-A. *Langmuir* **2014**, *30*, 8357.
- (117) Patil, R.; Miles, J.; Ko, Y.; Datta, P.; Rao, B. M.; Kiserow, D.; Genzer, J. *Macromolecules* **2018**, *51*, 10237.
- (118) Edmondson, S.; Huck, W. T. *Advanced Materials* **2004**, *16*, 1327.
- (119) Amin, I.; Steenackers, M.; Zhang, N.; Schubel, R.; Beyer, A.; Götzhäuser, A.; Jordan, R. *Small* **2011**, *7*, 683.
- (120) Kelby, T. S.; Huck, W. T. *Macromolecules* **2010**, *43*, 5382.
- (121) Turchanin, A.; Beyer, A.; Nottbohm, C. T.; Zhang, X.; Stosch, R.; Sologubenko, A.; Mayer, J.; Hinze, P.; Weimann, T.; Götzhäuser, A. *Advanced Materials* **2009**, *21*, 1233.
- (122) Edmondson, S.; Frieda, K.; Comrie, J. E.; Onck, P. R.; Huck, W. T. *Advanced Materials* **2006**, *18*, 724.
- (123) Welch, M. E.; Ober, C. K. *ACS Macro Letters* **2013**, *2*, 241.
- (124) Amin, I.; Steenackers, M.; Zhang, N.; Beyer, A.; Zhang, X.; Pirzer, T.; Hugel, T.; Jordan, R.; Götzhäuser, A. *Small* **2010**, *6*, 1623.
- (125) Fujie, T.; Haniuda, H.; Takeoka, S. *Journal of Materials Chemistry* **2011**, *21*, 9112.
- (126) Estillore, N. C.; Advincula, R. C. *Macromolecular Chemistry and Physics* **2011**, *212*, 1552.
- (127) Kohri, M.; Shinoda, Y.; Kohma, H.; Nannichi, Y.; Yamauchi, M.; Yagai, S.; Kojima, T.; Taniguchi, T.; Kishikawa, K. *Macromolecular Rapid Communications* **2013**, *34*, 1220.
- (128) Snaith, H. J.; Whiting, G. L.; Sun, B.; Greenham, N. C.; Huck, W. T.; Friend, R. H. *Nano Letters* **2005**, *5*, 1653.
- (129) Tokareva, I.; Minko, S.; Fendler, J. H.; Hutter, E. *Journal of the American Chemical Society* **2004**, *126*, 15950.
- (130) Tokarev, I.; Tokareva, I.; Minko, S. *ACS Applied Materials & Interfaces* **2011**, *3*, 143.

- (131) Gupta, S.; Agrawal, M.; Uhlmann, P.; Simon, F.; Stamm, M. *Chemistry of Materials* **2009**, *22*, 504.
- (132) Lee, S.; Pérez-Luna, V. H. *Langmuir* **2007**, *23*, 5097.
- (133) Choi, J.; Choi, M.-J.; Yoo, J.-K.; Park, W. I.; Lee, J. H.; Lee, J. Y.; Jung, Y. S. *Nanoscale* **2013**, *5*, 7403.
- (134) Gupta, S.; Agrawal, M.; Uhlmann, P.; Simon, F.; Oertel, U.; Stamm, M. *Macromolecules* **2008**, *41*, 8152.
- (135) Ambi, A.; Parikh, N.; Vera, C.; Burns, K.; Montano, N.; Sciorra, L.; Epstein, J.; Zeng, D.; Traba, C. *Biofouling* **2018**, *34*, 273.
- (136) Paripovic, D.; Klok, H.-A. *ACS Applied Materials & Interfaces* **2011**, *3*, 910.
- (137) Benetti, E. M.; Sui, X.; Zapotoczny, S.; Vancso, G. J. *Advanced Functional Materials* **2010**, *20*, 939.
- (138) Kim, J. U.; O'Shaughnessy, B. *Macromolecules* **2006**, *39*, 413.
- (139) Christau, S.; Möller, T.; Yenice, Z.; Genzer, J.; von Klitzing, R. *Langmuir* **2014**, *30*, 13033.
- (140) Ferhan, A. R.; Kim, D.-H. *Journal of Materials Chemistry* **2012**, *22*, 1274.
- (141) Bhat, R. R.; Genzer, J.; Chaney, B. N.; Sugg, H. W.; Liebmann-Vinson, A. *Nanotechnology* **2003**, *14*, 1145.
- (142) Gage, R.; Currie, E.; Cohen Stuart, M. *Macromolecules* **2001**, *34*, 5078.
- (143) Currie, E.; Norde, W.; Stuart, M. C. *Advances in Colloid and Interface Science* **2003**, *100*, 205.
- (144) Liu, Z.; Pappacena, K.; Cerise, J.; Kim, J.; Durning, C. J.; O'Shaughnessy, B.; Levicky, R. *Nano Letters* **2002**, *2*, 219.
- (145) Oren, R.; Liang, Z.; Barnard, J. S.; Warren, S. C.; Wiesner, U.; Huck, W. T. *Journal of the American Chemical Society* **2009**, *131*, 1670.
- (146) Bhat, R. R.; Genzer, J. *Applied Surface Science* **2006**, *252*, 2549.
- (147) Kim, B. J.; Bang, J.; Hawker, C. J.; Kramer, E. J. *Macromolecules* **2006**, *39*, 4108.
- (148) Bhat, R. R.; Tomlinson, M. R.; Genzer, J. *Macromolecular Rapid Communications* **2004**, *25*, 270.
- (149) Christau, S.; Thurandt, S.; Yenice, Z.; von Klitzing, R. *Polymers* **2014**, *6*, 1877.
- (150) Diamanti, S.; Arifuzzaman, S.; Genzer, J.; Vaia, R. A. *ACS Nano* **2009**, *3*, 807.
- (151) Ferhan, A. R.; Guo, L.; Zhou, X.; Chen, P.; Hong, S.; Kim, D.-H. *Analytical Chemistry* **2013**, *85*, 4094.

- (152) Pekdemir, S.; Karabel, S.; Kiremitler, N. B.; Liu, X.; Nealey, P. F.; Onses, M. S. *ChemPhysChem* **2017**, *18*, 2114.
- (153) Christau, S.; Moeller, T.; Genzer, J.; Koehler, R.; von Klitzing, R. *Macromolecules* **2017**, *50*, 7333.
- (154) Mei, S.; Qi, H.; Zhou, T.; Li, C. Y. *Angewandte Chemie* **2017**, *129*, 13833.
- (155) Panzarasa, G.; Aghion, S.; Soliveri, G.; Consolati, G.; Ferragut, R. *Nanotechnology* **2015**, *27*, 02LT03.
- (156) Zhang, Q.; Wang, X.-D.; Tian, T.; Chu, L.-Q. *Applied Surface Science* **2017**, *407*, 185.
- (157) Zhang, Q.; Yin, J. J.; Liu, F.; Zou, X. N.; Chu, L. Q. *Surface and Interface Analysis* **2017**, *49*, 316.
- (158) Iacono, M.; Connolly, D.; Heise, A. *RSC Advances* **2017**, *7*, 19976.
- (159) Wang, H.; Patil, A. J.; Liu, K.; Petrov, S.; Mann, S.; Winnik, M. A.; Manners, I. *Advanced Materials* **2009**, *21*, 1805.
- (160) Xu, Y.; Yuan, J.; Fang, B.; Drechsler, M.; Müllner, M.; Bolisetty, S.; Ballauff, M.; Müller, A. H. *Advanced Functional Materials* **2010**, *20*, 4182.
- (161) Yuan, J.; Gao, H.; Schacher, F.; Xu, Y.; Richter, R.; Tremel, W.; Muller, A. H. *ACS Nano* **2009**, *3*, 1441.
- (162) Yuan, J.; Schmalz, H.; Xu, Y.; Miyajima, N.; Drechsler, M.; Moeller, M. W.; Schacher, F.; Mueller, A. H. *Advanced Materials* **2008**, *20*, 947.
- (163) Sato, M.; Kato, T.; Shimamoto, H.; Kamitani, K.; Ohta, N.; Hirai, T.; Takahara, A. *ACS Macro Letters* **2018**, *7*, 148.
- (164) Wu, T.; Ge, Z.; Liu, S. *Chemistry of Materials* **2011**, *23*, 2370.
- (165) Taniguchi, T.; Inada, T.; Kashiwakura, T.; Murakami, F.; Kohri, M.; Nakahira, T. *Colloids and Surfaces A: Physicochemical and Engineering Aspects* **2011**, *377*, 63.
- (166) Liu, J.; Zhang, L.; Shi, S.; Chen, S.; Zhou, N.; Zhang, Z.; Cheng, Z.; Zhu, X. *Langmuir* **2010**, *26*, 14806.
- (167) Costantini, F.; Benetti, E. M.; Tiggelaar, R. M.; Gardeniers, H. J.; Reinhoudt, D. N.; Huskens, J.; Vancso, G. J.; Verboom, W. *Chemistry—A European Journal* **2010**, *16*, 12406.
- (168) Yan, J.; Ye, Q.; Wang, X.; Yu, B.; Zhou, F. *Nanoscale* **2012**, *4*, 2109.
- (169) Li, D.; Jang, Y. J.; Lee, J.; Lee, J.-E.; Kochuveedu, S. T.; Kim, D. H. *Journal of Materials Chemistry* **2011**, *21*, 16453.
- (170) Zhang, M.; Liu, L.; Wu, C.; Fu, G.; Zhao, H.; He, B. *Polymer* **2007**, *48*, 1989.

- (171) Gupta, S.; Agrawal, M.; Conrad, M.; Hutter, N. A.; Olk, P.; Simon, F.; Eng, L. M.; Stamm, M.; Jordan, R. *Advanced Functional Materials* **2010**, *20*, 1756.
- (172) Ye, Q.; Wang, X.; Hu, H.; Wang, D.; Li, S.; Zhou, F. *The Journal of Physical Chemistry C* **2009**, *113*, 7677.
- (173) Zhang, K.; Li, H.; Zhao, S.; Wang, W.; Wang, S.; Xu, Y.; Yu, W.; Wang, J. *Polymer Bulletin* **2006**, *57*, 253.
- (174) Park, J. T.; Koh, J. H.; Seo, J. A.; Cho, Y. S.; Kim, J. H. *Applied Surface Science* **2011**, *257*, 8301.
- (175) Gao, T.; Ye, Q.; Pei, X.; Xia, Y.; Zhou, F. *Journal of Applied Polymer Science* **2013**, *127*, 3074.
- (176) Llarena, I.; Romero, G.; Ziolo, R. F.; Moya, S. E. *Nanotechnology* **2009**, *21*, 055605.
- (177) Zhou, W.; Chen, Y.; Wang, X.; Guo, Z.; Hu, Y. *Journal of Nanoscience and Nanotechnology* **2011**, *11*, 98.
- (178) Zhang, M.; Drechsler, M.; Müller, A. H. *Chemistry of Materials* **2004**, *16*, 537.
- (179) Yang, Y.; Wang, W.; Chen, T.; Chen, Z.-R. *ACS Applied Materials & Interfaces* **2014**, *6*, 21468.
- (180) Yin, J. J.; Wahid, F.; Zhang, Q.; Tao, Y. C.; Zhong, C.; Chu, L. Q. *Macromolecular Materials and Engineering* **2017**, *302*, 1700069.
- (181) Stetsyshyn, Y.; Awsiuk, K.; Kusnezh, V.; Raczowska, J.; Jany, B. R.; Kostruba, A.; Harhay, K.; Ohar, H.; Lishchynskiy, O.; Shymborska, Y. *Applied Surface Science* **2019**, *463*, 1124.
- (182) Gupta, S.; Uhlmann, P.; Agrawal, M.; Chapuis, S.; Oertel, U.; Stamm, M. *Macromolecules* **2008**, *41*, 2874.
- (183) Lu, Y.; Mei, Y.; Walker, R.; Ballauff, M.; Drechsler, M. *Polymer* **2006**, *47*, 4985.
- (184) Ishizu, K.; Kakinuma, H.; Ochi, K.; Uchida, S.; Hayashi, M. *Polymers for Advanced Technologies* **2005**, *16*, 834.
- (185) Lu, Y.; Mei, Y.; Schrinner, M.; Ballauff, M.; Möller, M. W.; Breu, J. *The Journal of Physical Chemistry C* **2007**, *111*, 7676.
- (186) Li, L.; Da, Y.; Ying, S.; Zheng, W.; Zhang, X.; Yu, X. *Polymer Bulletin* **2017**, *74*, 505.
- (187) Xu, F.; Su, F.; Deng, S.; Yang, W. *Macromolecules* **2010**, *43*, 2630.
- (188) Azzaroni, O.; Brown, A. A.; Cheng, N.; Wei, A.; Jonas, A. M.; Huck, W. T. *Journal of Materials Chemistry* **2007**, *17*, 3433.

- (189) Wunder, S.; Polzer, F.; Lu, Y.; Mei, Y.; Ballauff, M. *The Journal of Physical Chemistry C* **2010**, *114*, 8814.
- (190) Xiao, L.; Qu, L.; Zhu, W.; Wu, Y.; Liu, Z.; Zhang, K. *Macromolecules* **2017**, *50*, 6762.
- (191) Cabana, S.; Lecona-Vargas, C. S.; Meléndez-Ortiz, H. I.; Contreras-García, A.; Barbosa, S.; Taboada, P.; Magarinos, B.; Bucio, E.; Concheiro, A.; Alvarez-Lorenzo, C. *Journal of Drug Delivery Science and Technology* **2017**, *42*, 245.
- (192) Mei, Y.; Sharma, G.; Lu, Y.; Ballauff, M.; Drechsler, M.; Irrgang, T.; Kempe, R. *Langmuir* **2005**, *21*, 12229.
- (193) Mei, Y.; Lu, Y.; Polzer, F.; Ballauff, M.; Drechsler, M. *Chemistry of Materials* **2007**, *19*, 1062.
- (194) Ghasemi, S.; Karim, S. *Colloid and Polymer Science* **2018**, *1*.
- (195) Ghasemi, S.; Karim, S. *Materials Chemistry and Physics* **2018**, *205*, 347.
- (196) Sun, C.; Li, Y.; Li, Z.; Su, Q.; Wang, Y.; Liu, X. *Journal of Nanomaterials* **2018**, *2018*.
- (197) Mogha, N. K.; Gosain, S.; Masram, D. T. *Arabian Journal of Chemistry* **2017**.
- (198) Zhang, T.; Du, Y.; Müller, F.; Amin, I.; Jordan, R. *Polymer Chemistry* **2015**, *6*, 2726.
- (199) Narupai, B.; Page, Z. A.; Treat, N. J.; McGrath, A. J.; Pester, C. W.; Discekici, E. H.; Dolinski, N. D.; Meyers, G. F.; Read de Alaniz, J.; Hawker, C. J. *Angewandte Chemie International Edition* **2018**, *57*, 13433.
- (200) Enciso, A. E.; Fu, L.; Russell, A. J.; Matyjaszewski, K. *Angewandte Chemie International Edition* **2018**, *57*, 933.
- (201) Chapman, R.; Gormley, A. J.; Stenzel, M. H.; Stevens, M. M. *Angewandte Chemie* **2016**, *128*, 4576.
- (202) Enciso, A. E.; Fu, L.; Lathwal, S.; Olszewski, M.; Wang, Z.; Das, S. R.; Russell, A. J.; Matyjaszewski, K. *Angewandte Chemie International Edition* **2018**, *57*, 16157.
- (203) Patil, R. R.; Turgman-Cohen, S.; Šrogl, J. í.; Kiserow, D.; Genzer, J. *Langmuir* **2015**, *31*, 2372.
- (204) Patil, R. R.; Turgman-Cohen, S.; Šrogl, J. í.; Kiserow, D.; Genzer, J. *ACS Macro Letters* **2015**, *4*, 251.

2. Synthesis of Loop Polymer Brushes via Chain-End Post-Polymerization Modification

2.1. Introduction

Polymer brushes are thin films composed of chain-end tethered polymer chains.¹⁻⁸ One strategy to synthesize polymer brushes is via surface-initiated polymerization (SIP). This approach allows to readily control chemical composition and film thickness and can provide access to high grafting density polymer brushes. Polymer brushes have attracted considerable attention as non-biofouling coatings,⁹⁻¹³ which are important for medical implants, biosensors or marine applications. Another attractive application of polymer brushes is their use as low friction surfaces,¹⁴⁻¹⁸ which are relevant for prosthetics, medical devices, such as blood pump bearings, endoscope surfaces or catheters as well as contact lenses or microelectromechanical devices.

The vast majority of polymer brushes, which have been reported so far are composed of polymer chains that are tethered via one end-group to the surface. Anchoring linear polymers via both chain-ends to a surface results in loop-type polymer brushes. In contrast to their linear counterparts, loop-type polymer brushes have received only relatively limited attention.¹⁷ Loop brushes in recent reports, for example, were shown to better resist non-specific protein adsorption as compared to their linear analogs.^{19,20} Loop poly(2-ethyl-2-oxazoline) (PEOXA) brushes grafted onto TiO₂ substrates showed lower friction coefficients as compared to single-chain end-tethered PEOXA brushes.¹⁹ Furthermore, loop polymer brushes can form Velcro-type interactions with linear polymer chains, which may be exploited to generate large scale adhesive interfaces.²¹ Velcro-type interactions were also demonstrated to modulate friction dynamics in water between linear and loop polymer brush modified surfaces.²² There are also theory and simulation studies that point towards significant differences in wetting behavior between linear and loop brushes.^{23,24}

Loop-type polymer brushes have been mostly prepared via grafting-onto strategies, using α,ω -telechelic polymers with thiol,^{20,25-27} siloxane,²⁸ carboxylic acid^{29,30} or catechol end-groups.^{19,31,32} Also, triblock copolymers³³⁻³⁶ with physisorbing hydrophobic,³³

neutral^{35,36} or charged³⁴ domains at both sides can be used. A very interesting grafting-onto strategy was proposed by Li et al., who prepared loop brushes by surface attachment of polymer single crystals obtained from α,ω -alkoxysilane telechelic poly(ϵ -caprolactone).³⁷ While the grafting-onto approach is very straightforward, it generally leads to polymer brush films with lower grafting densities and film thicknesses. Grafting-from strategies, which use SIP potentially could provide access to higher grafting density loop-type brushes. So far, only very few reports have described the use of grafting-from approaches to prepare loop brushes. In two articles, Rotzoll and Vana have explored surface-immobilized bipedal azo initiators and chain transfer agents to grow poly(methyl acrylate) loop brushes.^{38,39} This manuscript describes an alternative grafting-from methodology towards high grafting density loop-type polymer brushes (**Figure 2.1**). The strategy presented here starts with the preparation of linear polymer grafts via surface-initiated atom transfer radical polymerization (SI-ATRP) followed by a first chain-end functionalization to introduce allyl groups and a final metathesis reaction to induce loop-closure.

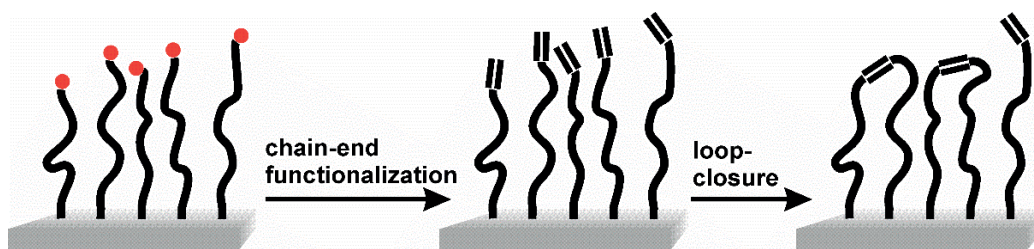


Figure 2.1. Synthesis of loop-type polymer brushes via chain-end functionalization and subsequent loop-closure metathesis.

2.2. Experimental Section

2.2.1. Materials

Methyl methacrylate (MMA) was obtained from Aldrich. The inhibitor from MMA was removed by passing the monomer through a column of activated, basic aluminium oxide. (6-(2-Bromo-2-methyl)propionyloxy)hexyldimethylchlorosilane was synthesized as previously described.⁴⁰ Allylamine, L-ascorbic acid, 2,2'-bipyridine (bpy), CuBr_2 (99.999%), CuBr (99.999%), CuCl (purity, $\geq 97\%$), ethyl 2-bromoisobutyrate (EBiB), ethyl 2-bromopropionate, tetraethoxysilane and tetra-n-butylammonium fluoride (TBAF, 1 M in THF) were purchased from Aldrich and used as received. 1st and 2nd Generation Grubbs catalysts were obtained from Sigma. Triethylamine trihydrofluoride ($\text{Et}_3\text{N}\cdot 3\text{HF}$) was obtained from Acros. 4,4'-Dinonyl-2,2'-bipyridyl (dNbpy) was purchased from TCI.

Allyl tributylstannane (95%) was purchased from ABCR. 1,1,4,7,10,10-Hexamethyltriethylenetetramine (HMTETA), *N,N,N',N'',N''*-pentamethyldiethylenetriamine (PMDETA) and triethylamine were purchased from Aldrich. Triethylamine was distilled before use. Silica gel was from SiliCycle Inc. and basic alumina from Sigma-Aldrich. Sulfuric acid (98%) was obtained from Merck. Hydrogen peroxide (30%), ammonia (25%), ammonium chloride, sodium bicarbonate, sodium sulfate, magnesium sulfate, acetone, DMSO, dichloromethane (DCM), ethanol, ethyl acetate, n-hexane, methanol and tetrahydrofuran (THF) were purchased from Reitolab SA. HPLC grade THF and toluene were obtained from Fisher Chemicals. Dry DCM and toluene were obtained from a solvent-purification system (PureSolv). Deionized water was obtained from a Millipore Elix 3 water purification system.

2.2.2. Analytical methods

Particle sizes and polymer brush film thicknesses were measured by Dynamic Light Scattering using a Malvern Nano ZS instrument. Thermogravimetric analysis (TGA) was performed using a Perkin Elmer TGA4000 instrument under nitrogen flow. The calculation of the initiator surface concentration, brush grafting densities and brush thicknesses from the TGA data are presented in the Supporting Information. The heating procedure involved three steps: (1) equilibration at 30 °C for 5 min; (2) ramp up at 10 °C/min to 900 °C; (3) hold at 900 °C for 10 min. The organic content of the samples was calculated from the weight loss between 200 °C and 800 °C. For Gel Permeation Chromatography analysis, an Agilent 1260 apparatus equipped with a Varian 390 MDS refractive index detector, 2x Agilent PL-Gel Mixed C columns and a guard column was used. THF was used as the eluent at a flow rate of 1 mL/min and analyses were performed at 40 °C. Sample concentrations of 2 mg/mL were used. Linear PMMA standards (PSS Mainz) with molecular weights between 2200 and 201 000 Da were used for GPC calibration. NMR spectra were recorded on a Bruker AvanceIII 400MHz spectrometer equipped with BBFO-Plus_z 5 mm probe. The ¹³C and ¹H signals were referenced to CDCl₃ carbon and residual proton signals.

2.2.3. Procedures

Ethyl 2-(2-propen-1-ylamino)isobutyrate. EBiB (5 mL, 34.1 mmol) and freshly distilled triethylamine (9.5 mL, 68.2 mmol) were mixed with 34.1 mL DMSO and 10 mL THF in a two-neck round bottom flask, previously purged with nitrogen. Then, 5.1 mL

allylamine (68.2 mmol) was added. The flask was heated to 40 °C and stirred overnight. After that, 100 mL saturated sodium bicarbonate solution was added to the reaction mixture and the product extracted 4 times with 50 mL ethyl acetate. The organic phase was dried over magnesium sulfate and the volatiles were removed on a rotary evaporator. The product was purified by column chromatography (3:2 hexane/ethyl acetate, v/v). Yield: 2.75 g, 47.2%. ¹H NMR (CDCl₃, 400 MHz), δ: 5.89 (ddt, ³J(*vic*) = 6 Hz, ³J(*trans*) = 17.1 Hz, ³J(*cis*) = 9.9 Hz, 1H, CH₂-CH=CH₂), 5.15 (dd, ³J(*trans*) = 17.1 Hz, ²J = 1.4 Hz, 2H, CH=CH₂), 5.05 (d, ³J(*cis*) = 9.9 Hz, 2H, CH=CH₂), 4.15 (q, 2H, CH₃-CH₂), 3.09 (d, 2H, NH-CH₂), 1.75 (s broad, 1H, NH), 1.30 (s, 6H, C-(CH₃)₂), 1.26 (s, 3H, CH₃-CH₂). ¹³C NMR (CDCl₃, 100 MHz), δ: 176.48 (C=O), 136.30 (CH=CH₂), 115.61 (CH=CH₂), 60.32 (CH₃-CH₂), 58.44 (C-(CH₃)₂), 46.93 (NH-CH), 24.91 (C-(CH₃)₂), 13.90 (CH₃-CH₂). ¹H NMR and ¹³C NMR spectra are included in **Figure S2.1** of the Supporting Information.

Ethyl 2-(2-propen-1-ylamino)propionate. Ethyl 2-bromopropionate (5 mL, 38.5 mmol) and freshly distilled triethylamine (10.7 mL, 77 mmol) were mixed with 38.5 mL DMSO and 10 mL THF in a two-neck round bottom flask, previously purged with nitrogen. Then, 5.8 mL allylamine (77 mmol) was added. The flask was heated to 40 °C and stirred overnight. After that, 100 mL saturated sodium bicarbonate solution was added to the reaction mixture and the product extracted 4 times with 50 mL ethyl acetate. The organic phase was dried over magnesium sulfate and the volatiles were removed on a rotary evaporator. The product was purified by column chromatography (3:2 hexane/ethyl acetate, v/v). Yield: 3.83 g, 63.3%. ¹H NMR (CDCl₃, 400 MHz), δ: 5.83 (ddt, ³J(*vic*) = 6.1 Hz, ³J(*trans*) = 17.4 Hz, ³J(*cis*) = 10.2 Hz, 1H, CH₂-CH=CH₂), 5.13 (dd, ³J(*trans*) = 17.4 Hz, ²J = 1.0 Hz, 1H, CH=CH₂), 5.05 (d, ³J(*cis*) = 10.2 Hz, 1H, CH=CH₂), 4.17 (q, 2H, CH₃-CH₂), 3.33 (q, 2H, CH-CH₃), 3.21 (dd, ²J(*gem*) = 13.7 Hz, ³J(*vic*) = 6.1, Hz, 1H, NH-CH₂), 3.13 (dd, ²J(*gem*) = 13.7 Hz, ³J(*vic*) = 6.1, Hz, 2H, NH-CH₂) (The resonances at 3.21 and 3.13 ppm are deformed dd signals due to ABM system with strongly coupled A and B (diastereotopic protons), which was confirmed by simulation with WinDNMR software), 1.69 (s broad, 1H, NH), 1.26 (t, 3H, CH₃-CH₂), 1.26 (d, 3H, CH₃-CH). ¹³C NMR (CDCl₃, 100 MHz), δ: 175.63 (C=O), 136.21 (CH=CH₂), 116.22 (CH=CH₂), 60.53 (CH-CH₃), 55.79 (CH₃-CH₂), 50.45 (NH-CH₂), 19.03 (CH₃-CH), 14.19 (CH₃-CH₂). ¹H NMR and ¹³C NMR spectra are included in **Figure S2.2** of the Supporting Information.

Metathesis of ethyl 2-(2-propen-1-ylamino)isobutyrate and ethyl 2-(2-propen-1-ylamino)propionate. Typically, 213.8 mg ethyl 2-(2-propen-1-ylamino)isobutyrate (1.25 mmol) or 196.3 mg ethyl 2-(2-propen-1-ylamino)propionate (1.25 mmol) were mixed with 5 mol% of 1st or 2nd Generation Grubbs catalyst (0.0625 mmol) in 2.5 mL dry DCM under nitrogen. The reactions were performed at room temperature or under reflux for 18 h. Then, DCM was removed under vacuum and the content was analyzed by ¹H-NMR spectroscopy in CDCl₃ to estimate conversions.

Ethyl 2,2-dimethyl-4-pentenoate. 20 mL THF, 15.8 mL allyltributyl stannane (51.11 mmol) and 407.4 μL HMTETA (1.50 mmol) were added into a Schlenk flask, which was sealed and subjected to three freeze-pump-thaw cycles. Then, 112.3 mg CuBr (0.78 mmol) and 5 mL EBiB (34.1 mmol) were added to the frozen mixture under positive nitrogen pressure. The flask was sealed again, evacuated, thawed and backfilled with nitrogen. Finally, it was placed into an oil bath and heated to 60 °C. The reaction mixture was stirred for 24 h. Then, the content was passed through a neutral alumina plug. The volatiles were removed on a rotary evaporator and the product was purified by vacuum distillation (61 °C, 17 Torr). Alternatively, the reaction product can be purified by column chromatography (4:96, EtOAc:Hex, v/v). Conversion of EBiB 99.5%. ¹H NMR (CDCl₃, 400 MHz), δ: 5.75 (m, 1H, CH₂-CH=CH₂), 5.07 (d, 2H, CH=CH₂), 4.13 (q, 2H, CH₃-CH₂), 2.29 (d, 2H, CH₂-CH), 1.25 (t, 3H, CH₃-CH₂), 1.17 (s, 6H, C-(CH₃)₂). ¹³C NMR (CDCl₃, 100 MHz), δ: 177.45 (C=O), 134.29 (CH=CH₂), 117.75 (CH=CH₂), 60.26 (CH₃-CH₂), 44.72 (C-CH₂), 42.12 (C-(CH₃)₂), 24.78 (C-(CH₃)₂), 14.21 (CH₃-CH₂). ¹H NMR and ¹³C NMR spectra are included in **Figure S2.3** of the Supporting Information.

In addition to the procedures discussed above, a number of other conditions were also evaluated for the synthesis of ethyl 2,2-dimethyl-4-pentenoate. These experiments were carried out in a similar fashion, only changing the reagents and solvents: 1 mL EBiB (6.82 mmol), 5 mL toluene, 2.12 mL allyltributylstannane (6.82 mmol), 53 μL PMDETA (0.25 mmol), 36 mg CuBr (0.25 mmol), 17 h 40 min, 65 °C, conversion 20.5%; 1 mL EBiB (6.82 mmol), 3 mL DMF, 2.12 mL allyltributylstannane (6.82 mmol), 53 μL PMDETA (0.25 mmol), 36 mg CuBr (0.25 mmol), 72 h, RT, conversion 94.2%; 0.2 mL EBiB (1.36 mmol), 1 mL MMA (9.35 mmol), 0.848 mL allyltributylstannane (2.73 mmol), 12.71 mg dNbpy (0.031 mmol), 1.67 mg CuCl (0.017 mmol), 72 h, RT, conversion 97.7%.

Diethyl 2,2,7,7-tetramethyloct-4-enedioate. First, 21.2 mg 2nd generation Grubbs' catalyst (0.025 mmol) was added into a 2-neck round-bottom flask, which was equipped with a stir bar and a reflux condenser. The set-up was sealed and purged with nitrogen. Then, 78.1 mg ethyl 2,2-dimethyl-4-pentenoate (0.5 mmol) and 1 mL dry DCM were injected into the flask, which was then heated to 40 °C and stirred for 72 h. After that, the catalyst was removed on a short neutral silica column. DCM was removed on a rotary evaporator and the product was isolated by flash column chromatography using 20:1 hexane/ethyl acetate, v/v ($R_f = 0.37$). Conversion of 2,2-dimethyl-4-pentenoate was 99.5%. When the same reaction was performed at room temperature for 72 h the conversion was 96.2%. When the 1st generation Grubbs catalyst was used, this protocol resulted in ethyl 2,2-dimethyl-4-pentenoate conversion of 54.8% (room temperature) or 98% (reflux).

¹H NMR (CDCl₃, 400 MHz) δ : 5.43, 5.38 (t, $J=4.61$ Hz, 2 H, (E, Z) $\underline{\text{CH}}=\underline{\text{CH}}$), 4.11 (q, $J=6.95$ Hz, 4 H, (E, Z) $\text{CH}_3-\underline{\text{CH}_2}\text{O}$), 2.28, 2.22 (d, $J=4.78$ Hz, 4 H, (E, Z) $\underline{\text{CH}_2}-\text{CH}=\text{CH}$), 1.24 (t, $J=6.83$ Hz, 6 H, (E, Z) $\underline{\text{CH}_3}-\text{CH}_2$), 1.17, 1.14 (s, 12 H, (E, Z) $\underline{\text{CH}_3}-\text{C}$). ¹³C NMR (CDCl₃, 100 MHz) δ :) 177.61, 177.57 (s, (E, Z) $\underline{\text{C}}(=\text{O})\text{O}$), 129.21, 127.61 (s, (E, Z) $\underline{\text{CH}}=\underline{\text{CH}}$), 60.33, 60.25 (s, (E, Z) $\text{CH}_3-\underline{\text{CH}_2}\text{O}$), 43.51 (s, (E, Z) $\underline{\text{C}}-\text{CH}_3$), 42.38, 42.32 (s, (E, Z) $\underline{\text{CH}_2}-\text{CH}=\text{CH}$), 37.76 (s, (E, Z) $\underline{\text{C}}-\text{CH}_3$), 24.85, 24.80 (s, (E, Z) $\underline{\text{CH}_3}-\text{C}$), 14.22 (s, (E, Z) $\underline{\text{CH}_3}-\text{CH}_2$). For several H and C resonances, two positions are reported, which are due to the presence of E and Z isomers. ¹H NMR and ¹³C NMR spectra are included in **Figure S2.4** of the Supporting Information.

Solution ATRP of MMA. The polymerization was carried out with MMA/EBiB/CuCl/dNbpy = 1000/1/2/4 molar ratio. 18.7 mL MMA (20 g, 199.6 mmol) and 326 mg dNbpy (0.798 mmol) were added to a Schlenk flask equipped with a magnetic stir bar. The flask was sealed and the solution was subjected to three freeze-pump-thaw cycles. Then, 39.5 mg CuCl (0.399 mmol) was added under positive nitrogen pressure. The flask was placed in preheated oil bath at 70 °C and the content was mixed for 15 min. Finally, 29 μL EBiB (38.9 mg, 0.200 mmol) was added under positive nitrogen pressure to start the polymerization. The reaction was allowed to proceed for 6 h at 70 °C and was stopped by diluting the content with 100 mL acetone and passing the reaction mixture through a short neutral alumina column. The PMMA was precipitated into 1 L of cold methanol, filtered and dried overnight under vacuum. $M_n(\text{GPC}) = 24.7$ kDa, $M_w/M_n = 1.15$.

Synthesis of silica nanoparticles. A mixture of tetraethoxysilane (10.7 mL, 47.92 mmol), ethanol (240 mL), deionized water (31.7 mL) and concentrated (25%) ammonium hydroxide (22.8 mL, 23.69 mmol) was stirred at room temperature under nitrogen for 3 h. The particles were collected by centrifugation (10 min, 8000 rpm). After that, the nanoparticles were cleaned in two consecutive washing (vortex dispersing in THF) and centrifugation cycles.

The solvent was then decanted and the silica particles freeze-dried and obtained as a white powder in a quantitative yield. Nanoparticles sizes were determined by DLS using the intensity size distribution. Using this protocol, several batches of nanoparticles with average sizes of 320, 332 and 411 nm were prepared. **Figure S2.5** shows the representative size distributions of these batches.

Immobilization of the ATRP initiator. Before immobilization of the initiator, the silica nanoparticles (3 g) were purified with 50 mL piranha solution (*Caution:* piranha solution reacts violently with organic substances and should be handled with care). Piranha was prepared by slowly adding 15 mL H₂O₂ to 35 mL H₂SO₄ (7:3, v:v) under stirring. After 3 h, the nanoparticles were centrifuged (10 min, 8000 rpm), collected and washed two times with water, once with ethanol (each time vortex dispersing before the separation) and freeze-dried. The dried particles (3 g) were washed with dry toluene and placed in a dry reaction flask with 48 mL dry toluene. Then, the flask was sealed and purged with nitrogen. After that, a solution of 25 μ L of the initiator (0.1 mmol) in 2 mL dry toluene was added. After stirring overnight at room temperature, the functionalized particles were collected by centrifugation and subsequently washed 3 times with toluene and 2 times with THF. Each time, particles were vortex dispersed and centrifuged for 10 min at 8000 rpm. Cleaned silica nanoparticles were freeze-dried and stored in dark under nitrogen atmosphere.

SI-ARGET-ATRP of MMA. SI-ARGET-ATRP of MMA was performed following a protocol adapted from a procedure for the polymerization of MMA from planar surfaces.⁴¹ Polymerizations were carried out with MMA/CuBr₂/bpy/ascorbic acid = 5667/1/10/10 molar ratio. In a typical experiment, 100 mg ATRP-initiator modified silica nanoparticles, 10 mL MMA (93.5 mmol), 6 mL MeOH and 2 mL water were placed in a Schlenk flask. Then 2 mL of a stock solution was added, which was prepared by mixing 18.5 mg CuBr₂ (82.8 mmol), 128.75 mg bpy (824.4 mmol) and 10 mL MeOH. The Schlenk flask was sealed and purged with nitrogen for 15 min. Then, the mixture was sonicated for 15 min

and the reaction was started by injecting 200 μL of a freshly prepared solution of ascorbic acid (145.25 mg, 824.7 μmol) in 1 mL water. The reaction was carried out at room temperature for 20 min – 15 h. After the specified time, the polymer-modified particles were centrifuged (10 min, 8000 rpm) and then washed 2 times with MeOH, THF and acetone. Each washing step consisted of vortex suspending and centrifuging. Cleaned particles were freeze-dried.

SI-ATRP OF MMA. Polymerizations were performed using a protocol that was a modification of an earlier published procedure.⁴² No sacrificial initiator was used here. Polymerization reactions were carried out with MMA/CuCl/dNbpy = 600/1/2 molar ratio. Typically, 150 mg ATRP-initiator modified silica nanoparticles, 204 mg dNbpy (0.5 mmol) and 14 mL MMA (15 g, 150 mmol) were added to a Schlenk flask equipped with a magnetic stir bar. The flask was sealed and the solution was subjected to three freeze-pump-thaw cycles. After equilibration at room temperature, 25 mg CuCl (0.25 mmol) was added under nitrogen flow and the flask was placed in a preheated oil bath at 70 °C. After a predetermined time, the flask was removed from the oil bath and opened to expose the catalyst to air. The polymer-modified particles were collected by centrifugation (10 k rpms, 10 min) and washed 2 times with THF and 2 times with MeOH. The cleaned particles were freeze-dried.

TBAF-mediated brush cleavage. Cleavage experiments were carried out in nitrogen purged flasks using a 0.05 M solution of TBAF in THF. For 20 mg nanoparticles, 1.5 mL TBAF solution was used. Reaction was carried out at room temperature or at 55 °C. After 24 or 70 hours, the particles were collected by centrifugation. The supernatant was saved. The particles were washed 2 times with 5 mL THF, 2 times with 5 mL water and 2 times with 5 mL ethanol on a vortex mixer, each time repeating centrifugation. Finally, the particles were freeze-dried overnight and stored for TGA. THF from the washing step was added to the previously saved supernatant. Then, 1.5 mL of a saturated aqueous NH_4Cl solution was added and the polymers extracted 3 times with dichloromethane. The organic phases were combined and dried over Na_2SO_4 . The mixture was filtered and concentrated on a rotary evaporator. Dried residue was dissolved in THF (to obtain 2 mg/mL concentration for GPC measurement) and stored at 2-10 °C.

Et₃N·3HF-mediated brush cleavage. Cleavage experiments were carried out in sealed flasks with 10% of Et₃N·3HF in HPLC grade THF. For 20 mg nanoparticles, 5 mL Et₃N·3HF solution was used. Reactions were carried out at room temperature. After 30 min, the reaction solution did not contain any residual particles and the reaction mixture was concentrated on a rotary evaporator. The resulting residue was dissolved in a minimal amount of acetone and precipitated 3 times into methanol and 3 times into hexane. Then, the precipitated PMMA was dried under vacuum and dissolved in THF to afford ca. 2 mg/mL concentration for GPC analysis. The samples were stored at 2-10 °C before the analysis.

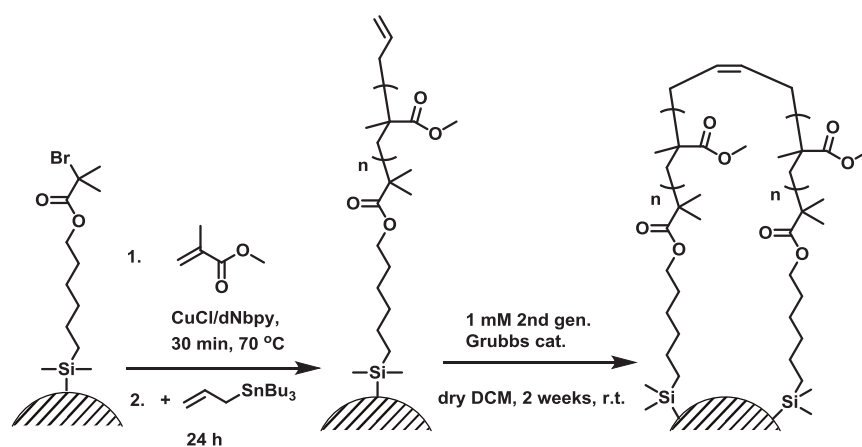
Chain-end functionalization of PMMA grafted silica nanoparticles with allylamine. To a nitrogen purged glass flask containing 140 mg PMMA-grafted silica nanoparticles (having in total $\sim 10^{-3}$ mmol bromine groups) and 28 mL DMSO, 0.21 mL allylamine (2.8 mmol) and 1.17 mL triethylamine (8.4 mmol) were injected and reaction was carried out for 48 h at 40 °C. After that, the particles were collected by centrifugation (10 min, 8000 rpm) and then washed twice with deionized water, methanol and THF. Each washing step consisted of vortex suspending and centrifuging. The cleaned particles were freeze-dried and stored.

Chain-end functionalization of PMMA grafted silica nanoparticles with allyltributylstannane. The functionalization was done by quenching SI-ATRP of MMA with 10 mol% allyltributylstannane against initial amount of MMA. After the injection, the reaction was allowed to proceed for 24 hours, while maintaining the inert atmosphere and keeping the same temperature (70 °C). After that, the PMMA-functionalized nanoparticles with allyl chain-ends were collected by centrifugation (10 k rpm, 10 min) and washed 2 times with THF, 2 times with n-hexane and 2 times with MeOH. The cleaned particles were freeze-dried.

Loop-closing metathesis of olefin end-functionalized PMMA brushes. 100 mg olefin end-functionalized PMMA-grafted silica nanoparticles were treated with 0.46 mg 2nd generation Grubbs catalyst in 50 mL DCM. The reaction was allowed to proceed at room temperature for two weeks and 0.5 mL of the catalyst solution (0.46 mg in 0.5 mL DCM) was added each day. Afterwards, the particles were collected by centrifugation (10 min, 8000 rpm), washed 3 times with DCM, freeze-dried and stored.

2.3. Results and Discussion

Scheme 2.1 illustrates the synthesis of PMMA loop brushes via post-polymerization loop-closure. In a first step, linear PMMA brushes are grown from silicon nanoparticles via surface-initiated atom transfer radical polymerization. Then, the chain-ends of the surface anchored PMMA chains are modified with an allyl end-group. In a final step the allyl chain-end functionalized brushes are exposed to a 2nd generation Grubbs catalyst in order to induce loop-formation. In what follows below, we will discuss in detail the different steps towards the synthesis of the loop-type polymer brushes.



Scheme 2.1.

2.3.1. PMMA brush synthesis

Polymer brushes were grown from silica particles, which were prepared via the Stöber process. To allow the grafting of the PMMA brushes, the nanoparticles were modified with the ATRP initiator, 6-(2-bromo-2-methylpropionyloxy)hexyldimethylchlorosilane. In a first series of polymerization experiments, PMMA brushes were grown by surface initiated – activators regenerated by electron transfer ATRP (SI-ARGET ATRP) from 332 nm diameter silica nanoparticles with an ATRP initiator surface concentration of 2.1 nm⁻² using reaction times that varied from 20 min to 6 hours. Brush growth was monitored by TGA analysis of the PMMA modified silica nanoparticles (**Figure 2.2A**). **Figure 2.2B** plots the PMMA weight loss, which is proportional to polymer molecular weight, and thus brush film thickness, as a function of polymerization time. After an initial linear increase in the observed weight loss, the film growth rate seems to decrease at polymerization times longer than 2 hours, indicating a loss of end-group fidelity. As high degrees of end-group fidelity

are important for an effective loop-closure, all of the PMMA brushes prepared via SI-ARGET-ATRP were obtained using polymerization times of at most 2 hours.

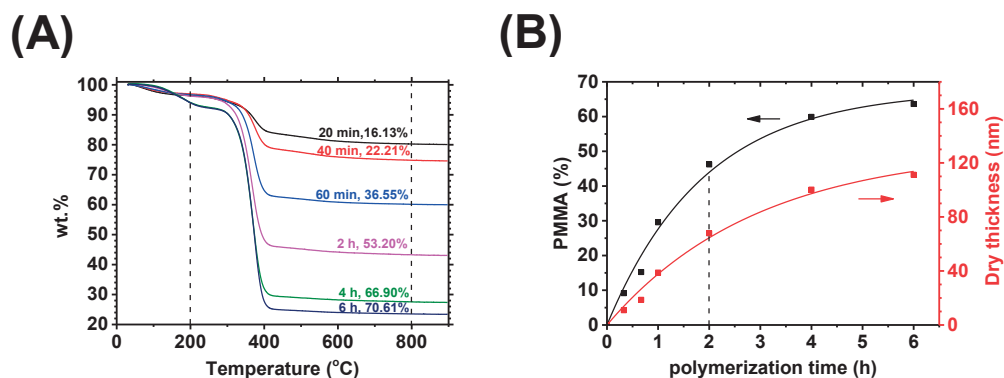


Figure 2.2. (A) TGA curves of PMMA-grafted silica nanoparticles ($\phi = 332$ nm) prepared by SI-ARGET-ATRP at different polymerization times. Heating ramp of 10 °C/min was used. (B) Percentage PMMA weight loss and brush thicknesses of PMMA-grafted silica nanoparticles as a function of polymerization time.

2.3.2. Brush cleavage

Determining the molecular weight of the surface grafted PMMA is important, not only to calculate the grafting density of the PMMA brushes, but also to characterize the loop-type brushes. Polymer molecular weights were measured by GPC. This requires a procedure that allows the surface-grafted polymer to be cleaved from the silica particles. First, TBAF was evaluated as a cleavage reagent.⁴³ For these experiments, 320 nm diameter silica particles, which were modified with PMMA brush layers of different thicknesses were incubated at room temperature (27, 46, 68 and 157 nm) or at 55 °C (4, 68 and 157 nm) in a 0.05 M solution of TBAF in HPLC grade THF for 72 and 24 h, respectively. The cleavage reaction was monitored by TGA of the residual nanoparticles. When the cleavage reaction was performed at room temperature, only partial cleavage of the PMMA brushes was observed (**Figure S2.6**). Increasing the temperature to 55 °C resulted in complete cleavage for all samples, except for particles modified with a 157 nm thick PMMA brush (**Figure S2.7**).

In order to allow quantitative brush cleavage at room temperature, triethylamine trihydrofluoride ($\text{Et}_3\text{N}\cdot 3\text{HF}$) was investigated.⁴⁴ When PMMA-brush modified silica nanoparticles were treated with a 10% $\text{Et}_3\text{N}\cdot 3\text{HF}$ solution in THF at room temperature, complete dissolution of the nanoparticles could be observed with the naked eye within 30 min.

Initially, the cleaved PMMA was isolated by quenching the reaction mixture with NaHCO_3 , neutralizing with HCl and extracting the polymers with DCM followed by drying over Mg_2SO_4 . Alternatively, and much more straightforward, the volatiles are removed from the reaction mixture on a rotary evaporator and the polymer isolated by precipitation in methanol and hexane.

To optimize and validate the $\text{Et}_3\text{N}\cdot 3\text{HF}$ cleavage protocol, 411 nm diameter silica nanoparticles modified with a 91 nm PMMA brush were exposed to $\text{Et}_3\text{N}\cdot 3\text{HF}$ for a period of 2 hours or overnight and the isolated, cleaved PMMA, analyzed by GPC. The results of these analyses are summarized in **Table S2.1** and **Figure S2.8**. Increasing the reaction time of the cleavage reaction leads to a decrease in the molecular weight of the cleaved polymer (see **Table S1**, entries #1 and #2 and **Figure S2.8**). This can either indicate that high molecular weight chains are cleaved easier (as reported in ⁴⁵) or could point towards degradation of PMMA upon prolonged exposure to $\text{Et}_3\text{N}\cdot 3\text{HF}$. In a control experiment, in which PMMA prepared by solution ATRP was exposed to $\text{Et}_3\text{N}\cdot 3\text{HF}$ for 2 hours and overnight, no significant or only very small changes in molecular weight could be observed (**Table S2.1**, entries #3, #4 and #5 and **Figure S2.9A**). As a result, cleavage reactions were carried out overnight to ensure complete brush cleavage. To validate the reproducibility of this method, two batches of 411 nm diameter silica nanoparticles modified with a 95 nm PMMA brush were separately incubated overnight in $\text{Et}_3\text{N}\cdot 3\text{HF}$. The molecular weights of the PMMA isolated in these two experiments differed less than 5% (**Table S2.1**, entries #6 and #7 and **Figure S2.9B**) indicating the reproducibility of this cleavage protocol.

2.3.3. Chain-end modification

In a first attempt to incorporate allyl chain-end functional groups, silica nanoparticles modified with PMMA brushes produced via SI-ARGET-ATRP with polymerization times of 20, 40, 60 or 120 min were reacted with allylamine. The allyl end functionalized brushes were subsequently exposed to a 1 mM solution of 1st generation Grubbs catalyst for 48 h. Successful chain-end metathesis would generate loop-type α,ω -chain-end tethered polymer that would possess increased molecular weight, as compared to the initial, linear PMMA grafts. Cleavage with $\text{Et}_3\text{N}\cdot 3\text{HF}$ after the metathesis reaction and subsequent GPC analysis, however, did not reveal any change in the molecular weight of the polymers as compared to the starting allyl end-functionalized PMMA grafts (Supporting Information **Figure S2.10** and **Table S2.2**).

To understand the difficulties in accomplishing loop-closure, model metathesis experiments were done with ethyl 2-(2-propen-1-ylamino)isobutyrate and ethyl 2-(2-propen-1-ylamino)propionate. For these model reactions, 1.25 mmol of ethyl 2-(2-propen-1-ylamino)isobutyrate or ethyl 2-(2-propen-1-ylamino)propionate were dissolved in 2.5 mL dichloromethane in the presence of 1 mM solution of 1st generation Grubbs catalyst. The reactions were run at room temperature or at reflux for 18 h. ¹H-NMR analysis of the products of these model reactions indicated significant loss of the allyl groups upon exposure to the Grubbs catalyst. As an example, **Figure 2.3** compares the ¹H-NMR spectra of ethyl 2-(2-propen-1-ylamino)isobutyrate at the beginning of the reaction (**Figure 2.3A**) and after exposure to 1st generation Grubbs catalyst for 18 hours under reflux (**Figure 2.3B**). The ¹H-NMR spectrum of the 1st generation Grubbs catalyst is included in **Figure S2.11**. Comparison of the integrals of signals “d” and “c” at t=0 and after 18 hours indicates almost 70% loss of allyl groups. In case of ethyl 2-(2-propen-1-ylamino)propionate, the effect was slightly less pronounced and ~60% of allyl groups were lost (compare integrals of the signals “e” and “g” at t=0 and after 18 hours in **Figure S2.12**). In addition, none of the NMR spectra did indicate the formation of secondary olefins. Carrying out these metatheses at room temperature or the use of the 2nd generation Grubbs catalyst mitigated, but could not help to completely prevent allyl group loss. With ethyl 2-(2-propen-1-ylamino)isobutyrate as the substrate, allyl group losses of 22, 38 and 59% were observed when using the 1st generation Grubbs catalyst at room temperature, or the 2nd generation Grubbs catalyst at room temperature or under reflux and still no dimerization was observed (**Figure S2.13**, **Figure S2.14** and **Figure S2.15**). The observed losses of allyl groups during the attempted metathesis reaction explain why the loop-closure attempts with the allyl amine end functionalized PMMA brushes were not successful. These results are also in agreement with other reports that have described the loss of allylic amines under the action of Grubbs catalyst.⁴⁶

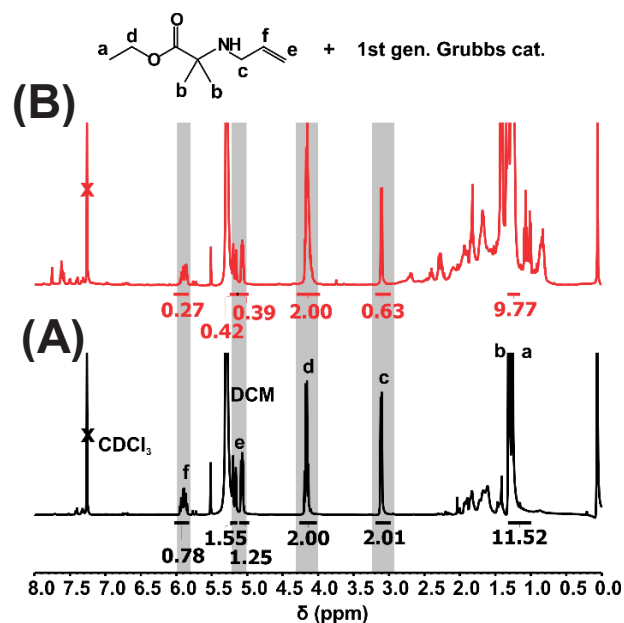
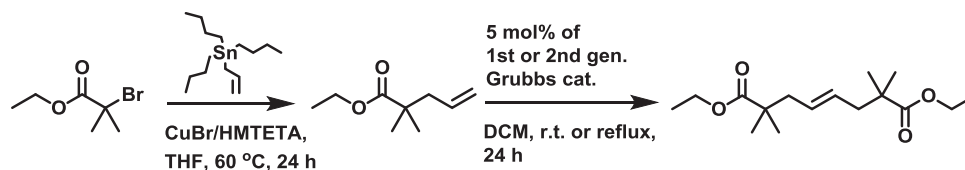


Figure 2.3. ¹H NMR spectra of ethyl 2-(2-propen-1-ylamino)isobutyrate in the presence of 1st Generation Grubbs catalyst, taken at (A) the beginning (t=0) and (B) after 18h of the reaction under reflux. The unlabeled signals are due to the active and decomposed catalyst.

As an alternative for allylamine, allyltributylstannane was explored for the chain-end functionalization of the PMMA grafts.⁴⁷⁻⁴⁹ First, the reaction of allyltributylstannane with ethyl 2-bromoisobutyrate to produce ethyl 2,2-dimethyl-4-pentenoate and the subsequent metathesis reaction were studied in model experiments (**Scheme 2.2**). In these experiments, ethyl 2-bromoisobutyrate and allyltributylstannane were reacted in a 1:1 molar ratio in different solvents. The progress of the reaction was monitored by measuring the conversion of EBiB with ¹H-NMR spectroscopy. Using toluene as a solvent and PMDETA as a ligand resulted in 20.5% conversion of ethyl 2-bromoisobutyrate at 65 °C after 17 hours (**Figure S2.16**, **Figure S2.17** and **Figure S2.18**). The reaction proceeded much better in polar solvents. In DMF at room temperature an EBiB conversion of 94% was obtained after 72 hours (**Figure S2.19**). Due to its high boiling point DMF, however, can be difficult to remove. Instead, in THF and with HMTETA as a ligand at 60 °C, with 1:1.5 EBiB/allyltributylstannane stoichiometry, 99.5% of EBiB conversion was reached within 24 h reaction time (**Figure 2.4**).



Scheme 2.2.

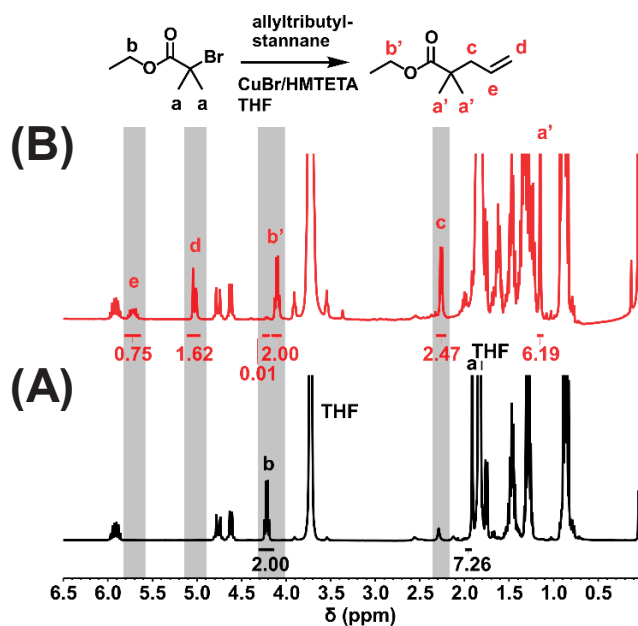


Figure 2.4. ^1H NMR analysis of the reaction between ethyl 2-bromoisobutyrate and allyltributyl stannane (1:1.5 molar ratio) in THF with CuBr/HMTETA at 60°C at (A) $t = 0$ and (B) after 24 h. Signals b and b' were used to calculate the conversion: $2.00/(0.01+2.00) \cdot 100\% = 99.5\%$.

An additional experiment was performed in the presence of MMA to investigate whether allyltributylstannane can be used as a quenching reagent concluding SI-ATRP. The NMR spectra of the reaction mixture after 70 h showed that the allylation competes with the polymerization of MMA and is completed only after certain conversion of MMA (more detailed discussion is provided in Supporting Information with the ^1H -NMR spectrum in **Figure S2.20**). To the best of our knowledge, this observation has not been reported in the literature. However the researchers tend to use high excess of allyltributylstannane and quench the polymerizations at high conversions, which may mitigate this effect.⁴⁷⁻⁴⁹

Subsequently, ethyl 2,2-dimethyl-4-pentenoate was subjected to metathesis reaction using 1st or 2nd generation Grubbs' catalyst in dichloromethane at room temperature or

under reflux over 72 h. The progress of these reactions was followed by $^1\text{H-NMR}$ spectroscopy. Carrying out the metathesis reaction in the presence of 1st generation Grubbs catalyst at room temperature resulted in 38% conversion (**Figure S2.21**). When the reaction was performed at reflux, the conversion increased to 96% (**Figure S2.22**). Using the 2nd generation Grubbs catalyst resulted in 92.4% conversion when the reaction was performed at room temperature (Figure S2.23, Figure S2.24), respectively 98.9% at reflux (**Figure 2.5**).

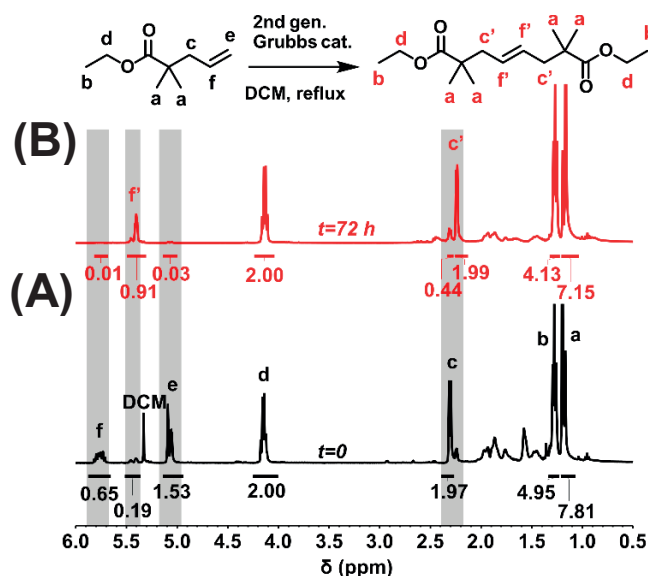


Figure 2.5. $^1\text{H-NMR}$ spectrum of a reaction mixture of ethyl 2,2-dimethyl-4-pentenoate and 2nd generation Grubbs' catalyst under reflux (DCM was removed under vacuum) at (A) $t = 0$ and (B) after 72 h. Signals f and f' were used to calculate the conversion: $0.91/(0.01+0.91)\cdot 100\% = 98.9\%$.

2.3.4. Synthesis of PMMA loop brushes

The chain-end functionalization and metathesis procedures, which were elaborated in the previous sections, were finally applied to the synthesis of PMMA loop brushes. For these experiments, PMMA brushes were grown from 411 nm diameter silica nanoparticles via bulk SI-ATRP. **Figure 2.6A** shows the results of thermogravimetric analysis of PMMA brush modified nanoparticles obtained at polymerization times ranging from 10 min to 2 hours. The evolution of the PMMA weight loss as a function of polymerization time is presented in **Figure 2.6B**. To determine the molecular weight of the surface-grown PMMA and the grafting density of the PMMA brush, the polymer was cleaved overnight using a 10% $\text{Et}_3\text{N}\cdot 3\text{HF}$ solution in THF and analyzed by GPC. **Figure 2.7A** presents the GPC chromatograms and **Figure 2.7B** the evolution of the number average molecular weights

(M_n) and dispersities (M_w/M_n) of the PMMA grafts as a function of polymerization time. Both **Figure 2.6B** and **Figure 2.7B** show a slight decrease in the growth of polymer molecular weight at reaction times longer than 20-30 min, indicating the loss of reactive chain-ends. The polymer molecular weights, dispersities, film thicknesses and grafting densities of the PMMA brushes are also listed in **Table 2.1**.

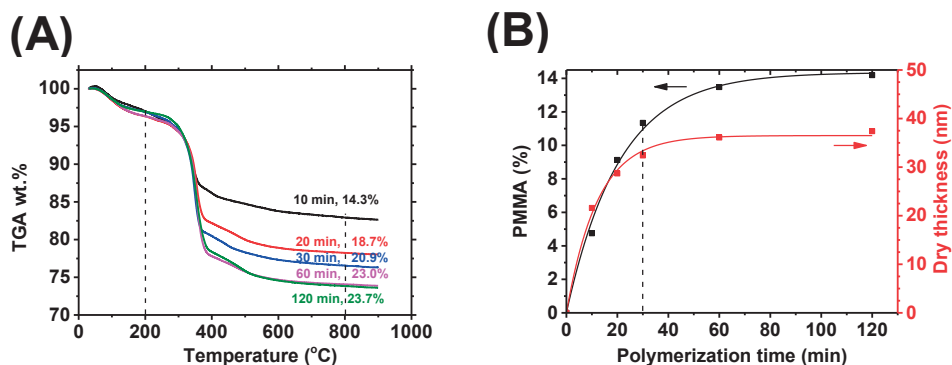


Figure 2.6. (A) TGA curves of PMMA-grafted silica nanoparticles ($\phi = 411$ nm) prepared by bulk SI-ATRP at different polymerization times. Heating ramp of 10 °C/min was used. (B) Percentage PMMA weight loss and brush thicknesses of PMMA-grafted silica nanoparticles as a function of polymerization time.

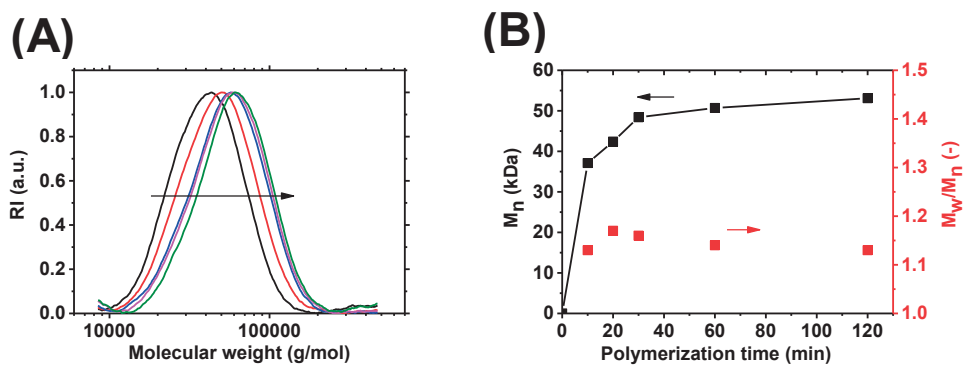


Figure 2.7. (A) GPC traces for PMMA brushes grown from silica nanoparticles ($\phi = 411$ nm) with polymerization times of 10 (black), 20 (red), 30 (blue), 60 (pink) and 120 min (green); (B) evolution of GPC number average molecular weights and dispersities of the grafted PMMA.

Table 2.1. Molecular weights, film thicknesses and grafting densities of PMMA brushes grown from silica nanoparticles ($\phi = 411$ nm) by SI-ATRP.

Entry	Polymerization time [min]	M_n [kDa]	M_w [kDa]	\bar{D} [-]	M_p [kDa]	GD ^a [chains/nm ²]	Brush thickness ^b [nm]
#1	10	37.1	41.9	1.13	41.7	0.12	21.6
#2	20	42.4	49.5	1.17	47.5	0.23	28.7
#3	30	48.4	56.3	1.16	53.3	0.26	32.4
#4	60	50.7	57.9	1.14	54.1	0.30	36.1
#5	120	53.1	60.3	1.13	56.9	0.31	37.4

a – calculated using M_n of PMMA-grafts, DLS diameter of initial, non-modified silica nanoparticles and TGA wt. loss of PMMA-modified nanoparticles, b – calculated using DLS diameter of initial, non-modified silica nanoparticles and TGA wt. loss of PMMA-modified nanoparticles.

For the synthesis of the PMMA loops, two batches of PMMA-grafted silica nanoparticles (silica core $\phi = 411$ nm) were prepared using a polymerization time of 30 min followed by quenching using 10 mol% allyltributylstannane against initial amount of MMA for 24 h. The resulting allyl chain-end functionalized PMMA brush modified nanoparticles were analyzed by TGA and the molecular weights and molecular weight distributions of the PMMA grafts measured by GPC. The polymer molecular weights as well as film thicknesses and grafting densities of the PMMA brushes are given in **Table 2.2**. In a final step, the silica nanoparticles with allyl-functionalized polymer brushes were exposed to 2nd generation Grubbs catalyst in dry DCM at room temperature. During a period of two weeks 0.5 mL dry DCM with 0.46 mg of catalyst was added daily to the reaction. After that, the nanoparticles were collected, washed and dried. Finally, the polymer brush modified nanoparticles were exposed to $\text{Et}_3\text{N}\cdot 3\text{HF}$ and the cleaved PMMA was analyzed by GPC (**Figure 2.8**, **Table 2.2**).

Table 2.2. Molecular weights, film thicknesses and grafting densities of allyl end-functionalized PMMA brushes before and after the loop-closure.

Entry	Sample	M _n [kDa]	M _w [kDa]	Đ	M _p [kDa]	GD ^a [chains/nm ²]	Brush thickness ^b [nm]
#1	Before metathesis	109.1	153.0	1.40	142.5	0.88	117.4
	After metathesis	176.5	276.8	1.57	237.7	N.A.	N.A.
#2	Before metathesis	116.3	150.5	1.29	147.5	0.52	88.5
	After metathesis	153.9	209.0	1.36	188.2	N.A.	N.A.

a – calculated using M_n of PMMA-grafts, DLS diameter of initial, non-modified silica nanoparticles and TGA wt. loss of PMMA-modified nanoparticles, b – computed using DLS diameter of initial, non-modified silica nanoparticles and TGA wt. loss of PMMA-modified nanoparticles.

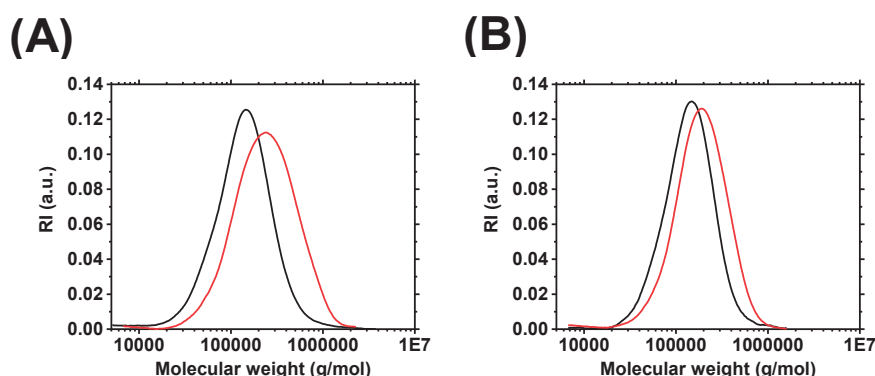


Figure 2.8. GPC traces of linear- and loop- PMMA cleaved from silica nanoparticles using 10% Et₃N·3HF in THF overnight. The PMMA brushes were obtained by 30 min SI-ATRP followed by quenching with 10 mol% allyltributylstannane vs. initial MMA in the feed (**A** – first, **B** – second batch). Then, the loop closure was carried out for 2 weeks, each day dosing 0.46 mg 2nd Generation Grubbs catalyst, ca. 10 mol% against amount of the grafted initiator. Batch 2 was additionally quenched with DMSO at the end of the metathesis. The traces were normalized by area under the curves.

Table 2.2 and **Figure 2.8** compare the molecular weights and dispersities of the allyl end-functionalized PMMA grafts and the product obtained after the metathesis reaction. Quantitative loop-closure would result in a doubling of the molecular weight of the surface-

grafted polymers. The molecular weights of the polymers after loop-closure metathesis are indeed significantly higher as compared to the initial linear allyl end-functionalized PMMA grafts, which indicates that the metathesis reaction indeed results in the formation of PMMA loops. The molecular weights of the samples analyzed after metathesis, however, are less than twice the molecular weights of the initial PMMA grafts. This indicates that loop formation is not quantitative and that the brushes obtained after the metathesis reaction are a mixture of loop type and linear PMMA grafts. There are a number of factors that may contribute to the less than quantitative formation of PMMA loops. A first factor, which may contribute to the lower than expected molecular weight of the PMMA loops, is a not 100% bromine end-functionalization of the initial PMMA brush. A less than quantitative conversion of the halide chain-ends with allyltributylstannane could be a second contributor. Finally, steric barrier could also prevent effective chain-end metathesis loop-closure.

2.4. Conclusions

The monitoring of loop-closure of linear polymer brushes is not trivial, as it implies small chemical changes that are difficult to detect. However, the closure connects two chains and thus implies an increase of molecular weight. We synthesized loop PMMA brushes via metathesis of allyl end-functionalized PMMA chains, which were cleaved and analyzed by GPC. The analysis showed nearly doubled molecular weights of the PMMA grafts after the modification, which indicates the successful synthesis of loop polymer brushes via this new approach.

Part of this work was carried out by the graduate student Maxence Ménetrey who contributed with the development of the Et₃N·3HF mediated cleavage protocol. GPC measurements were carried out by Jacques Morisod (LP, EPFL). XPS measurements were performed by Pierre Mettraux from the MHMC of the EPFL.

2.5. References

- (1) Zhao, B.; Brittain, W. J. *Progress in Polymer Science* **2000**, *25*, 677.
- (2) Pyun, J.; Kowalewski, T.; Matyjaszewski, K. *Macromolecular Rapid Communications* **2003**, *24*, 1043.

- (3) Edmondson, S.; Osborne, V. L.; Huck, W. T. *Chemical Society Reviews* **2004**, *33*, 14.
- (4) Senaratne, W.; Andruzzi, L.; Ober, C. K. *Biomacromolecules* **2005**, *6*, 2417.
- (5) Jain, P.; Baker, G. L.; Bruening, M. L. *Annual Review of Analytical Chemistry* **2009**, *2*, 387.
- (6) Barbey, R.; Lavanant, L.; Paripovic, D.; Schüwer, N.; Sugnaux, C.; Tugulu, S.; Klok, H.-A. *Chemical Reviews* **2009**, *109*, 5437.
- (7) Azzaroni, O. *Journal of Polymer Science Part A: Polymer Chemistry* **2012**, *50*, 3225.
- (8) Zoppe, J. O.; Ataman, N. C.; Mocny, P.; Wang, J.; Moraes, J.; Klok, H.-A. *Chemical Reviews* **2017**, *117*, 1105.
- (9) Hucknall, A.; Rangarajan, S.; Chilkoti, A. *Advanced Materials* **2009**, *21*, 2441.
- (10) Banerjee, I.; Pangule, R. C.; Kane, R. S. *Advanced Materials* **2011**, *23*, 690.
- (11) Yang, W. J.; Neoh, K.-G.; Kang, E.-T.; Teo, S. L.-M.; Rittschof, D. *Progress in Polymer Science* **2014**, *39*, 1017.
- (12) Moroni, L.; Gunnewiek, M. K.; Benetti, E. M. *Acta Biomaterialia* **2014**, *10*, 2367.
- (13) Lowe, S.; O'Brien-Simpson, N. M.; Connal, L. A. *Polymer Chemistry* **2015**, *6*, 198.
- (14) Klein, J. *Friction* **2013**, *1*, 1.
- (15) Mocny, P.; Klok, H.-A. *Molecular Systems Design & Engineering* **2016**, *1*, 141.
- (16) Kreer, T. *Soft Matter* **2016**, *12*, 3479.
- (17) Benetti, E. M.; Divandari, M.; Ramakrishna, S. N.; Morgese, G.; Yan, W.; Trachsel, L. *Chemistry—A European Journal* **2017**, *23*, 12433.
- (18) Morgese, G.; Benetti, E. M.; Zenobi-Wong, M. *Advanced Healthcare Materials* **2018**, 1701463.
- (19) Divandari, M.; Morgese, G.; Trachsel, L.; Romio, M.; Dehghani, E. S.; Rosenboom, J.-G.; Paradisi, C.; Zenobi-Wong, M.; Ramakrishna, S. N.; Benetti, E. M. *Macromolecules* **2017**, *50*, 7760.
- (20) Yamada, K.; Katoono, R.; Yui, N. *Polymer Journal* **2011**, *44*, 286.
- (21) Zhou, T.; Han, B.; Qi, H.; Pan, Q.; Smith, D. M.; Han, L.; Li, C. Y. *Nanoscale* **2018**, *10*, 18269.
- (22) Seo, J.-H.; Tsutsumi, Y.; Kobari, A.; Shimojo, M.; Hanawa, T.; Yui, N. *Soft Matter* **2015**, *11*, 936.
- (23) Shull, K. R. *Faraday Discussions* **1994**, *98*, 203.

- (24) Pei, H.-W.; Liu, X.-L.; Liu, H.; Zhu, Y.-L.; Lu, Z.-Y. *Physical Chemistry Chemical Physics* **2017**, *19*, 4710.
- (25) Lu, H. B.; Campbell, C. T.; Castner, D. G. *Langmuir* **2000**, *16*, 1711.
- (26) Patton, D.; Knoll, W.; Advincula, R. C. *Macromolecular Chemistry and Physics* **2011**, *212*, 485.
- (27) Han, Y.; Ma, J.; Hu, Y.; Jin, J.; Jiang, W. *Langmuir* **2018**.
- (28) Sakurai, S.; Watanabe, H.; Takahara, A. *Polymer Journal* **2013**, *46*, 117.
- (29) Huang, Z.; Ji, H.; Mays, J. W.; Dadmun, M. D. *Macromolecules* **2008**, *41*, 1009.
- (30) Huang, Z.; Ji, H.; Mays, J.; Dadmun, M.; Smith, G.; Bedrov, D.; Zhang, Y. *Langmuir* **2010**, *26*, 202.
- (31) Kang, T.; Banquy, X.; Heo, J.; Lim, C.; Lynd, N. A.; Lundberg, P.; Oh, D. X.; Lee, H.-K.; Hong, Y.-K.; Hwang, D. S. *ACS Nano* **2016**, *10*, 930.
- (32) Li, L.; Yan, B.; Zhang, L.; Tian, Y.; Zeng, H. *Chemical Communications* **2015**, *51*, 15780.
- (33) Ren, X.; Weng, L. T.; Fu, Y.; Ng, K. M.; Chan, C. M. *Surface and Interface Analysis* **2015**, *47*, 953.
- (34) Banquy, X.; Burdynska, J.; Lee, D. W.; Matyjaszewski, K.; Israelachvili, J. *Journal of the American Chemical Society* **2014**, *136*, 6199.
- (35) Alonzo, J.; Huang, Z.; Liu, M.; Mays, J. W.; Toomey, R. G.; Dadmun, M. D.; Kilbey, S. M. *Macromolecules* **2006**, *39*, 8434.
- (36) Liu, S.; Jamali, S.; Liu, Q.; Maia, J.; Baek, J.-B.; Jiang, N.; Xu, M.; Dai, L. *Macromolecules* **2016**, *49*, 7434.
- (37) Zhou, T.; Qi, H.; Han, L.; Barbash, D.; Li, C. Y. *Nature Communications* **2016**, *7*, 11119.
- (38) Rotzoll, R.; Vana, P. *Journal of Polymer Science Part A: Polymer Chemistry* **2008**, *46*, 7656.
- (39) Rotzoll, R.; Vana, P. *Australian Journal of Chemistry* **2009**, *62*, 1473.
- (40) Schüwer, N.; Klok, H. -A. *Advanced Materials* **2010**, *22*, 3251.
- (41) Zhu, B.; Edmondson, S.
- (42) Ohno, K.; Akashi, T.; Huang, Y.; Tsujii, Y. *Macromolecules* **2010**, *43*, 8805.
- (43) Patil, R. R.; Turgman-Cohen, S.; Šrogl, J.; Kiserow, D.; Genzer, J. *ACS Macro Letters* **2015**, *4*, 251.
- (44) Westman, E.; Stromberg, R. *Nucleic Acids Research* **1994**, *22*, 2430.

- (45) Melzak, K. A.; Yu, K.; Bo, D.; Kizhakkedathu, J. N.; Toca-Herrera, J. L. *Langmuir* **2015**, *31*, 6463.
- (46) Alcaide, B.; Almendros, P.; Alonso, J. M.; Aly, M. F. *Organic Letters* **2001**, *3*, 3781.
- (47) Adachi, K.; Honda, S.; Hayashi, S.; Tezuka, Y. *Macromolecules* **2008**, *41*, 7898.
- (48) Coessens, V.; Pyun, J.; Miller, P. J.; Gaynor, S. G.; Matyjaszewski, K. *Macromolecular Rapid Communications* **2000**, *21*, 103.
- (49) Vojtova, L.; Turro, N. J.; Koberstein, J. T. *Chemické Listy, Symposia* **2002**, *96*, S227.

2.6. Supporting Information

Model reaction for quenching ATRP of MMA from EBiB using allyltributylstannane. This is a model experiment that imitates conditions during quenching ATRP of MMA with allyltributylstannane at low monomer conversions. A Schlenk flask was charged with 12.71 mg dNbpv (0.26 mmol), 0.2 mL EBiB (1.364 mmol), 1.0 mL MMA (9.35 mmol) and 0.848 mL allyltributylstannane (2.73 mmol). The flask was sealed and three freeze-pump-thaw cycles were carried out. Then, 1.67 mg of CuCl (0.017 mmol) was added into the frozen mixture under positive nitrogen pressure. The flask was sealed again, evacuated, thawed and backfilled with nitrogen. Finally it was placed into an oil bath and heated to 70°C. The reaction mixture was stirred for 72 h. NMR sample was taken and analyzed after MMA was removed on a rotary evaporator (**Figure S2.20**). The conversion was 97.5%. Some amounts of polymerized MMA were observed as marked by a methoxy signal at 3.59 and the signal's integral account for degree of polymerization (DP) of 7.07 (M_n of 708 Da), as compared to theoretical 6.85 for non-quenched polymerization. Only slightly higher DP indicates much slower stannane-induced deactivation compared to propagation of MMA.

Determination of initiator surface concentration, polymer brush grafting densities and film thicknesses from TGA. TGA derived weight losses refer to a corrected value, which was obtained according to the equation below (following a similar treatment as in ¹):

$$\varphi_{\text{grafted}} = \frac{\text{wt.}\%(200-800^\circ\text{C})}{100\% - \text{wt.}\%(30-200^\circ\text{C})} \quad (\text{Eq. S2.1})$$

$$\varphi_{\text{silica}} = 100\% - \varphi_{\text{grafted}} \quad (\text{Eq. S2.2})$$

where ϕ_{grafted} and ϕ_{silica} refer to weight fractions of grafted species and silica core, respectively, wt.% is the TGA recorded weight loss between indicated temperature range. This way, any physisorbed species (water, organic solvents), shown as weight loss between 30 and 200°C, are excluded.

ATRP initiator surface concentrations were obtained by first calculating specific surface area (SA) of synthesized silica nanoparticles:

$$SA = \frac{\pi d^2}{\frac{\pi d^3}{6} \cdot \rho_{\text{silica}}} = \frac{6}{d \rho_{\text{silica}}} \left[\frac{\text{cm}^3}{\text{nm} \cdot \text{g}} \right] = \frac{6 \cdot 10^3}{d \rho_{\text{silica}}} \left[\frac{\text{m}^2}{\text{g}} \right] \quad (\text{Eq. S2.3})$$

where d: diameter of silica nanoparticles [nm], ρ_{silica} : density of silica, 2.3 [g/cm³]. Then, grafting density of grafted initiator molecules:

$$GD = \frac{\frac{\text{wt.\%}_{\text{initiator+silica}}}{100\% - \text{wt.\%}_{\text{initiator+silica}}} - \frac{\text{wt.\%}_{\text{silica}}}{100\% - \text{wt.\%}_{\text{silica}}}}{M} \cdot 10^6 \left[\frac{\mu\text{mol}}{\text{g}} \right] \quad (\text{Eq. S2.4})$$

$$GD = \frac{\frac{\text{wt.\%}_{\text{initiator+silica}}}{100\% - \text{wt.\%}_{\text{initiator+silica}}} - \frac{\text{wt.\%}_{\text{silica}}}{100\% - \text{wt.\%}_{\text{silica}}}}{M \cdot SA} \cdot N_{AV} \cdot 10^{-18} \left[\frac{\text{molecules}}{\text{nm}^2} \right] \quad (\text{Eq. S2.5})$$

where wt.%_{silica}, wt.%_{initiator+silica}: TGA wt.% loss between 200 and 800°C for pristine, and grafted silica nanoparticles, respectively, M: molecular weight of initiator on the surface (308.31 g/mol), N_{AV} : Avogadro number (6.02·10²³ molecules/mol).

Brush grafting densities was obtained in similar manner:

$$GD = \frac{\frac{\text{wt.\%}_{\text{initiator+silica}}}{100\% - \text{wt.\%}_{\text{initiator+silica}}} - \frac{\text{wt.\%}_{\text{silica}}}{100\% - \text{wt.\%}_{\text{silica}}}}{M_n \cdot SA} \cdot N_{AV} \cdot 10^{-18} \left[\frac{\text{molecules}}{\text{nm}^2} \right] \quad (\text{Eq. S2.6})$$

were wt.%_{polymer} is wt.% loss between 200 and 800°C for polymer grafted silica nanoparticles, and M_n is number average molecular weight of cleaved polymers obtained from GPC [g/mol].

To calculate dry brush thickness we consider the polymer grafted nanoparticles ($V_{\text{polymer}} + V_{\text{silica}}$) and silica core (V_{silica}) as spheres with diameters of d+2h, and d, respectively. Then, the volumes are written using mass fractions and densities of a polymer (for PMMA, 1.1 g/cm³) and silica core (2.3 g/cm³).

$$\frac{V_{\text{polymer}} + V_{\text{silica}}}{V_{\text{silica}}} = \frac{\pi/6 \cdot (d+2h)^3}{\pi/6 \cdot d^3} = \left(\frac{d+2h}{d} \right)^3 \quad (\text{Eq. S 2.7})$$

$$\frac{V_{\text{polymer}} + V_{\text{silica}}}{V_{\text{silica}}} = \frac{\phi_{\text{polymer}} / \rho_{\text{polymer}}}{\phi_{\text{silica}} / \rho_{\text{silica}}} + 1 = \frac{\phi_{\text{polymer}} \rho_{\text{silica}}}{\phi_{\text{silica}} \rho_{\text{polymer}}} + 1 \quad (\text{Eq. S2.8})$$

Finally, equating the two above expressions we have:

$$\left(\frac{d+2h}{d}\right)^3 = \frac{\varphi_{\text{polymer}}\rho_{\text{silica}}}{\varphi_{\text{silica}}\rho_{\text{polymer}}} + 1 \quad (\text{Eq. S2.9})$$

Because we are interested only in positive real numbers:

$$\frac{d+2h}{d} = \left(\frac{\varphi_{\text{polymer}}\rho_{\text{silica}}}{\varphi_{\text{silica}}\rho_{\text{polymer}}} + 1\right)^{1/3} \quad (\text{Eq. S2.10})$$

$$h = \frac{d}{2} \cdot \left(\left(\frac{\varphi_{\text{polymer}}\rho_{\text{silica}}}{\varphi_{\text{silica}}\rho_{\text{polymer}}} + 1\right)^{1/3} - 1\right) \quad (\text{Eq. S2.11})$$

Amount of bromine groups in m mass of PMMA-modified silica nanoparticles was calculated as following:

$$n_{Br} = m_{\text{core}} \cdot GD = m \cdot (1 - \varphi_{\text{grafted}}) \cdot GD \quad (\text{Eq. S2.12})$$

where m and m_{core} correspond to masses of PMMA-modified silica nanoparticles and silica core, respectively; GD is the grafting density of attached initiator expressed in $\mu\text{mol/g}$.

Example analysis and calculations. Silica nanoparticles synthesized via Stöber process were freeze-dried and subjected to thermogravimetric analysis (TGA) and dynamic light scattering (DLS) measurements. The results indicated average diameter of particles of 332 nm with polydispersity of 0.037 (calculated specific surface area, SA, $7.86 \text{ m}^2/\text{g}$, **Eq. S2.3**). The ATRP initiator (6-(2-bromo-2-methyl)propionyloxy)hexyldimethylchlorosilane) was grafted onto the silica particles and resulted in loading of ca. $24.2 \mu\text{mol/g}$ of the initiator (wt.% initiator+silica = 6.99%, wt% silica = 6.34%, **Eq. S2.4**). Difference between functionalized SiNPs and pristine ones, along with DLS diameter of silica core 332 nm was used to calculate grafting density (GD) $1.85 \text{ molecules/nm}^2$ (**Eq. S2.5**). Then, PMMA brushes were grown by 20 min – 6 h SI-ARGET ATRP reaction. Weight loss during 200-800°C step of TGA was associated with degradation of a polymer (**Figure 2.2A**). Weight loss fraction of the PMMA grafted silica particles was in the range of 16.1 – 70.6 %. The TGA weight losses were plotted against polymerization time to reveal linear pseudo-living polymerization regime (**Figure 2.2B**). From this part of the plot we selected a maximum reaction time of 2 hours, as beyond, the bromine end-group fidelity may be lost.²

Another batch of silica nanoparticles was used to grow PMMA brushes via SI-ATRP in bulk (SiNPs size 411 nm, PDI 0.03, SA $6.3 \text{ m}^2/\text{g}$, loading of the initiator $123.5 \mu\text{mol/g}$, grafting density of the initiator $11.8 \text{ molecules/nm}^2$, wt.% initiator+silica = 9.48%, wt% silica = 6.25%). Weight loss during 200-800°C step of TGA was associated with degradation of a polymer (**Figure 2.6A**). Weight loss fraction of the PMMA grafted silica

particles was in the range of 14.3 – 23.7%. The TGA weight losses were plotted against polymerization time (**Figure 2.6B**). A maximum reaction time of 30 min was selected.

Amount of bromine groups in 140 mg PMMA-modified silica nanoparticles was calculated according to mass of their silica core. For 45% PMMA wt. fraction (determined with TGA) and thus 77 mg silica core, and grafting density of 17.55 $\mu\text{mol/g}$, the amount of bromine groups is $1.35 \cdot 10^{-3}$ mol.

Table S2.1. Molecular weights and dispersities of PMMA cleaved from silica nanoparticles exposed to $\text{Et}_3\text{N} \cdot 3\text{HF}$ (entries 1, 2, 6, 7) as well as of PMMA prepared by solution ATRP before (#3) and after the treatment (#4, #5).

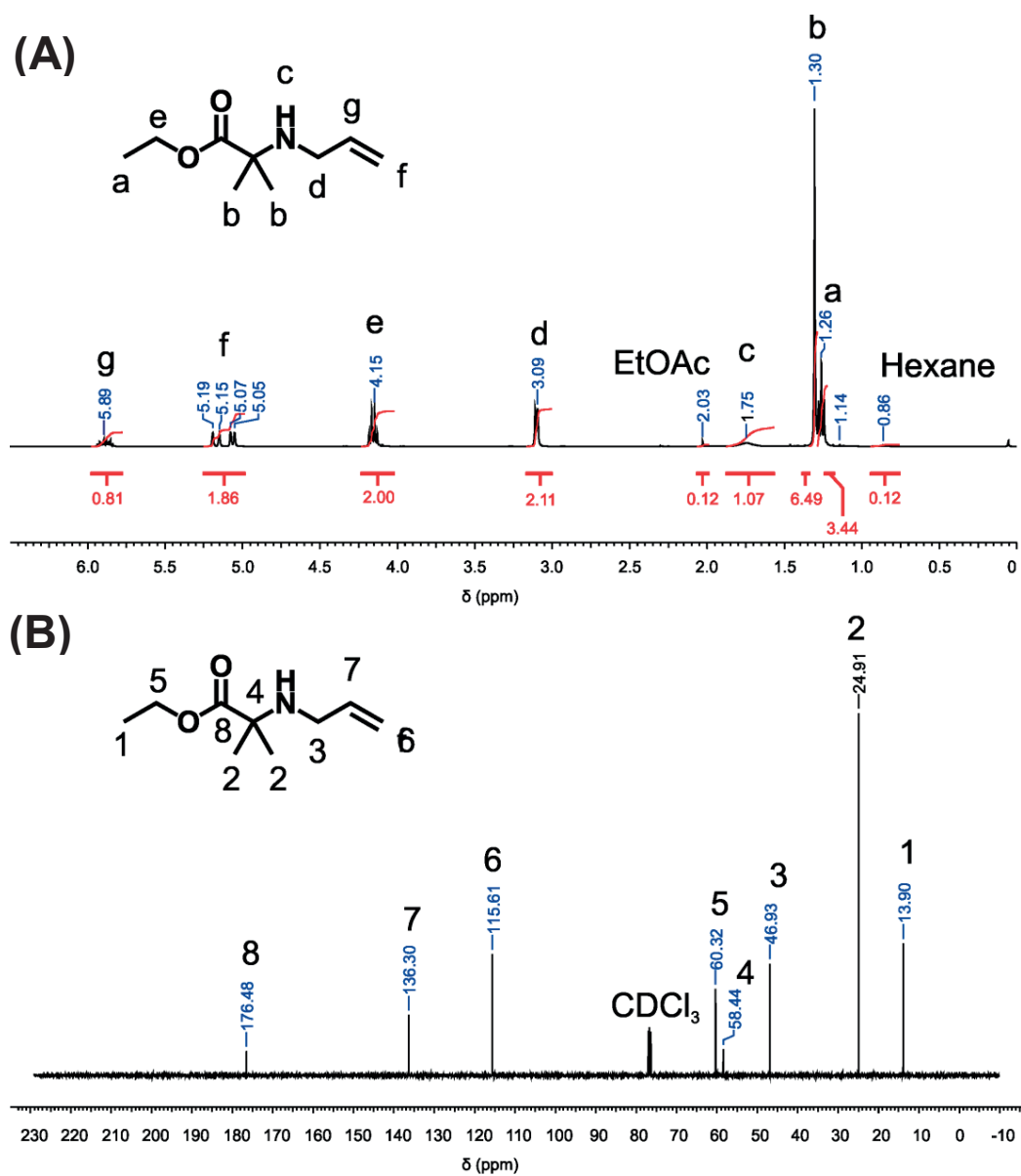
Entry	Sample	Synthesis conditions	Cleavage conditions	M_n [kDa]	M_w [kDa]	\bar{D} [-]	M_p [kDa]
1	SiNPs-PMMA	$d_{\text{core}} = 411$ nm, $d_{\text{PMMA}} = 91$ nm, 30 min SI-ATRP quenched with allyltributylstannane	2h cleaving with quenching	161.4	235.7	1.44	245.8
2	SiNPs-PMMA		overnight cleaving with quenching	109.0	161.0	1.48	142.5
3	PMMA		N.A.	24.7	28.3	1.15	28.5
4	PMMA	Free polymer chains, 6 h ATRP	2h cleaving	25.9	29.2	1.12	29.0
5	PMMA		overnight cleaving	26.6	29.6	1.11	29.5
6	SiNPs-PMMA	$d_{\text{core}} = 411$ nm, $d_{\text{PMMA}} = 95$ nm, 60 min SI-ATRP quenched with allyltributylstannane	overnight cleaving #1	219.0	280.5	1.28	279.0
7	SiNPs-PMMA		overnight cleaving #2	208.9	272.7	1.31	269.0

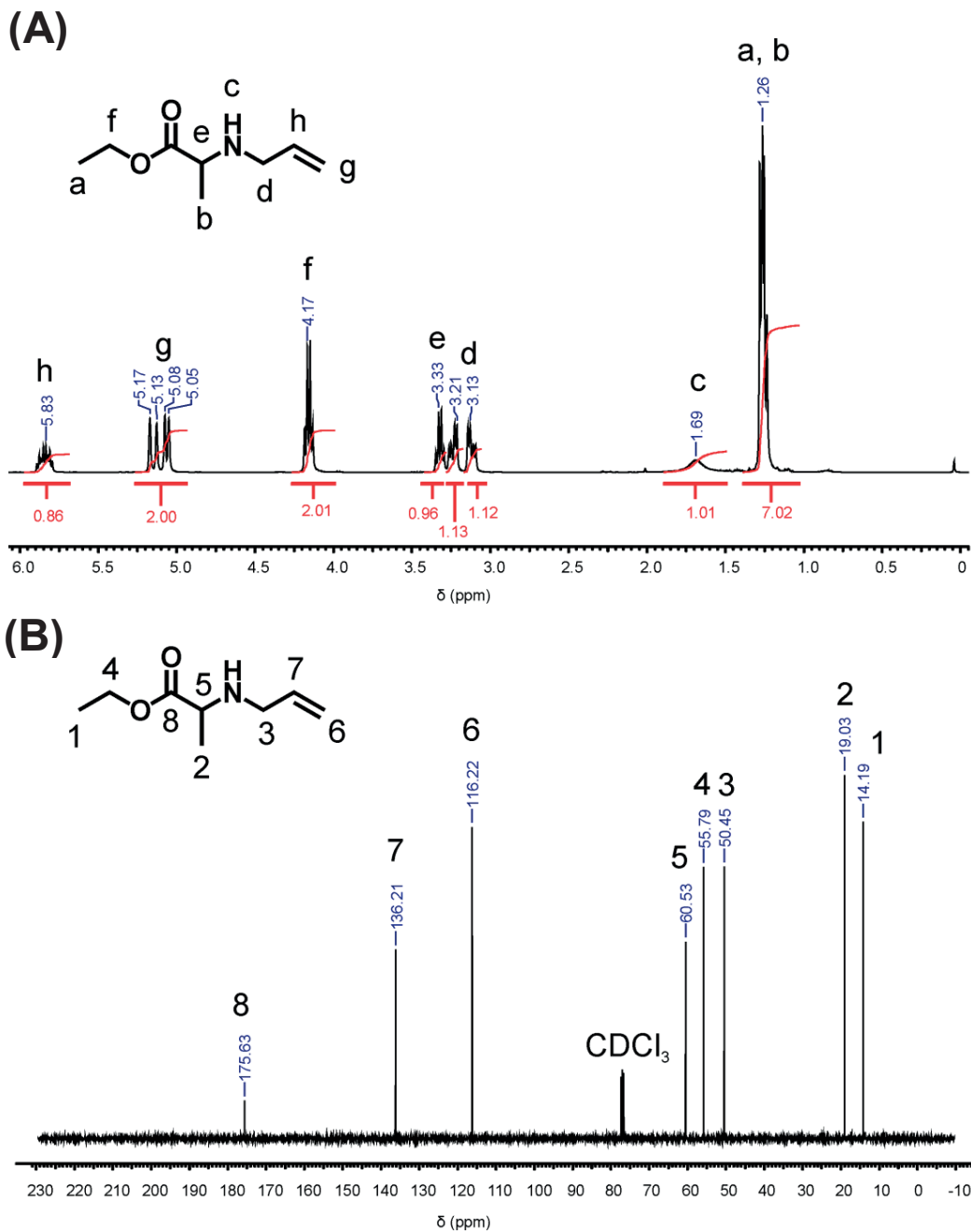
d_{core} – diameter of silica nanoparticle core, d_{PMMA} – PMMA brush thickness

Table S2.2. Molecular weights, film thickness and grafting densities of PMMA brushes on the samples before and after chain-end modification with allylamine as well as after exposure to 1 mM 1st generation Grubbs catalyst.

En-try	Polymeri- zation time [min]	Sample	M _n [kDa]	M _w [kDa]	Đ [-]	GD [chains/nm ²] ^a	dry brush thickness [nm] ^b
#1	20	PMMA-Br	92.3	142.3	1.54	0.18	22.7
		PMMA-allylamine	92.9	143.5	1.54	-	-
		PMMA-loops	102	151.9	1.49	-	-
#2	40	PMMA-Br	150.4	251.9	1.67	0.42	55.6
		PMMA-allylamine	151.5	259.2	1.72	-	-
		PMMA-loops	165.5	276.3	1.7	-	-
#3	60	PMMA-Br	203.6	355.7	1.75	0.47	80.4
		PMMA-allylamine	201.9	370.3	1.83	-	-
		PMMA-loops	218	394.7	1.81	-	-
#4	120	PMMA-Br	315.3	563.7	1.79	0.62	138.1
		PMMA-allylamine	331	645.3	1.95	-	-
		PMMA-loops	303	568.2	1.88	-	-

a – calculated using M_n of PMMA-grafts, DLS diameter of initial, non-modified silica nanoparticles and TGA wt. loss of PMMA-modified nanoparticles, b – computed using DLS diameter of initial, non-modified silica nanoparticles and TGA wt. loss of PMMA-modified nanoparticles.





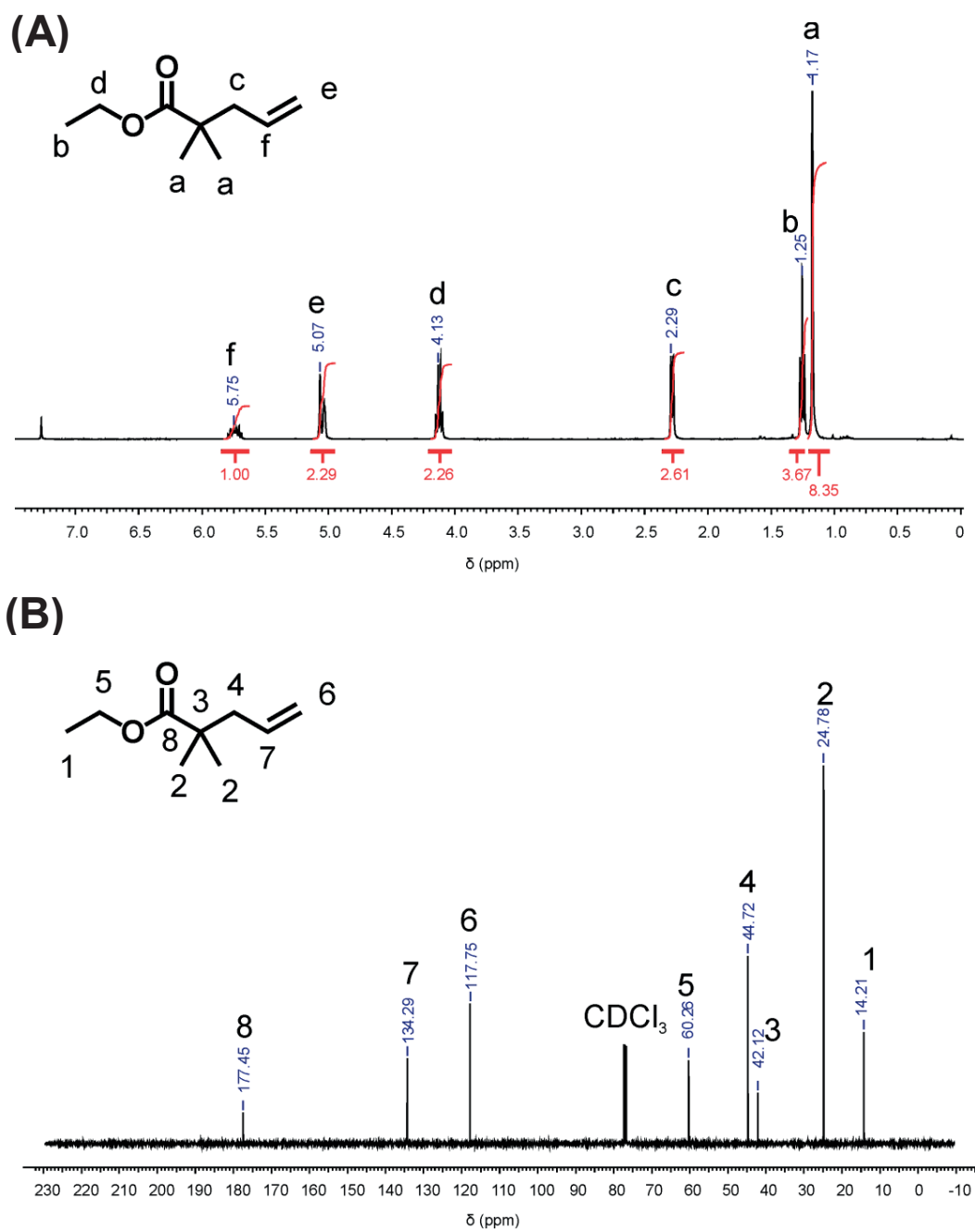


Figure S2.3. (A) ^1H NMR spectrum and (B) ^{13}C NMR spectrum of ethyl 2,2-dimethylpent-4-enoate. Recorded in CDCl_3 .

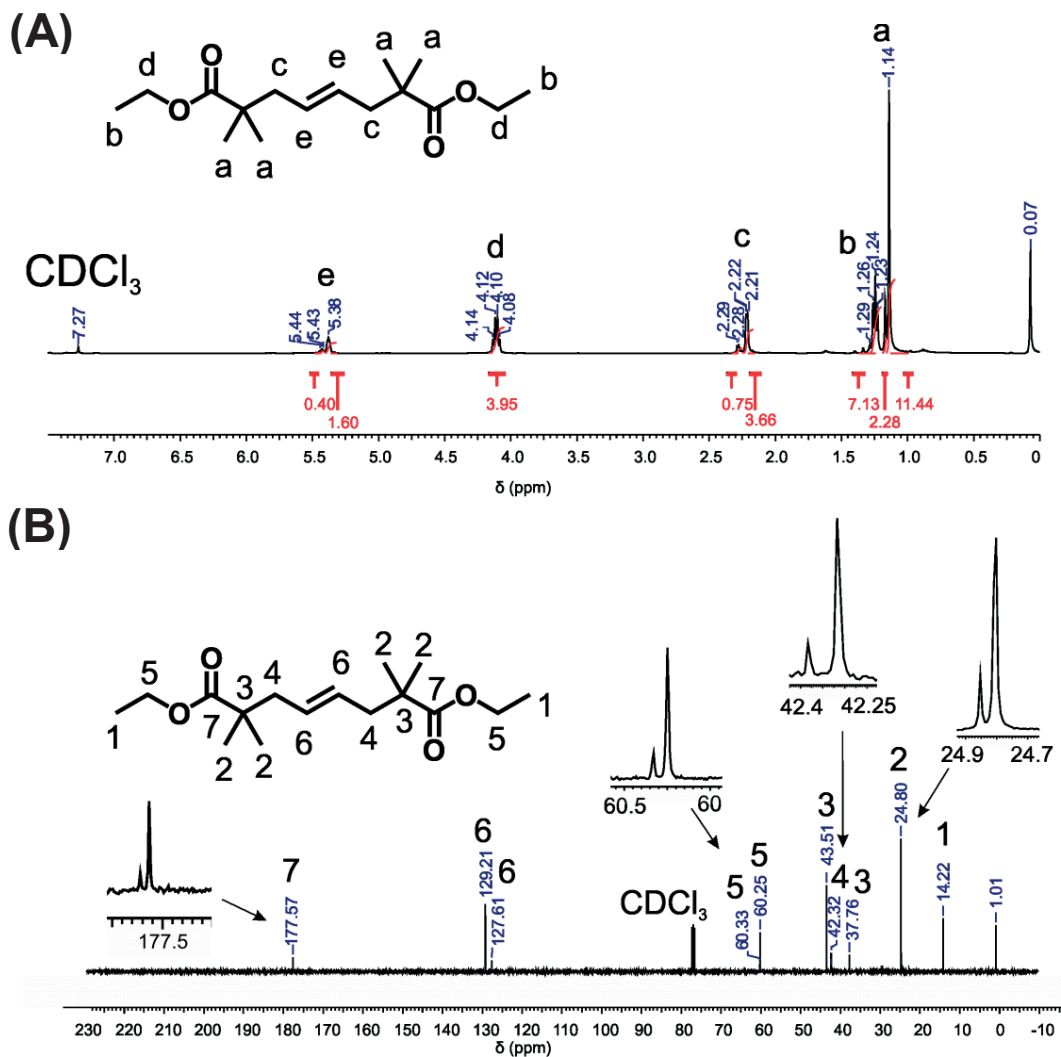


Figure S2.4. (A) ^1H NMR and (B) ^{13}C NMR spectra of diethyl 2,2,7,7-tetramethyloct-4-enedioate. Some of the signals are accompanied by smaller peaks (insets), which can be attributed to the presence of (E) and (Z)-isomers. Recorded in CDCl_3 .

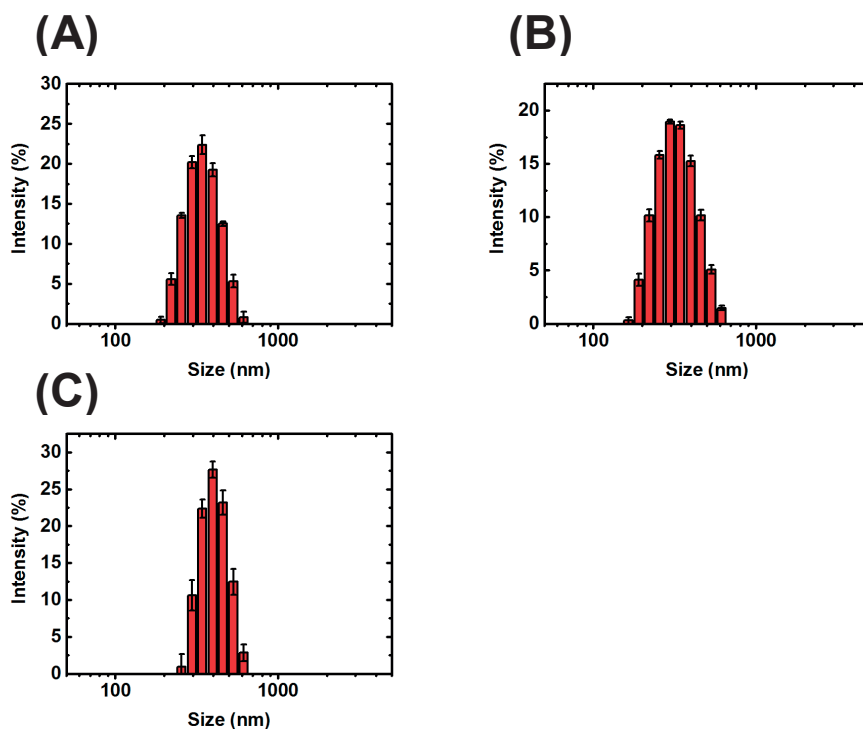


Figure S2.5. DLS size distributions from three batches of silica nanoparticles: (A) Z-average diameter = 332.4 nm, PDI = 0.037, (B) Z-average diameter = 320 nm, PDI = 0.014, (C) Z-average diameter = 411.1 nm, PDI = 0.051.

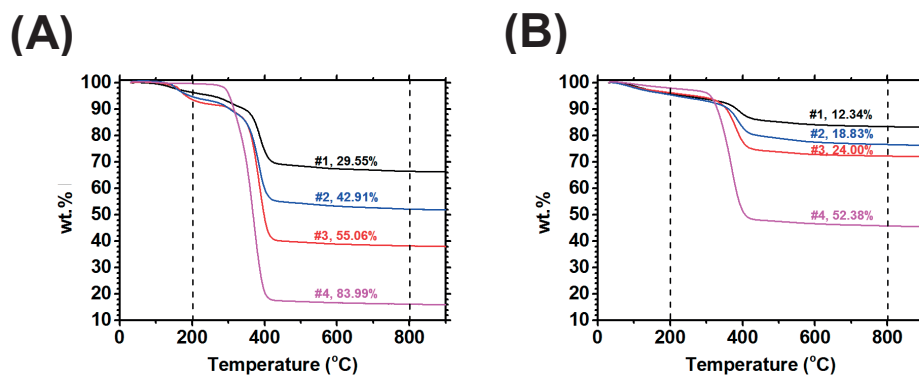


Figure S2.6. Thermogravimetric curves of silica nanoparticles grafted with PMMA brushes (A) before and (B) after cleavage at room temperature for 72 h in 0.05 M TBAF solution in HPLC grade THF. Diameter of silica nanoparticle core was 320 nm and PMMA brush thicknesses were (A) 27 (#1), 46 (#2), 68 (#3) and 157 nm (#4) before and (B) 5.5 (#1), 13.1 (#2), 19.5 and 62.8 nm (#4) after the cleavage.

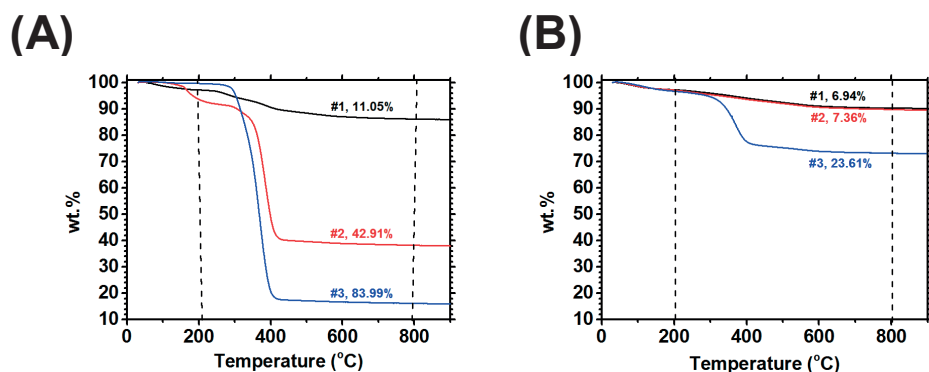


Figure S2.7. Thermogravimetric curves of silica nanoparticles grafted with PMMA brushes (A) before and (B) after cleavage at 55°C for 24 h in 0.05 M TBAF solution in HPLC grade THF. Diameter of silica nanoparticle core was 320 nm and PMMA brush thicknesses were (A) 4 (#1), 68 (#2) and 157 nm (#3) before and (B) 0 (#1, #2) and 19 (#3) nm after the cleavage.

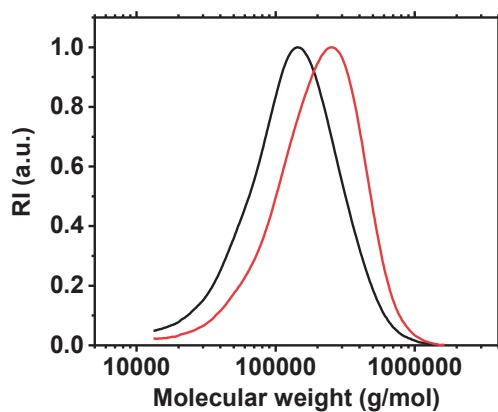


Figure S2.8. GPC traces of PMMA cleaved from silica nanoparticles ($\phi = 411$ nm) grafted by 30 min bulk SI-ATRP ($d = 91$ nm) with 10% Et₃N·3HF in THF using a reaction time of 2h (red trace) or overnight (black trace), followed by quenching and extraction.

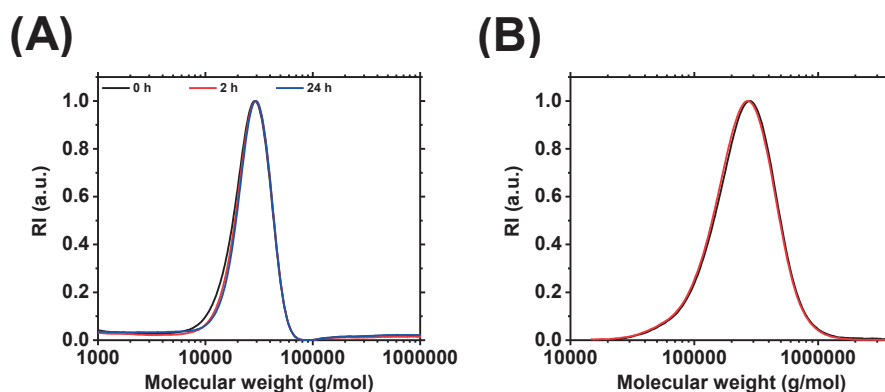


Figure S2.9. GPC traces of PMMA: (A) free PMMA chains before (black trace, #3 in **Table S2.1**) and after exposure to $\text{Et}_3\text{N}\cdot 3\text{HF}$ for 2 (red trace, #4 in **Table S2.1**) and 24 h (blue trace, #5 in **Table S5**), (B) PMMA degraded from silica nanoparticles in two separate cleaving experiments (black - #6, red trace - #7 in **Table S2.1**).

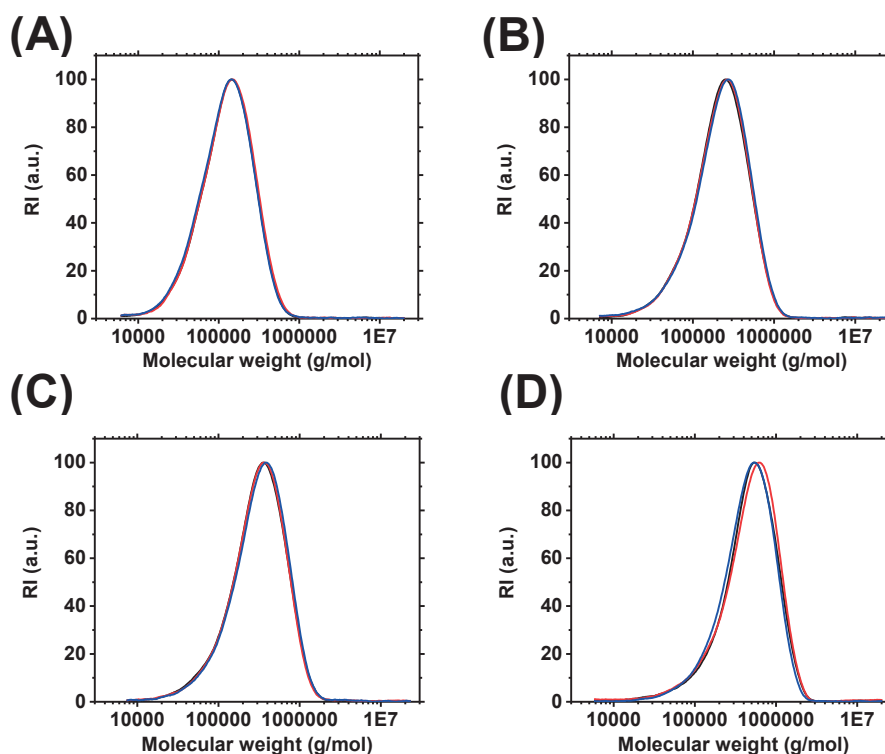


Figure S2.10. GPC traces of PMMA cleaved from PMMA-modified silica nanoparticles: (black) after SI-ARGET ATRP, (red) after functionalization with allylamine and (blue) after exposure to 1 mM 1st generation Grubbs catalyst. PMMA brushes were synthesized using polymerization time of (A) 20 min, (B) 40 min, (C) 60 min and (D) 120 min.

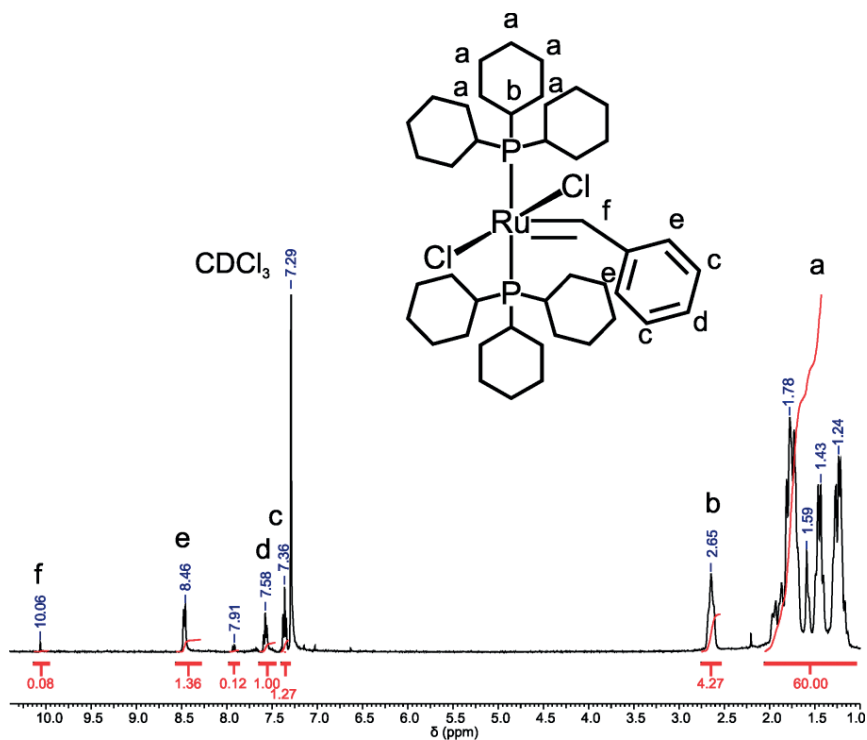


Figure S2.11. ^1H NMR spectrum of 1st generation Grubbs catalyst. Recorded in CDCl_3 . The signals were assigned according to ^{3,4}.

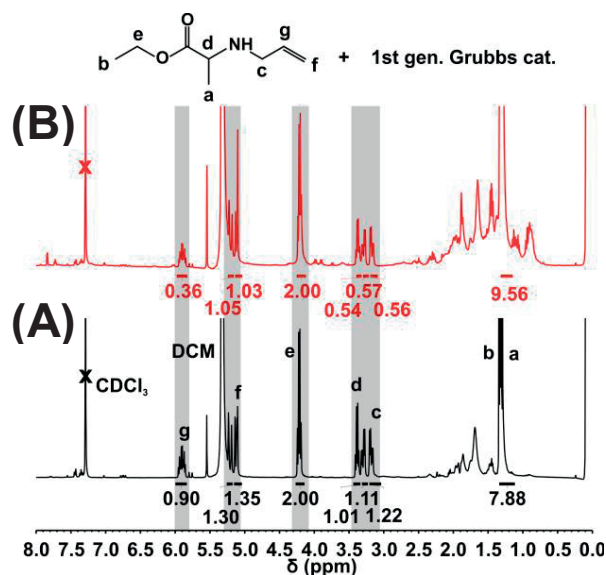


Figure S2.12. ^1H NMR spectra of ethyl 2-(2-propen-1-ylamino)propionate in the presence of 1st Generation Grubbs catalyst, taken at (A) the beginning ($t=0$) and (B) after 17 h of the reaction under reflux. The unlabeled signals can be due to the active and decomposed catalyst.⁵

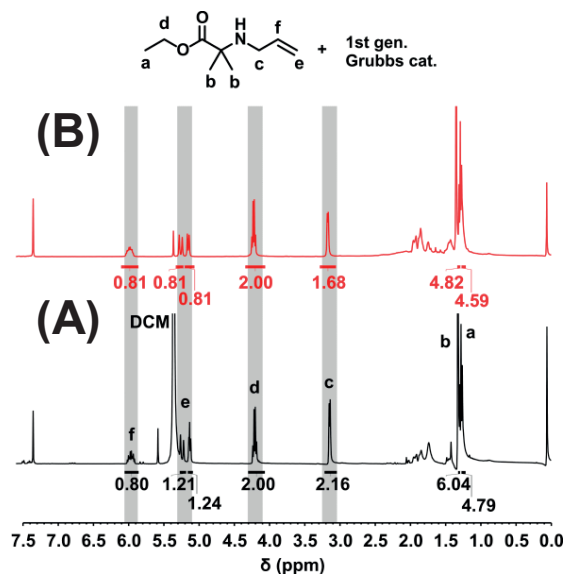


Figure S2.13. ¹H NMR spectra of ethyl 2-(2-propen-1-ylamino)isobutyrate in the presence of 1st Generation Grubbs catalyst, taken at (A) the beginning (t=0) and (B) after 18h of the reaction at room temperature. The unlabeled signals can be due to the active and decomposed catalyst.⁵

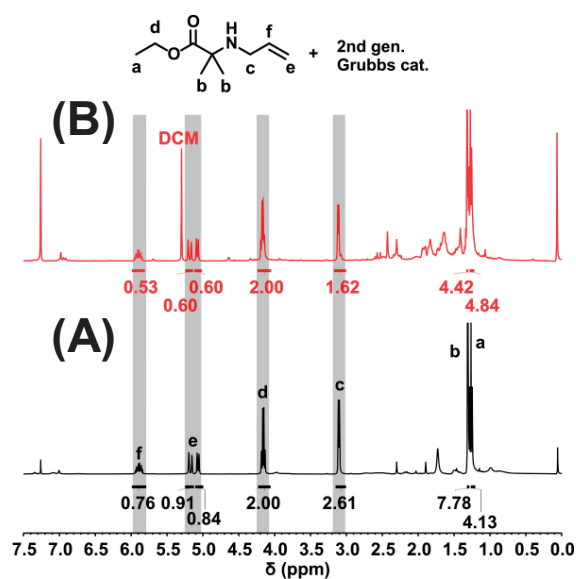


Figure S2.14. ¹H NMR spectra of ethyl 2-(2-propen-1-ylamino)isobutyrate in the presence of 2nd Generation Grubbs catalyst, taken at (A) the beginning (t=0) and (B) after 18h of the reaction at room temperature. The unlabeled signals can be due to the active and decomposed catalyst.⁵

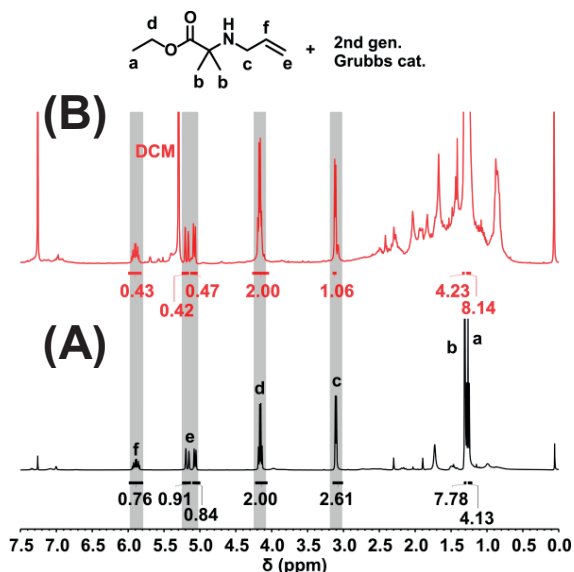


Figure S2.15. ^1H NMR spectra of ethyl 2-(2-propen-1-ylamino)isobutyrate in the presence of 2nd Generation Grubbs catalyst, taken at (A) the beginning ($t=0$) and (B) after 18h of the reaction under reflux. The unlabeled signals can be due to the active and decomposed catalyst.⁵

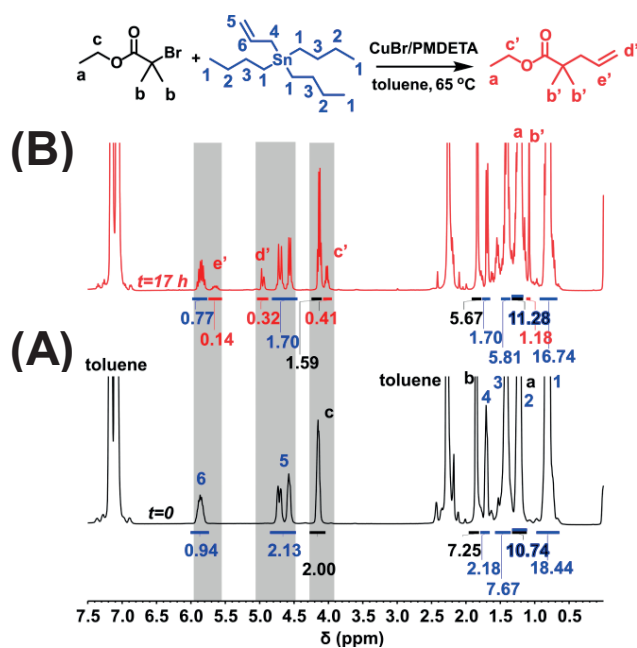


Figure S2.16. ^1H NMR spectra of ethyl 2-bromoisobutyrate, allyltributyl stannane in toluene with CuBr/PMDETA (A) at the beginning ($t=0$) and (B) after 17 h of the reaction at 65°C; signals c and c' were used to calculate the conversion: $0.41/(1.59+0.41) \cdot 100\% = 20.5\%$.

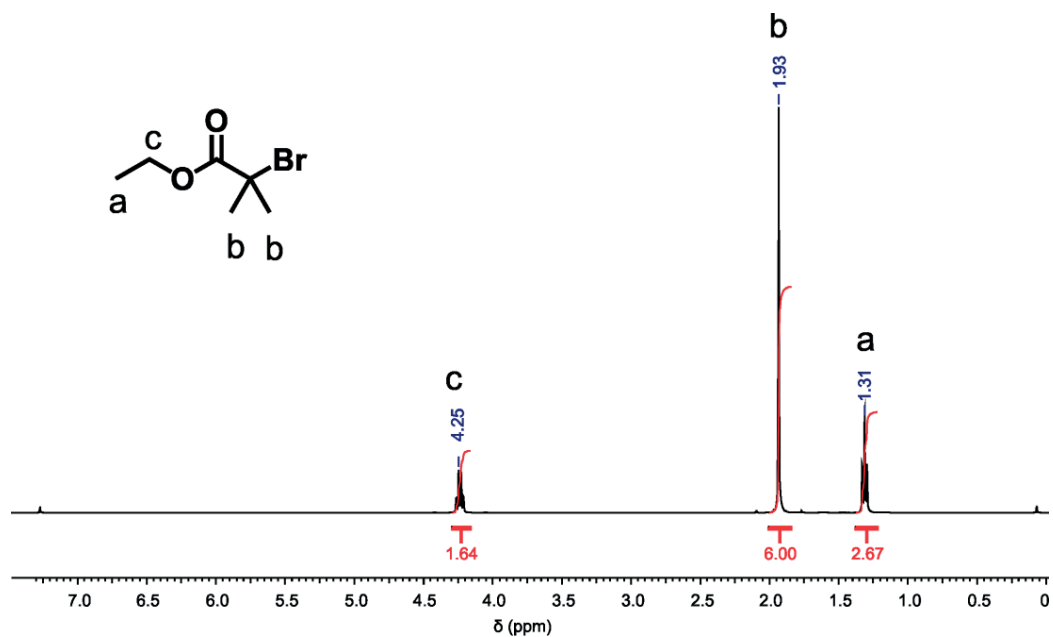


Figure S2.17. ^1H NMR spectrum of ethyl α -bromoisobutyrate. Recorded in CDCl_3 .

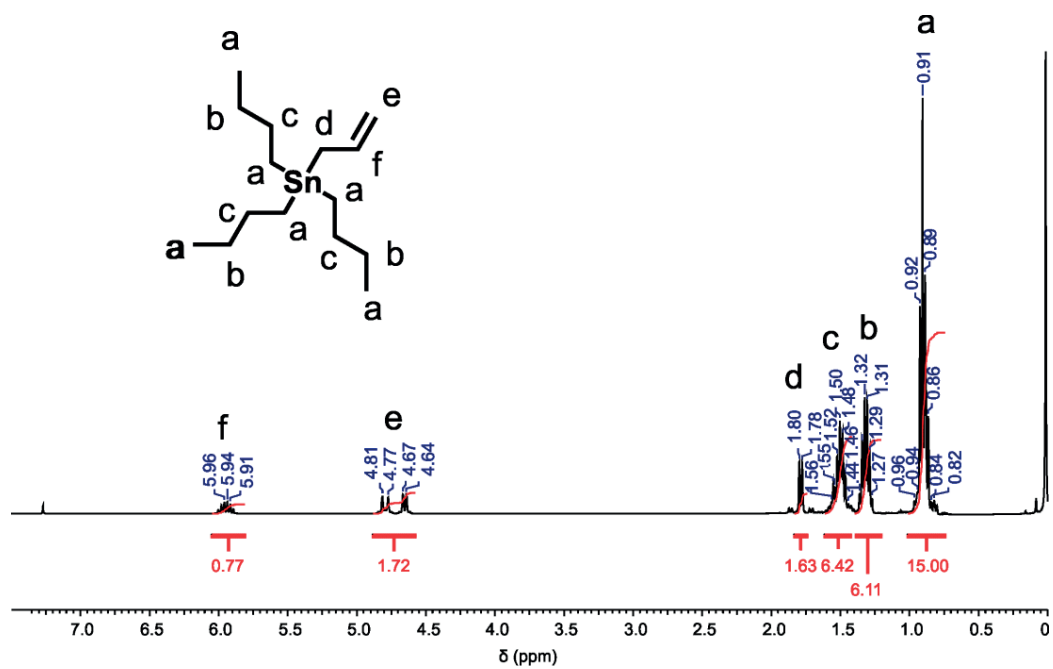


Figure S2.18. ^1H NMR spectrum of allyltributylstannane. Recorded in CDCl_3 .

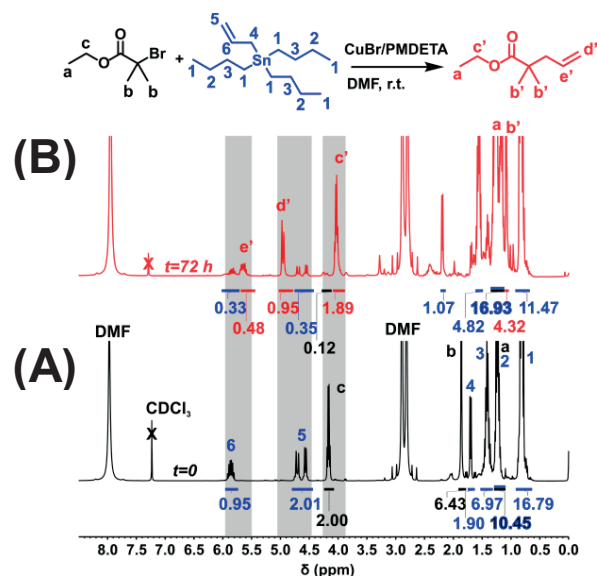


Figure S2.19. ¹H NMR spectra of ethyl 2-bromoisobutyrate and allyltributyl stannane in DMF with CuBr/PMDETA (A) at the beginning (t=0) and (B) after 72 h of reaction at room temperature. Signals c and c' were used to calculate the conversion: $1.89/(0.12+1.89) \cdot 100\% = 94.0\%$.

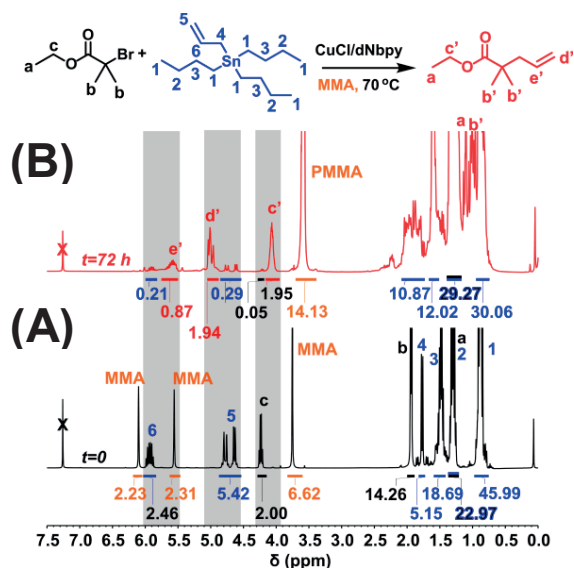


Figure S2.20. ¹H NMR spectra of ethyl 2-bromoisobutyrate and allyltributyl stannane in MMA with CuCl/dNbpy (most of the MMA was removed on a rotary evaporator) (A) at the beginning (t=0) and (B) after 72 h at 70°C. Signals c and c' were used to calculate the conversion: $1.95/(0.05+1.95) \cdot 100\% = 97.5\%$. Degree of the polymerization before complete quenching was calculated according to signals of PMMA (3.59 ppm), c and c': $14.13/(1.95+0.05) = 7.07$.

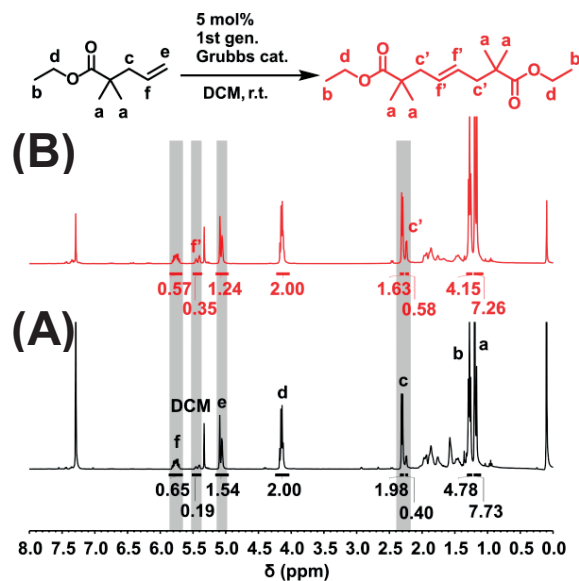


Figure S2.21. ¹H NMR spectra of ethyl 2,2-dimethyl-4-pentenoate in the presence of 1st generation Grubbs' catalyst in DCM (A) at the beginning (t=0) and (B) after 72 h of the reaction at room temperature. Product conversion can be calculated from signals f and f', $0.35/(0.57+0.35) \cdot 100\%=38.0\%$.

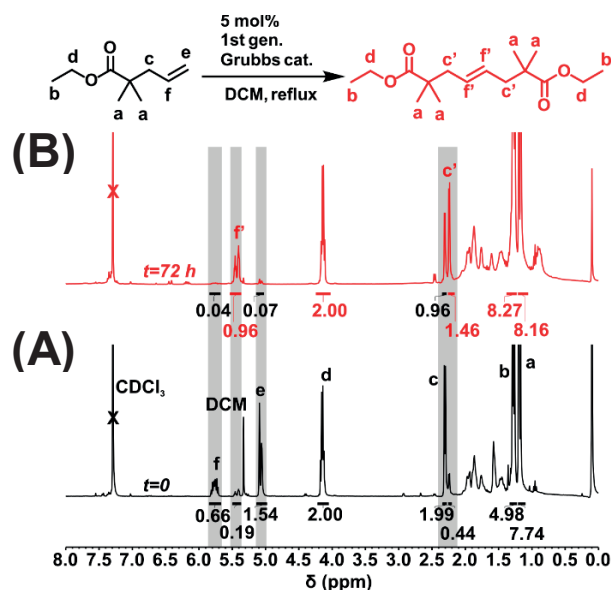


Figure S2.22. ¹H NMR spectra of ethyl 2,2-dimethyl-4-pentenoate in the presence of 1st generation Grubbs' catalyst in DCM (A) at the beginning (t=0) and (B) after 72 h of the reaction under reflux. Product conversion can be calculated from: signals f and f', $0.96/(0.04+0.96) \cdot 100\%=96.0\%$.

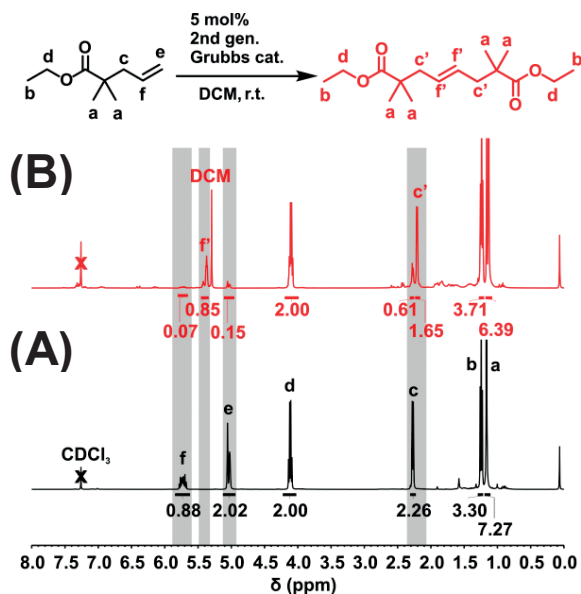


Figure S2.23. ^1H NMR spectra of ethyl 2,2-dimethyl-4-pentenoate in the presence of 2nd generation Grubbs' catalyst in DCM (A) at the beginning ($t=0$) and (B) after 72 h of the reaction at room temperature. Product conversion can be calculated from: signals f and f', $0.85/(0.07+0.85) \cdot 100\% = 92.4\%$.

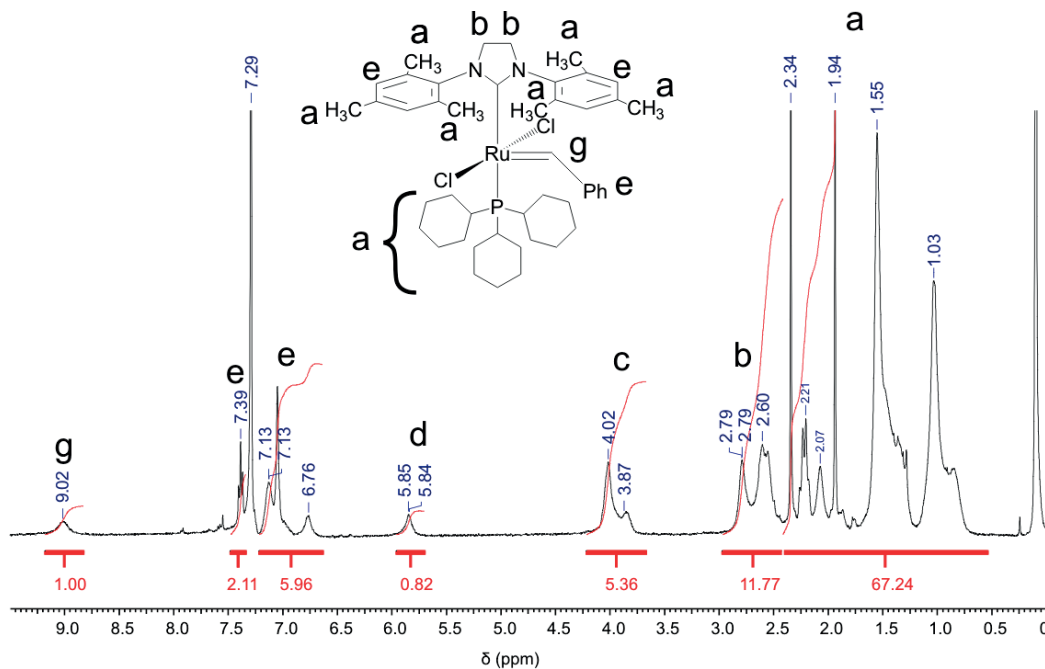


Figure S2.24. ^1H NMR spectrum of 2nd generation Grubbs catalyst. Recorded in CDCl₃. The signals were assigned according to ⁶.

References

- (1) Bartholome, C.; Beyou, E.; Bourgeat-Lami, E.; Chaumont, P.; Zydowicz, N. *Macromolecules* **2003**, *36*, 7946.
- (2) Kim, J.-B.; Huang, W.; Bruening, M. L.; Baker, G. L. *Macromolecules* **2002**, *35*, 5410.
- (3) Schwab, P.; France, M. B.; Ziller, J. W.; Grubbs, R. H. *Angewandte Chemie International Edition* **1995**, *34*, 2039.
- (4) Dinger, M. B.; Mol, J. C. *Organometallics* **2003**, *22*, 1089.
- (5) Hong, S. H.; Wenzel, A. G.; Salguero, T. T.; Day, M. W.; Grubbs, R. H. *Journal of the American Chemical Society* **2007**, *129*, 7961.
- (6) Scholl, M.; Ding, S.; Lee, C. W.; Grubbs, R. H. *Organic Letters* **1999**, *1*, 953.

3. Reversibly Crosslinked Polymer Brushes

3.1. Introduction

Tethering polymer chains via one of their chain-ends to a surface results in thin polymer films, which are referred to as polymer brushes. One approach to synthesize polymer brushes is via surface-initiated polymerization (SIP). In particular when using controlled radical polymerization (CRP) techniques, the SIP approach is versatile and allows the preparation of high grafting density polymer brushes with good control over film thickness and composition.¹⁻⁵ Although surface-initiated CRP (SI-CRP) is mostly used to produce linear surface-grafted polymers, also more complex chain-end tethered polymer topologies, such as branched, block copolymer and crosslinked brushes can be produced.

The introduction of interchain crosslinks can enhance the robustness and improve the mechanical properties of polymer brushes.⁶⁻⁹ It also leads to lower hydration / solvation and swelling ratios of the brushes. Most crosslinked polymer brushes contain permanent interchain crosslinks. An interesting, but much less explored alternative strategy is the use of reversible crosslinks. The introduction of reversible interchain crosslinks allows to dynamically modulate the crosslink density and properties of polymer brush films. There are a number of approaches that have been explored to prepare reversibly crosslinked polymer brushes.

One approach to introduce reversible interchain crosslinks is based on the complexation of ions or low molecular guests, which can bind to two (or more) functional groups in adjacent surface attached polymer chains. Poly(acrylic acid) (PAA) brushes can be crosslinked upon exposure to Ca^{2+} ions. The disruption and reformation of these physical crosslinks has been proposed to provide an energy dissipation pathway in friction experiments.¹⁰ At relatively high concentrations, poly(*N*-isopropylacrylamide) (PNIPAAm) brushes can be crosslinked by urea, which can form hydrogen bonds with the amine side-chain functional groups of the brush.¹¹ Craig, Zauscher and coworkers prepared reversibly crosslinked brushes by addition of bis(Pd^{II} -pincer) complexes to poly(4-vinylpyridine) (P4VP) brushes.¹² The authors used two different pincer-based crosslinks, which had different dissociation rates. Importantly these rates had a dramatic effect on

coefficients of friction of the layers. In addition to non-covalent interactions, also reversible covalent bonds can be used to prepare polymer brushes that contain reversible crosslinks. An interesting functional group in this context is the coumarin motif, which forms a dimer upon UV-irradiation with $\lambda > 300$ nm. UV-irradiation with $\lambda < 260$ nm leads to cleavage of these dimers. Ji and coworkers incorporated a small fraction of coumarin groups in poly(2-(dimethylamino)ethyl methacrylate) (PDMAEMA), which were grown from silica nanoparticles.¹³ By monitoring the hydrodynamic radius of the nanoparticles, these authors could demonstrate that the brushes can be crosslinked and decrosslinked over up to four cycles by alternating UV-irradiation with a wavelength of 365 and 254 nm.

Another example of a reversible covalent bond is the disulfide motif. Disulfides are formed under oxidative conditions from thiols. Under reducing conditions the disulfide bond is cleaved and the thiol group regenerated. The reductive cleavage of disulfide crosslinked polymer brushes has been used to trigger guest release from polymer brush coated mesoporous silica nanoparticles¹⁴ and has also been explored to relieve buckling patterns in planar polymer brushes.¹⁵ In these examples, the reversibility of the disulfide bond has only taken advantage of a single, reductive cleavage step. This manuscript explores the use of the disulfide motif to produce polymer brushes that can reversibly crosslink and decrosslink over multiple cycles by alternating exposure to oxidizing and reducing conditions.

3.2. Experimental Section

3.2.1. Materials

All chemicals and solvents were used as received unless stated otherwise. Dendritic copper, CuBr_2 (99.999%), CuCl (purum, $\geq 97\%$), N,N,N',N'',N''' -pentamethyldiethylenetriamine (PMDETA), tris(2-carboxyethyl)phosphine hydrochloride (TCEP) and sodium thiomethoxide (NaSAc) were purchased from Aldrich. Sodium azide, glycidyl methacrylate, propargyl bromide solution (80% in toluene) and anhydrous magnesium sulfate were supplied by Sigma. Propargyl alcohol was purchased from ABCR. 2,2'-Bipyridyl (bpy), potassium iodide and anhydrous potassium phosphate monobasic were purchased from Fluka. Potassium thioacetate was purchased from AlfaAesar. Dibasic anhydrous potassium phosphate was purchased from Fisher Scientific. Sodium bicarbonate was purchased from Riedel-de Haën. Hydrochloric acid (12 M) was purchased from VWR. Triethylamine (Merck) was distilled over KOH directly before using. 2-

(Dimethylamino)ethyl methacrylate (DMAEMA) was passed through basic alumina column to remove inhibitor. Sodium hydroxide and potassium hydroxide were purchased from Rectolab SA together with n-hexane, n-pentane, ethyl acetate and dichloromethane. Chloroform was obtained from Merck and was dried by distillation over P₂O₅. Anhydrous toluene was purified and dried using a solvent purification system (PureSolv). Deionized water was obtained from a Millipore Elix 3 purification water system. The ATRP initiator, (6-(2-bromo-2-methyl)propionyloxy)hexyldimethylchlorosilane, was synthesized as previously reported.¹⁶ 3-Azido-2-hydroxypropyl methacrylate (AzHPMA)¹⁷ and *S*-propargyl thioacetate (Pg-SAc)¹⁸ were synthesized according to literature protocols. AzHPMA was additionally purified one day before polymerization by column chromatography (silica gel, 5:2 hexane/ethyl acetate, v/v, R_f=0.5). Phosphate buffers were prepared using potassium phosphate monobasic and dibasic salts and desired pH was adjusted with potassium hydroxide or phosphoric acid using a calibrated pH-meter (SevenEasy, Mettler-Toledo).

3.2.2. Analytical methods

NMR spectroscopy. NMR spectra were recorded on a Bruker AvanceIII 400MHz spectrometer equipped with a BBFO-Plus_z 5 mm probe.

Fourier-transform reflectance infrared spectroscopy. Fourier-transform reflectance infrared spectra were acquired using a Nicolet 6700 instrument from ThermoFisher Scientific with a VariGATR grazing angle ATR accessory from Harrick Scientific Products, which was equipped with a Ge ATR crystal at an angle of incidence of 60° with 128 scans.

Water contact angle measurements. Water contact angles were determined using DataPhysics OCA 35 contact angle measurement system.

Ellipsometric analysis of dry brush film thickness. Brush thicknesses on silicon wafers were determined by means of a variable angle spectroscopic ellipsometer from Semilab ZRt (Semilab SE2000). Ellipsometric data were recorded at an incidence angle of 70° and a wavelength range of 245 – 990 nm. The ellipsometric data, consisting of the Ψ and Δ values, were analyzed using the software provided with the instrument (Spectroscopic Ellipsometry Analyzer v1.6.1 (Semilab). The calculation method was based

on a four-layer silicon/silicon oxide/polymer brush/ambient model, assuming the polymer brush to be isotropic and homogeneous. The refractive index (n) of a polymer brush layer for which no nk -file was provided is described by the Cauchy approximation ($n = A_n + B_n/\lambda^2$) and was fitted accordingly by the software together with the layer thickness. All reported ellipsometric film thicknesses were corrected for the approx. 2.5 nm-thick native oxide layer on the silicon substrates.

Ellipsometric analysis of brush crosslinking and decrosslinking. First, a silicon wafer modified with a polymer brush was mounted on a holder and immersed in 0.1 M phosphate buffer (pH 7.4) in a liquid cell. After 5 min equilibration, a measurement was taken and the sample was removed and placed in 0.1 M phosphate buffer (pH 7.4) containing 1 mg/mL TCEP for 10 min. Then, the sample was washed for 10 min in the buffer without TCEP and placed back to the liquid cell to take a measurement. After that, the sample on the holder was incubated for 2 h in an oven preheated to 60 °C under air. Once again the sample on the holder was placed to the liquid cell containing 0.1 M phosphate buffer (pH 7.4), equilibrated for 5 min and analyzed. The cycles were repeated as desired. Throughout the cycles the sample was not removed from the holder so that each time the same spot could be analyzed.

To analyze the thickness of swollen brushes, a multiple layer box model consisting of silicon/silicon oxide/ n swollen brush layers ($n=1-5$)/water was used. Parameters for Cauchy model of optical properties of a given brush were determined from dry polymer brush measurements carried out at 65, 70 and 75° incidence angles. Swollen brush thicknesses were estimated using a model composed of several (typically $n = 3-5$) slabs, with water contents that increased as the slabs were located closer to the brush-water interface. The problem with this approach is that the number of fitting variables increase with the number of slabs, which can result in high uncertainties in the film thickness. Swollen brushes were analyzed by gradually increasing the number of slabs to improve the goodness of the fit. The number of slabs was increased until the addition of a further slab only resulted in a minor improvement of the fit, while dramatically increasing uncertainties. All reported ellipsometric swollen film thicknesses include fitting uncertainties.

QCM-D experiments. Quartz crystal microbalance (QCM) experiments were carried out with a Q-Sense E4 system (Q-Sense, Sweden) using silicon oxide quartz crystals purchased from Q-sense and by analyzing third overtones of the fundamental resonance

frequency and dissipation factors. To monitor crosslinking/decrosslinking of the brushes, polymer brush coated QCM-D sensors were first exposed to deoxygenated 0.1 M phosphate buffer (pH 7.4) at 0.15 mL/min at 25 °C for 20 min. Phosphate buffer was deoxygenated by purging with nitrogen for 1 hour and subsequent sonication for 5 minutes. After that, the brush coated sensors were presented with 0.1 M phosphate buffer containing 1 mg/mL TCEP for 20 minutes at 0.15 mL/min and then with 0.1 M phosphate buffer without TCEP for 20 min. Next, air was pumped at the maximum speed of 0.579 mL/min for 2-3 min to remove the solvent from the sensor chamber. The rate was reduced back to 0.150 mL/min and the sensors were subjected to a heating ramp to 60 °C with 2 °C/min rate. Then, 60 °C temperature was maintained for 2 h to induce crosslinking by formation of disulfide bonds. The subsequent cooling to 25 °C was performed with 2 °C/min rate and simultaneous pumping the phosphate buffer at 0.15 mL/min. The cycle was repeated a desired number of times. At the end of the day the instrument was flushed with water and air, left overnight without removing the sensors and the experiment was continued the next day for more cycles. Sensors were equilibrated for 20 min after each solvent change.

3.2.3. Procedures

Preparation of ATRP initiator-modified substrates. Silicon wafers were first sonicated in acetone, ethanol, water and acetone (5 min each). The wafers were dried under a flow of nitrogen and exposed to oxygen plasma for 10 min (100 W, 5 mL/min O₂ flow). Then, the wafers were transferred immediately to a reactor, which was sealed and evacuated for at least 30 min before adding dry toluene and the ATRP initiator to afford a 5 mM initiator solution. The functionalization was allowed to proceed for 16 h at room temperature, while stirring the solution at 300 rpm. Finally, the modified substrates were removed from the reaction mixture and rinsed extensively with toluene and acetone, sonicated for 15 seconds in acetone, rinsed with ethanol, sonicated for 15 seconds in ethanol and rinsed with water and ethanol. The washed initiator-functionalized silicon wafers were dried under a flow of nitrogen and stored under nitrogen in the dark.

Surface-initiated atom transfer radical copolymerization (SI-ATRP) of 2-(dimethylamino)ethyl methacrylate (DMAEMA) and ethylene glycol dimethacrylate (EGDMA). First, ATRP-initiator functionalized silicon wafers were placed into glass vials, sealed and purged with N₂ for 15 min. Monomer stock mixture containing 5 mol% EGDMA in DMAEMA was prepared and stored under nitrogen at -20°C. 68.3 mg bpy (0.437 mmol)

was placed in a Schlenk flask. Then, 3 mL of the monomer mixture, 2.4 mL water and 3 mL methanol were added. 2.0 mg CuBr₂ (0.0090 mmol) together with 2.76 mg bpy (0.017 mmol) were added using 606 µL of a stock solution (33 mg CuBr₂, 45.6 mg bpy, 10 mL H₂O). Three freeze-pump-thaw cycles were performed to remove oxygen. 17.3 mg CuCl (0.175 mmol) was added to the frozen mixture under positive nitrogen pressure. Ratio of monomer/CuCl/CuBr₂/bpy was 2000 : 20 : 1 : 50, while volume ratio of monomer/H₂O/MeOH was 1:1:1. The flask was sealed back, evacuated, thawed and backfilled with nitrogen. Finally, the resulting dark solution was transferred with a nitrogen purged syringe into the glass vials with silicon wafers. Polymerizations were conducted at room temperature. After a predetermined polymerization time, the wafers were removed and washed with water, MeOH and acetone. Finally, the brush-modified substrates were dried and stored under N₂ at -20°C. The growth profile of these brushes is displayed in **Figure S3.1**.

Surface-initiated atom transfer radical (co)polymerization (SI-ATRP) of 2-(dimethylamino)ethyl methacrylate (DMAEMA) and 3-azido-2-hydroxypropyl methacrylate (AzHPMA). In a typical experiment, ATRP-initiator functionalized silicon wafers were placed into glass vials, sealed and purged with N₂ for 15 min. Monomer stock mixtures containing 0, 1, 5 and 10 mol% AzHPMA in DMAEMA were prepared and stored under nitrogen at -20°C for no more than one day. 68.3 mg bpy (0.437 mmol) was placed in a Schlenk flask. Then, 3 mL of the monomer mixture, 2.4 mL water and 3 mL methanol were added. After that, 2.0 mg CuBr₂ (0.0090 mmol) together with 2.76 mg bpy (0.017 mmol) were added using 606 µL of a stock solution (33 mg CuBr₂, 45.6 mg bpy, 10 mL H₂O) followed by three freeze-pump-thaw cycles. Finally, 17.3 mg CuCl (0.175 mmol) was added to the frozen mixture under positive nitrogen pressure. The flask was sealed, evacuated, thawed and backfilled with nitrogen. Ratio of monomer/CuCl/CuBr₂/bpy was 2000 : 20 : 1 : 50, while volume ratio of monomer/H₂O/MeOH was 1:1:1. Finally, the resulting dark solution was transferred with a nitrogen purged syringe into the glass vials with silicon wafers. Polymerizations were conducted at room temperature. After a predetermined polymerization time, the wafers were removed and washed with water, MeOH and acetone. Finally, the brush-modified substrates were dried and stored under N₂ at -20°C.

Surface-initiated atom transfer radical copolymerization (SI-ATRP) of 2-(dimethylamino)ethyl methacrylate (DMAEMA) with 50 mol% 3-azido-2-hydroxypropyl methacrylate (AzHPMA). For the synthesis of polymer brushes from an equimolar mixture of DMAEMA and AzHPMA, a protocol was used that is slightly different from the one presented above. First, ATRP-initiator functionalized silicon wafers were placed into glass vials, sealed and purged with N₂ for 15 min. A monomer stock mixture containing equimolar amounts of AzHPMA and DMAEMA was prepared and stored under nitrogen at -20°C for no more than one day. 34.2 mg bpy (0.219 mmol) was placed in a Schlenk flask. Then, 1.5 mL of the monomer mixture, 0.45 mL water and 2.25 mL methanol were added. After that, 1.0 mg CuBr₂ (0.0045 mmol) together with 1.38 mg bpy (0.0088 mmol) were added using 303 µL of a stock solution (33 mg CuBr₂, 45.6 mg bpy, 10 mL H₂O). Next, the mixture was subjected to three freeze-pump-thaw cycles and 8.7 mg CuCl (0.088 mmol) was added to the frozen mixture under positive nitrogen pressure. The flask was sealed back, evacuated, thawed and backfilled with nitrogen. Ratio of monomer/CuCl/CuBr₂/bpy was 2000 : 20 : 1 : 50, while volume ratio of monomer/H₂O/MeOH was 1:0.5:1.5. Finally, the resulting dark solution was transferred with a nitrogen purged syringe into the glass vials with silicon wafers. Polymerizations were conducted at room temperature. After a predetermined polymerization time, the wafers were removed and washed with water, MeOH and acetone. Finally, the brush-modified substrates were dried and stored under N₂ at -20°C.

Surface-initiated atom transfer radical polymerization (SI-ATRP) of 3-azido-2-hydroxypropyl methacrylate (AzHPMA). ATRP-initiator functionalized silicon wafers were placed into glass vials, sealed and purged with N₂ for 15 min. Then, 1.8 mg CuCl₂ (0.01339 mmol) and 92.5 mg bpy (0.5922 mmol), 2 mL water, 2 mL MeOH and 2 mL AzHPMA were added into a round bottom flask. 12.7 mg copper powder (0.1998 mmol) was added. The flask was sealed with a rubber septum and purged with a nitrogen for 30 min. Finally, the resulting dark solution was transferred with a nitrogen purged syringe into the glass vials with silicon wafers. Ratio of AzHPMA/Cu(0)/CuCl₂/bpy was 885 : 14.92 : 1 : 44.2, while volume ratio of monomer/H₂O/MeOH was 1:1:1. Polymerizations were conducted at room temperature. After a predetermined polymerization time, the wafers were removed and washed with water, MeOH and acetone. Finally, the brush-modified substrates were dried and stored under N₂ at -20°C. This protocol resulted in brushes with

a film thickness of 136 nm after a polymerization time of 5 minutes. Longer reaction times resulted in gelation of the polymerization medium.

Post-polymerization modification of P(DMAEMA-co-AzHPMA) brushes with *S*-propargyl thioacetate. First, 5 mL DMF together with Pg-SAc (11.4 mg, 10.8 μ L, 0.1 mmol) and PMDETA (17.3 mg, 21.1 μ L, 0.1 mmol) were added into a Schlenk flask with a magnetic stir bar. The flask was sealed with a rubber septum and subjected to 2 freeze-pump-thaw cycles. Then, CuBr (14.4 mg, 0.1 mmol) was added under positive nitrogen pressure. The mixture was stirred until complete dissolution of the catalyst and then transferred into previously nitrogen purged glass vessels containing the polymer brush modified surfaces. The reaction proceeded for 30 min at 0 °C at orbital shaker. The wafers were washed with DMF and methanol.

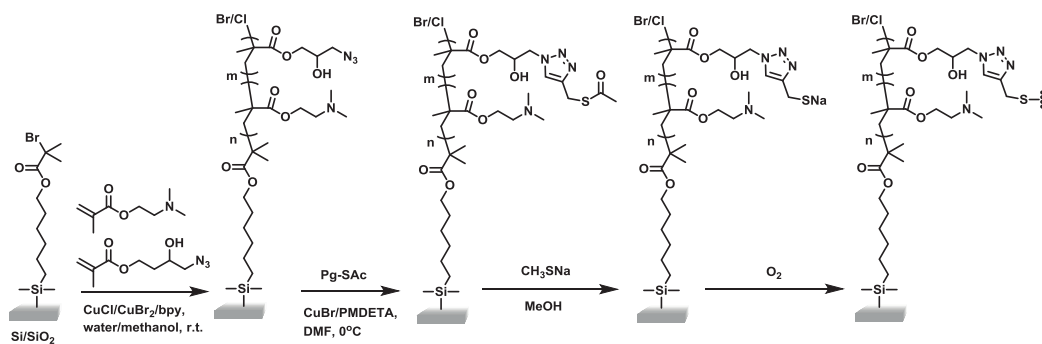
Deprotection of P(DMAEMA-co-AzHPMA)-SAC brushes. Thioacetate deprotection was performed following a literature protocol.¹⁹ To this end, P(DMAEMA-co-AzHPMA)-SAC brushes were immersed in 5 mL of a 0.2 mM solution of sodium thiomethoxide in methanol for 30 minutes under nitrogen at room temperature. After that, the samples washed with methanol and water, dried under stream of nitrogen and stored at -20°C under nitrogen.

3.3. Results and Discussion

3.3.1. Synthesis and characterization of P(DMAEMA-co-AzHPMA) copolymer brushes

Scheme 3.1 outlines the synthetic strategy that was used for the preparation of the disulfide crosslinked polymer brushes. The first step of the synthesis of these brushes is the surface-initiated atom transfer radical copolymerization of 3-azido-2-hydroxypropyl methacrylate (AzHPMA) and 2-(dimethylamino)ethyl methacrylate (DMAEMA). These copolymerization experiments were performed at room temperature using a monomer/CuCl/CuBr₂/bpy ratio = 2000/20/1/50. Initially, SI-ATRP experiments were performed in a reaction medium composed of monomer/MeOH/water 5/4/1 (v/v/v). These

reaction conditions, however, only afforded very thin brushes (below 20 nm) after 2 hours, while film thicknesses of 310-340 nm brushes were obtained after a polymerization time of 4 days. These very long reaction times also resulted in a dramatic increase in the viscosity of the reaction medium and in the formation of free (i.e. non-surface attached) polymer, which could be precipitated by the addition of water. This may be due to side reactions of the AzHPMA monomer that can lead to branching or intermolecular coupling.²⁰⁻²² To mitigate these side reactions, the water content in the reaction medium was increased and polymerizations were performed in a medium composed of monomer/MeOH/water 1:1:1. Under these conditions, copolymer brushes with thicknesses of 150 – 250 nm could be obtained within 4-10 hours from monomer feeds containing 0-10 mol% AzHPMA (**Figure 3.1**). For monomer feeds containing 50 mol% AzHPMA however, the use of these concentrations resulted in very fast polymerization and gelation of the polymerization medium already after 10 minutes. Polymerization of equimolar mixture of AzHPMA and DMAEMA therefore were performed in monomer/MeOH/water ratio of 1:1.5:0.5. Brush growth was also found to be accelerated, when AzHPMA was used that had been stored for more than a few days. In order to assure reproducible brush growth, the AzHPMA monomer was purified by column chromatography a day before each polymerization.



Scheme 3.1.

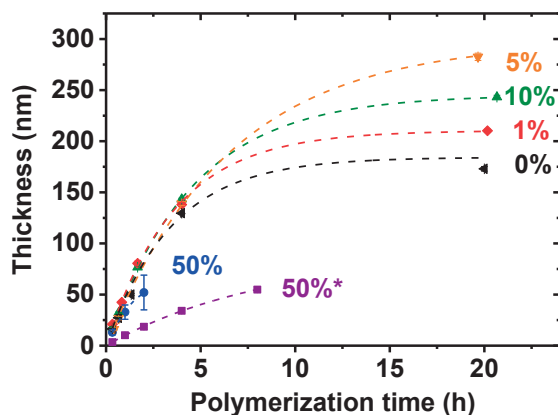


Figure 3.1. Evolution of dry film thickness as a function of polymerization time for the SI-ATRP of DMAEMA and AzHPMA with different contents of AzHPMA in the feed; monomer/MeOH/water ratio (vol./vol.) was 1:1:1, and for experiment (*) it was 1:1.5:0.5. (\blacktriangleleft) PDMAEMA, (\blacklozenge) P(DMAEMA-co-1%AzHPMA), (\blacktriangledown) P(DMAEMA-co-5%AzHPMA), (\blacktriangle) P(DMAEMA-co-10%AzHPMA), (\bullet , \blacksquare) P(DMAEMA-co-50%AzHPMA). Lines are used to guide the eye.

All of the copolymer brushes that will be discussed in the remainder of this manuscript were prepared with a polymerization time of 4 hours. The P(DMAEMA-co-AzHPMA) brushes were analyzed by FTIR spectroscopy and XPS. **Figure 3.2** shows FTIR spectra of a PDMAEMA homopolymer brush and P(DMAEMA-co-AzHPMA) copolymer brushes generated from monomer feeds containing 1%, 5%, 10% or 50% AzHPMA. Incorporation of the AzHPMA comonomer resulted in the appearance of a signal at 2101 cm^{-1} , which can be assigned to the N=N=N stretching band. The intensity of this signal gradually increased as the relative amount of AzHPMA in the monomer feed increased.

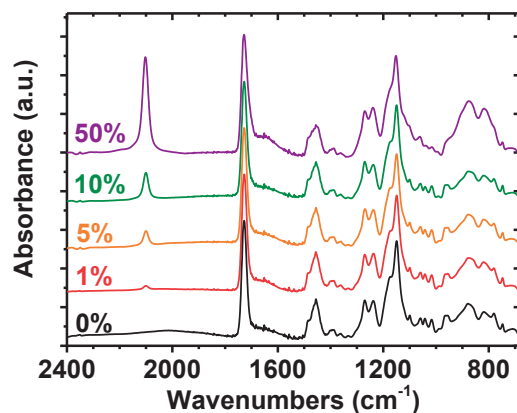


Figure 3.2. ATR-FTIR spectra of a PDMAEMA homopolymer brush (black) and P(DMAEMA-co-AzHPMA) copolymer brush generated from monomer feeds containing 1 (red), 5 (orange), 10 (green) or 50 mol% (purple) AzHPMA. The spectra have been normalized to the signal at 1727 cm^{-1} .

Figure 3.3 compares C 1s and N 1s XPS high resolution scans of a PDMAEMA homopolymer brush, a P(DMAEMA-co-AzHPMA) copolymer brush obtained from a monomer feed containing equimolar amounts of the two monomers, and PAzHPMA homopolymer brush (discussion, high resolution scans and binding energies for different copolymer brush compositions are provided in Supporting Information, **Figure S3.2** and **Table S3.1**). In C 1s scans intensity of a signal “3” at $285.7\text{--}285.9\text{ eV}$, associated with $\underline{\text{C}}\text{-N/C-OH}$, is decreasing with increasing AzHPMA content in the brush. However, the amount of $\underline{\text{C}}\text{-N}$ species is lower than calculated according to the chemical composition, i.e. 21.7 vs. 33.1% for P(DMAEMA-co-50%AzHPMA), but it applies also for PAzHPMA, where it is only 14% , as compared to theoretical 28.6% . The N 1s scans revealed more substantial changes. PDMAEMA sample features an amine ($\underline{\text{N}}\text{-C}$ species) signal “a” at $399.3\text{--}399.6\text{ eV}$ and small fraction (less than 10%) of protonated amine species. The copolymer brush shows additionally strongly shifted azide components at “c” 400.9 ($\underline{\text{N}}=\underline{\text{N}}^+=\underline{\text{N}}^-$) and “d” 404.6 eV ($\text{N}=\underline{\text{N}}^+=\underline{\text{N}}^-$). Their theoretical relative ratio is $2:1$, while we observed it at $3.7:1$. We also observed slightly lower nitrogen atomic concentration than expected, i.e. 12.4 vs. 16.1% . Similar result was observed for PAzHPMA, for which the signal ratio c/d is $2.5:1$ (vs. theoretical $2:1$) and the nitrogen atomic concentration is 12.8% , lower than theoretical 23.1% . We associate all these discrepancies with the decomposition of azides under X-ray irradiation during the XPS analysis. The ratio of azide “d” at 404.6 eV to amine “a” component at $399.3\text{--}399.6\text{ eV}$ in P(DMAEMA-co-50%AzHPMA)

copolymer brush suggests incorporation of only 20.6% of AzHPMA in the brush (= d/a ratio), however the degradation of azides and build-up of degradation side products falling at 399.3-399.6 eV leads to a severe underestimation.^{23,24} In fact, the signal ratio d/a for PAzHPMA homopolymer brush is only 54.9% and thus half of the azide groups could have transformed into amine species under X-ray irradiation and contributed to the “a” signal. If similar extent of the degradation occurred for P(DMAEMA-co-50%AzHPMA), the AzHPMA content would be close to its content in the feed.

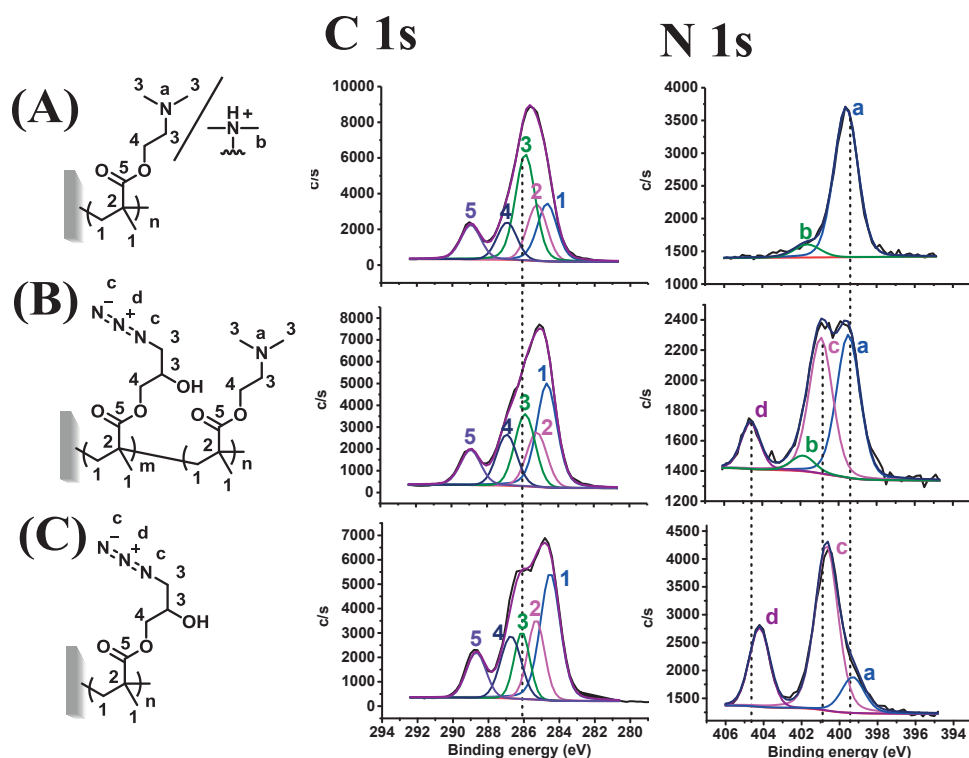


Figure 3.3. XPS C 1s and N 1s high resolution scans of (A) a PDMAEMA homopolymer brush, (B) a P(DMAEMA-co-AzHPMA) copolymer brush produced from a monomer feed containing equimolar amounts of DMAEMA and AzHPMA, and (C) PAzHPMA homopolymer brush.

3.3.2. Post-polymerization modification of P(DMAEMA-co-AzHPMA) copolymer brushes

To introduce the thiol side chain functional groups, the P(DMAEMA-co-AzHPMA) brushes were modified with *S*-propargyl thioacetate (Pg-SAc) via copper(I)-catalyzed azide-alkyne cycloaddition (CuAAC). CuAAC post-polymerization modification of the copolymer brushes was performed using CuBr/PMDETA in DMF at 0 °C for 30 min.

Figure 3.4 compares FTIR spectra of P(DMAEMA-co-AzHPMA) brushes produced from monomer feeds containing 1-50 mol% AzHPMA before and after CuAAC post-polymerization modification with *S*-propargyl thioacetate. Reaction of brushes obtained using 1-10 mol% AzHPMA with *S*-propargyl thioacetate resulted in complete disappearance of the azide signal at 2101 cm^{-1} . For brushes prepared from a monomer feed containing 50 mol% AzHPMA, the FTIR analysis also revealed a strong decrease in the intensity of the azide signal. In this case however, the spectrum of the post-polymerization modified brush still indicated the presence of remaining, unreacted azide groups ($\sim 35\%$). Analysis of the carbonyl region of the FTIR spectrum of this sample reveals a shoulder at $\sim 1693 \text{ cm}^{-1}$, which can be attributed to the thioacetate carbonyl stretching band.

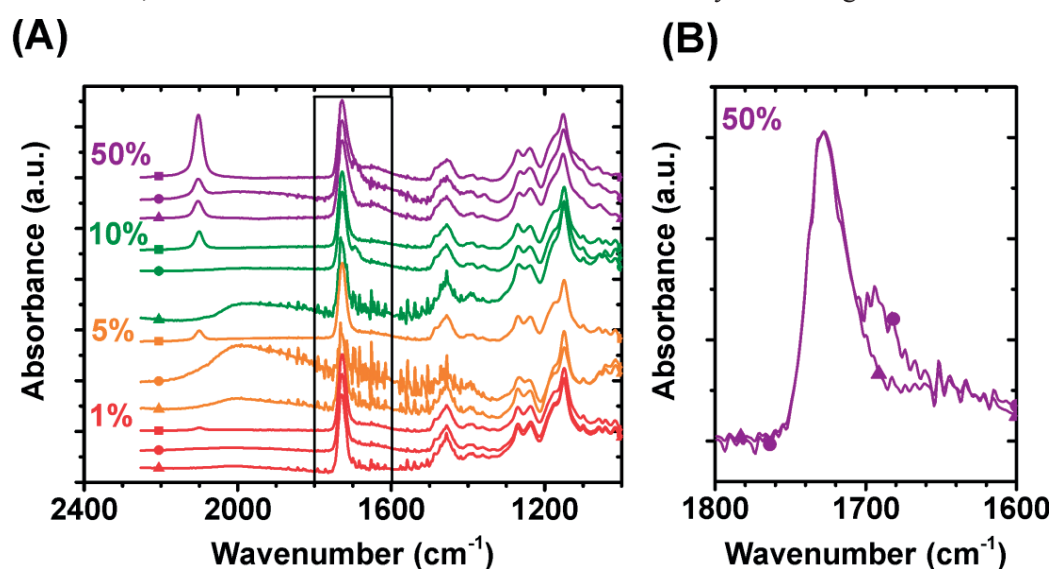


Figure 3.4. (A) ATR-FTIR spectra of P(DMAEMA-co-AzHPMA) brushes produced from monomer feeds containing 1%, 5%, 10% and 50% AzHPMA before post-polymerization modification (\blacksquare), after CuAAC with *S*-propargyl thioacetate (\bullet), and after reaction with sodium thiomethoxide (\blacktriangle). (B) Carbonyl region of FTIR spectra of a P(DMAEMA-co-AzHPMA) copolymer brush obtained from equimolar amounts of DMAEMA and AzHPMA after CuAAC of *S*-propargyl thioacetate (\bullet) and after reaction with sodium thiomethoxide (\blacktriangle). The spectra are normalized with respect to the signal at 1727 cm^{-1} .

Figure 3.5 compares C 1s, N 1s and S 2p high resolution scans of a P(DMAEMA-co-AzHPMA) brushes prepared from an equimolar mixture of DMAEMA and AzHPMA before and after CuAAC post-polymerization modification with *S*-propargyl thioacetate. First, triazole components “f” and “b” at 400.1-400.3 and 401.4-401.9 eV^{25,26} replaced the azide signals “c” and “d” in N 1s scans. Their relative ratio was 2.3:1, close to the theoretical 2:1, which may suggest a full conversion. On the first sight it may seem like a

discrepancy between FTIR and XPS. However, penetration depths of these two techniques are dramatically different, i.e. for ATR-FTIR it is in the range of a few micrometers, while for XPS it is limited to ca. 10 nm. Therefore, it seems that the reaction does not occur homogeneously, but its yield is higher at the surface. Finally, the S 2p scans revealed further evidence for the successful attachment of thioacetate. The copolymer brush prior to modification did not display any sulfur species. After the CuAAC, the brush showed a major signal “I” at 162.4 eV, associated with thioacetate groups.²⁷ Worth noting are the small signals of more oxidized sulfur species “II” and “III” (sulfinate $-\text{SO}_2^-$ and sulfonate $-\text{SO}_3^{2-}$) at 164.9, and 167.3 eV.²⁸ It shows that the installed thioacetate can over-oxidize on air. The surfaces were also analyzed ellipsometrically after the modification, but because of the small molecular weight of introduced thioacetate, the changes were very small (Table 3.1).

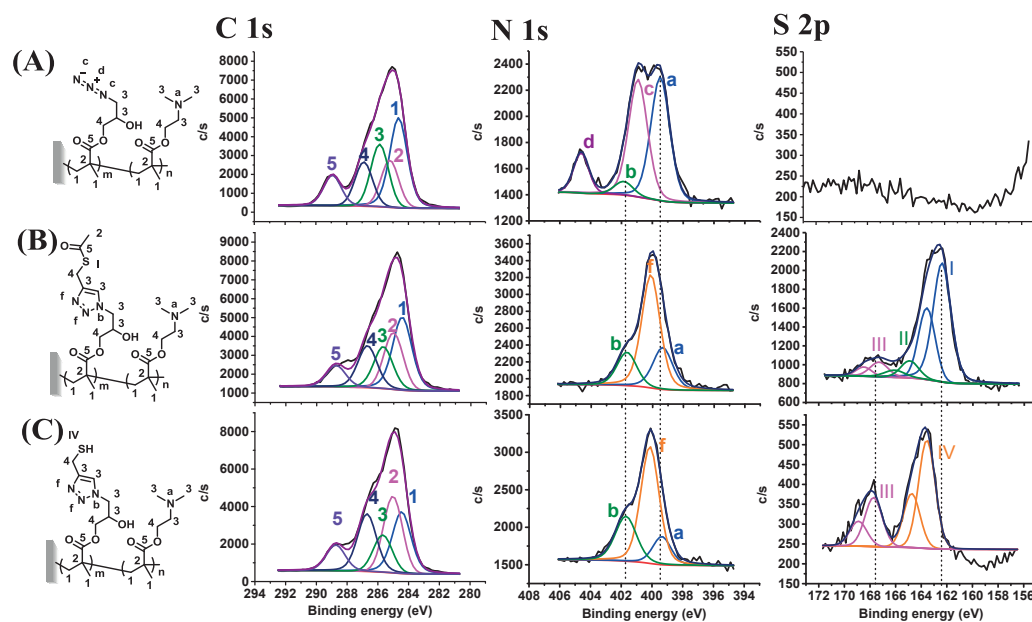


Figure 3.5. XPS C 1s, N 1s and S 2p high resolution scans of (A) P(DMAEMA-co-AzHPMA) copolymer brush produced from a monomer feed containing equimolar amounts of DMAEMA and AzHPMA, and its modified counterparts: (B) after CuAAC with *S*-propargyl thioacetate and (C) after subsequent deprotection of thioacetate with sodium thiomethoxide.

Table 3.1. List of dry thicknesses of the non-modified and modified P(DMAEMA-co-AzHPMA) brushes obtained by 4 h SI-ATRP. Theoretical thicknesses upon post-polymerization modification are given in parentheses. The measured thicknesses were determined by ellipsometry; mean values and standard deviations represent measurements taken at 9 equally spaced points of each sample.

Func-tion-aliza-tion	PDMAEMA	PDMAEMA-co-X%AzHPMA			
		X = 1%	X = 5%	X = 10%	X = 50%
-	N.A.	104.4 ± 6.1	126.9 ± 2.9	131.2 ± 3.9	N.A.
SAc	N.A.	97.1 ± 7.9 (105.1)	134.2 ± 1.5 (131.5)	142.5 ± 2.5 (140.6)	N.A.
SH	N.A.	80.0 ± 4.5 (104.9)	124.16 ± 0.95 (129.8)	136.5 ± 1.4 (137.1)	N.A.

The first step of the synthesis of the thiol side-chain functionalized brushes included the deprotection of the thioacetate groups with thiomethoxide in methanol. This reaction was monitored with FTIR spectroscopy and XPS. In the FTIR spectra of a brush obtained by copolymerization of equimolar amounts of DMAEMA and AzHPMA, treatment with thiomethoxide resulted in disappearance of the thioester carbonyl bands at 1693 cm^{-1} (**Figure 3.4**). Comparison of the S 2p high resolution scans of the same brush before and after reaction with thiomethoxide also revealed changes that are consistent with the (quantitative) deprotection of the thioacetate groups (**Figure 3.5**). In the S 2p high resolution scan of the protected brush, the main signal, which is due to the sulfur atoms in the thioacetate side-chain functional groups, is located at 162.4 eV. In the spectrum of the corresponding deprotected brush, the main signal is shifted to 163.6 eV, which is consistent with the formation of thiol/disulfide groups.²⁷ However again, the S 2p scans revealed presence of oxidized species “III”, this time only at higher binding energy of 167.3 eV and at higher content, which may indicate higher tendency of deprotected brushes to over-oxidize on air.

Worth noting are also side effects of using sodium thiomethoxide for deprotecting the polymer brushes. Ellipsometry measurements of the samples exposed to thiomethoxide revealed a small decrease of film thicknesses, which was mostly pronounced for the brush comprising 1% of AzHPMA (**Table 3.1**). The thicknesses decreased by 17.1, 10.0 and 6.0

nm for the brushes with 1%, 5% and 10% AzHPMA, respectively. Thus, the degrafting of polymer chains seems to be more pronounced at lower contents of relatively hydrophobic AzHPMA. The degrafting behavior of the samples exposed to the media used in our post-polymerization modification reactions are displayed in **Figure S3.3**.

3.3.3. Dynamic behavior of reversibly crosslinked polymer brushes

The introduction of interchain disulfide bonds is expected to change the swelling behavior as well as the viscoelastic properties of the brushes. To study the effect of crosslinking and decrosslinking on the swelling behavior and viscoelastic properties, the polymer brushes were studied with ellipsometry and quartz crystal microbalance with dissipation monitoring (QCM-D). For the formation of disulfides from thiols, a number of reaction conditions can be used, including DMSO,²⁹ H₂O₂,²⁹ H₂O₂/I₂,³⁰ H₂O₂/NaI³⁰ and Fenton reagent (Fe(II)/citrate/cysteine).³¹

The use of H₂O₂, however, may lead to overoxidation and the use of iodide, iodine or the Fenton reagent leads to complexation of I⁻ or Fe²⁺ by the DMAEMA units in the brush, which would complicate ellipsometry and QCM-D experiments. The P(DMAEMA-co-AzHPMA) copolymer brushes investigated in this study, however, were already found to crosslink upon exposure to ambient air for 30 min. The process could be accelerated and driven to completion by exposing the brush films to air at 60 °C for 2 hours. Decrosslinking could be accomplished by incubating the polymer brushes in a 1 mg/mL solution of TCEP in 0.1 M phosphate buffer at pH 7.4. Decrosslinking of the brushes results in an increase in the swelling ratio. In a series of experiments with P(DMAEMA-co-AzHPMA) brushes, obtained from polymerization feed containing 10% AzHPMA, the influence of the incubation time of the TCEP solution on the swelling ratio was studied. These experiments revealed a relatively rapid increase in the swelling ratio at short incubation times, which levelled off at incubation times longer than 10 minutes (**Figure S3.4**). As a consequence, a reaction time of 10 min was used for the decrosslinking of the brushes.

To study the swelling behavior of the brushes in the crosslinked and decrosslinked states, polymer brush samples were analyzed by ellipsometry. Samples were first exposed to 1 mg/mL TCEP in 0.1 M phosphate buffer for 10 min to cleave disulfide bonds and induce decrosslinking. Then, the brushes were washed by incubation in the buffer for 10 min and placed in a liquid cell, where the swollen film thickness was measured. After that, the brush samples were dried under a flow of air during 5 seconds, and crosslinked by heating at 60 °C for 2 h at ambient air.

Subsequently, the brush films were placed back in 0.1 M phosphate buffer in the liquid cell and the swollen thickness of the crosslinked brush was measured. This cycle was repeated several times and the dry film thickness measured after each crosslinking and decrosslinking step. **Figure 3.6** compares the swelling ratios of thiol functionalized P(DMAEMA-co-AzHPMA) brushes, which were obtained from monomer feeds containing 10% AzHPMA, with two different film thicknesses, with those of a PDMAEMA homopolymer brush and a permanently crosslinked P(DMAEMA-co-EGDMA) brush. **Figure 3.6** clearly illustrates the reversible nature of the disulfide crosslinks. The swelling ratios of the P(DMAEMA-co-AzHPMA)-SH brushes increase and decrease in a repeating and reversible fashion for up to 8 steps of exposure to TCEP and air. However, we noticed that after multiple steps (7 or 5 steps for **Figure 3.6A** and **Figure 3.6B**) the trends become inconsistent, which can be attributed to potential over-oxidation or degrafting of the brushes, which complicates the ellipsometric measurement. The non-crosslinked and permanently crosslinked control brushes, in contrast, do not reveal any variations in swelling behavior upon exposure to the same conditions.

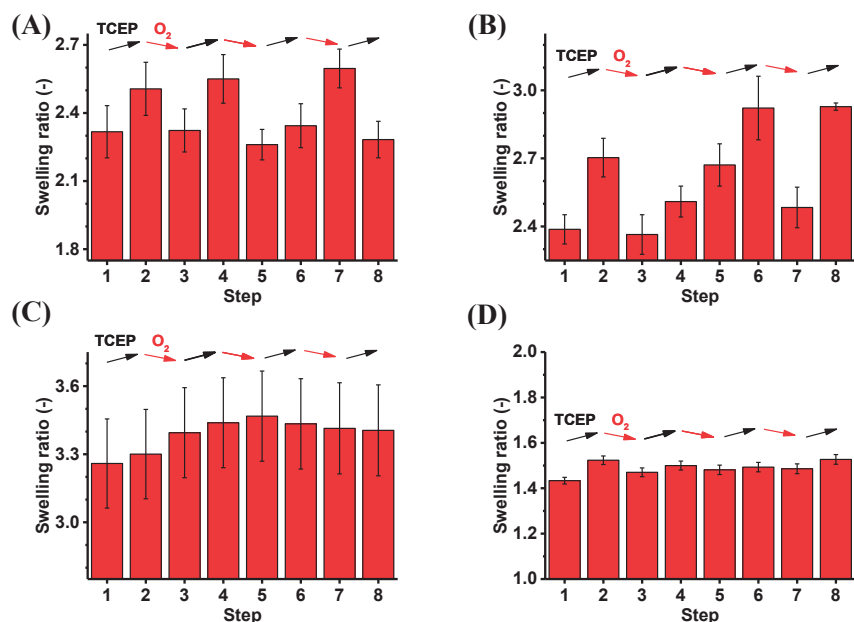


Figure 3.6. P(DMAEMA-co-AzHPMA) copolymer brush bearing thiol groups (161 nm, **A** and 86 nm, **B**), PDMAEMA homopolymer brush (57 nm, **C**), and P(DMAEMA-co-EGDMA) copolymer brush (94 nm, **D**) after exposure to TCEP (1 mg/mL in 0.1 M phosphate buffer, pH 7.4), and air while heated at 60°C; these steps caused the thiol-functionalized brushes to decrosslink and crosslink, respectively. The copolymer brushes were obtained from monomer feeds containing either 10% AzHPMA or 5% EGDMA to afford similar number of crosslinks.

The reversible crosslinking and decrosslinking of thiol functionalized brushes obtained from SI-ATRP copolymerization of a monomer feed containing 10 mol% AzHPMA was also studied by QCM-D. **Figure 3.7** plots changes in frequency (Δf) and dissipation (ΔD) of the 3rd harmonic overtone measured on a QCM-D sensor chip modified with a 129.1 nm thick brush. At $t = 0$, the crosslinked brush is placed in the liquid cell. Starting at $t = 7.5$ min a 0.1 M phosphate buffer (pH 7.4) is pumped over the QCM-D chip at a flow rate of 0.150 mL/min. This results in a sharp drop in frequency and an increase in the dissipation. These changes reflect the hydration (uptake of water) of the brush and the concomitant increase in viscoelastic character of the brush film. At $t = 31$ min, 1 mg/mL TCEP is introduced in the buffer, which is passed over the brush-modified sensor chip. This results in an instantaneous decrease in Δf and, more importantly, an increase in ΔD . The latter indicates a further increase in the viscoelastic properties of the brush, which is consistent with decrosslinking of the brush. At $t = 52$ min, the temperature of the sample chamber was set to 60 °C and air pumped over the brush for 120 min in order to re-crosslink the brush. When the brush was then exposed again to 0.1 M phosphate buffer at 25 °C, the Δf and ΔD were similar to those observed at the beginning of the 1st cycle, indicating the reversibility of the process. **Figure S3.5** shows the evolution of Δf and ΔD when this brush sample is exposed to 7 subsequent cycles of crosslinking and decrosslinking. The bonding is fully reversible in the first two cycles. At a later stage, however, the changes in Δf and ΔD upon treatment with TCEP become gradually less pronounced. This would be consistent with a slow reduction of the crosslink density of the brush, which may be the result of overoxidation and loss of thiol groups. Other figures displaying raw QCM data (with up to 13th overtones) for 22.4 and 129.1 nm brushes are given in Supporting information in **Figure S3.6**, **Figure S3.7** and **Figure S3.8** and they follow the same trends described here. Additionally, the evolutions of shifts of 3rd harmonic frequencies and dissipation factors are displayed in **Figure S3.9**. They indicate the lowering contrast between two opposite states at further cycles, which could be due to degrafting of polymer chains.

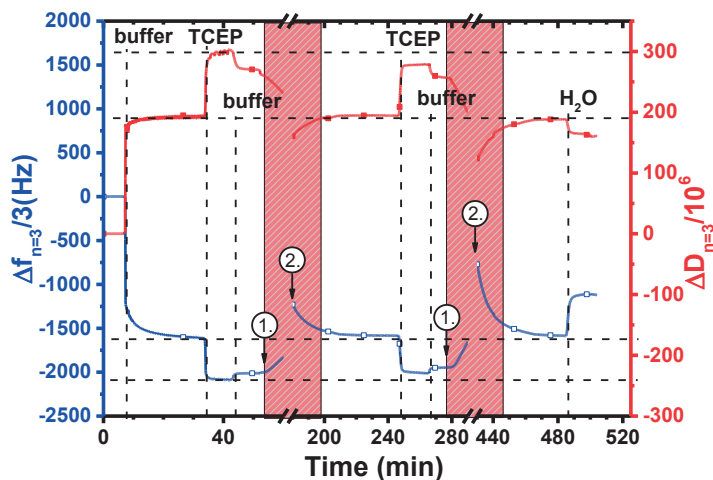


Figure 3.7. Shifts of harmonic frequencies and dissipation factor recorded for a QCM chip grafted with 129.1 nm thick PDMAEMA-co-AzHPMA copolymer brush bearing thiol groups upon exposure to phosphate buffer (pH 7.4, 0.1 M), TCEP (1 mg/mL in the buffer), air (heated up to 60°C, **1.**) and again cooled with the buffer (temperature was set to 20°C, **2.**) (a crosslinking step, marked in red). The copolymer brush was obtained from monomer feed containing 10% AzHPMA. To improve readability heating steps were cut out (see x-axis breaks at 60-180 and 290-430 min). The test was concluded with flushing with water and air to reduce degrafting during overnight storage.

3.4. Conclusions

We presented a synthetic strategy to install different crosslinks onto polymer brush platforms, which will allow for the systematic investigation of their impact on the stability and properties of polymer brushes. The synthesis comprises a two step-process: SI-ATRP to generate P(DMAEMA-co-AzHPMA) copolymer brush platform, and post-polymerization modification with CuAAC of *S*-propargyl thioacetate. Prior protection of the thiol linker with acetate was necessary for compatibility with CuAAC. The polymerization of DMAEMA with AzHPMA with up to 50% AzHPMA was well controlled and films with up to 280 nm could be generated. The modifications were readily followed by FTIR (azide signals) and ellipsometry (thickness changes). XPS provided a supporting evidence for chemical changes, including among others transformation of azide groups into triazole rings (shifts from 400.9, 404.6 to 399.5, 400.2 eV), attachment of thioacetate (S 2p signal at 162.4 eV) and deprotection to thiols (thiol S 2p signal at 163.6 eV).

The reversible crosslinking within PDMAEMA-co-10%AzHPMA-SH brushes was shown by ellipsometric swelling tests, and QCM-D measurements. Shifts in resonance frequency and dissipation marked changes in both swelling and chain mobility. The oxidation and reduction steps could have been easily carried out by 2 h 60°C heating stage under air and incubation in 1 mg/mL TCEP in 0.1 M phosphate buffer, pH 7.4.

XPS measurements were performed by Pierre Mettraux from the MHMC of the EPFL.

3.5. References

- (1) Zoppe, J. O.; Ataman, N. C.; Mocny, P.; Wang, J.; Moraes, J.; Klok, H.-A. *Chemical Reviews* **2017**, *117*, 1105.
- (2) Barbey, R.; Lavanant, L.; Paripovic, D.; Schüwer, N.; Sugnaux, C.; Tugulu, S.; Klok, H.-A. *Chemical Reviews* **2009**, *109*, 5437.
- (3) Gosecka, M.; Basinska, T. *Polymers for Advanced Technologies* **2015**, *26*, 696.
- (4) Wu, L.; Glebe, U.; Boeker, A. *Polymer Chemistry* **2015**, *6*, 5143.
- (5) Chen, W.-L.; Cordero, R.; Tran, H.; Ober, C. K. *Macromolecules* **2017**, *50*, 4089.
- (6) Ramakrishna, S. N.; Cirelli, M.; Kooij, E. S.; Klein Gunnewiek, M.; Benetti, E. M. *Macromolecules* **2015**, *48*, 7106.
- (7) Dehghani, E. S.; Spencer, N. D.; Ramakrishna, S. N.; Benetti, E. M. *Langmuir* **2016**, *32*, 10317.
- (8) Zhang, J.; Xiao, S.; Shen, M.; Sun, L.; Chen, F.; Fan, P.; Zhong, M.; Yang, J. *RSC Advances* **2016**, *6*, 21961.
- (9) Lilge, I.; Schönherr, H. *European Polymer Journal* **2013**, *49*, 1943.
- (10) Dunér, G.; Thormann, E.; Ramström, O.; Dédinaité, A. *Journal of Dispersion Science and Technology* **2010**, *31*, 1285.
- (11) Micciulla, S.; Michalowsky, J.; Schroer, M. A.; Holm, C.; von Klitzing, R.; Smiatek, J. *Physical Chemistry Chemical Physics* **2016**, *18*, 5324.
- (12) Loveless, D. M.; Abu-Lail, N. I.; Kaholek, M.; Zauscher, S.; Craig, S. L. *Angewandte Chemie International Edition* **2006**, *45*, 7812.
- (13) Dong, Z.; Mao, J.; Wang, D.; Yang, M.; Ji, X. *Langmuir* **2015**, *31*, 8930.
- (14) Wan, X.; Wang, D.; Liu, S. *Langmuir* **2010**, *26*, 15574.

- (15) Guo, W.; Reese, C. M.; Xiong, L.; Logan, P. K.; Thompson, B. J.; Stafford, C. M.; Ievlev, A. V.; Lokitz, B. S.; Ovchinnikova, O. S.; Patton, D. L. *Macromolecules* **2017**, *50*, 8670.
- (16) Schüwer, N.; Klok, H. -A. *Advanced Materials* **2010**, *22*, 3251.
- (17) Gao, C.; Zheng, X. *Soft Matter* **2009**, *5*, 4788.
- (18) Schuster, T.; Schellenberger, S.; Friedrich, R.; Klapper, M.; Müllen, K. *Journal of Fluorine Chemistry* **2013**, *154*, 30.
- (19) Wallace, O. B.; Springer, D. M. *Tetrahedron letters* **1998**, *39*, 2693.
- (20) Anderson, G. T.; Henry, J. R.; Weinreb, S. M. *The Journal of Organic Chemistry* **1991**, *56*, 6946.
- (21) Broeckx, W.; Overbergh, N.; Samyn, C.; Smets, G.; L'abbé, G. *Tetrahedron* **1971**, *27*, 3527.
- (22) Li, Y.; Yang, J.; Benicewicz, B. C. *Journal of Polymer Science Part A: Polymer Chemistry* **2007**, *45*, 4300.
- (23) Saad, A.; Abderrabba, M.; Chehimi, M. M. *Surface and Interface Analysis* **2017**, *49*, 340.
- (24) Zorn, G.; Liu, L.-H.; Árnadóttir, L.; Wang, H.; Gamble, L. J.; Castner, D. G.; Yan, M. *The Journal of Physical Chemistry C* **2013**, *118*, 376.
- (25) Heinrich, T.; Traulsen, C. H.-H.; Darlatt, E.; Richter, S.; Poppenberg, J.; Traulsen, N. L.; Linder, I.; Lippitz, A.; Dietrich, P. M.; Dib, B. *RSC Advances* **2014**, *4*, 17694.
- (26) Gouget-Laemmel, A.; Yang, J.; Lodhi, M.; Siriwardena, A.; Aureau, D.; Boukherroub, R.; Chazalviel, J.-N.; Ozanam, F.; Szunerits, S. *The Journal of Physical Chemistry C* **2012**, *117*, 368.
- (27) Wenzler, L.; Moyes, G.; Raikar, G.; Hansen, R.; Harris, J.; Beebe, T.; Wood, L.; Saavedra, S. *Langmuir* **1997**, *13*, 3761.
- (28) Willey, T. M.; Vance, A. L.; Van Buuren, T.; Bostedt, C.; Terminello, L.; Fadley, C. *Surface Science* **2005**, *576*, 188.
- (29) Yiannios, C.; Karabinos, J. *The Journal of Organic Chemistry* **1963**, *28*, 3246.
- (30) Kirihara, M.; Asai, Y.; Ogawa, S.; Noguchi, T.; Hatano, A.; Hirai, Y. *Synthesis* **2007**, *2007*, 3286.
- (31) Goessl, A.; Tirelli, N.; Hubbell, J. A. *Journal of Biomaterials Science, Polymer Edition* **2004**, *15*, 895.

3.6. Supporting Information

Calculation of swollen brush thicknesses

Brush thickness at swollen state was calculated as twice the first moment of the thickness profile that was obtained by fitting the ellipsometric results. This strategy transforms more complicated brush profiles into equivalent single box profiles with the same integrated areas and the same first moments.¹ Such obtained swollen brush thickness d^* serves as a representative value and is used to calculate swelling ratios.

The fitted thickness profiles consisted of maximum 5 layers ($n = 5$) of constant hydration that was increasing towards the bulk water medium. Number of layers was selected to maximize the fit and minimize resulting uncertainties of thickness of each layer and the percentages of its polymer/water components.

The d^* was calculated as follows:

$$d^* = \frac{2 \int_0^\infty z\varphi(z)dz}{\int_0^\infty \varphi(z)dz} = \frac{\sum_{i=1}^n [(\sum_{j=1}^i z_j)^2 - (\sum_{j=1}^{i-1} z_j)^2] \cdot \varphi_i}{\sum_{i=1}^n z_i \varphi_i} =$$

$$= \frac{z_1^2 \varphi_1 + \dots + ((z_1 + \dots + z_n)^2 - (z_1 + \dots + z_{n-1})^2) \varphi_n}{z_1 \varphi_1 + \dots + z_n \varphi_n}$$

Calculation of theoretical brush thicknesses of post-polymerization modified brushes

The theoretical thickness changes were calculated according to the equations below. Knowing that molecular weights of DMAEMA, AzHPMA units and introduced Pg-SAC linkers are 157.21, 184.17 and 114.17 g/mol, and assuming $x\%$ AzHPMA content in the brushes we can calculate average molecular weight of a monomer unit in the initial ($M_{av,1}$) and modified ($M_{av,2}$) brush:

$$M_{av,1} = 157.21 \cdot \left(1 - \frac{x}{100\%}\right) + 184.17 \cdot \frac{x}{100\%}$$

$$M_{av,2}(SAC) = 157.21 \cdot \left(1 - \frac{x}{100\%}\right) + (184.17 + 114.17) \cdot \frac{x}{100\%}$$

Then, theoretical thickness of a final brush with a full conversion is:

$$d_{theo} = d_{initial} \cdot \frac{M_{av,2}}{M_{av,1}}$$

Therefore, a yield for the CuAAC protocol is:

$$\eta_{CuAAC} = \frac{d}{d_{theo}} \cdot 100\%$$

CuAAC of the 131.2 nm copolymer brushes with 10% AzHPMA units with Pg-SAC resulted in dry thickness of 142.5 nm, and:

$$d_{theo} = 131.2 \text{ nm} \cdot \frac{171.3}{159.9} = 140.6 \text{ nm}$$

$$\eta_{CuAAC} = \frac{142.5 \text{ nm}}{140.6 \text{ nm}} \cdot 100\% > 100\%$$

Similarly, the results for other brushes comprising 1 and 5% AzHPMA also suggest quantitative reactions. The next step for installation of thiol linkers, i.e. the deprotection of thioacetate functionalized brushes resulted in a decrease of dry film thickness, which cannot be explained by the loss of acetate group. These results suggest degrafting of the polymer chains during the process. A control experiment for degrafting was carried out on homopolymer PDMAEMA brushes in the media used for post-polymerization modification (**Figure S3.3A**). Additionally, swelling of the PDMAEMA in these media is shown in **Figure S3.3B**. The experiment indicates that degrafting of polymer chains occurs in DMF, but to a substantial degree only when sodium thiomethoxide is added. It is interesting to note that this reagent is considered to be mild and not interfering with functional groups, such as enone, lactone, carboxylic acid, hydroxyl and ester.² Because the experiment was done on a non-crosslinked brushes and for twice as long exposure time, the degrafting should be reduced in the applied post-polymerization modification protocols. No alternative deprotection strategies were explored.

Discussion of XPS signals. XPS measurements served as a supplementary technique to FTIR to confirm successful (co)polymer brush synthesis and post-polymerization modification. **Figure S3.2a** shows deconvoluted C 1s and N 1s scans, which fit well to the PDMAEMA chemical structure.³ In C 1s high resolution scans C sp³ signals are observed at 284.5-284.7 eV (**Figure S3.2a**, curve 1).³⁻⁵ The characteristic C-C=O, C-O-C=O and C=O signals of PDMAEMA are observed at 285.0-285.2, 286.7-286.9 and 288.7-289.0, respectively (**Figure S3.2a**, curves 2, 4 and 5, respectively).^{3,4} The carbon atoms adjacent to tertiary amine display binding energy (BE) of 285.7-285.9 eV (**Figure S3.2a**, curve 3).^{3,4} In N 1s high resolution scans, the pronounced feature at 399.3-399.6 eV (**Figure S3.2a**, curve a) is attributed to the amine group,⁴ while the signal at 401.4-401.9 eV has been previously associated with a partial protonation of the PDMAEMA amine (**Figure S3.2a**, curve b).^{4,6} XPS binding energies for each chemical state of carbon and nitrogen together with respective component concentrations are listed in **Table S3.1**. Unfortunately, the XPS measurements did not reveal any substantial changes between copolymer brushes composed of 0 – 10% AzHPMA. Additional measurements were carried out on PAzHPMA brushes to identify its characteristic signals. The deconvolutions fit well to the chemical

structure of PAzHPMA.⁷ In C 1s high resolution scans C sp³ signals are observed at 284.5 eV (**Figure S3.2f**, curve 1).⁷ The C-C=O, C-O-C=O and C=O signals of DMAEMA and AzHPMA units are observed at 285.3, 286.7 and 288.7, respectively (**Figure S3.2f**, curves 2, 4' and 5', respectively). The azide and hydroxyl carbon signal is placed at a BE of 286.1 eV (**Figure S3.2f**, curve 3').⁷ Although the nitrogen content (12.4% instead of 23.1%) and C-N/C-OH chemical state contribution (286.1 eV, 14% instead of 28.6%) seem to be rather low, they can be rationalized by instability of azide groups under X-rays during XPS measurement.^{8,9} The degradation of azide groups has been previously associated with formation of nitrene species.⁸ This supports an observation of an amine signal at 399.3 eV, which is a product of an intercalation of a reactive nitrene into -C-H, C-C or C-OH bonds. Nevertheless, the azide group is clearly visible on N 1s scan with its characteristic features of well separated signals at 400.7 and 404.2 eV at a ratio of 2.5:1 (close to theoretical 2:1), which is a consequence of the charged resonance structure of this group.^{7,10,11} However, these signals were only observed on copolymer brush P(DMAEMA-co-AzHPMA) sample composed of 50% AzHPMA. This could be a result of a degradation of azide groups, which are there otherwise only in small amounts. On the other hand, there are examples of azide-type monolayers in the literature that have been successfully characterized by XPS. Monolayers could be more prone to damage by X-rays, because their functional groups are much more exposed. However, their analysis can be facilitated by limiting the measurement time to a few seconds. Typical solutions include either a “snapshot” mode or high pass energy settings (e.g. 80 eV) that allow researchers to obtain high number of counts with a good resolution.⁸

Table S3.1. Elements and their chemical state concentrations, derived from XPS on PDMAEMA, P(DMAEMA-co-AzHPMA) and PAZHPMA brush samples. Values in parentheses represent theoretical values according to the chemical structures.

Element	Overall							
	PDMAEMA	PDMAEMA-co-1%AzHPMA	PDMAEMA-co-5%AzHPMA	PDMAEMA-co-10%AzHPMA	PDMAEMA-co-50%AzHPMA	PAZHPMA	PDMAEMA-co-50%AzHPMA-SAC	PDMAEMA-co-50%AzHPMA-SH
C	68.9% (72.7%)	68.1% (72.5%)	70.7% (71.8%)	67.0% (70.8%)	61.1% (63.3%)	57.8% (53.8%)	61.3% (66.4%)	62.5% (65.8%)
N	6.7% (9.1%)	5.7% (9.2%)	7.4% (9.8%)	5.9% (10.5%)	12.4% (16.1%)	12.4% (23.1%)	7.4% (12.1%)	7.4% (13.4%)
O	21.8% (18.2%)	23.4% (18.2%)	21.9% (18.4%)	23.4% (18.7%)	26.2% (20.7%)	26.2% (23.1%)	22.9% (19.1%)	24.4% (17.9%)
S	-	-	-	-	-	-	4.7% (2.5%)	0.9% (3%)
Si	2.6% (0%)	2.9% (0%)	0.1% (0%)	3.7% (0%)	3.7% (0.0%)	3.7% (0.0%)	3.7% (0%)	4.8% (0.0%)
N/C ratio	0.097 (0.125)	0.084 (0.127)	0.105 (0.136)	0.088 (0.148)	0.203 (0.277)	0.215 (0.429)	0.121 (0.182)	0.118 (0.204)
S/C ratio	-	-	-	-	-	-	0.077 (0.038)	0.014 (0.046)

Table S3.1. (Continued)

Band position	N 1s							
	PDMAEMA	PDMAEMA- co- 1%AzHPMA	PDMAEMA- co- 5%AzHPMA	PDMAEMA- co- 10%AzHPMA	PDMAEMA- co- 50%AzHPMA	PAzHPMA	PDMAEMA-co- 50%AzHPMA-SAC	PDMAEMA-co- 50%AzHPMA-SH
399.3-399.6 (a, N- C/triazole)	91.4% (100%)	86.5% (97.1%)	87.1% (86.4%)	87.7% (75.0%)	43.1% (25%)	13.5% (N.A.)	23.5% (25%)	14.2% (25%)
400.1-400.3 (f, triazole)	-	-	-	-	-	-	58.7% (50%)	59.5% (50%)
400.9 (c, N=N ⁺ =N ⁻)	0% (0%)	0% (1.9%)	0% (9.1%)	0% (16.7%)	41.0% (50%)	61.9% (66.7%)	-	-
401.4-401.9 (b, NH ⁺ - C/triazole)	8.7% (N.A.)	13.5% (N.A.)	12.9% (N.A.)	12.3% (N.A.)	4.7% (N.A.)	-	17.8% (25%)	26.3% (25%)
404.6 (d, N=N ⁺ =N ⁻)	0% (0%)	0% (1.0%)	0% (4.5%)	0% (8.3%)	11.2% (25%)	24.6% (33.3%)	-	-

Table S3.1. (Continued)

Band position	C 1s							
	PDMAEMA	PDMAEMA- CO- 1%AzHPMA	PDMAEMA- CO- 5%AzHPMA	PDMAEMA- CO- 10%AzHPMA	PDMAEMA- CO- 50%AzHPMA	PzHPMA	PDMAEMA-co- 50%AzHPMA-SAC	PDMAEMA-co- 50%AzHPMA-SH
284.5-								
284.7 (1, C-C)	20.8% (25.0%)	22.5% (25.0%)	29.3% (25.2%)	14.6% (25.4%)	34.9% (26.8%)	38.1% (28.6%)	32.5% (20.9%)	25.3% (22.5%)
285.0-								
285.2 (2, C-C=O)	18.6% (12.5%)	22.2% (12.5%)	14.6% (12.6%)	20.1% (12.7%)	16.6% (13.4%)	19% (14.3%)	22.3% (14.6%)	27.8% (11.3%)
285.7-								
285.9 (3, C-N/C-OH/C-S)	36.6% (37.5%)	31.6% (37.4%)	29.5% (37.1%)	36.3% (36.6%)	21.7% (33.1%)	14% (28.6%)	17.9% (35.4%)	13.7% (43.8%)
286.7-								
286.9 (4, C-O-C=O/C-S-C=O)	12.2% (12.5%)	12.4% (12.5%)	17.1% (12.6%)	15.9% (12.7%)	15.5% (13.4%)	17.1% (14.3%)	18.1% (14.6%)	23.0% (11.3%)
288.7-								
289.0 (5, C=O)	11.8% (12.5%)	11.3% (12.5%)	9.6% (12.6%)	13.1% (12.7%)	11.3% (13.4%)	11.7% (14.3%)	9.1% (14.6%)	10.2% (11.3%)

Table S3.1. (Continued)

S 2P_{3/2}

Band position	Percentage							
	PDMAEMA	PDMAEMA- CO- 1%AzHPMA	PDMAEMA- CO- 5%AzHPMA	PDMAEMA- CO- 10%AzHPMA	PDMAEMA- CO- 50%AzHPMA	PAzHPMA	PDMAEMA-co- 50%AzHPMA-SAC	PDMAEMA-co- 50%AzHPMA-SH
162.4 (S-Ac)	-	-	-	-	-	-	79.6% (100%)	-
163.6 (S-H)	-	-	-	-	-	-	-	67.9% (100%)
164.9 (SO ₂ ⁻)	-	-	-	-	-	-	10.8% (N.A.)	-
167.3 (SO ₃ ²⁻)	-	-	-	-	-	-	9.6% (N.A.)	32.1% (N.A.)

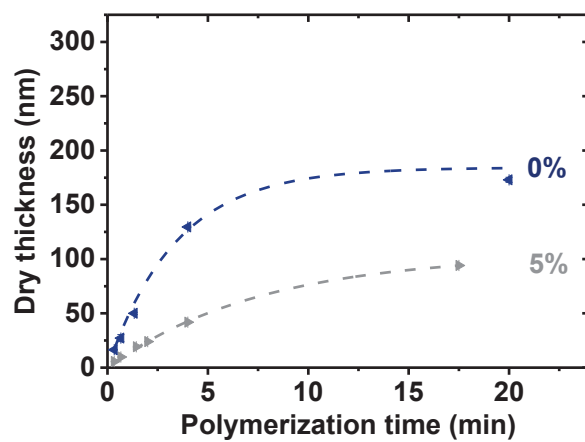


Figure S3.1. Growth profiles of (◄) PDMAEMA homopolymer brush and (►) P(DMAEMA-co-EGDMA) copolymer brush; monomer/MeOH/water ratio (vol./vol.) was 1:1:1. Lines are used to guide the eye.

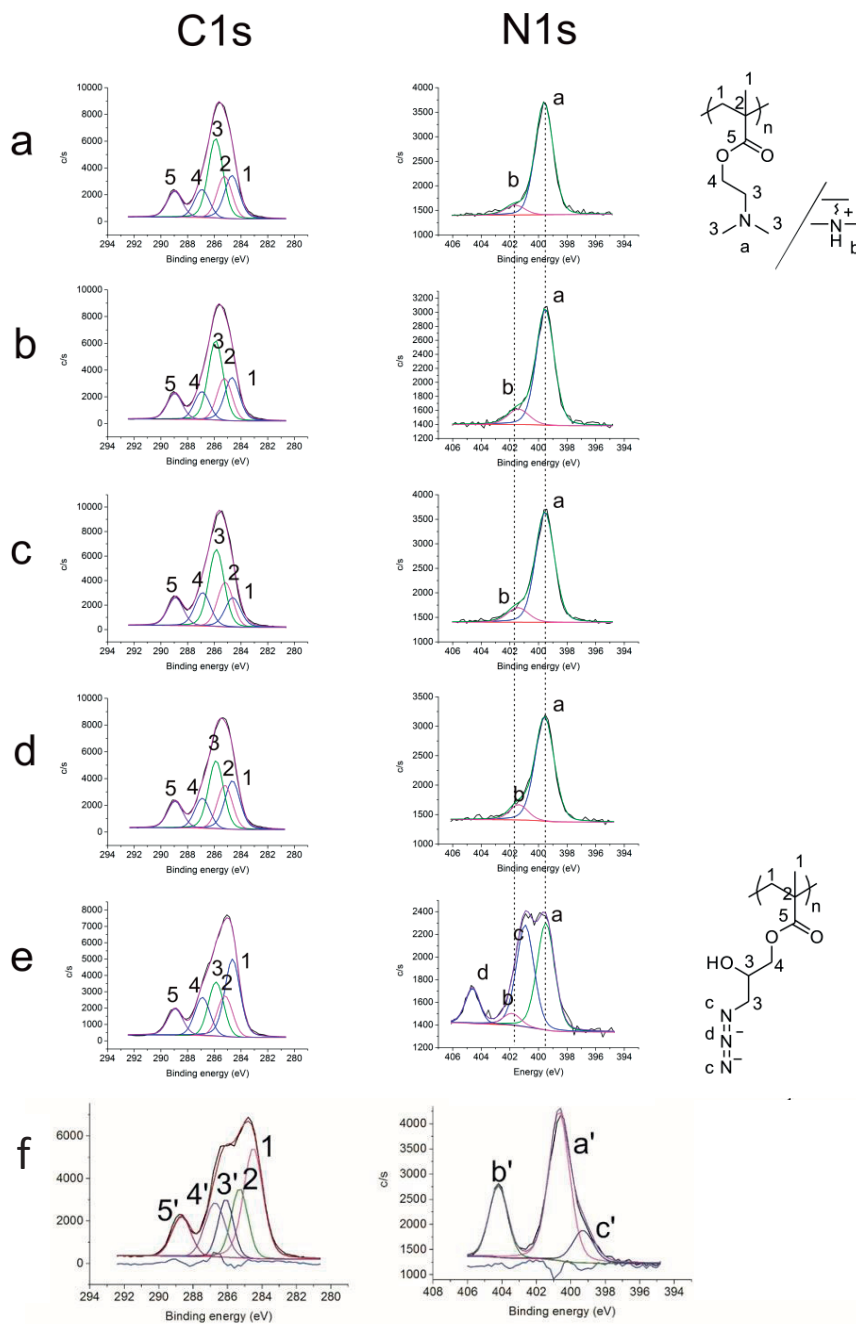


Figure S3.2. XPS C 1s and N 1s high resolution scans of (a) PDMAEMA, (b, c, d, e) P(DMAEMA-co-AzHPMA) with (b) 1%, (c) 5%, (d) 10% and (e) 50% of DMAEMA, and (f) PAzHPMA brushes. Signal shapes were deconvoluted according to a PDMAEMA and PAzHPMA chemical structure presented on the right.

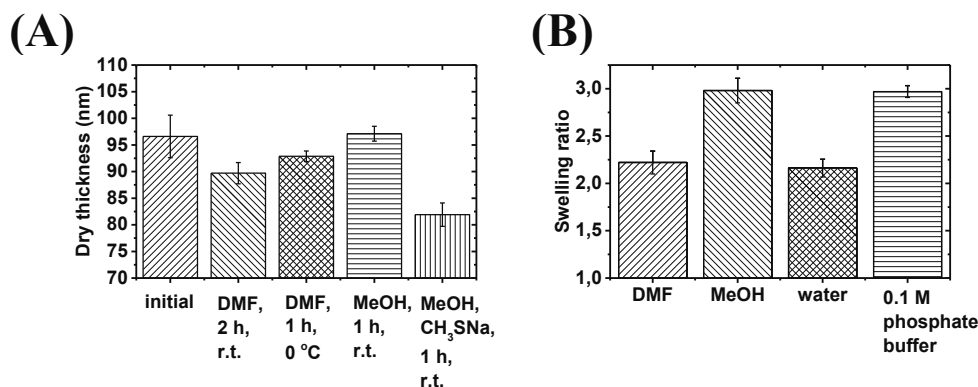


Figure S3.3. (A) Thickness changes of 96.6 nm PDMAEMA upon exposure to different media; (B) swelling ratios in different media given for a correlation to the degrafting process; importantly, besides swelling also a presence of nucleophile is necessary to cause degrafting of polymer chains; freshly distilled DMF was used for the tests; MeOH was used as received.

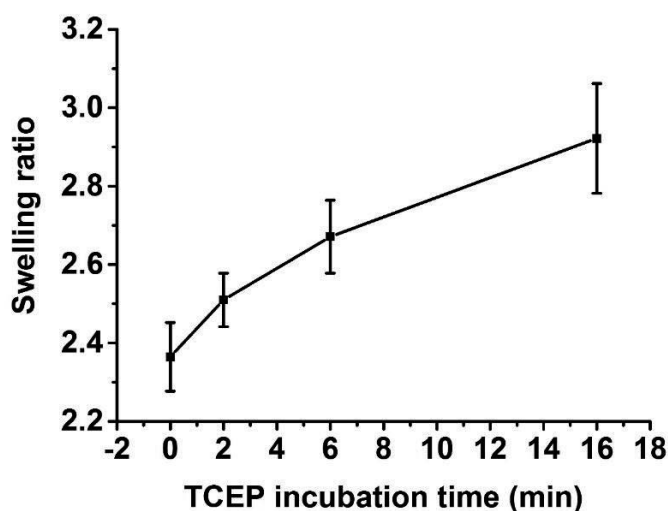


Figure S3.4. Decrosslinking of P(DMAEMA-co-AzHPMA) copolymer brush bearing disulfide crosslinks by incubating with 1 mg/mL TCEP solution in phosphate buffer (pH 7.4, 0.1M) for increasing amount of time. The reduction results in higher swelling of the brush. The copolymer brush was obtained from monomer feed containing 10% AzHPMA.

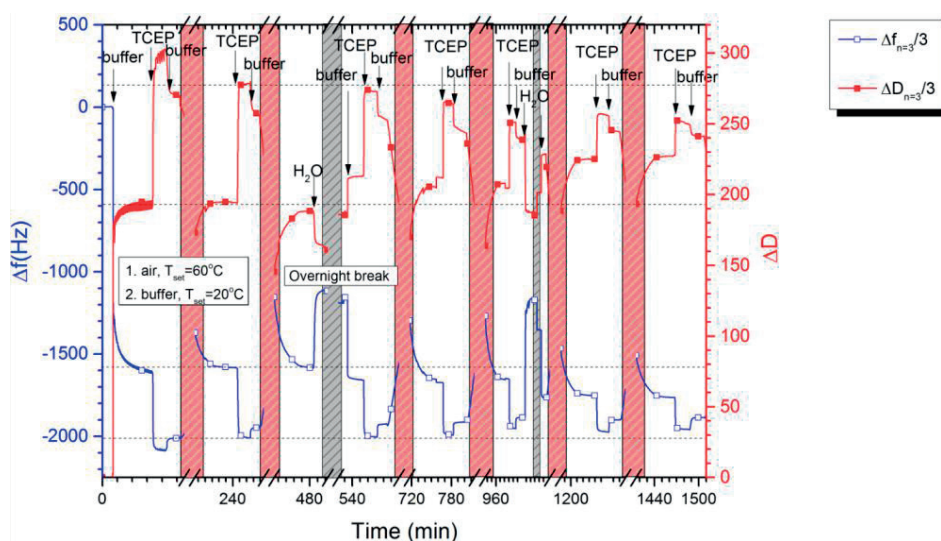


Figure S3.5. Shifts of harmonic frequencies and dissipation factor recorded for a QCM chip grafted with 129.1 nm thick PDMAEMA-co-AzHPMA copolymer brush bearing thiol/disulfide groups upon exposure to phosphate buffer (pH 7.4, 0.1 M), TCEP (1 mg/mL in the buffer), air (heated up to 60°C) and again cooled with the buffer (down to 20°C) (a crosslinking step, marked in red). The copolymer brush was obtained from monomer feed containing 10% AzHPMA. To improve readability, heating and storage steps were cut out (see x-axis breaks at 55-185, 285-435, 503-522, 600-717, 815-935, 1085-1183 and 1290-1415 min). Note that the time only express the measurement time and does not count the storing time. Overnight storage breaks are marked in grey. The test was concluded with flushing with water and air to reduce degrafting during overnight storage.

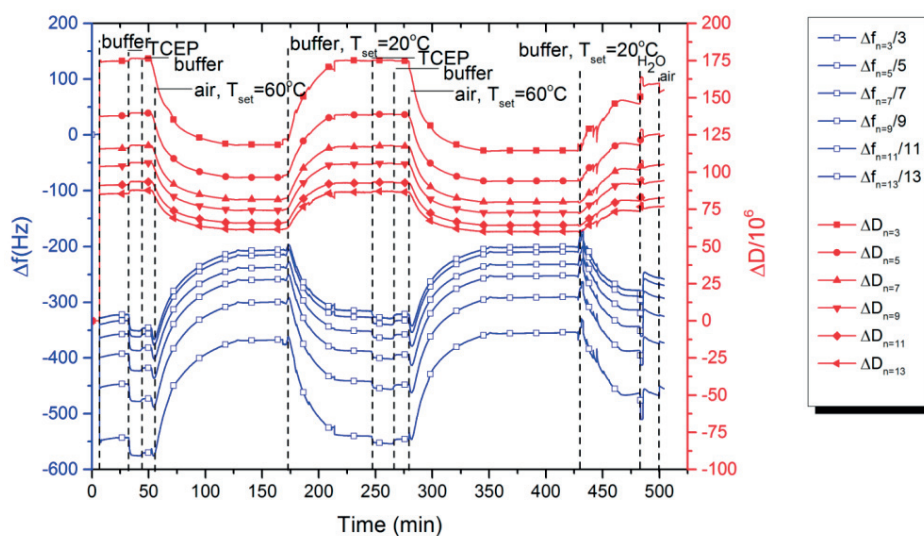


Figure S3.6. Shifts of harmonic frequencies and dissipation factor recorded for a QCM chip grafted with 22.4 nm thick PDMAEMA-co-AzHPMA brush bearing thiol/disulfide groups upon exposure to phosphate buffer (pH 7.4, 0.1 M), TCEP (1 mg/mL in the buffer), air (heated up to 60°C) and again cooled with the buffer (down to 20°C). The test was concluded with flushing with water and air to reduce degrafting during overnight storage. The copolymer brush was generated from monomer feed containing 10% AzHPMA.

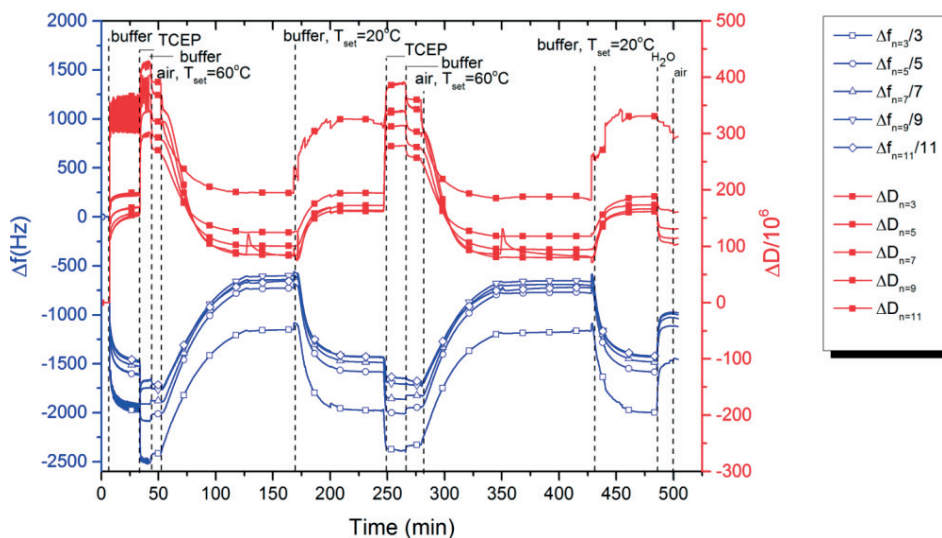


Figure S3.7. Shifts of harmonic frequencies and dissipation factor recorded for a QCM chip grafted with 129.1 nm thick PDMAEMA-co-AzHPMA copolymer brush bearing thiol/disulfide groups upon exposure to phosphate buffer (pH 7.4, 0.1 M), TCEP (1 mg/mL in the buffer), air (heated up to 60°C) and again cooled with the buffer (down to 20°C). The test was concluded with flushing with water and air to reduce degrafting during overnight storage. The brush was obtained from monomer feed containing 10% AzHPMA.

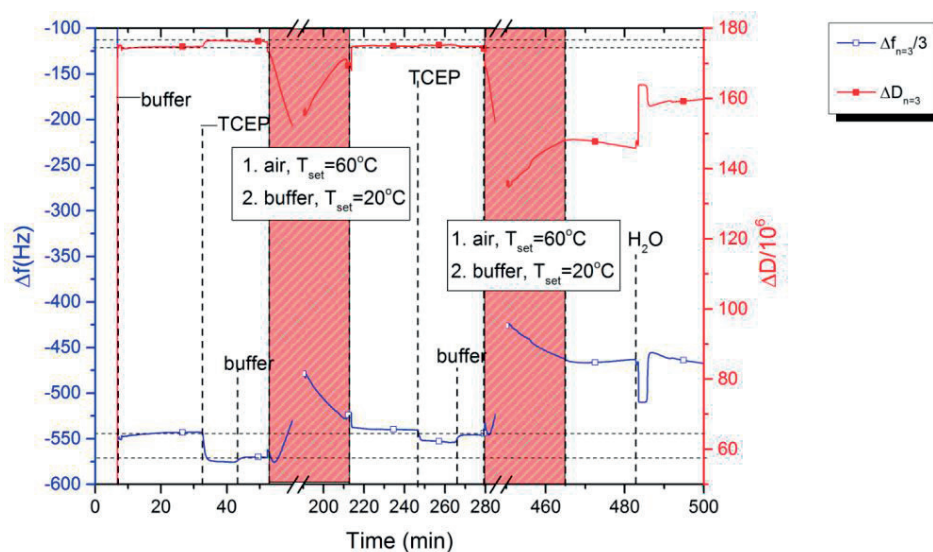


Figure S3.8. Shifts of harmonic frequencies and dissipation factor recorded for a QCM chip grafted with 22.4 nm thick PDMAEMA-co-AzHPMA copolymer brush bearing thiol/disulfide groups upon exposure to phosphate buffer (pH 7.4, 0.1 M), TCEP (1 mg/mL in the buffer), air (heated up to 60°C) and again cooled with the buffer (down to 20°C) (a crosslinking step, marked in red). To improve readability heating steps were cut out (see x-axis breaks at 60-190 and 285-450 min). The test was concluded with flushing with water and air to reduce degrafting during overnight storage. The copolymer brush was obtained from monomer feed containing 10% AzHPMA.

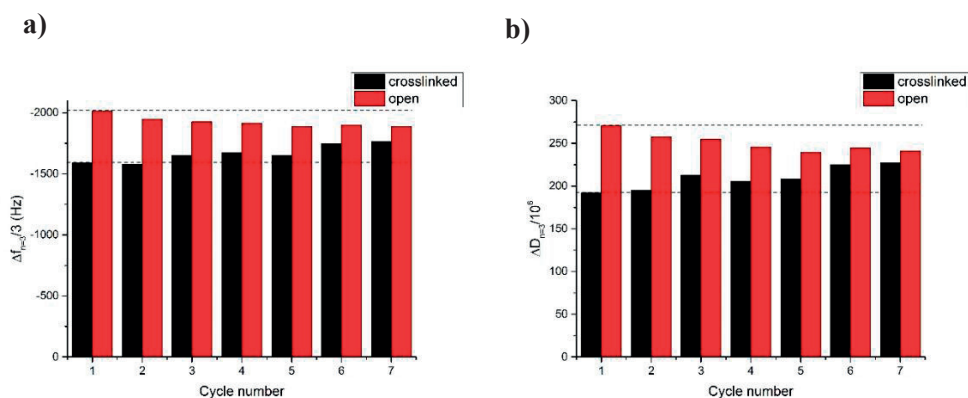


Figure S3.9. Evolution of shifts in (a) 3rd harmonic frequency and (b) dissipation factor at 3rd harmonic frequency over crosslinking/opening cycles of 129.1 nm thick PDMAEMA-co-AzHPMA copolymer brush bearing thiol/disulfide groups obtained from monomer feed containing 10% AzHPMA.

References

- (1) Biesalski, M.; R uhe, J.; Johannsmann, D. *The Journal of Chemical Physics* **1999**, *111*, 7029.
- (2) Wallace, O. B.; Springer, D. M. *Tetrahedron Letters* **1998**, *39*, 2693.
- (3) Bilgi  Tune, T. *Polymer Brushes - Engineered Model Interfaces and Functional Surface Coatings for DNA Biosensing and Electrocatalysis*, Ph. D. Thesis, EPFL, Lausanne, 2015.
- (4) Zengin, A.; Karakose, G.; Caykara, T. *European Polymer Journal* **2013**, *49*, 3350.
- (5) Karamdoust, S.; Yu, B.; Bonduelle, C. V.; Liu, Y.; Davidson, G.; Stojcevic, G.; Yang, J.; Lau, W. M.; Gillies, E. R. *Journal of Materials Chemistry* **2012**, *22*, 4881.
- (6) Yang, Y.; Liu, L.; Zhang, J.; Li, C.; Zhao, H. *Langmuir* **2007**, *23*, 2867.
- (7) Bog, U.; de los Santos Pereira, A.; Mueller, S. L.; Havenridge, S.; Parrillo, V.; Bruns, M.; Holmes, A. E.; Rodriguez-Emmenegger, C.; Fuchs, H.; Hirtz, M. *ACS Applied Materials & Interfaces* **2017**, *9*, 12109.
- (8) Saad, A.; Abderrabba, M.; Chehimi, M. M. *Surface and Interface Analysis* **2017**, *49*, 340.
- (9) Zorn, G.; Liu, L.-H.;  rnad ttir, L.; Wang, H.; Gamble, L. J.; Castner, D. G.; Yan, M. *The Journal of Physical Chemistry C* **2013**, *118*, 376.
- (10) Eisenblaetter, J.; Bruns, M.; Fehrenbacher, U.; Barner, L.; Barner-Kowollik, C. *Polymer Chemistry* **2013**, *4*, 2406.
- (11) Collman, J. P.; Devaraj, N. K.; Eberspacher, T. P.; Chidsey, C. E. *Langmuir* **2006**, *22*, 2457.

4. A Polymer-Brush Templated Three-Dimensional Molybdenum Sulfide Catalyst for Hydrogen Evolution

4.1. Introduction

Hydrogen is considered to be the energy carrier of the future.¹ One of the most promising techniques for sustainable hydrogen production is water splitting. Water splitting consists of two half reactions, namely the hydrogen evolution reaction (HER) and the oxygen evolution reaction (OER). Electrocatalysts are employed to minimize the overpotential required to drive these reactions. Noble-metal electrocatalysts, notably Pt and its alloys, exhibit the highest reported activity for HER. However, due to the scarcity and high cost of Pt, large-scale implementation of water electrolyzers employing this material is not feasible. The development of Earth-abundant electrocatalysts for HER has become an active area of energy research. While many new classes of catalysts with promising activities, such as metal chalcogenides, phosphides, carbides, borides, nitrides have been reported,²⁻⁵ much less attention has been paid to the microscopic assembly of the catalysts. Typically, the catalysts are simply casted from their suspensions onto supporting electrodes. Potential issues from this method include, but are not limited to, aggregation of nanoparticles and inhibition of individual active sites, low bulk conductivity, and hindered mass transport. Because a significant current density is required to produce a sufficient amount of hydrogen in HER, any practical device will consist of a catalyst layer of substantial thickness. Thus, the optimization of the 3D assembly of HER catalysts becomes important.⁶

MoS_x-polymer composites have previously been utilized for a number of applications.⁷⁻¹⁰ The incorporation of MoS₂ within a polymer matrix has resulted in improved thermal, mechanical, and tribological properties of the materials.¹¹⁻¹² Addition of MoS₂ to conductive polymers such as polypyrrole, polyaniline, poly(3,4-ethylenedioxythiophene) leads to better supercapacitors.¹³ Because MoS_x has been reported as an archetypical non-precious HER catalyst,¹⁴⁻¹⁶ MoS_x-polymer hybrids have also been evaluated for HER.¹⁷⁻¹⁹ However, the performances of these composites is still modest.

Herein, we describe an approach to use polymer brushes as a template to control the 3D assembly of amorphous MoS_x. Polymer brushes are thin (typically 10 -200 nm thick) films consisting of chain end-surface tethered polymers. Polymer brush films are most frequently prepared by surface-initiated controlled radical polymerization chemistries, which allow precise control over polymer molecular weight (film thickness) and interchain distance (grafting density). As they can be prepared with precise control over film thickness, grafting density and can incorporate a range of chemical functional groups, polymer brush films are attractive templates for the templated formation of thin metal and metal oxide (composite) films.²⁰⁻²³ In this report, we explore the use of polymer brushes to prepare a series of MoS_x-polymer composites on highly oriented pyrolytic graphite (HOPG) with variable heights, grafting densities, and site densities, which allowed a systematic study of parameters influencing the HER activity. HOPG is based on carbon which is abundant, and it is highly conductive and has a relatively flat surface. Thus, HOPG is preferred over silicon, which is highly resistive, and gold, which is rare and expensive. In terms of turnover frequency (TOF), a fundamental parameter in catalysis, our best catalyst is superior to most previously reported nanostructured molybdenum sulfide catalysts, with turnover frequencies of 1.3 and 4.9 s⁻¹ at overpotentials of 200 mV and 250 mV, respectively. The study also reveals some of the challenges in this approach.

4.2. Experimental Section

4.2.1. Materials

Unless stated otherwise, commercially available materials were used as received. 4-Nitroaniline (C₆H₆N₂O₂, ≥ 99%, Aldrich), aniline (C₆H₇N, purum, ≥ 99.0% (GC), Fluka), tetrafluoroboric acid solution (HBF₄, 48 wt.% in water, Aldrich), sodium nitrite (NaNO₂, RegaentPlus[®], ≥ 99.0%, Aldrich), tetrabutylammonium tetrafluoroborate (NBu₄BF₄, 99%, Aldrich), acetonitrile (ACN, HPLC grade, Fischer), potassium chloride (KCl, puriss. p.a., ≥ 99.5% (AT), Aldrich), hydrochloric acid (HCl, fuming 37% for analysis, VWR), iodomethane (methyl iodide, MeI, 99%, stabilized, Acros), 2,6-dimethylpyridine (2,6-lutidine, C₇H₉N, 99+%, Aldrich), 2-bromo-2-methylpropionyl bromide (BiBB, 98%, Aldrich), N,N-dimethylaminoethyl methacrylate (DMAEMA, 98%, Aldrich), 2,2'-bipyridine (bpy, ≥ 99%, Aldrich), copper (I) bromide (CuBr, 99.999%, Aldrich), ethylenediaminetetraacetic acid (EDTA, ≥ 99%, Fluka), ammonium tetrathiomolybdate ((NH₄)₂MoS₄, 99.97% trace metals basis, Aldrich), platinum (II) chloride (PtCl₂, 98%,

Aldrich), ethylene glycol (EG, 99+%, extra pure, Acros), sodium perchlorate monohydrate (NaClO₄·H₂O, puriss, p.a., ACS reagent, ≥ 98% (T), Aldrich), sulfuric acid (H₂SO₄, volumetric, 1 M H₂SO₄ (2 N), Fluka). Triethylamine (Et₃N, ≥ 98%, Fluka) was distilled over KOH. Both toluene and DMF were purified and dried using a solvent-purification system (PureSolv). Organic solvents such acetone, dichloromethane (DCM), methanol (MeOH), ethanol (EtOH), and diethyl ether (Et₂O) used for washing were of technical grade. The water used was first purified using Millipore Milli-Q[®] Integral water purification system (18.2 MΩ·cm resistivity). DMAEMA was passed through basic alumina column to remove inhibitor just before a polymerization. 6-(chlorodimethylsilyl)hexyl 2-bromo-2-methylpropanoate was prepared according to previous literature report.¹ HOPG was used as substrate for the polymer brushes. The HOPG ZYA plates were purchased from Optigraph. HOPG support was cleaved prior to use.

4.2.2. Analytical methods

Physical characterization. XPS measurements were performed at the Molecular and Hybrid Materials Characterization Centre at the École Polytechnique Fédérale de Lausanne. The instrument used for surface analysis of the HOPG ZYH electrodes was an Axis Ultra instrument from Kratos Analytical equipped with a conventional hemispheric analyzer. The X-ray source employed was a monochromatic Al K_α source (1486.7 eV) source operating at 100 W and 10⁻⁹ mbar. The instrument used for HOPG ZYA plates surface analysis was a PHI5000 VersaProbe II XPS system by Physical Electronics (PHI) with a detection limit of 1 atomic percent. Analysis was performed using a monochromatic Al K_α X-ray source (1486.7 eV) of 24.8 W power with a beam size of 100 μm. The spherical capacitor analyser was set at 45° take-off angle with respect to the sample surface. The pass energy was 46.95 eV yielding a full width at half maximum of 0.91 eV for the Ag 3d 5/2 peak. Curve fitting was performed using the PHI Multipak software. For survey analysis the pass energy was 187.8 eV with 0.8 eV/step. For multiplex analysis the pass energy was 46.9 eV with 0.2 eV/step or 23.9 eV with 0.1 eV/step. The diameter of the analysed area was 10 μm.

FTIR experiments were performed on a Vertex 80 from Bruker. The resolution was of 0.2 cm⁻¹. The infrared spectra were recorded on a 4000-400 cm⁻¹ window using the attenuated total reflectance (ATR) mode. A platinum ATR crystal was used. The scan velocity was 10 kHz. A KBr beamsplitter was used.

Electrochemical measurements. Electrochemical measurements were recorded using a Gamry Instruments Reference 3000™ potentiostat. A traditional three-electrode configuration was used. For polarization and electrolysis measurements, a platinum wire was used as the counter electrode and a double-junction Ag/AgCl (KCl saturated) electrode was used as the reference electrode. Both the counter and reference electrode were rinsed with distilled water and dried with compressed air prior to measurements. The processed HOPG (home-made electrodes or plates) was used as working electrode unless stated otherwise. Potentials were referenced to a reversible hydrogen electrode by adding a value of $(0.2 + 0.059 \times \text{pH})$ V. All potentials were converted and referred to the RHE unless stated otherwise. The current density was normalised over the geometric surface area of the electrode. The value j_u , used to obtain a dimensionless logarithm, corresponds to a unit current density of 1 A cm^{-2} . The ohmic drop was corrected using the current interrupt method.

4.2.3. Procedures

Synthesis of (4-Nitrophenyl)diazonium tetrafluoroborate (4-NDT). The diazonium salt was prepared in accordance with previous literature protocol.²⁴ A solution of 25 mmol NaNO₂ in 4 mL water was cooled down in an ice bath. 25 mmol of the corresponding aniline, in this case 4-nitroaniline (3.4 g), was added to 10 mL water. 9 mL HBF₄ was added to the aniline mixture and stirred vigorously. The reaction mixture turned brown after addition of the acid. The mixture was kept in an ice bath and left stirring for 5 to 10 minutes. Then the previously prepared sodium nitrite solution was added dropwise to the reaction mixture. Fumes were emitted upon the addition and the reaction mixture turned from brown to a mocha colour. The solution was left for 15 minutes. Meanwhile, some HBF₄ is cooled down in the meantime. Then, the reaction mixture was filtered. The filtered product was washed sequentially with the filtrate, the cold HBF₄ solution, ethanol and diethyl ether. The resulting (4-nitrophenyl)diazonium tetrafluoroborate was obtained as a khaki coloured paste. The reaction yield was 29% (1.1 g). The product was collected using a plastic spatula to reduce potential explosive hazards from diazonium compounds. ¹H NMR (D₂O, 400 MHz): δ (ppm) 8.95-8.92 (m, 2H), 8.79-8.76 (m, 2H).

Electrografting of the diazonium salt onto HOPG support. The details of the electrolyte bath composition are given in previous literature reports.²⁵ The grafting solution consisted in 0.1 M of NBu₄BF₄ and about 5 mM of diazonium salt in 30 mL acetonitrile

(ACN). Depending on the grafting density desired, the 4-NDT and benzenediazonium tetrafluoroborate (BDT) concentrations were varied. A grafting density of 100% required 5 mM of 4-NDT, while 50% grafting density required 2.5 mM of BDT and 2.5 mM of 4-NDT in ACN. A grafting density of 10% required 4.5 mM of BDT and 0.5 mM of 4-NDT in ACN. The potentiostatic deposition was performed at a potential of -0.7 V vs. Ag/AgCl for 6 minutes. Each HOPG sample was carefully washed with water and acetone after grafting and dried with nitrogen gas. After each grafting, the electrolyte was renewed and both the counter and the reference electrode were carefully rinsed with acetone and dried under nitrogen.

Preparation of poly(2-(methacryloyloxy)ethyl ammonium iodide) (PMETAI) brushes. Poly(2-(dimethylamino)ethyl methacrylate) (PDMAEMA) brushes were prepared according to a previous literature procedure.²² Briefly, 15 mmol of DMAEMA (2.528 mL, 2.3583 g) and 0.3 mmol of the 2,2'-bipyridine ligand (0.0468 g) were mixed in deionized water (15 mL) and the mixture subjected to three consecutive freeze-pump-thaw cycles. Copper bromide (0.0215 g, 0.15 mmol) was then added under nitrogen atmosphere. Subsequent degassing by two additional cycles of freeze-pump-thaw was performed. All remaining solid was dissolved by continuous stirring at room temperature for 15 minutes. The mixture was then cannula transferred into a nitrogen-purged reaction vessel containing an HOPG plate with the attached ATRP initiator (for multiple surface grafting, the plates were mounted onto a custom made PEEK holders). The reaction was allowed to proceed at room temperature. The polymerization time was varied in order to evaluate the influence of the molecular weight of the polymer brush films on HER catalysis. On ZYA grade HOPG, polymerization times of 1, 5, 20, 40 and 60 minutes were used. Once the brushes were prepared, the HOPG plates were washed successively for 5 min with water, methanol and ethanol under nitrogen atmosphere. The prepared samples were then immersed in a 0.1 M solution of ethylenediaminetetraacetic acid (EDTA, adjusted to pH 8 with sodium hydroxide) for 1 hour. Final steps prior to quaternization included washing using water and ethanol and drying the samples in a stream of nitrogen. The resulting PDMAEMA brushes were placed within a PEEK holder into a glass reactor. The reactor was evacuated and backfilled with nitrogen 3 times. The samples were then quaternized using a 10 vol.% solution of methyl iodide in acetone for 16 hours. The resulting PMETAI brushes were rinsed twice with each of the following solvent: acetone, ethanol, water and then again with ethanol. The quaternized brushes were then dried using nitrogen.

HER precatalyst incorporation. The iodide counter-anion was replaced by dipping the PMETAI-brush coated HOPG into a 40 mM solution of (NH₄)₂MoS₄ in dry dimethylformamide (DMF). Prior to submersion of the HOPG plates, the dipping mixture was stirred for 1 hour. Then, the mixture was filtered using a HPLC-syringe-filter made of a Nylon membrane with a pore size of 0.2 μm. The HOPG plates were placed separately in different vials. The filtrate was added to each vial and the HOPG plates were left submersed for one hour. Then, the plates were removed from the solution and washed carefully with water and acetone and dried under nitrogen. The as-prepared samples contained MoS₄²⁻, which had replaced the iodide anions.

4.3. Results and Discussion

4.3.1. Synthesis and characterization of polymer-brush templated 3D MoS_x catalysts

Figure 4.1 summarizes the synthetic strategy for the preparation of the MoS_x-polymer composites. First, (4-nitrophenyl)diazonium tetrafluoroborate was used to electrograft nitrobenzene onto the HOPG surface (**Figure 4.1**, step 1).^{25,26} Electrochemical reduction of the nitro group resulted in surface-bound aniline (**Figure 4.1**, step 2). Reaction of this amino-functionalized surface with 2-bromo-2-methylpropionyl bromide (BiBB) (**Figure 4.1**, step 3) followed by CuBr-catalyzed surface-initiated atom transfer radical polymerization (SI-ATRP) of dimethylaminoethyl methacrylate (DMAEMA) yielded a surface-attached polymer brush film (**Figure 4.1**, step 4). The as-obtained PDMAEMA brushes were subsequently quaternized by methyl iodide to afford cationic PMETAI brushes (**Figure 4.1**, step 5). This reaction was carried out using a previously reported procedure, which has been shown to result in quantitative conversion of the tertiary amine groups.²² Ion exchange of the iodide anion in PMETAI with MoS₄²⁻ (**Figure 4.1**, step 6), followed by oxidation resulted in an assembly containing MoS₃ as HER precatalyst.^{15,27} The latter was converted to the active MoS_x catalyst during HER,^{27,28} typically through 10 cathodic polarization scans. Detailed procedures for each of the steps in **Figure 4.1** are provided in the Experimental Part and the Supporting Information.

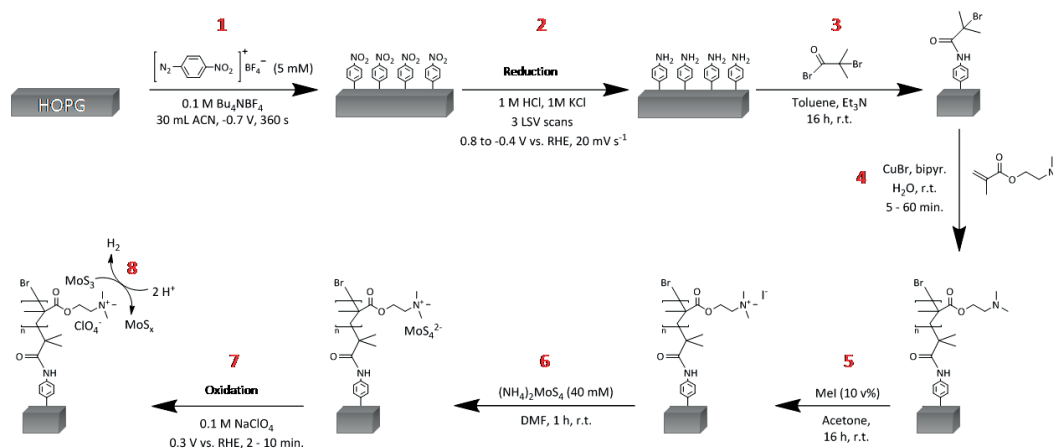


Figure 4.1. Synthetic procedure for the preparation of the MoS_x-polymer brush assemblies. A number is associated to each step of the process. For clarity, the number of anchoring molecules is reduced from four to one after step 3; (1) electrografting of nitrobenzene, (2) reduction of the nitro-anchored groups, (3) attachment of the ATRP initiator, (4) polymer brush growth, (5) quaternization of the polymer brushes, (6) catalyst incorporation via anion-exchange, (7) precatalyst formation, (8) HER catalysis.

Several HOPGs of different grades were used for the assembly. First HOPG ZYH plates were used (**Figure S4.1**). X-ray photoelectron spectroscopy (XPS) measurements (**Figure S4.2**) confirmed the formation of the desired assemblies. The wetting properties of the substrate at different stages of fabrication were evaluated using water contact-angle measurements (**Figure S4.3**). The catalytic performance of the systems using HOPG ZYH substrates is summarized in **Table S4.1**. The performance of the reference sample prepared using Pt as catalyst indicates that the polymer network is not limiting the conductivity of the catalytic system for HER, probably because of the limited height of the polymer. The data in **Table S4.1** indicate poor reproducibility of these systems, as significant variance in activity was observed on similar samples. We suspect that the varying surface roughness of the HOPG ZYH substrates (**Figure S4.4**) is the origin of this non-reproducibility. To mitigate this problem, the highest commercial grade of HOPG, *i.e.*, ZYA, was then employed as support. ZYH and ZYA HOPG bear a similar chemical composition, however, their mosaic spread, a measure of the parallelism of the crystalline grains in the materials, is different. ZYA has a lower mosaic spread (0.4°) than ZYH (3.5°),²⁹ and thus, has a significantly smoother surface. The ZYA samples are essentially flat on the nanometer level (**Figure S4.5**).

AFM was used to monitor the evolution of the film thickness of PMETA brushes grafted from HOPG ZYA and PDMAEMA brushes grafted from Si as a function of polymerization time. PDMAEMA brush films grafted from on Si samples were used as reference because the polymer heights could be reliably measured by ellipsometry. On the other hand, although HOPG is flat at a nanoscale, pronounced surface roughness can be observed at a micrometer scale (**Figure S4.6a**), making the measurements of polymer heights by AFM less accurate. Despite the uncertainty, there is a visible correlation between polymerization time and brush film thickness for experiments on both HOPG plates and Si wafers (**Figure S4.6b**). It was therefore possible to tune the length of the grafted polymer chains by varying time in the range of 5 to 60 minutes. We chose 20 minutes as an optimal polymerization time. On Si wafer the polymer growth started to slow down after 20 min, while on HOPG ZYA longer polymerization time seemed to lead to uncontrolled side reactions and non-reproducible polymer heights. Thus, for the following experiments the maximum polymerization time was set to 20 minutes.

To verify successful preparation of MoS_x-polymer assemblies, characterization of the samples at different stages of the assembly was performed. **Figure 4.2** shows Fourier-transform infrared (FTIR) spectra recorded at different stages of the fabrication process. Upon electrografting using (4-nitrophenyl)diazonium tetrafluoroborate, absorption peaks of the nitro groups were observed at 1523 cm⁻¹ and 1350 cm⁻¹ in the infrared spectra (**Figure 4.2**, red line).³⁰ The bands at 1590 cm⁻¹ and 890 cm⁻¹ were attributed to the HOPG support.³⁰ After the growth of the polymer brush film (**Figure 4.2**, blue curve), the IR spectra of the samples were significantly modified and characteristic features of the PDMAEMA were revealed. Notably, the peak at 1730 cm⁻¹ and the doublet observed at 1155 cm⁻¹ were attributed to the C=O and C-O-C moieties, respectively.^{31,32} The tertiary amine feature was present at 1400 cm⁻¹.³¹ The signals attributed to the alkane moieties (CH₃, CH₂) of the brushes were found at 2950 cm⁻¹ and 1475 cm⁻¹.^{31,32} After anion-exchange (**Figure 4.2**, green line), a new signal at 490 cm⁻¹ is observed and is attributed to the Mo-S bond stretching vibration.³³ The HER catalysis converts the precatalyst MoS₃ to MoS_x. This conversion was reflected by the observation of new IR signals. The broad peak at 1650 cm⁻¹ was attributed to MoS_x.³⁴ The slight shift of this peak compared to that of MoS₂ at 1630 cm⁻¹ is consistent with the amorphous nature of our MoS_x catalyst (**Figure 4.2**, orange curve). Overall the FTIR spectra indicate the successful preparation of the MoS_x-polymer composites.

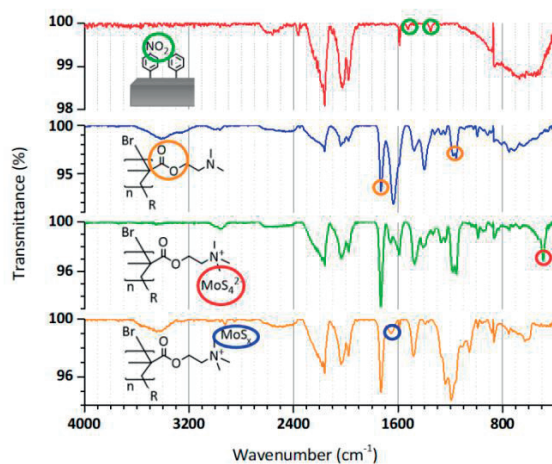


Figure 4.2. FTIR spectra of the MoS_x/polymer brush composite at different stages of fabrication. The corresponding chemical structure is drawn for reference. The circled features on the spectra refer to the circled chemical moiety on the corresponding chemical structure. The “R” on the chemical structures is used to designate the covalent link between the polymer brush and the HOPG substrate, fabricated by the electrografting species and the ATRP initiator attachment. The features from 1900 to 2300 cm⁻¹ are attributed to the oxidation of the support material, water and CO₂ traces.³⁵

The successful preparation of the polymer composite films was also confirmed by XPS measurements, which were carried out at the different steps in the fabrication process (**Figure S4.7**). N 1s high resolution XPS spectra were obtained for the first stages of brush-assembly preparation (**Figure 4.1**, step 1-4). The main binding energies feature observed successively at 406.1 eV (**Figure S4.7b**), 399.7 eV (**Figure S4.7e**), 399.9 eV (**Figure S4.7h**), and 399.8 eV (**Figure S4.7l**), correspond respectively to the nitro, amino, amide, and tertiary amine moieties. The presence of these specific features indicates the successful fabrication of the brush-assembly. Characteristic C 1s signals of PDMAEMA were also observed (**Figure S4.7m**). The binding energies at 289.3, 286.9, and 285.3 eV, correspond respectively to the C-C=O, C=O, and C-O-C=O moieties of PDMAEMA. The O 1s features observed at 533.5 and 531 eV correspond to the O-C=O and O-C signals of the PDMAEMA brush (**Figure S4.7n**). Deconvolution analysis of the XPS survey, high resolution spectra, and additional discussion is provided in the Supporting Information. **Figure 4.3a** and **b** show Mo 3d and S 2p deconvoluted XPS signals of the composite after catalyst incorporation (**Figure 4.1**, step 6), while **Figure 4.3c** and **d** present results for a composite sample after HER catalysis. After incorporation of the catalyst, the XPS signals indicate

the presence of MoS₄²⁻ (230.9 eV), MoO₃ (232.8 eV), and molybdenum oxysulfide (231.8 eV).²⁷ The latter two are surface-bound impurities formed when the samples were exposed to air prior to XPS analysis; they are not expected to be present under catalytic conditions. For the catalyst after HER catalysis, the expected bridging S₂²⁻ and the terminal S²⁻ associated with MoS_x are observed.²⁷ In addition, the S 2p XPS spectra reveals signals attributed to H₂S and H₂SO₄.³⁶⁻³⁸ H₂SO₄ originates from the electrolyte. It has been reported that ammonium tetrathiomolybdate can generate H₂S under mild conditions.³⁹ The H₂S might remain in the composite, either being adsorbed by the polymer, or being dissolved in the electrolyte and trapped by the polymer. In addition, in-situ generation of H₂S via decomposition of the sample in the XPS experiments is possible.

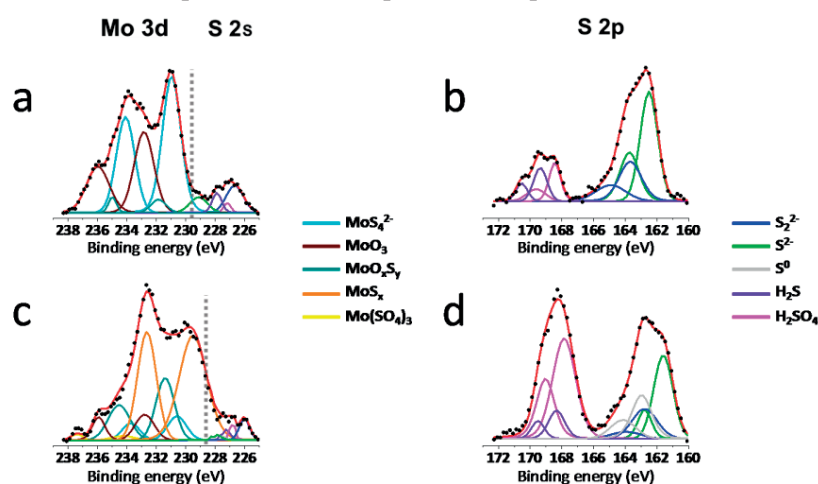


Figure 4.3. (a - c) Mo 3d high resolution XPS spectra for the composite sample after (a) catalyst incorporation and after (c) hydrogen evolution reaction. (b - d) S 2p high resolution XPS spectra for the composite sample after (b) catalyst incorporation and after (d) HER. The deconvolution follows a simple color code: the experimental data correspond to the black dots, the fitting envelope is the red line. Each coloured curve corresponds to a specific chemical moiety. Due to the degeneracy nature of the orbitals in S 2p and Mo 3d, each moiety possesses a doublet of signals. S 2s singlets are within the binding energy window of Mo 3d (right-hand side of the grey dashed line). The S 2s peak was deconvoluted using a curve for each moiety identified in the S 2p peaks deconvolution.

TEM images and corresponding elemental mapping information confirmed the successful incorporation of the catalyst after step 7 (**Figure 4.4**). Focused-ion beam (FIB) was necessary to prepare the samples for imaging. The sample preparation process included the deposition of an amorphous carbon layer, to protect the composite from the milling step of the FIB process. To ensure a clear distinction from the carbon substrate and the

protective carbon layer, a longer polymerization time, 40 minutes, was employed for the sample fabrication. **Figure 4.4a** shows the cross-section TEM image of the sample, where the zones of HOPG, polymer layer, and protective carbon layer are visible. A higher resolution image is shown in **Figure 4.4b**. The corresponding elemental mapping images (**Figure 4.4c** and **d**) confirm the presence of molybdenum sulfide within the polymer network. As expected, C signals have a lower intensity in the polymer layer than in the HOPG substrate and the protective carbon layer. Molybdenum is homogeneously distributed in the polymer layer.

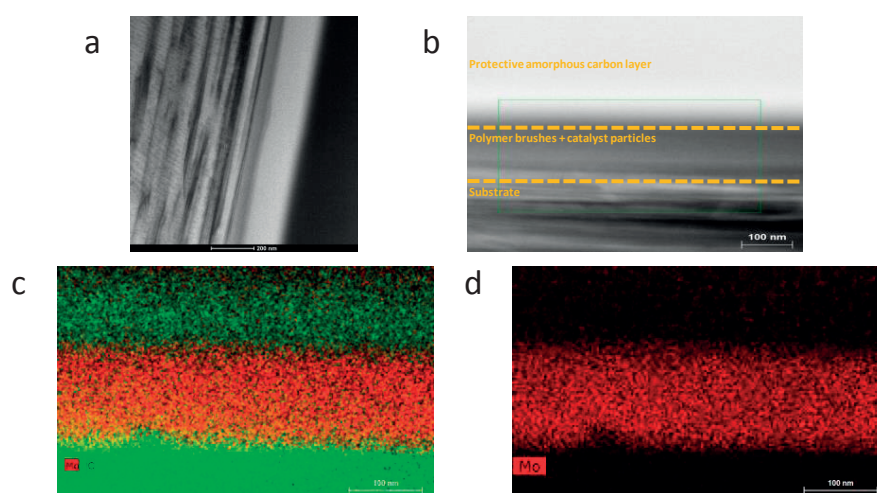


Figure 4.4. TEM and EDX images of the MoS_x-polymer composite on HOPG ZYA. The sample was prepared using focused-ion beam (FIB) to obtain a thin lamella sample that is measurable under TEM. (a) Overall cross section picture of the assembly (scale bar 200 nm). (b) Cross section image which served for EDX elemental mapping measurements. The dashed lines separate different regions of the sample. From bottom to top: substrate (HOPG) layer; polymer brushes with homogeneous incorporation of MoS_x; protective amorphous carbon layer (c) C and Mo elemental mapping. The brushes are sandwiched between the two carbon layers. (d) Mo elemental mapping. The polymer height is about *ca.* 150 nm.

4.3.2. Hydrogen evolution using polymer-brush templated 3D MoS_x catalysts

The hydrogen evolving properties of the MoS_x-polymer composite films were tested using linear sweep voltammetry (LSV) in 1 M H₂SO₄. The samples were carefully insulated so that only a specific surface area of one HOPG face was exposed to the acidic media (**Figure S4.8**). **Figure 4.5** shows representative LSV curves of the MoS_x-polymer composites made with polymerization time of 1, 5, and 20 minutes. The samples prepared

with 20 minutes of polymerization time exhibited the highest net activity. An overpotential of 344 mV was required to generate a current density of 0.5 mA cm⁻². The relatively small current density achieved by the catalytic systems is largely due to a very small catalyst loading (Table S4.2). The intrinsic activity of the catalyst, however, can be described by turnover frequency (TOF). The loadings of MoS_x in these systems were measured using electrochemistry (Supporting Information). Based on these data, the TOF at $\eta = 250$ mV was calculated (Figure 4.5, inset). It is noted that the TOFs of these composites are quite high, and are one order of magnitude higher than a previously reported MoS_x-polymer composite system.¹⁹

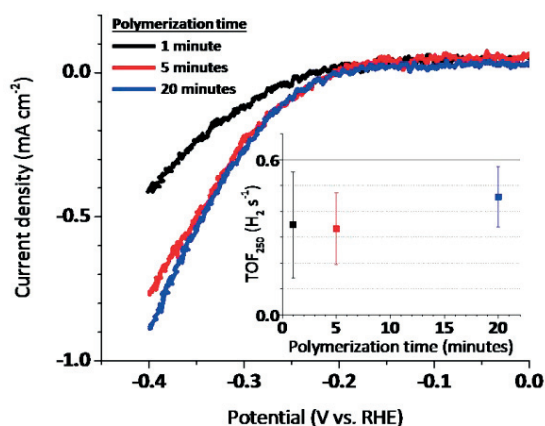


Figure 4.5. LSV scans (of MoS_x-loaded polymer brush films prepared using different polymerization times). The assemblies underwent 10 consecutive LSV scans from 0.1 V to -0.4 V vs. RHE in 1 M H₂SO₄ to convert the precatalyst MoS₃ to the catalytic active species MoS_x. The scans displayed correspond to the 11th LSV measurement performed on the assemblies. Conditions: scan rate 5 mV s⁻¹, ohmic drop corrected. The catalyst loading for the polymer assemblies prepared at 1, 5, and 20 minutes polymerization times were 0.10, 0.18, and 0.17 μg cm⁻², respectively. Inset: turnover frequencies at $\eta = 250$ mV.

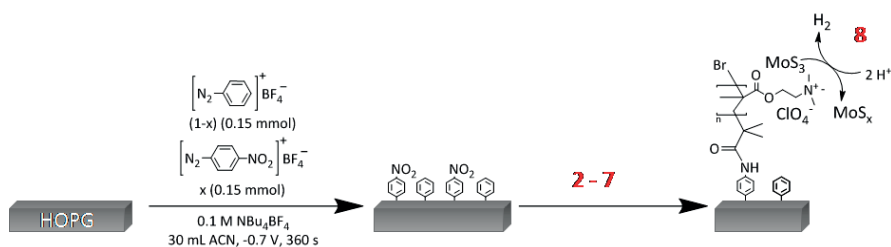


Figure 4.6. Schematic drawing of the method to vary the grafting density on HOPG. Parts 2-8 are identical to the steps described in Figure 4.1.

Tafel analysis was conducted for the LSV curves of the assemblies (**Table S4.2**). The Tafel slopes are much higher than those of amorphous MoS_x^{27,40-43}, which suggests hindered electron and/or proton transport. The latter might originate from the hydrophobic nature of the polymer brushes. Water contact-angle measurements on the composites at several fabrication stages support this hypothesis (**Figure S4.9**). The bare HOPG substrate possesses a water-contact angle of 88.3°, indicative of a hydrophobic surface. Upon quaternization of the polymer brushes, a water-contact angle of 19.7° is observed (**Figure S4.9c**). The surface prior to catalyst incorporation is thus hydrophilic. However, after catalyst incorporation and subsequent activation, the resulting assembly has a water-contact angle of above 95°, indicative of a very hydrophobic surface.

In the preparation of the above assemblies, HOPG was electrografted with nitrobenzene in a presumed 100% site density. As a consequence, the polymer brushes have a 100% grafting density. To probe the influence of the grafting density, polymer brushes with 50% and 10% grafting densities were also prepared. These samples were obtained by the introduction of non-polymerization active (“dummy”) sites, i.e., benzene groups in the initial electrografting step. The benzene groups cannot be functionalized by the ATRP precursor, preventing the growth of polymer brushes from these sites (**Figure 4.6**). When polymer brush films are grown at identical polymerization times (~ molecular weights), the lower surface concentration of polymerization initiators on the 10% and 50% grafting density surfaces leads to an increased average interchain distance and thus a more collapsed polymer chain conformation and small film thickness.²⁰ **Figure 4.7a** compares the LSV curves of three MoS_x-polymer assemblies, all made in 20 minutes but with different grafting densities. **Table S3** and **Figure S4.10** describe further electrocatalytic data of additional samples. The overpotential required to generate a current density of 0.5 mA cm⁻² for the composites prepared at 100%, 50%, and 10% grafting densities are 344, 254, and 211 mV, respectively. Thus, the catalytic performance is significantly improved upon reduction of the grafting density. Several factors contribute to the higher activity at reduced grafting density: (1) a higher catalyst loading (**Table S4.3**); (2) higher intrinsic activity (TOF) due to more accessible active sites (see below). (3) Additionally, mass transport might be more facile on samples with a lower grafting density. The stability of the best catalyst was tested in a potentiostatic electrolysis for 10 hours. After an activation period (about 1 h), the current density remained largely stable (**Figure 4.7b**). This result indicates a good stability of the activity of our catalyst.

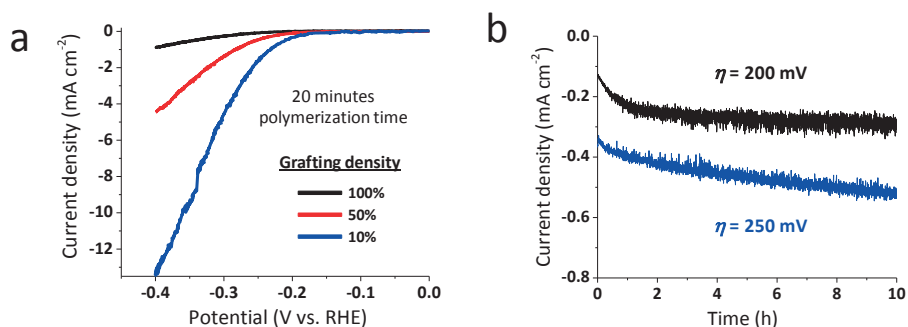


Figure 4.7. (a) LSV scans of MoS_x-coated polymer brush assemblies, prepared using 20 minutes of polymerization time and different grafting densities, in 1 M H₂SO₄. The assemblies underwent 10 consecutive LSV scans from 0.1 V to -0.4 V vs. RHE in 1 M H₂SO₄ to convert the precatalyst MoS₃ to the catalytic active species MoS_x. The scans displayed correspond to the 11th LSV measurement performed on the assemblies. Conditions: scan rate 1 mV s⁻¹, ohmic drop corrected. The catalyst loadings for the polymer assemblies prepared at 100%, 50%, and 10% grafting density were respectively 0.17, 0.12, and 0.35 μg cm⁻². (b) Potentiostatic electrolysis over 10 hours. The tested sample (catalyst loading of 0.35 μg cm⁻²) was prepared under 10% grafting density and 20 minutes of polymerization time.

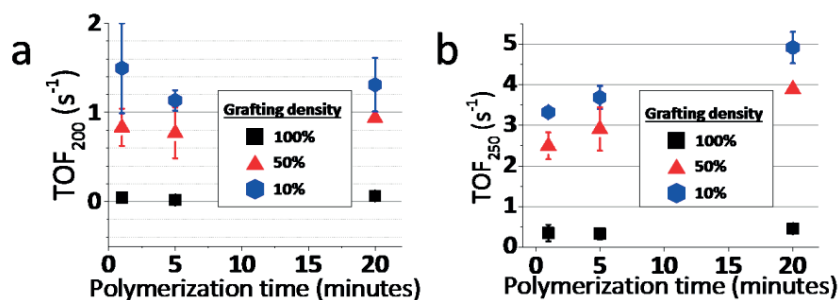


Figure 4.8. TOFs of the MoS_x polymer brush composites at different polymerization times and grafting densities. (a) TOFs at η = 200 mV; (b) TOFs at η = 250 mV. The averaged values of 3-4 samples in the same batch are displayed; error bars refer to standard deviation.

Figure 4.8 shows the TOFs at η = 200 and 250 mV for the various samples prepared in this study. The figure shows that grafting density has a strong influence in TOF, while polymerization time (i.e. polymer chain length) has only a modest influence. Despite different catalytic loadings (**Table S4.3**) of the samples prepared with identical polymerization time and grafting density, the activity in terms of TOF is similar. The most active catalyst is the sample with 10% grafting density and generated by 20 minutes

polymerization of DMAEMA. TOFs of 1.3 and 4.9 s⁻¹ at $\eta = 200$ and 250 mV were obtained. **Figure S4.11** shows that the activity of this catalyst is much higher than the catalyst directly deposited on HOPG. As mentioned above, the higher TOFs for the samples with lower grafting densities might be due to more accessible reaction sites. This may be due to the reduced steric hindrance as well as the smaller film thicknesses of the polymer composite films prepared from the lower grafting densities brushes.

The TOF values of the different catalysts are compared to some state-of-the-art molybdenum sulfide catalysts (**Figure 4.9**).^{19,27,44-48} Additional catalytic parameters including mass and specific activity, as well as TOFs, of the different catalytic systems are compared in **Table S4.4** and **Table S4.5**.

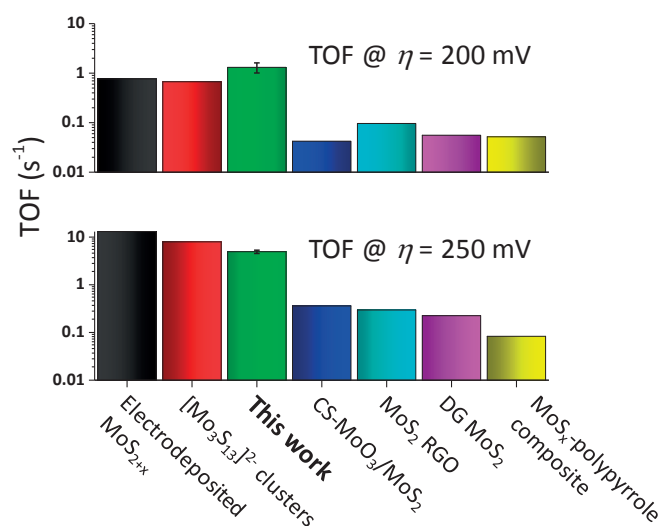


Figure 4.9. Comparison of TOFs of various state-of-the-art molybdenum sulfide catalysts. The electrodeposited MoS_{2+x} catalyst was previously developed by our group.¹⁵ Jaramillo et al. developed the tetrathiomolybdate clusters [Mo₃S₁₃]²⁻,⁴⁴ the core-shell (CS) MoO₃/MoS₂ nanowires,⁴⁵ and the double gyroid (DG) MoS₂ catalysts.⁴⁶ The MoS₂ RGO corresponds to molybdenum sulfide nanoparticles grown on reduced graphene oxide sheets suspended in solution.⁴⁷ The MoS_x polypyrrole composite corresponds to electrodeposited molybdenum sulfide onto a poly(pyrrole-alkylammonium) matrix.¹⁹

It can be seen that the best MoS_x-polymer brush composite has higher TOFs than many MoS₂ nanoparticle catalysts. Its TOF is similar to that of [Mo₃S₁₃]²⁻ clusters absorbed on HOPG which are rich in active edge sites, suggesting an optimal 3D assembly. Interestingly, the electrodeposited MoS_{2+x} film has also the highest activity among all these

molybdenum sulfide catalysts, which serves as a fortuitous example of optimal random assembly.

Despite their high TOFs, the MoS_x-polymer brush composites have modest current densities at low overpotentials, which is due to low catalyst loadings. The maximum loadings of the catalyst in the polymer brushes (it is assumed that the molecular weight (Mw) of MoS_x catalyst is similar to MoS₂, i.e. 160.1 g/mol) can be estimated according to this formula: mass loading = Mw(MoS₂)*hd/(2M_{METAL})* where h is dry PMETAI brush thickness, d is polymer density of 1g/cm³, and M_{METAL} = 299.1 g/mol. Thus, the maximum loadings are 1.04 μg cm⁻² for 5 min polymerization time (assuming 38.8 nm brush height) and 2.14 μg cm⁻² for 20 min polymerization time (assuming 80 nm brush height). Nevertheless, the measured actual catalyst loadings are typically lower and for highest film thicknesses they are as low as 10% of maximum values. We hypothesize that the entry of the catalyst in the polymer brush film is hindered due to the sterics of the polymer chains. This steric hindrance is reduced upon decreasing both film thickness and the grafting density, although the maximum loading is decreased as well.

4.4. Conclusions

In summary, a multiple-step synthetic protocol to prepare polymer brush-templated amorphous molybdenum sulfide catalysts has been successfully developed. The polymer brushes direct the 3D assembly of the MoS_x catalyst. Systematic investigations have led to an optimal catalyst template which is prepared by 20 minutes of polymerization of DMAEMA from ZYA HOPG substrate with 10% grafting density of the ATRP initiator. This catalyst shows turnover frequencies of 1.3 and 4.9 s⁻¹ at η = 200 and 250 mV in 1 M H₂SO₄, which is among the highest reported for molybdenum sulfide catalysts. On the other hand, the geometrically averaged current densities at low overpotentials are comparatively small due to a very small loading of catalysts. How to significantly increase the catalyst loading in this system is the next challenge. The work demonstrates a novel approach for the 3D assembly of HER catalysts, revealing its advantages and current limitation.

The results presented in this chapter are part of a collaborative project with Prof. Xile Hu from the Laboratory of Inorganic Synthesis and Catalysis (LSCI) of the EPFL. Lucas-Alexandre Stern contributed with the diazonium synthesis, and the electrochemical experiments, as well as the anion-exchange, and the FTIR measurements. Tuğba Bilgiç

Tune and Piotr Mocny both contributed for the ATRP initiator attachment, SI-ATRP, quaternization of the polymer brushes, and their analysis by ellipsometry and AFM. Tuğba Bilgiç Tune worked on the first HOPG support reported in this Chapter, while Piotr Mocny on the second and third HOPG support. Water contact angle measurements were both performed by Tuğba Bilgiç Tune and Piotr Mocny. The interdisciplinary centre for electron microscopy (CIME) of the EPFL provided the high-resolution SEM pictures. Fang Song performed the electron microscopic measurements (HRTEM). XPS measurements were performed by Nicolas Xanthopoulos and Pierre Mettraux from the MHMC of the EPFL.

This work was published in “Stern, L. -A., Mocny, P., Vrabel, H., Bilgic, T., Klok, H. -A., Hu, X. *ACS applied materials & interfaces*, **2018**, 10, 6253-6261.”

4.5. References

- (1) Anderson, D.; Holdren, J. P.; Jefferson, M.; Jochem, W.; Nakićenović, N.; Reddy, A. K. N.; Rogner, H.-H.; Smith, K. R.; Turkenburg, W. C.; Williams, R. H. *World Energy Assessment*, United Nations Development Programme, New York, 2000.
- (2) Zou, X.; Zhang, Y. *Chemical Society Reviews* **2015**, 44, 5148.
- (3) Roger, I.; Shipman, M. A.; Symes, M. D. *Nature Reviews Chemistry* **2017**, 1, 0003.
- (4) Jiao, Y.; Zheng, Y.; Jaroniec, M.; Qiao, S. Z. *Chemical Society Reviews* **2015**, 44, 2060.
- (5) Faber, M. S.; Jin, S.; *Energy & Environmental Science* **2014**, 7, 3519.
- (6) Zhao, H.; Zhu, Y.-P.; Yuan, Z.-Y. *European Journal of Inorganic Chemistry* **2016**, 13-14, 1916.
- (7) Coleman, J. N.; Lotya, M.; O'Neill, A.; Bergin, S. D.; King, P. J.; Khan, U. et al. *Science* **2011**, 331, 568.
- (8) Rao, C. N. R.; Ramakrishna Matte, H. S. S.; Maitra, U. *Angewandte Chemie International Edition* **2013**, 52, 13162.
- (9) Zhou, K.; Liu, J.; Zeng, W.; Hu, Y.; Gui, Z. *Composites Science and Technology* **2015**, 107, 120.
- (10) Wang, X.; Xing, W.; Feng, X.; Song, L.; Hu, Y. *Polymer Reviews* **2017**, 57, 440.
- (11) Naffakh, M.; Díez-Pascual, A. M.; Remškar, M.; Marco, C. *Journal of Materials Chemistry* **2012**, 22, 17002.
- (12) Yuan, H.; Yang, S.; Liu, X.; Wang, Z.; Ma, L.; Hou, K.; Yang, Z.; Wang, J. *Composites: Part A* **2017**, 102, 9.

- (13) Zhang, W. J.; Huang, K. J. *Inorganic Chemistry Frontiers* **2017**, *4*, 1602.
- (14) Laursen, A. B.; Kegnæs, S.; Dahl, S.; Chorkendorff, I. *Energy & Environmental Science* **2012**, *5*, 5577.
- (15) Merki, D.; Hu, X. *Energy & Environmental Science* **2011**, *4*, 3878.
- (16) Benck, J. D.; Hellstern, T. R.; Kibsgaard, J.; Chakthranont, P.; Jaramillo, T. F. *ACS Catalysis* **2014**, *4*, 3957.
- (17) Zeng, X.; Niu, L.; Song, L.; Wang, X.; Shi, X.; Yan, J. *Metals*, **2015**, *5*, 1829.
- (18) Dai, X.; Du, K.; Li, Z.; Sun, H.; Yang, Y.; Zhang, X.; Li, X.; Wang, H. *Chemical Engineering Science* **2015**, *134*, 572.
- (19) Lattach, Y.; Deronzier, A.; Moutet, J. C. *ACS Applied Materials & Interfaces*, **2015**, *7*, 15866.
- (20) Zoppe, J. O.; Ataman, N. C.; Mocny, P.; Wang, J.; Moraes, J.; Klok, H.-A. *Chemical Reviews* **2017**, *117*, 1105.
- (21) Tugulu, S.; Harms, M.; Fricke, M.; Volkmer, D.; Klok, H.-A. *Angewandte Chemie* **2006**, *118*, 7619; *Angewandte Chemie International Edition* **2006**, *45*, 7458.
- (22) Paripovic, D.; Klok, H.-A. *ACS Applied Materials & Interfaces* **2011**, *3*, 910.
- (23) Sugnaux, C.; Mallorquí, A. D.; Herriman, J.; Klok, H.-A.; Fontcuberta i Morral, A. *Advanced Functional Materials* **2015**, *25*, 3958.
- (24) Starkey, E. B. *Organic Syntheses* **1939**, *19*, 40.
- (25) Delamar, M.; Hitmi, R.; Pinson, J.; Saveant, J. M. *Journal of the American Chemical Society* **1992**, *114*, 5883.
- (26) Allongue, P.; Delamar, M.; Desbat, B.; Fagebaume, O.; Hitmi, R.; Pinson, J.; Savéant, J. M. *Journal of the American Chemical Society* **1997**, *119*, 201.
- (27) Vrubel, H.; Hu, X. *ACS Catalysis* **2013**, *3*, 2002.
- (28) Lassalle-Kaiser, B.; Merki, D.; Vrubel, H.; Gul, S.; Yachandra, V. K.; Hu, X.; Yano, J. *Journal of the American Chemical Society* **2015**, *137*, 314.
- (29) Patel, A. N.; Collignon, M. G.; O'Connell, M. A.; Hung, W. O.; McKelvey, K.; Macpherson, J. V.; Unwin, P. R. *Journal of the American Chemical Society* **2012**, *134*, 20117.
- (30) Leitner, T.; Kattner, J.; Hoffmann, H. *Applied Spectroscopy* **2003**, *57*, 1502.
- (31) Zhang, X.; Li, G.; Zhang, H.; Wang, X.; Qu, J.; Liu, P.; Wang, Y. *Soft Matter*, **2013**, *9*, 6159.
- (32) Taktak, F.; Yildiz, M.; Sert, H.; Soykan, C. *Journal of Macromolecular Science Part A* **2015**, *52*, 39.

- (33) Zhang, J.; Hu, S. P.; Feng, Y. L.; Xu, B.; Guo, Y. H. *Advanced Materials Research* **2011**, 287, 2049.
- (34) Maugé, F.; Lamotte, J.; Nesterenko, N. S.; Manoilova, O.; Tsyganenko, A. A. *Catalysis Today* **2001**, 70, 271.
- (35) Socrates, G. *Infrared and Raman Characteristic Group Frequencies*, John Wiley & Sons, Ltd., Chichester, 2001.
- (36) Sodhi, R. N.; Cavell, R. G. *Journal of Electron Spectroscopy and Related Phenomena* **1986**, 41, 1.
- (37) Benck, J. D.; Chen, Z. B.; Kuritzky, L. Y.; Forman, A. J.; Jaramillo, T. F. *ACS Catalysis* **2012**, 2, 1916.
- (38) Weber, T.; Muijsers, J. C.; Niemantsverdriet, J. W. *The Journal of Physical Chemistry* **1995**, 99, 9194.
- (39) Xu, S.; Yang, C. T.; Meng, F. H.; Pacheco, A.; Chen, L.; Xian, M. *Bioorganic & Medicinal Chemistry Letters* **2016**, 26, 1585.
- (40) Merki, D.; Fierro, S.; Vrubel, H.; Hu, X. *Chemical Science* **2011**, 2, 1262.
- (41) Merki, D.; Vrubel, H.; Rovelli, L.; Fierro, S.; Hu, X. *Chemical Science* **2012**, 3, 2515.
- (42) Vrubel, H.; Merki, D.; Hu, X. *Energy & Environmental Science* **2012**, 5, 6136.
- (43) Vrubel, H.; Moehl, T.; Grätzel, M.; Hu, X. *Chemical Communications*, **2013**, 49, 8985.
- (44) Kibsgaard, J.; Jaramillo, T. F.; Besenbacher, F. *Nature Chemistry* **2014**, 6, 248.
- (45) Chen, Z.; Cummins, D.; Reinecke, B. N.; Clark, E.; Sunkara, M. K.; Jaramillo, T. F. *Nano Letters* **2011**, 11, 4168.
- (46) Kibsgaard, J.; Chen, Z.; Reinecke, B. N.; Jaramillo, T. F. *Nature Materials* **2012**, 11, 963.
- (47) Li, Y.; Wang, H.; Xie, L.; Liang, Y.; Hong, G.; Dai, H. *Journal of the American Chemical Society* **2011**, 133, 7296.
- (48) Li, D. J.; Maiti, U. N.; Lim, J.; Choi, D. S.; Lee, W. J.; Oh, Y.; Lee, G. Y.; Kim, S. O. *Nano Letters* **2014**, 14, 1228.

4.6. Supporting Information

Synthesis of Benzenediazonium Tetrafluoroborate (BDT). The synthesis of BDT followed the same procedure than that of 4-NDT synthesis. The difference consisted in using aniline (2.3 g) as starting material. Color changes were also affected by the change

of starting material. The reagent concentrations were unchanged compared to the 4-NDT synthesis. Upon dissolution of the aniline, the solution turned white. The resulting product corresponds to a white paste (2.79 g). The reaction was quantitative. ¹H NMR (D₂O, 400 MHz): δ (ppm) 8.69-8.56 (m, 2H), 8.24-8.19 (m, 1H), 8.00-7.95 (m, 2H).

Physical Characterization. High resolution scanning electron microscopy images were taken on a ZEISS MERLIN. The treated HOPG plates were directly used for imaging. HRTEM images were taken on a FEI Tecnai Osiris equipped with an 11 megapixel Gatan Orius CCD camera. TEM images were taken on a Philips FEI CM12 with a LaB₆ source operated at 120 kV accelerating voltage. The samples were prepared by scrapping off HOPG plates using a scalpel. The extracted samples were then dispersed in ethanol and sonicated. The slurries were mixed with a micropipette by several suction-release cycles to ensure representative and reproducible TEM samples. A few drops of the mixed suspensions were deposited onto the carbon-coated grids.

To image the cross-section of HOPG ZYA samples, preparation of the sample through Focused ion beam was necessary. A TEM lamella was prepared by focused ion beam (FIB) milling using a Zeiss NVision40, applying ion beam voltages of 30 kV down to 5 kV for final thinning. During milling, the sample surface was protected by a layer of amorphous carbon made first by electron beam induced deposition and then by ion beam induced deposition.

Transmission electron microscopy (TEM) and scanning TEM (STEM) analyses of HOPG ZYA samples' cross sections were performed using an FEI Talos F200S, operated at 80 kV high tension in order to reduce the possibility of electron beam induced damage during imaging. Energy dispersive X-ray spectroscopy (EDXS) hyperspectral mapping was performed in STEM mode using a ~0.75 nA electron beam, with data recorded using Bruker Esprit software.

Atomic force microscopy was performed in tapping mode on a Veeco Multimode Nanoscope IIIa SPM controller (Digital Instruments, Santa Barbara, CA) using NSC14/no Al MikroMasch (Tallinn, Estonia) cantilevers. Micropatterned initiator-coated substrates were prepared using a protocol previously reported in the literature.² The prepared patterns on HOPG were used to determine the height profile of polymer-coated HOPG.

Reduction of the Nitro Functional Groups to Amino Moieties. Electrochemical reduction was performed in an electrolyte composed of 1 M HCl and 1 M KCl. A 2 L stock

solution of the electrolyte was prepared prior to reduction. The HOPG plates, bearing nitro groups after electrografting, were immersed in the electrolyte and were employed as working electrodes. Three consecutive cyclic voltammetry scans were performed to ensure large conversion of the nitro groups. The starting and ending potential of the cyclic scan was of 0.8 V vs. RHE, the vertex potential was of -0.4 V vs. RHE. The scan rate applied was of 20 mV s⁻¹. After reduction, the HOPG sample was carefully washed with water and dried with nitrogen gas. The counter and reference electrode were both washed with water, acetone and dried under nitrogen between each reduction. The electrolyte was renewed between each HOPG samples' reduction.

Fabrication of a Monolayer of Trimethylammonium onto HOPG. For comparison purposes with the polymer composites on HOPG ZYH electrodes, monolayer of trimethylammonium were fabricated on HOPG electrodes; which were previously modified with 4-NDT followed by reduction. The electrode tips were immersed into a 2 mL solution of DMF including 50 μ L of methyl iodide (114 mg, 0.8 mmol) and 5 μ L of 2,6-lutidine (4.6 mg, 0.04 mmol) for 16 h at room temperature. Thereafter, the electrodes were washed with deionized water and dried under compressed air.

Attachment of the ATRP Initiator on HOPG Plates. The prepared HOPG plates were then placed within a PEEK holder into a glass reactor. Once the reactor was sealed, it was evacuated and backfilled with nitrogen 3 times. Dry toluene (20 mL) was added to the reactor. Freshly distilled trimethylamine (0.4 mL) was then added and the mixture is well stirred. The system was then cooled down to 0 °C in ice bath. Afterwards, BiBB, the ATRP initiator, is added dropwise (0.4 mL) to the solution. The reaction was kept at 0 °C for 1 h, then the ice bath was removed and the reaction is kept at room temperature for 16 hours. The HOPG plates were then washed extensively with toluene, dichloromethane for 5 minutes and dried with nitrogen.

Attachment of the ATRP Initiator on Si Substrates. Silicon wafers (0.8x1.0 cm) were sonicated 5 minutes in acetone, 5 minutes in ethanol and 5 minutes in distilled water. The wafers were dried using compressed air flow. The substrates were then exposed to microwave-induced oxygen plasma (200 W, Diner electronic GmbH, Germany) for 15 minutes. The wafers were then immersed for 16 h at room temperature under inert atmosphere in a 2 mM solution of 6-(chlorodimethylsilyl)hexyl 2-bromo-2-

meethylproponoate in dry toluene. The prepared wafers were rinsed with dichloromethane and methanol, and dried under nitrogen flow.

Insulation of HOPG ZYA Plates Prior to Anion Exchange. The HOPG ZYA samples were insulated so that only one face of the HOPG was exposed to the electrolyte (cf. **Figure S7**). To ensure conductivity of the isolated material, Ag paste was used to attach a Cu wire at the back of the HOPG support. Once connected, the assembly was isolated so that the HOPG face opposite to the silver paste is exposed. After insulation, the surface area exposed to the electrolyte was determined by means of optical photography (prior to HER). The pixel area of the exposed surface was then determined. By comparison with a sample, whose pixel and geometric area is known, the exact geometric area of the sample was calculated. In addition, the edge sites of HOPG were isolated from deposition of molybdenum sulphide.

Oxidation to Obtain the MoS₃ Precatalyst. MoS₄-incorporated polymers underwent electrochemical oxidation to form the MoS₃ precatalyst prior to the HER. The electrolyte solution contained 0.1 M of NaClO₄. The potentiostatic oxidation was performed at a potential of 0.3 V *vs.* RHE for several minutes. In all cases, the oxidation was complete before 10 minutes of reaction. The oxidation was stopped when the current change between two consecutive minutes was in the order sub-micro-ampere. The oxidized samples were washed with water and dried under nitrogen. Both the counter and reference electrodes were washed with water and acetone and dried using nitrogen gas. In regard of the small amount of currents generated during oxidation, the electrolyte solution was not renewed between each sample.

Evaluation of the HER Activity of the MoS_x-Polymer Brush Composite. The prepared samples were subjected to electrolysis in 1 M H₂SO₄. 10 consecutive LSV scans were performed using a potential window of 0.1 V to -0.4 V *vs.* RHE. These measurements prior to the catalytic activity recordings were performed without iR drop correction. The preliminary scans ensured the effective transformation of the MoS₃ pre-catalyst to the catalytic active species, *i.e.*, MoS_x.³ The 11th LSV was thus used to evaluate the catalytic performance of the MoS_x-polymer brush composite for HER. The potential window of this LSV scan was similar, that is the potential ranged from 0.1 V to -0.4 V *vs.* RHE. However, in this instance, the iR drop was corrected using the current interrupt method. After

electrolysis, the samples were washed with water, dried with nitrogen gas and stored under inert atmosphere. The auxiliary and reference electrodes were both rinsed with water and acetone and dried using nitrogen in between each sample measurement. The electrolyte was renewed for each sample.

Evaluation of the TOF of the MoS_x-Polymer Composite and References.

This Work. Based on the following electrochemical oxidation reaction (corresponding to the step 7 in **Figure 4.1**),³



it was possible to determine the electrochemical active loading of catalyst using the following relation

$$\begin{aligned} \text{Loading } [\mu\text{g cm}^{-2}] \\ = \frac{Q [C] \times 10^6 [\mu\text{g/g}] \times 192 [g/\text{mol}_{\text{MoS}_3}]}{2 [\text{mol}_{\text{e}^-}/\text{mol}_{\text{MoS}_3}] \times 96485 [C/\text{mol}_{\text{e}^-}] \times A [\text{cm}^2]} \end{aligned} \quad (\text{Eq. S4.2})$$

By assuming that all catalyst molecules included in the loading act as active sites for HER, the TOF was determined by:

$$\text{TOF } [H_2 \text{ s}^{-1}] = \frac{j \left[\frac{\text{mA}}{\text{cm}^2} \right] \times 10^{-3} \left[\frac{\text{A}}{\text{mA}} \right] \times \frac{1}{96485} \left[\frac{\text{mol}_{\text{e}^-}}{\text{A}\cdot\text{s}} \right] \times \frac{1}{2} \left[\frac{\text{mol}_{H_2}}{\text{mol}_{\text{e}^-}} \right] \times 6.022 \times 10^{23} \left[\frac{\text{molecules } H_2}{\text{mol}_{H_2}} \right]}{\text{cat.loading} \left[\frac{\text{g}_{\text{cat.}}}{\text{cm}^2} \right] \times M_{\text{cat.}}^{-1} \left[\frac{\text{mol}_{\text{cat.}}}{\text{g}_{\text{cat.}}} \right] \times 6.022 \times 10^{23} \left[\frac{\text{molecules cat.}}{\text{mol}_{\text{cat.}}} \right]} \quad (\text{Eq. S4.3})$$

Upon simplification we obtain:

$$\text{TOF } [H_2 \text{ s}^{-1}] = \frac{3.12 \times 10^{15} \times j}{\# \text{ active sites}/\text{cm}^2} \quad (\text{Eq. S4.4})$$

A samples' batch consisted of 3 to 4 samples with identical preparation conditions (identical polymerization time and grafting density). The TOFs for the samples in a batch were calculated individually. TOFs described in the main-text and shown in **Figure 4.8** correspond to the average of the TOFs obtained for the samples from the same batch. The standard deviation was determined and is depicted as error-bar in the corresponding figure.

TOF of electrodeposited MoS_{2+x}.³ It was based on the given catalytic loading (15 μg cm⁻²) and the calculated current density at 200 and 250 mV of overpotential. The latter

current density was determined using the Tafel slope, and exchange current density given in the report. Once the values were obtained, the relation **Eq. S4.4** was applied.

TOF of [Mo₃S₁₃]²⁻ clusters⁴. The TOF values at both overpotential are given within the maintext. Detailed calculations of the TOF are given in the corresponding literature and are similar to the method employed for this work.

TOF of CS-MoO₃/MoS₂⁵. Determined on the basis of the reported value of active site $7.4 \cdot 10^{16}$ MoS₂/cm² and of the current densities at 200 and 250 mV overpotential. Using these parameters, **Eq. S4.4** was applied.

TOF of MoS₂ RGO⁶. Based on the reported loading ($285 \mu\text{g cm}^{-2}$), the active site value was calculated using the molecular mass of MoS₂. The current density at 200 mV and 250 mV of overpotential were calculated using an extrapolation of the catalytic activity reported. Using these parameters, **Eq. S4.4** was applied.

TOF of DG MoS₂⁷. Based on the reported loading ($60 \mu\text{g cm}^{-2}$), the active site value was calculated using the molecular mass of MoS₂. The current density at 200 mV overpotential is given in the corresponding report. The current density at 250 mV was calculated using an extrapolation of the catalytic activity reported. Using these parameters, **Eq. S4.4** was applied.

TOF of MoS_x-polypyrrole composite⁸. It was based on the reported value of active site ($5 \cdot 10^{-8}$ molMoS₂/cm²) and on the current densities at 200 and 250 mV overpotential. Using these parameters, **Eq. S4.4** was applied.

Evaluation of the mass activity (j_m) and specific activity (j_s). Mass activities were obtained by a simple operation. The current density was divided by the catalytic loading.

Specific activities were determined by normalizing the current generated with the electrochemical surface area (ESCA). The ESCA was determined by the ratio of the double layer capacitance with the specific capacity. A general specific capacity value of 0.035 mF cm^{-2} was used for acidic electrolyte.⁹

If not reported, the double layer capacitance was determined with the charge passed during oxidation of the molybdenum sulfide species. Given the charge and the oxidation

potential, the capacitance was determined as the ratio of the coulombic charge over the oxidation potential.

Discussion of XPS signals. Figure S4.7 shows the XPS spectra of the composites at different stages of fabrication. Survey spectra suggest successful preparation of the MoS_x-polymer composite (Figure S4.7a, d, g, k, o and r). Silicon signals were due to frequently reported XPS chamber contamination. The N 1s high resolution XPS spectra (Figure S4.7b, e, h and l) of the samples revealed the NO₂ signal (406 eV) at several stages of the sample preparation.^{10,11} The signal at 400 eV after the electrografting might be attributed to azo groups formed during electrografting. Alternatively partial reduction of nitro groups to amines by the X-ray in XPS measurements might give rise to this signal.¹¹

The presence of the nitro group after electrochemical reduction underlines that the conversion was not complete. Interestingly, signals corresponding to partial reduction of the nitro group into azo (399.9 eV), hydroxylamine (401.8 eV, Figure S4.7b, e, h magenta curve) and nitroso (402.4 eV, Figure S4.7b, e, h cyan curve) moieties were observed.¹¹⁻¹³ Small features at 403.8 eV and 405.1 eV (Figure S4.7b, e, h green and dark green curve) were attributed to the diazonium moiety.^{14,15} The feature at 407 eV has been previously observed but the origin of this signal is yet unexplained.^{11,13} After polymerization, traces signals from the previous reaction steps were not observed. The sharp feature at 399 eV (Figure S4.7l, blue curve “D”) is attributed to the amine moiety.¹⁶ The 401 eV was attributed to the amine group under hydrogen binding environment (Figure S4.7l, turquoise curve).¹⁷ Adventitious traces of water after polymerization growth might explain this observation. The signal at 402 eV has been previously observed and corresponds to the partial protonation of the PDMAEMA amine (Figure S4.7l, light cyan curve).^{16,17} Due to significant overlap between the Mo 3p and N 1s signals, deconvolution of the N 1s features after catalyst incorporation was not possible.

High resolution C 1s XPS spectra are shown in Figure S4.7c, f, i, m, p and s. Prior to polymerization, five main features can be considered. At 284.6 eV the signal corresponding to the HOPG substrate was observed (Figure S4.7c, f, i, dark grey “0” curve).¹⁸⁻²⁰ The most important signal, 284.9 eV, corresponded to the C=C bond (Figure S4.7c, f, i, orange “1” curve).²¹ The feature at *ca.* 286 eV was attributed to C-N species (Figure S4.7c, f, grey “2” curve).^{21,22} Upon initiator attachment a signal feature at 286 eV increased and was attributed to the C-Br bond.²³ The trace feature at about 289 eV was correlated with carbonate moieties and might arise from air oxidation of the samples.²² After polymerization, several

features corresponding to carbon in PDMAEMA, PMETAI were observed (**Figure S4.7m, p and s**). C sp³ signal was observed at 284.8 eV (**Figure S4.7m, p and s**, blue “7” curve).^{16,24,25} The characteristic C-O-C=O, C-O-C=O and C-C=O signals of PDMAEMA were observed at 289.3 eV, 286.9 eV and 285.3 eV, respectively (**Figure S4.7m, p and s**, pink, curve “8”, “9” and “10”, respectively).^{16,24} The tertiary amine and its quaternized counterpart were observed at a binding energy of 285.9 eV and 286.3 eV, respectively.^{16,24}

The broad feature at 533 eV on **Figure S4.7j** explains the significant O 1s peaks in the XPS survey spectra of the composite at precedent fabrication’s steps; the observed signal corresponds to the binding energy of oxygen in nitro groups.²⁶ This indicates that residual electrografted nitrophenyl groups remain on the surface prior to polymerization. A broad feature above at 534 eV was attributed to the C=O bond after initiator attachment (**Figure S4.7j**, blue “a” curve).¹⁶ After polymerization three signals corresponding to the oxygen of the PDMAEMA polymer were observed **Figure S4.7n, q and t**, curve “b”, “c” and “d”). The O-C=O and O-C signals were found at 533.5 eV and 531 eV, respectively.²⁷ The C=O binding energy is of 532.5 eV.¹⁶ Water traces are the cause of the small feature at high binding energy on **Figure S4.7n and q**.²⁸

Table S4.1. Summary of catalytic activity measured on different MoS_x-polymer composites films grafted from HOPG ZYH electrodes highlighting the irreproducibility of data due to the use of HOPG ZYH electrodes; the catalytic activity was measured in 1 M sulfuric acid.

Catalyst	Grafting density [%]	Polymer brush film thickness [nm]	Anion-exchange solvent	Oxidation time [hour]	Loading [$\mu\text{g cm}^{-2}$]	η_{10}^a [mV]	Tafel slope [mV dec ⁻¹]	TOF ₂₀₀ ^b [s ⁻¹]
	100	44	DMF	1	0.23	N/A	179	0.18
		44			0.62	N/A	66	N/A
		44			2	497	51	0.02
		100			0.03	384	50	2.53
	10	25	DMF	3	0.06	N/A	92	0.85
		30			0.1	235	91	39.48
		34			0.79	327	66	0.19
PtCl ₂	10	34	DMF	1	N/A	35	24	N/A

^a η_{10} corresponds to the overpotential value obtained at a current density of 10 mA cm⁻². ^b TOF₂₀₀ corresponds to the turnover frequency at an overpotential value of 200 mV.

Table S4.2. Catalytic parameters of MoS_x/polymer composites on HOPG ZYA electrodes at 100% grafting density.

Sample	Polymerization time [min]	Loading [μg cm ⁻²]	$\eta_{0.5}$ ^a [mV]	Tafel slope [mV dec ⁻¹]	Exchange current density [A cm ⁻²]
1	1	0.78	321	132	-1.4 10 ⁻⁶
2		0.33	321	111	-6.4 10 ⁻⁷
3		0.10	N/A	137	-6.5 10 ⁻⁷
4	5	0.28	348	172	-4.6 10 ⁻⁶
5		0.18	351	136	-1.3 10 ⁻⁶
6		0.15	379	140	-1.1 10 ⁻⁶
7	20	0.38	296	141	-3.6 10 ⁻⁶
8		0.12	354	152	-2.5 10 ⁻⁶
9		0.17	344	148	-2.0 10 ⁻⁶

^a $\eta_{0.5}$ corresponds to the overpotential required to attain a current density of 0.5 mA cm⁻².

Table S4.3. Catalytic parameters of representative MoS_x/polymer composites on HOPG ZYA electrodes at different grafting densities.

Sample	Grafting density [%]	Polymerization time [min]	Loading [$\mu\text{g cm}^{-2}$]	$\eta_{0.5}$ ^a [mV]	Tafel slope [mV dec ⁻¹]	TOF @ $\eta = 200$ mV [s ⁻¹]	TOF @ $\eta = 250$ mV [s ⁻¹]	Exchange current density [A cm ⁻²]
1		1	0.10	N/A	137	N/A	0.50	$-6.5 \cdot 10^{-7}$
2	100	5	0.18	351	136	0.02	0.47	$-1.3 \cdot 10^{-6}$
3		20	0.17	344	148	0.06	0.53	$-2.0 \cdot 10^{-6}$
4		1	0.05	350	147	0.76	2.15	$-2.1 \cdot 10^{-6}$
5	50	5	0.15	251	114	0.69	3.21	$-2.8 \cdot 10^{-6}$
6		20	0.12	254	106	0.88	3.81	$-1.9 \cdot 10^{-6}$
7		1	0.04	345	145	0.97	3.46	$-2.1 \cdot 10^{-6}$
8	10	5	0.05	306	134	1.19	3.64	$-2.4 \cdot 10^{-6}$
9		20	0.35	211	104	0.98	4.77	$-5.4 \cdot 10^{-6}$

^a $\eta_{0.5}$ corresponds to the overpotential required to attain a current density of 0.5 mA cm^{-2} .

Table S4.4. Catalytic parameters of several molybdenum sulfide catalyst systems^a

Catalyst	Loa- ding [$\mu\text{g cm}^{-2}$]	j_{200} [mA cm ⁻²]	j_{250} [mA cm ⁻²]	$j_{m 200}$ [mA μg^{-1}]	$j_{m 250}$ [mA μg^{-1}]	$j_{s 200}$ [mA cm ⁻²]	$j_{s 250}$ [mA cm ⁻²]	Ref.
MoS_x polymer composite	0.35	-0.34	-1.65	-0.97	-4.71	-0.01	-0.05	This work
Electrodepo sited	15	-11.5	-196	-0.77	-13	N/A	N/A	3
MoS _{2+x} [Mo ₃ S ₁₃] ⁻² clusters	N/A	-0.03	-0.18	N/A	N/A	N/A	N/A	4
CS- MoO ₃ /MoS ₂	60	-1	-8.5	-0.02	-0.07	-0.22	-1.83	5
MoS ₂ RGO	280	-32.9	-100.9	-0.12	-0.36	N/A	N/A	6
DG MoS ₂	60	-4	-16.1	-0.07	-0.27	-0.03	-0.12	7
MoS _x polypyrrole composite	8	-0.1	-0.4	-0.01	-0.05	N/A	N/A	8

^a j , j_m , j_s correspond respectively to the current density, the mass activity and the specific activity. Current density is normalized over the geometric surface area while the specific activity is normalized over the ESCA. The subscripts related to these activities indicate the overpotential value at which the current is calculated. For the three variables, the overpotential evaluated are 200 and 250 mV of overpotential.

Table S4.5. TOF of several molybdenum sulfide systems at 200 and 250 mV of overpotential

Catalyst	TOF @ $\eta = 200$ mV [s ⁻¹]	TOF @ $\eta = 250$ mV [s ⁻¹]	Ref.
MoS_x polymer composite	1.31	4.92	This work
Electrodeposited MoS _{2+x}	0.76	13	3
[Mo ₃ S ₁₃] ⁻² clusters	0.67	7.91	4
CS-MoO ₃ /MoS ₂	0.04	0.36	5
MoS ₂ RGO	0.10	0.30	6
DG MoS ₂	0.06	0.22	7
MoS _x polypyrrole composite	0.05	0.08	8
MoS _x /N-doped CNT forest	3.5	-	29
[Mo ₃ S ₁₃] ⁻² clusters	3.3 ^a	22 ^a	4
UHV MoS ₂	8 ^{a,b}	-	4

^a TOF determined by active sites count. ^b TOF at an overpotential of 150 mV.

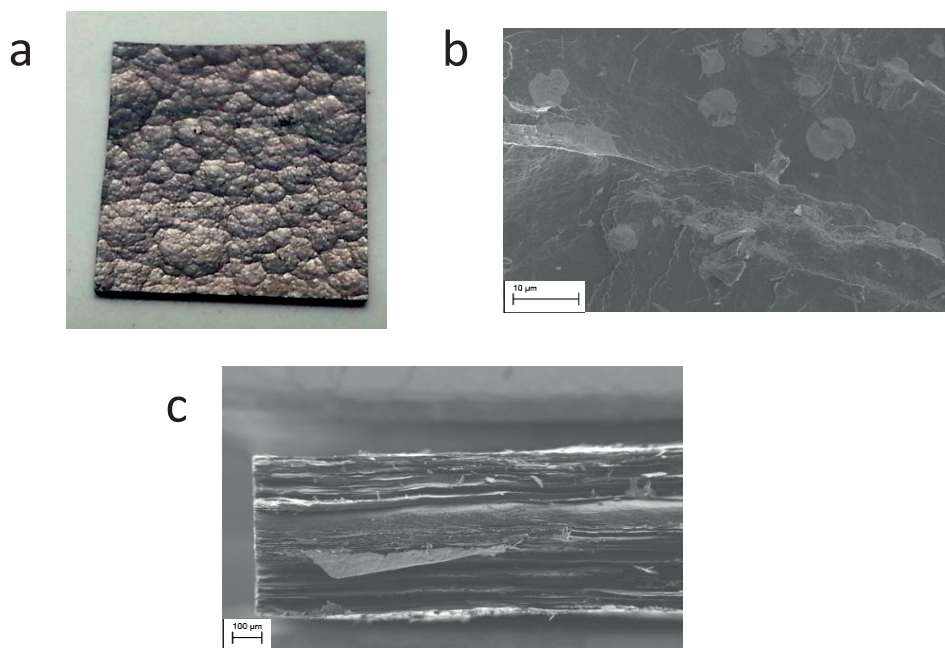


Figure S4.1. (a) Optical photograph of low-grade HOPG ZYH plate (ca. 1x1x0.2 cm). (b - c) High resolution SEM (HRSEM) images of the HOPG plate. (b) Top-view. (c) Cross-section view.

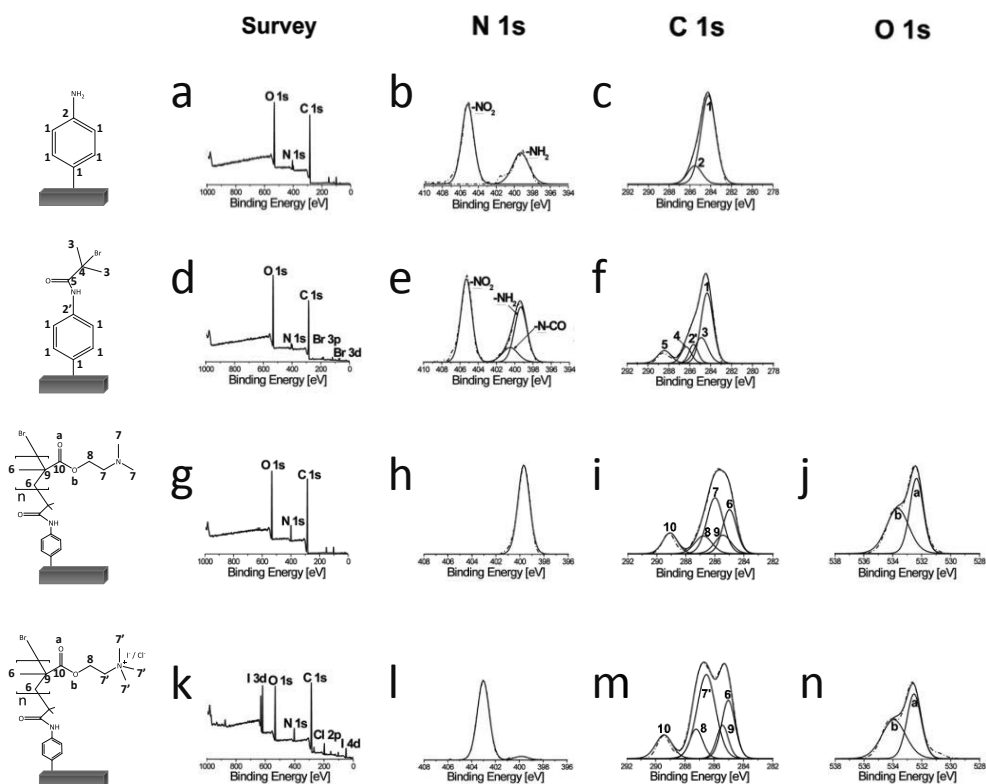


Figure S4.2. (a - n) XPS spectra of the MoS_x-polymer brush composites on HOPG ZYH at different stages of the assembly fabrication on HOPG. Each row of spectra corresponds to the composite at a different step of the process shown in **Figure 4.1**. The corresponding chemical structure of the assembly is shown for reference. The numbers and letters displayed on the spectra refer to specific atoms on the corresponding chemical structure. (a, d, g, k) XPS survey spectra at different stages of the assembly preparation. (b, e, h, l) High resolution N 1s XPS spectra. (c, f, i, m) High-resolution C 1s XPS spectra. (j, n) High-resolution O 1s XPS spectra.

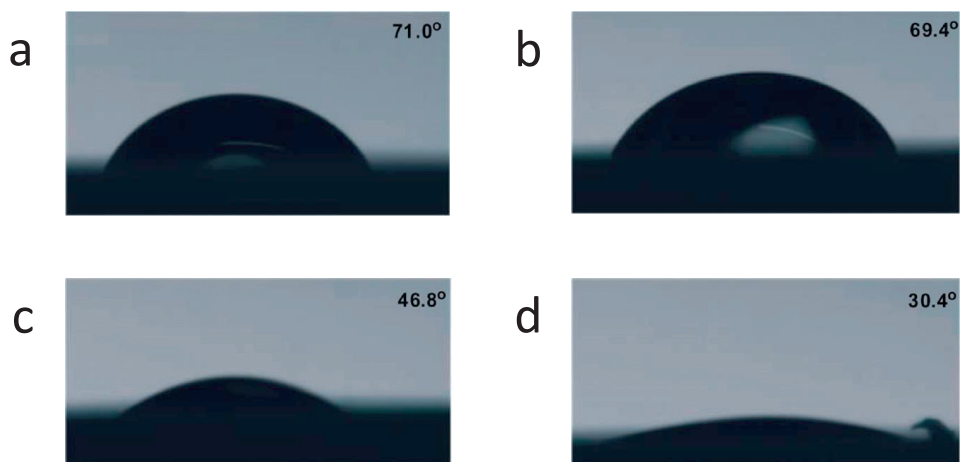


Figure S4.3. Water-contact angle measurements at different stages during the fabrication of the MoS_x composite films on HOPG ZYH (water droplets of 5 μ L). (a) Prior to and (b) after step 3. (c) Prior to and (d) after step 5. The step number refers to the steps indicated in **Figure 4.1** of the article.

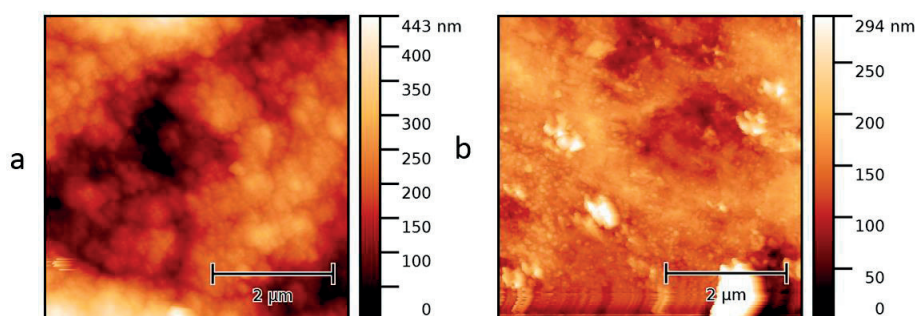


Figure S4.4. AFM images of non-functionalized HOPG ZYH plates (a) before and (b) after mechanical polishing. (a) Average roughness (Ra) = 54.7 nm, roughness mean square (Rms) = 68.3 nm, (b) Ra = 30.4 nm, Rms = 41.3 nm. Mechanical polishing did not sufficiently improve topography of the surface.

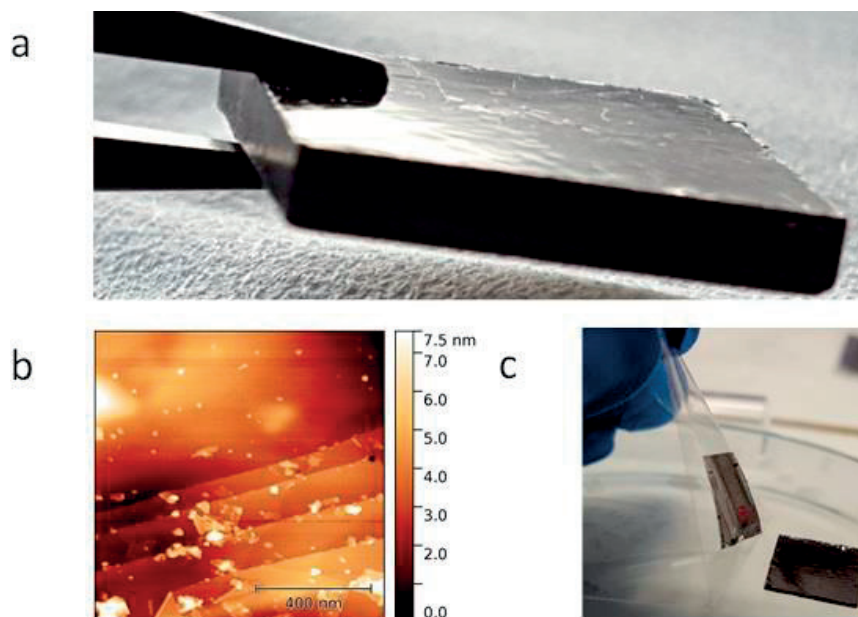


Figure S4.5. (a) Optical photograph of the HOPG ZYA. Plate dimension: 10x10x0.5 mm. (b) AFM image of the HOPG ZYA. (c) Optical photograph depicting the simple scotch-tape technique to cleave and renew the HOPG ZYA surface.

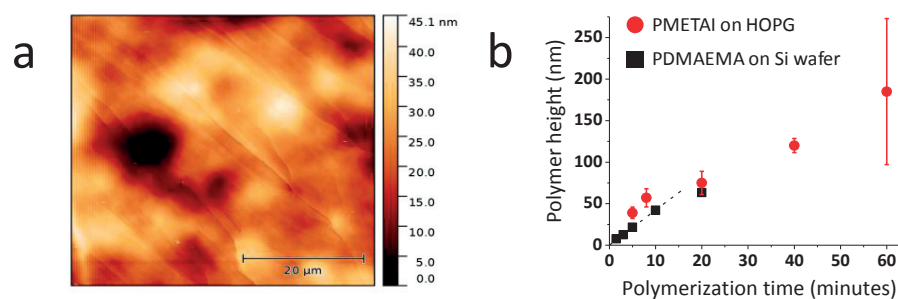


Figure S4.6. (a) AFM image representative of bare HOPG ZYA surface after cleaving. The roughness of the material on the micron scale and the possible defects underline the difficulty of accurate AFM measurements on HOPG grown polymers. Average roughness = 5.4 nm, roughness mean square = 6.9 nm. (b) Evolution of polymer brush film thickness as a function of polymerization time on both Si wafers (black squares) and HOPG (red circles). The height profile was determined by AFM measurements. Around 20 minutes of polymerization, the polymer growth slows down on Si wafer.

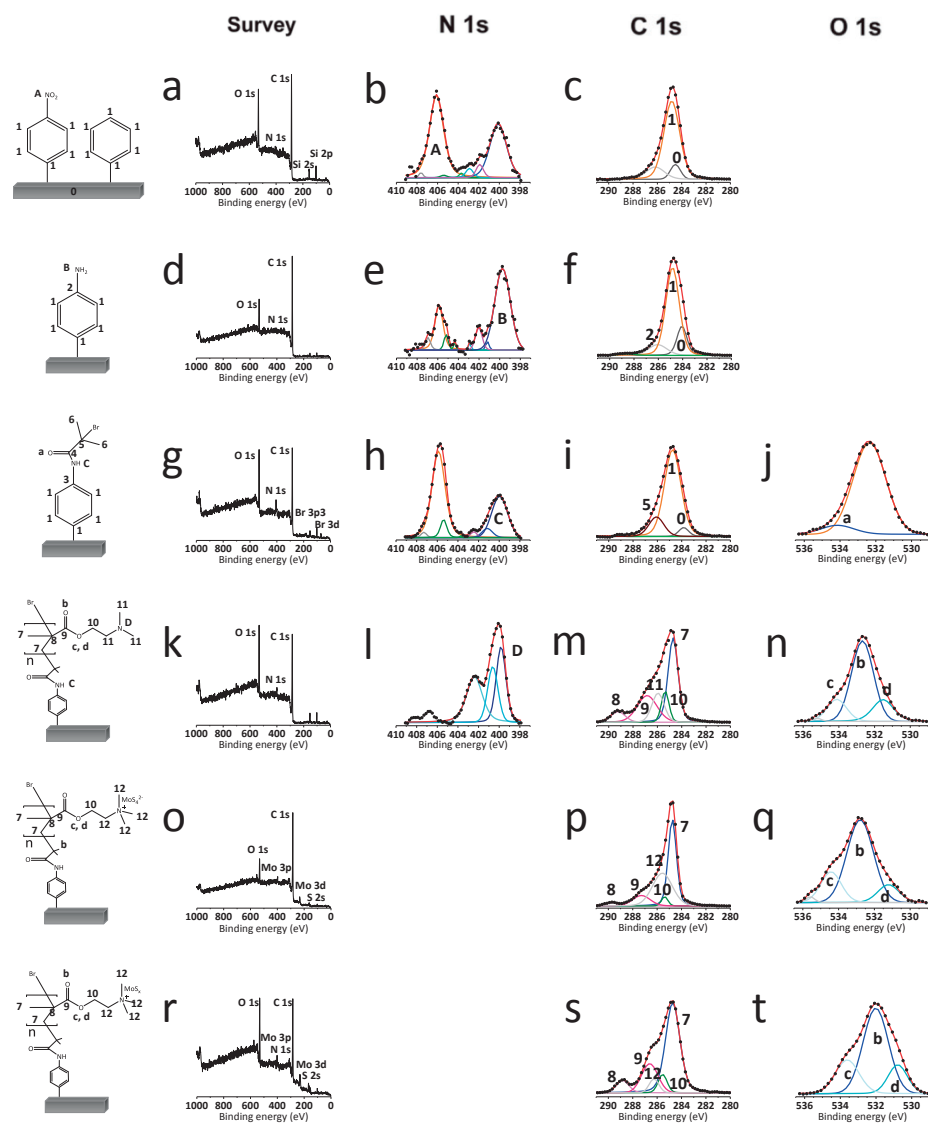


Figure S4.7. (a - t) XPS spectra of MoS_x-polymer brush composite films on HOPG ZYA at different stages of fabrication. Each row of spectra corresponds to the sample at a different step of the process shown in **Figure 4.1**. The corresponding chemical structure of the assembly is shown for reference. The numbers and letters displayed on the spectra refer to specific atoms on the corresponding chemical structure. The deconvolution follows a simple color code: the experimental data correspond to the black dots, the fitting envelope is the red line. For the same element, each color represents a unique moiety. Peaks of similar colors indicate, thus, the same signal at different stages of the polymer fabrication. (a, d, g, k, o, r) XPS survey spectra at different stages of the assembly preparation. (b, e, h, l) High resolution N 1s XPS spectra. (c, f, i, m, p, s) High-resolution C 1s XPS spectra. (j, n, q, t) High-resolution O 1s XPS spectra.

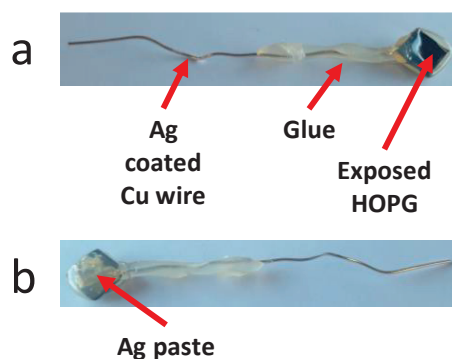


Figure S4.8. Insulated HOPG ZYA electrode. The exposed surface shown in (a) is in direct contact with the electrolyte. (b) Silver paste was used to connect a Cu wire to the back of the HOPG electrode. The connection was also insulated prior to treatment of the electrode. Insulation of the electrode is made after successful SI-ATRP (**Figure 4.1**, step 5). The remaining steps in the catalytic process were done on isolated electrodes. The process ensures that only the exposed surface is affected by the subsequent chemical modifications operated on the electrode assembly. The exposed surface area was determined by means of optical photography and subsequent image analysis. Any shape could be selected and the software provided a number of pixels of the selected area, which could be related to a real value in cm².

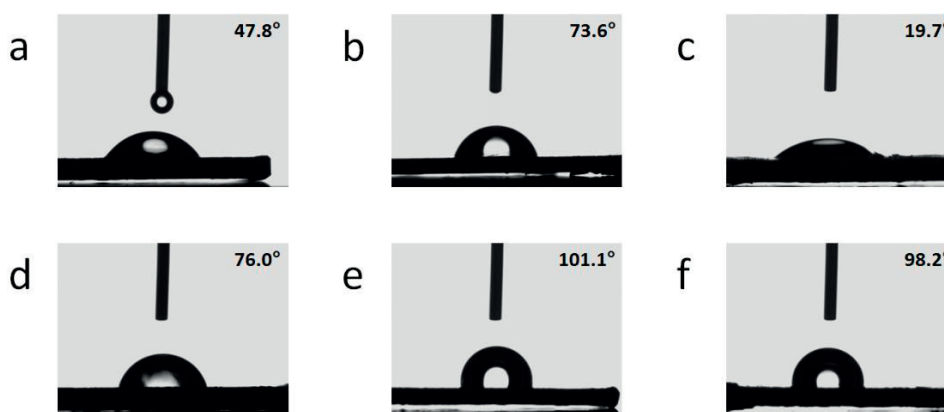


Figure S4.9. Water-contact angle measurements at different stages of the composite fabrication on HOPG ZYA (water droplets of 5 μ L). (a) After step 2. (b) Image after step 3. (c) After step 5 (d) After step 6. (e) After pre-catalyst formation (step 7). (f) After HER catalysis (step 8). The step number refers to the steps indicated in **Figure 4.1**.

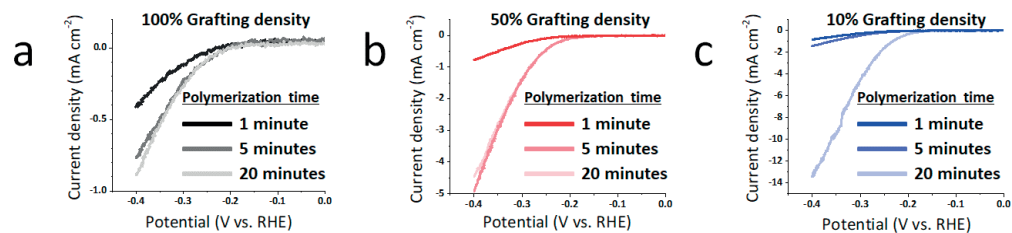


Figure S4.10. LSV scans of MoS_x-polymer brush assemblies, prepared using different polymerization times and different grafting densities, in 1 M H₂SO₄. The assemblies underwent 10 consecutive LSV scans from 0.1 V to -0.4 V vs. RHE in 1 M H₂SO₄ to convert the precatalyst MoS₃ to the catalytic active species MoS_x. The scans displayed correspond to the 11th LSV measurement performed on the assemblies. Conditions: scan rate 5 mV s⁻¹, ohmic drop corrected. The catalytic activities correspond to the samples described in Table S4.3.

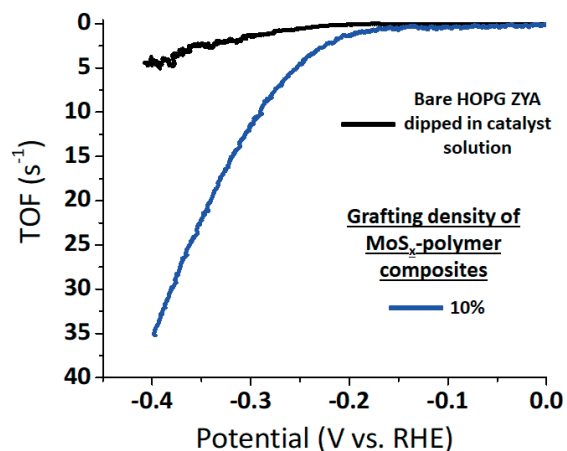


Figure S4.11. Comparison of TOF between a representative MoS_x polymer composite at 10% grafting density and a bare substrate sample dipped in catalyst solution for 1 hour. Details of the TOF calculations are given in the supporting information (Eq. S4).

References

- (1) Schüwer, N.; Klok, H. -A. *Advanced Materials* **2010**, *22*, 3251.
- (2) Tugulu, S.; Harms, M.; Fricke, M.; Volkmer, D.; Klok, H.-A. *Angewandte Chemie International Edition* **2006**, *45*, 7458.
- (3) Vrabel, H.; Hu, X. *ACS Catalysis* **2013**, *3*, 2002.
- (4) Kibsgaard, J.; Jaramillo, T. F.; Besenbacher, F.; *Nature Chemistry* **2014**, *6*, 248.
- (5) Chen, Z.; Cummins, D.; Reinecke, B. N.; Clark, E.; Sunkara, M. K.; Jaramillo, T. F. *Nano Letters* **2011**, *11*, 4168.
- (6) Li, Y.; Wang, H.; Xie, L.; Liang, Y.; Hong G.; Dai, H. *Journal of the American Chemical Society* **2011**, *133*, 7296.
- (7) Kibsgaard, J.; Chen, Z.; Reinecke, B. N.; Jaramillo, T. F. *Nature Materials* **2012**, *11*, 963.
- (8) Lattach, Y.; Deronzier, A.; Moutet, J. C. *ACS Applied Materials & Interfaces* **2015**, *7*, 15866.
- (9) McCrory, C. C. L.; Jung, S.; Ferrer, I. M.; Chatman, S. M.; Peters, J. C.; Jaramillo, T.F. *Journal of the American Chemical Society* **2015**, *137*, 4347.
- (10) Allongue, P.; Delamar, M.; Desbat, B.; Fagebaume, O.; Hitmi, R.; Pinson, J.; Savéant, J. M. *Journal of the American Chemical Society* **1997**, *119*, 201.
- (11) Yu, S. S.; Tan, E. S.; Jane, R. T.; Downard, A. J. *Langmuir* **2007**, *23*, 11074.
- (12) Gui, A. L.; Liu, G.; Chockalingam, M.; Le Saux, G.; Luais, E.; Harper, J. B.; Gooding, J. J. *Electroanalysis* **2010**, *22*, 1824.
- (13) Menanteau, T.; Levillain, E.; Downard, A. J.; Breton, T. *Physical Chemistry Chemical Physics* **2015**, *17*, 13137.
- (14) Finn, P.; Jolly, W. L. *Inorganic Chemistry* **1972**, *11*, 1434.
- (15) Ullien, D.; Thüne, P. C.; Jager, W. F.; Sudhölter, E. J.; de Smet, L. C. *Physical Chemistry Chemical Physics* **2014**, *16*, 19258.
- (16) Zengin, A.; Karakose, G.; Caykara, T. *European Polymer Journal* **2013**, *49*, 3350.
- (17) Yang, Y.; Liu, L.; Zhang, J.; Li, C.; Zhao, H. *Langmuir* **2007**, *23*, 2867.
- (18) Fujimoto, A.; Yamada, Y.; Koinuma, M.; Sato, S. *Analytical Chemistry* **2016**, *88*, 6110.
- (19) Yang, D.-Q.; Sacher, E. *Langmuir* **2006**, *22*, 860.
- (20) Schmiegel, S. J.; Belton, D. N. *Surface Science Spectra* **1992**, *1*, 333.

- (21) Chuang, C. H.; Ray, S. C.; Mazumder, D.; Sharma, S.; Ganguly, A.; Papakonstantinou, P.; Chiou, J.-W.; Tsai, H.-M.; Shiu, H.-W.; Chen, C.-H.; Lin, H.-J.; Guo, J.; Pong, W. F. *Scientific Reports* **2017**, *7*, 42235.
- (22) Moulder, J. F.; Stickle, W. F.; Sobol P. E.; Bomben, K. D. *Handbook of X-ray Photoelectron Spectroscopy*, Physical Electronics, Inc., Minnesota, 1995.
- (23) Matrab, T.; Chancolon, J.; L'hermite, M. M.; Rouzaud, J. N.; Deniau, G.; Boudou, J. P.; Chehimi, M. M.; Delamar, M. *Colloids and Surfaces A: Physicochemical and Engineering Aspects* **2006**, *287*, 217.
- (24) Bilgiç Tune, T. *Polymer Brushes - Engineered Model Interfaces and Functional Surface Coatings for DNA Biosensing and Electrocatalysis*, Ph. D. Thesis, EPFL, Lausanne, 2015.
- (25) Karamdoust, S.; Yu, B.; Bonduelle, C. V.; Liu, Y.; Davidson, G.; Stojcevic, G.; Yang, J.; Lau, W. M.; Gillies, E. R. *Journal of Materials Chemistry* **2012**, *22*, 4881.
- (26) Folkesson, B.; Sundberg, P. *Spectroscopy Letters* **1987**, *20*, 193.
- (27) Endo, K.; Maeda, S.; Aida, M. *Polymer Journal* **1997**, *29*, 171.
- (28) Schulze, P. D.; Shaffer, S. L.; Hance, R. L.; Utley, D. L. *Journal of Vacuum Science & Technology A: Vacuum, Surfaces and Films* **1983**, *1*, 97.
- (29) Li, D. J.; Maiti, U. N.; Lim, J.; Choi, D. S.; Lee, W. J.; Oh, Y.; Lee, G. Y.; Kim, S. O. *Nano Letters* **2014**, *14*, 1228.

5. Conclusions and Perspectives

Surface-initiated controlled radical polymerization has enabled the generation of plethora of architectures of polymer brushes. Manipulation of the chemical composition and topology has a great effect on the final properties of polymer brushes. Loop or reversibly crosslinked polymer brushes are examples of brush architectures that feature superior properties as compared to their linear counterparts. Also, incorporation of functional groups that can bind or stabilize nanoparticles is interesting, as it can provide complementary features like catalytic activity. While classic linear polymer brushes are easily accessible with SI-CRP, architecturally advanced assemblies are more difficult to obtain. Therefore, the development of feasible synthetic approaches is required.

After an introduction to the field of complex polymer brush structures in **Chapter 1**, which presented synthetic strategies toward different brush topologies and polymer-nanoparticles hybrid films, **Chapter 2** described challenges associated with post-polymerization modification loop-closure of linear polymer brushes. The monitoring of loop-closure of linear polymer brushes is not trivial, as it implies small chemical changes that are difficult to detect. However, the closure connects two chains and thus implies an increase of molecular weight. Therefore, the first part of this Chapter focused on the development and optimization of polymer brush cleavage protocols from silica nanoparticles using $\text{Et}_3\text{N}\cdot 3\text{HF}$. Then, post-polymerization loop-closure strategy was proposed using allylamine to install olefin chain-ends. However, this step was incompatible with subsequent metathesis. This was confirmed by model experiments on small molecules. Allylamine-functionalized ATRP initiators did not undergo dimerization in the presence of 1st and 2nd generation Grubbs catalysts. Thus, the final part explored attachment of olefin chain-ends using an alternative reagent, allyltibutylstannane, followed by exposure to Grubbs catalysts. The analysis of cleaved PMMA chains after the loop-closure showed nearly doubled molecular weights of the PMMA grafts after the modification, which indicates the successful synthesis of loop polymer brushes via this new approach. The modification could be further optimized for better yields, for example by reducing polymerization time of SI-ATRP to minimize losses of halide chain-ends. Also, the reaction with allyltributylstannane may be performed with less active ATRP ligands to avoid radical terminations and thus inefficient trapping by the stannane. Finally, there may be an optimal grafting density and polymer brush thickness, at which the chain-ends are close enough to promote efficient loop-closure. The post-polymerization loop-closure is an attractive

strategy to enhance properties of conventional linear polymer brushes, whose synthesis is easily accessible. Further research should aim at investigation of tribological and fouling properties of these loop polymer brushes and comparison with loops obtained by grafting-onto method. Importantly, contrary to the grafting-onto, post-polymerization loop-closure enables high grafting densities and thus brush-topology studies in regimes systematically not explored before.

In **Chapter 3** synthesis of a P(DMAEMA-co-AzHPMA) copolymer platform for subsequent CuAAC click chemistry post-polymerization modification was described. The copolymerization of DMAEMA with AzHPMA with up to 50% AzHPMA was well controlled and films with up to 280 nm could be generated. *S*-propargyl thioacetate could react with azide groups of AzHPMA and crosslink the brushes after deprotection of thioacetate and 10 min exposure to air. The modifications were readily followed by FTIR spectroscopy (azide signals at 2101 cm⁻¹) and XPS provided additional evidence for the chemical changes, including among others transformation of azide groups into triazole rings (shifts from 400.9, 404.6 to 399.5, 400.2 eV), attachment of thioacetate (S 2p signal at 162.4 eV) and deprotection to thiols (thiol S 2p signal at 163.6 eV). The crosslinking could be reversed by 10 min incubation in TCEP, 0.1 M phosphate buffer solution (pH 7.4) and repeated by simple heating at 60°C under air for 2 h. This reversibility was confirmed by changes in swelling (ellipsometry), chain hydration and mobility (quartz crystal microbalance with dissipation monitoring (QCM-D)). The dynamics of this system can be used to tune lubrication and non-fouling properties of polymer brushes. Further investigations should cover attachment of different crosslinks (e.g. bearing hydrogen bonding ureidopyrimidinone) to systematically study their effect on final properties of the brushes. Importantly, this strategy not only allows the formation of polymer brushes with crosslinks of different dynamics, but also the attachment of complex functions and biomolecules. Hence, these platforms can be used for different applications.

In **Chapter 4**, a multi-step synthetic protocol to prepare polymer brush-templated amorphous molybdenum sulfide catalysts was presented. HOPG surfaces were electrografted with a mixture of nitrobenzene and benzene to afford initiator surface concentrations of 10, 50 and 100%. Then, PDMAEMA brushes were grown via SI-ATRP and after quaternization with iodomethane and ion exchange with MoS₄²⁻ the precursor was reduced to MoS_x in cyclic voltammetry sweeps (from 0.8 to -0.4 V vs RHE at 20 mV/s). The polymer brushes directed the 3D assembly of the MoS_x catalyst. The hydrogen evolving properties of the MoS_x-polymer composite films were tested using linear sweep

voltammetry in 1 M H₂SO₄, which revealed that the lowest grafting densities (10%) featured the highest intrinsic activity (TOF). It was concluded that this activity could be a result of a higher catalyst loading, more accessible sites and facilitated mass transport to the active sites. The systematic investigations led to an optimal catalyst template, which was prepared by 20 minutes polymerization of DMAEMA from HOPG substrates bearing 10% of the ATRP initiator. This catalyst showed turnover frequencies of 1.3 and 4.9 s⁻¹ at $\eta = 200$ and 250 mV in 1 M H₂SO₄, which is among the highest reported for molybdenum sulfide catalysts. Additionally, during 10 h potentiostatic electrolysis the MoS_x-polymer assemblies displayed stable currents, which indicated a good stability of these catalysts. However, the geometrically averaged current densities at low overpotentials were comparatively small due to a very small loading of catalysts. It is therefore crucial to develop strategies to maximize catalyst loadings in similar systems in future. This could be done by growing thick polymer brushes of low grafting densities. Alternatively, MoS_x nanoparticles could be synthesized *ex situ* and incorporated in the brushes by “in-stacking” method described in the Introduction.

This Thesis has explored three routes of post-polymerization modification of SI-ATRP generated polymer brushes that affect them in different ways, viz. transforming topology to form loop-type brush architectures, introducing reversible crosslinks and incorporating catalyst nanoparticles by *in situ* synthesis. The versatile combination of SI-CRP with post-polymerization modification enables many ways to enrich and enhance functions of polymer brushes. Importantly, the strategies presented here are straightforward modifications that can be used to tune numerous polymer brushes that have been reported so far in the literature.

Piotr Mocny

Route Aloys-Fauquez 109
1018 Lausanne
Switzerland
+41 76 700 93 66
piotr.mocny@gmail.com

OrcID: [0000-0001-6456-8373](https://orcid.org/0000-0001-6456-8373)

ResearcherID: [C-4002-2019](https://pubs.acs.org/author/4002-2019)



EDUCATION:

École polytechnique fédérale de Lausanne (EPFL)

08.2014 - present **Ph.D.** in Materials Science

Gdańsk University of Technology (GUT)

02.2012 - 12.2013 **M.Sc. in Chemical Technology** (with A grade), Specialization: Organic Technology.

10.2009 – 03.2013 **B.Eng. degree, Applied Physics** (with A grade), Specialization: Nanotechnology.

10.2008 – 01.2012 **B.Eng. degree, Chemical Technology** (with B+ grade), Specialization: Organic Technology.

PROFESSIONAL EXPERIENCE:

08.2014 – present **Doctoral Assistant at Polymers Laboratory**, École polytechnique fédérale de Lausanne (EPFL)

Ph.D. Thesis: “**Controlling topology, dynamics and function of polymer brushes via post-polymerization modification**”

Supervisor: **Prof. Harm-Anton Klok**

Description:

Synthesized loop-polymer brushes via post-polymerization modification (olefin metathesis) of surface-initiated atom transfer radical polymerization (SI-ATRP) generated linear brushes for improvement of their non-biofouling and lubrication. Developed characterization strategy to confirm successful loop-closure, which comprised cleaving and GPC analysis of the polymer chains.

Designed and developed a project to synthesize polymer brushes with reversible crosslinks controlled by redox (thiol/disulfide linkers) stimulus to be applied as boundary lubricants of tunable properties. The synthesis included modification of polymer brush side-chains with CuAAC. The reversibility was studied with QCM-D and liquid cell ellipsometry.

Synthesized MoS_x-polymer brush catalysts supported on HOPG for hydrogen evolution reaction (HER) with high turnover frequencies and high stabilities - a green technology for renewable energy.

Additional duties:

Supervised **three master student projects** and **co-supervised a Master Thesis**.

Teaching assistant for practical exercises (TP) on **crystallography** (in English) during **spring semester 2017**.

Responsibilities for equipment: AFM, QCM-D, water contact angle machine (**management, troubleshooting, trainings**), and for a laboratory (**management, organization, scheduling duties**).

03.2013-09.2013 **Intern, SABIC-Europe, Sabic Technology Center**, Unimodal HDPE & UHMWPE, Geleen, the Netherlands

M.Sc. Thesis: “**Compatibilizer development through reactive extrusion**”

Supervisors: **Dr. Lidia Jasińska-Walc and Dr. Robbert Duchateau**

Description:

Investigated functionalization of polyolefins. Involved synthesis on a laboratory scale (multigram scale) via reactive extrusion, purification of the products (Soxhlet extraction) and analysis by (variable temperature) FTIR, NMR, GPC/SEC and DSC.

2011-2012 **Department of Chemistry and Technology of Functional Materials**, Gdańsk University of Technology, Poland

B.Sc. Thesis: “**Chemical functionalization of carbon nanotubes**”

Supervisor: **Prof. Jan F. Biernat**

Description:

Covalent functionalization of single-walled carbon nanotubes (SWCNTs) for application as electrode material in biocatalytical fuel cell using glucose oxidase (from *Aspergillus niger* AM-11) and laccase (from *Cerrena unicolor* C-139) as enzymes.

09.2011 **Internship, Polpharma Pharmaceutical Works**, Department of Operational Excellence – Starogard Gdański, Poland

06-07.2011 **Internship, Water and Sewer Treatment Plant**, Tczew, Poland

PUBLICATIONS:

6. Michl, T. D., Jung, D., Pertoldi, A., Schulte, A., **Mocny, P.**, Klok, H. -A., Schönherr, H., Giles, C., Griesser, H. J., and Coad, B. R. “**An Acid Test: Facile SI-ARGET-ATRP of Methacrylic Acid.**” *Macromolecular Chemistry and Physics* **2018**, 219(15), 1800182.
5. Stern, L. A., **Mocny, P.**, Vrabel, H., Bilgic, T., Klok, H. -A., and Hu, X. “**Polymer-Brush-Templated Three-Dimensional Molybdenum Sulfide Catalyst for Hydrogen Evolution.**” *ACS applied materials & interfaces* **2018**, 10(7), 6253-6261.
4. Michl, T. D., Giles, C., **Mocny, P.**, Futrega, K., Doran, M. R., Klok, H. -A., Griesser, H. J., and Coad, B. R. “**Caspofungin on ARGET-ATRP grafted PHEMA polymers: Enhancement and selectivity of prevention of attachment of Candida albicans.**” *Biointerphases* **2017**, 12(5), 05G602.
3. Krammer, A., Magrez, A., Vitale, W. A., **Mocny, P.**, Jeanneret, P., Guibert, E., Whitlow, H. J., Ionescu, A. M., and Schüler, A. “**Elevated transition temperature in Ge doped VO₂ thin films.**” *Journal of Applied Physics* **2017**, 122(4), 045304.
2. Zoppe, J. O., Ataman, N. C., **Mocny, P.**, Wang, J., Moraes, J., and Klok, H. -A. “**Surface-initiated controlled radical polymerization: state-of-the-art, opportunities, and challenges in surface and interface engineering with polymer brushes.**” *Chemical reviews* **2017**, 117(3), 1105-1318.
1. **Mocny, P.**, Klok, H. -A. “**Tribology of surface grafted polymer brushes**”, *Molecular Systems Design & Engineering* **2016**, 1, 141-154.

PUBLICATIONS IN PREPARATION:

3. **Mocny, P., Klok, H. -A.** “Complex polymer topologies and polymer – nanoparticles hybrid films prepared via surface-initiated polymerization”, Manuscript in preparation, invited for submission to *Progress in Polymer Science*.
2. **Mocny, P., Ménetrey, M., Klok, H. –A.** “Synthesis of loop polymer brushes via post-polymerization modification”, Manuscript in preparation.
1. **Mocny, P., Klok, H. -A.** “Reversibly crosslinked polymer brushes”, Manuscript in preparation.

PATENTS:

Patent application for European Procedure (Patents) 14POLY0121-EP-EPA “Process for the preparation of Functionalized Polyolefins with improved properties by reactive extrusion and the resulting Functionalized Polyolefins with improved properties”, filed on 17.11.2017, received search report on 29.05.2018.

PRESENTATIONS:

3. **Mocny, P., González Alanís, M. A., Klok, H. -A.** “Reversibly crosslinked polymer brushes by covalent and hydrogen bonding.” *SCS Fall Meeting*, EPFL, Lausanne, Switzerland, September 2018 poster presentation.
2. **Mocny, P., Stern, L.- A., Bilgic, T., Klok, H.- A., Hu, X.** “Preparation of PMETAI brushes on HOPG for hydrogen evolution reaction.” *EDMX Research Day*, EPFL, Lausanne, Switzerland, June 2017 poster presentation.
1. **Mocny, P., Klok, H.- A.** “Synthesis of PPEGMEMA loop brushes via post-polymerization loop-closure”, *EDMX Research Day*, EPFL, Lausanne, Switzerland, November 2015 poster presentation.

TECHNICAL SKILLS:

Synthesis:	SI-ATRP, post-polymerization modification , click chemistry (CuAAC), olefin metathesis, reactive extrusion, functionalization of silica nanoparticles, polystyrene microspheres, and silicon, HOPG, CoCrMo alloy, Ta ₂ O ₅ flat surfaces
Characterization:	NMR, GPC/SEC , (variable temperature) ATR-FTIR , AFM (dry or within liquid), ellipsometry (dry or within liquid), DLS , DSC , TGA , QCM-D , XPS , ToF-SIMS-MS , Langmuir-Blodgett trough , nanotribometry , water contact angle measurements
IT:	MS Office , VBA Excel Macros , OriginLab , AutoCAD , ChemCAD , InDesign , 3ds Max , CorelDRAW , C++ , LabVIEW , Arduino

LANGUAGES:

- English – fluent spoken and written (C2),
- German – intermediate in spoken and written (B1),
- French – intermediate in spoken and written (B1),
- Polish – native.

PERSONAL DETAILS:

Polish nationality, married, two children

